

Physical characterization of red blood cell aggregation

Dissertation

im Rahmen eines Cotutelle-Verfahrens zur Erlangung des Grades
des Doktors der Naturwissenschaften
der Naturwissenschaftlich-Technischen Fakultät
der Universität des Saarlandes

Thèse

dans le cadre d'une cotutelle pour obtenir le grade de
Docteur de l'Université Grenoble
Spécialité: Physique pour les sciences du vivant
et de Doktor der Naturwissenschaften der Universität des Saarlandes

von/présentée par

Daniel Amadeus Dominic Flormann

Saarbrücken/Grenoble

2016

Tag des Kolloquiums: 29.03.2017

Dekan: Prof. Dr. Guido Kickelbick

Mitglieder des Prüfungsausschusses:

Vorsitzender: Prof. Dr. Rolf Pelster

Berichterstatter: Prof. Dr. Christian Wagner

Berichterstatter: Jun.-Prof. Dr. Stephan Gekle

Akademischer Mitarbeiter: Dr. Andreas Tschöpe

Weiteres Mitglied: Prof. Dr. Thomas Podgorski

Weiteres Mitglied: Prof. Dr. Abdul Barakat

Weiteres Mitglied: Dr.-Ing. Claude Verdier

Eidesstattliche Versicherung

Hiermit versichere ich an Eides statt, dass ich die vorliegende Arbeit selbstständig und ohne Benutzung anderer als der angegebenen Hilfsmittel angefertigt habe. Die aus anderen Quellen oder indirekt übernommenen Daten und Konzepte sind unter Angabe der Quelle gekennzeichnet. Die Arbeit wurde bisher weder im In- noch im Ausland in gleicher oder ähnlicher Form in einem Verfahren zur Erlangung eines akademischen Grades vorgelegt.

Saarbrücken, 25.11.2016

Daniel Flormann

Abstract

Abstract

In this work, five aspects of the red blood cell aggregation induced by macromolecules are investigated. A rheological approach focused on the normalization of viscosity as a function of the macromolecular adsorption rates using a commercial rheometer is proposed. Derived from that approach, the yield stress of aggregating red blood cell suspensions is investigated. The sedimentation rates of the utilized biological system are then studied. Microscopical investigations, including measurements of the microscopical aggregation index, lead to the conclusion that the C-reactive protein, a plasma protein, does not influence the aggregation behavior of red blood cells. Detailed microscopical studies on the morphology of the interaction zones of aggregated red blood cells show that these strongly depend on the macromolecular concentration in good agreement with numerical simulations that allow to derive an approximation of the interaction energies. The latter are also directly measured with single cell force spectroscopy using an atomic force microscope with the additional result that the viscosity of the surrounding medium can influence the results significantly. Finally, the physical origin of aggregation is discussed and supported by several additional measurements. This allows to combine two existing theories and explain the bell-shape of interaction energy versus macromolecular concentration curve in a new way.

Résumé

Ce travail a été réalisé autour de cinq aspects de l'agrégation des globules rouges (RBCs) sanguins induite par des macromolécules. Une approche rhéologique, ciblée sur la normalisation de la viscosité en fonction du taux d'adsorption des macromolécules et mesurée par un rhéomètre commercial, est proposée. Par cette approche, la contrainte seuil de suspensions de cellules sanguines agrégées est aussi évaluée. De plus, les taux de sédimentation des solutions biologiques utilisées sont aussi mesurés. Nos données microscopiques, incluant des mesures d'indice d'agrégation microscopique, ont eu pour conclusion que la protéine C réactive, une protéine du plasma, n'a pas d'influence sur le phénomène d'agrégation des RBCs. Des mesures microscopiques détaillées de la morphologie des zones de contact des RBCs ont montrées que ces dernières dépendent fortement de la concentration de macromolécules,

en accord avec des simulations numériques dont ont pu être extraites des valeurs d'énergie d'interaction. Ces dernières ont en outre pu être directement mesurées par microscopie à force atomique avec pour résultat supplémentaire que la viscosité du milieu peut influencer la mesure de manière significative. Enfin, l'origine physique de l'agrégation est discutée et confirmée par des mesures additionnelles. Ceci permet de concilier deux théories et permet d'expliquer la forme en cloche de l'énergie d'interaction en fonction de la concentration en macromolécules d'une nouvelle manière.

Kurzzusammenfassung

In dieser Arbeit werden fünf Aspekte der makromolekül-induzierten Aggregation roter Blutzellen untersucht. Ein rheologischer Ansatz unter Verwendung eines kommerziellen Rheometers beinhaltet die Viskositätsnormierung als Funktion der Adsorptionsraten von Makromolekülen. Hiervon abgeleitet werden die Fließspannung von Suspensionen aggregierter roter Blutzellen untersucht. Außerdem werden die Sedimentationsraten des verwendeten biologischen Systems analysiert. Mikroskopische Untersuchungen, einschließlich des mikroskopischen Aggregationsindex, führen zu dem Schluss, dass das C-reaktive Protein (ein Plasmaprotein) die Aggregationseigenschaften roter Blutzellen nicht beeinflusst. Detaillierte mikroskopische Studien der Morphologie von Interaktionszonen aggregierter roter Blutzellen zeigen eine starke Abhängigkeit von der molekularen Konzentration, was gut mit numerischen Simulationen, die eine Annäherung an die Interaktionsenergien zulassen, übereinstimmt. Letztere wurden direkt mit Einzelzellkraftmikroskopie unter Verwendung eines Atomkraftmikroskops gemessen, was zu dem Resultat führt, dass die Viskosität des umgebenden Mediums einen signifikanten Einfluss auf die Ergebnisse haben kann. Am Ende wird der physikalische Ursprung der Aggregation diskutiert und durch verschiedenen Messungen ergänzt. Dies erlaubt es, beide existierenden Theorien zu vereinen und die Glockenkurve der Interaktionsenergie als Funktion der Makromolekülkonzentration auf eine neue Weise zu erklären.

Nomenclature

AFM	atomic force microscope
BSA	bovine serum albumin
CCD	charge-coupled device
CMOS	Complementary Metal Oxide Semiconductor
CP	cone-plate
CR	controlled rate
CRP	C-reactive protein
CS	controlled stress
DC motor	drag-cup motor
Dex	dextran
DSLR	digital single lens reflex camera
EC motor	electronically commutated synchronous motor
EDTA	ethylenediaminetetraaceticacid
ESR	erythrocyte sedimentation rate
Fib	Fibrinogen
FITC	fluorescein isothiocyanate
HES	hydroxyethylated starch
HSA	human serum albumin
HyD	high-sensitive hybrid detector
IDT	interdigital transducer
IgG	immunoglobulin G

IgM	immunoglobulin M
kDa	kilo-Dalton
LSCM	line scanning confocal microscopy
MAI	microscopical aggregation index
MP	megapixel
NA	numerical aperature
PBS	phosphate buffered saline
PEG	poly(ethylene glycol)
PMT	photomultiplier tube
PSCM	point scanning confocal microscopy
RBC	red blood cells
SAW	surface acoustic waves
SCFS	single cell force spectroscopy
SD	standard deviation
SDCM	spinning disk confocal microscopy
SE	standard error
SMT	seperate motor transducer
TC	Taylor-Couette
TEM	transmission electron microscopy
UV/Vis	ultraviolet/visible
WBC	white blood cells

Contents

Nomenclature	V
1 Introduction	1
1.1 Introduction	1
1.2 Literature overview	8
2 Materials and methods	11
2.1 Blood, red blood cell aggregation introduction and theoretical back- round	12
2.1.1 Blood and red blood cells	12
2.1.2 Macromolecules	16
2.1.3 Bridging and Depletion	19
2.2 General techniques	30
2.2.1 Confocal microscopy	30
2.2.2 Rheology	36
2.2.3 AFM	44
2.2.4 UV/Vis Spectroscopy	49
2.2.5 Surface acoustic waves (SAW)	52
2.3 Measurement techniques and preparation protocols	55
2.3.1 Sedimentation measurements	55
2.3.2 Microscopical aggregation index	56
2.3.3 RBC preparation	57
2.3.4 Hematocrit concentration of the pellet	57
2.3.5 Osmolality	57
2.3.6 Filtering of fibrinogen and used macromolecular concentra- tions	58
2.3.7 Cell-Tak functionalization protocol	59
2.3.8 BSA coating protocol	59
2.3.9 CellMask protocol	60
2.3.10 Overview of main devices and consumables	60
3 Results	63
3.1 Rheology and sedimentation	63
3.1.1 Separation of the clustering induced viscosity from the sus- pending phase viscosity	64
3.1.2 The yield stress of aggregated red blood cells	73

3.1.3	The sedimentation of aggregated red blood cells	78
3.2	Microscopical aggregation index investigations	86
3.3	C-reactive protein influence on the RBC aggregation	91
3.4	Interaction zones of RBCs	96
3.4.1	Doublets	97
3.4.2	Clusters larger than six cells per aggregate	105
3.5	AFM	108
3.5.1	Elasticity	109
3.5.2	Cell-Cell adhesion	113
3.6	Depletion versus bridging discussion	133
3.6.1	Adsorption of macromolecules	133
3.6.2	Ghosts and macromolecules	141
3.6.3	Particle induced RBC aggregation	144
3.6.4	Single cell force spectroscopy induced cell deformation	146
3.6.5	Summary of the depletion/bridging discussion	146
4	Summary and conclusion	151
5	Appendices	157
5.1	Rheology	157
5.2	Concentration converting	164
5.3	MAI	165
5.4	Supplements	168
5.5	Tethers	170
6	Acknowledgments	173
7	Publications	175
	Bibliography	193

1 Introduction

1.1 Introduction

Introduction (english)

Already in the ancient time, the classic Greek philosopher Heraklit realized that $\pi\acute{\alpha}\nu\tau\alpha\ \rho\acute{\epsilon}\tilde{\iota}$ (panta rhei) “everything flows”. Here Heraklit means that the Sein is in movement due to “war as the father of all things”, whereby he means the conflict between polarities in life, such as life and death, good times and bad times etc., are essential for our “Sein”. Obviously “the Sein” is in focus in Shakespeare’s Hamlet “To be or not to be: That is the question!”. In the natural science, this could be connected to the rheological questions to “how does it flow; Newtonian or non-Newtonian?”, “aggregation or no aggregation?” and “depletion or no depletion?”. Since the answer to all these questions is part of our “Sein” and the explanation of “Sein” is consequently the key question of natural science.

Compared to what was the case in the ancient world, where a direct classification of the existing natural sciences, e.g. physics, biology, medicine etc., was not proposed, science is nowadays becoming again more interdisciplinary. The issues are rather complex and hence the explanations involve advanced numerical and experimental techniques and concepts from different branches of science [179].

One such complex interdisciplinary question requiring investigations by a multitude of approaches is the mechanism of blood coagulation. On the one hand, it is essential for wound healing and on the other hand, it can causes thrombi formations in pathological cases with fatal clinical repercussions. The process of coagulation involves many parameters and interactions. For example, a “red thrombus” consists of a huge amount of red blood cells (RBCs) and blood platelets that are entrapped by a fibrin network. Fibrin is a protein derived from fibrinogen via the coagulation cascade [17, 18]. Even if the platelets are very important for thrombi formation, the interaction between red blood cells cannot be neglected in the process. In addition, erythrocytes aggregate in normal blood flow induced by proteins and antibodies, e.g. fibrinogen and immunoglobulins. Due to their appearance similar to a stack of coins, they are commonly called rouleaux as depicted in fig. 1.1 (b). Artificially, they can be induced by the addition of macromolecular plasma expanders, e.g. dextran or hydroxyethyl starch (HES). Initially, the single red blood cells aggregate with increasing macromolecule concentration up to a maximum at the concentration c_1 as shown in fig. 1.1 (a) and (b). A further concentration increase leads to a

disaggregation and at c_2 no aggregation is observed as illustrated in fig. 1.1 (c). In the presented work this phenomenon is referred to as “bell-shape” for simplicity. In contrast, for human proteins that induce the clustering process, a linear increase of the RBC aggregation with increasing protein concentration is found.

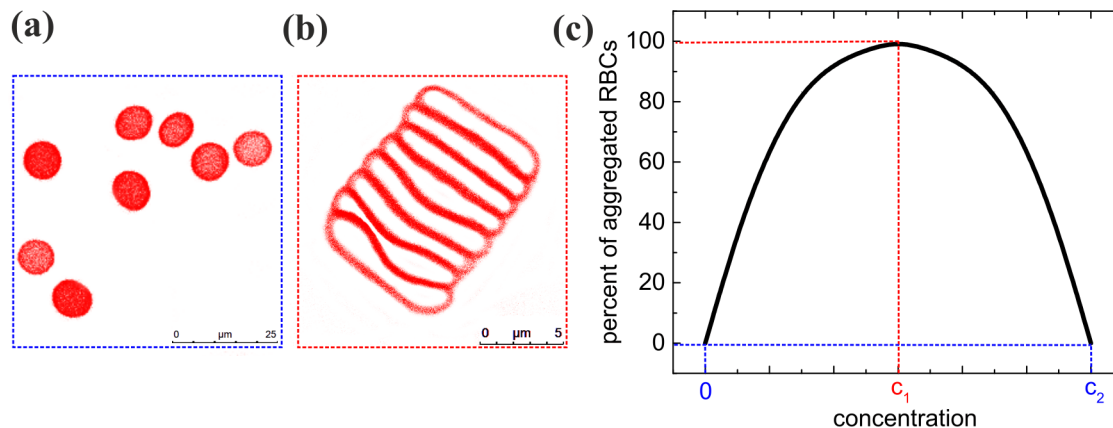


Figure 1.1: (a) Single red blood cells in buffer solution can (b) aggregate into rouleaux induced by proteins or other macromolecules (here, the example of 8 mg/ml fibrinogen). Images were taken with a confocal microscope and cell membranes are marked in red by the cell membrane dye CellMask. (c) For the case of fibrinogen a further concentration increase does not lead to a disaggregation, i.e. even at c_2 and at higher concentrations the percentage of aggregated cells is assumed (and observed) to remain at 100 %. In contrast, for polysaccharides like dextran or HES a further concentration increase can lead to a complete disaggregation. The concentration c_1 at which 100 % of the RBC are aggregated is marked in red, while the concentration c_2 where no RBCs are aggregated is marked in blue.

In vivo, such reversible aggregates or clusters are perpetually formed and break up due to shear stresses in veins and capillaries. At low shear rates more cells aggregate, which enhances blood viscosity, while the break-up of the rouleaux at high shear rates causes a decrease of blood viscosity (shear thinning). This effect is known since many decades and is further investigated in this work to reach a better understanding of the influence of aggregation on blood flows [56]. The results are published in [79].

Despite the fact that RBCs can sediment, the influence of sedimentation on the rheological investigations was analysed without finding a significant effect on the results by properly chosen geometries and experimental time scales.

In addition, clusters of RBCs do not just enhance the viscosity of blood but also lead to faster sedimentation of the cells. The erythrocyte sedimentation rate (ESR) is a common unspecific pathological test for inflammatory diseases in the human body

[17, 18]. Since the ESR tubes used in hematological tests are not standardized, the ESR was investigated as a function of tube diameter, which results in the finding that an increase of tube diameter leads to an increasing sedimentation velocity of the RBCs. In some clinical studies the ESR is directly correlated with the concentration of the C-reactive protein [1, 191]. It is shown with sedimentation and confocal microscopy that this correlation is an artifact most probably induced by a coincident elevated fibrinogen concentration. This result is published in [78].

A combination of sedimentation and confocal microscopy was as well used to analyse the interaction shapes of aggregated RBCs induced by dextran and fibrinogen. Flat intercal zones for low interaction energies and buckled ones for high interaction energies were found, which may have consequences on the stability and behavior of clusters in flow. This was related to a buckling process and published in [77]. A direct measurement of the interaction energy with atomic force microscopy leads to similar results as well as a discussion about the viscosity influence in such measurements.

The origin of RBC aggregation is still unclear. There are two coexisting models that can explain it. On the one hand, there is the depletion theory that refers to a colloidal osmotic pressure of the macromolecules as the main reason for rouleaux formation [143]. On the other hand, the bridging theory assumes the adsorption of macromolecules onto the RBC membranes and hence a potential adhesion between two cells as the origin of rouleau formations [133]. These models are confronted with experiments and are discussed by giving the approach for a new combined theory derived from colloidal physics [70].

After the introduction of the used biological materials, theoretical models and the experimental setups, the experimental part of this manuscript is structured from large to small scales of investigation: Starting with macroscopical investigations with rheology and sedimentation via microscopical investigations to interaction energies of RBC and ending with approaching studies regarding the depletion and bridging theories.

Introduction (français)

Déjà à l'Antiquité, le philosophe grec classique Héraclite a observé que $\pi\acute{\alpha}\nu\tau\alpha \rho\epsilon\tilde{\iota}$ (panta rhei), « tout coule » ou « tout passe ». Par cela Héraclite veut dire l'Être est en mouvement par « la guerre, père de toute chose », c'est-à-dire que le conflit entre les choses extrêmes de la vie, tels que la vie contre la mort, les bons moments contre les mauvais etc. est essentiel pour notre « Être ». Bien sûr, ce même « être » est central dans Hamlet des Shakespeare « Être ou ne pas être : telle est la question ! ». Dans les sciences naturelles cela peut être mis en relation avec les questions en rhéologie « quel type d'écoulement : newtonien ou non-newtonien ? », « agrégation ou non ? » ou « déplétion ou non ? ». La réponse à toutes ces questions est inscrite au cœur de notre « Être » et de fait, la description de notre « Être » est le défi majeur des sciences naturelles.

Par rapport à l'Antiquité, où une classification directe des sciences naturelles existantes comme la physique, la biologie ou la médecine par exemple n'était pas proposée, la science moderne est multidisciplinaire. Les questions sont plus complexes et de fait leurs réponses nécessitent à la fois des techniques expérimentales et numériques et font appel à des concepts de différents domaines scientifiques [179].

Une de ces questions complexes interdisciplinaires, nécessitant de nombreuses études abordées de différentes manières est le mécanisme de la coagulation du sang. Alors qu'elle est essentielle pour la cicatrisation, elle peut à l'opposé provoquer des thromboses pouvant avoir des conséquences cliniques fatales. Ce mécanisme de coagulation implique beaucoup de paramètres et d'interactions. Par exemple, un « thrombus rouge » est formé par un grand nombre de globules rouges (en anglais, Red Blood Cells, ou RBCs) et de plaquettes sanguines qui sont emmêlés dans un réseau de fibrine. La fibrine est une protéine issue du fibrinogène lors de la coagulation [17, 18]. Bien que les plaquettes soient un élément important dans la formation des thrombus, l'interaction entre globules rouges ne peut être négligée dans ce phénomène. De surcroît, les érythrocytes s'agrègent dans le sang circulant sous l'effet de protéines ou anticorps comme le fibrinogène ou les immunoglobulines. Du fait leur ressemblance à un empilement de pièces de monnaie, ces agrégats sont communément appelés rouleaux comme on le voit sur la figure 1.1 (b). De manière artificielle, ils se forment par l'ajout de succédané du plasma comme le Dextran ou l'hydroxyéthylamydon (HEA ou HES en anglais). Initialement, la proportion de globules rouges agrégés augmente avec la concentration en macromolécules jusqu'à ce que cette dernière atteigne un maximum c_1 (figure 1.1 (a) et (b)). Une augmentation supplémentaire de la concentration entraîne alors une désagrégation et à la concentration c_2 il n'y a alors plus d'agrégats observables, comme illustré par la figure 1.1 (c). Dans ce travail, il sera fait référence à ce phénomène par le terme « courbe en cloche (ou Bell-shape en anglais). A l'inverse, pour les protéines humaines responsables de ce phénomène d'agrégation, une réponse linéaire entre l'agrégation des RBCs et la concentration a été trouvée.

In vivo, de tels agrégats réversibles sont continuellement formés et détruits à cause du cisaillement exercé dans les vaisseaux ou capillaires sanguins. A faible taux de cisaillement, plus de cellules sont agrégées, ce qui augmente la viscosité du sang alors que la destruction des rouleaux à fort taux de cisaillement entraîne une diminution de la viscosité sanguine (rhéo-fluidification). Ce phénomène, connu depuis des décennies, est l'objet de ce travail de thèse, ceci afin d'améliorer notre compréhension de l'influence de l'agrégation dans les écoulements sanguins [56]. Les résultats ont fait l'objet d'une publication [79].

Malgré le fait que les RBCs puissent sédimenter, l'analyse de la contribution de la sédimentation aux mesures de rhéologie n'a pas montré d'effet significatif sur les résultats, lorsque les mesures sont réalisées dans des géométries et sur des échelles de temps adéquats.

De plus, les groupes des RBCs en solution ne se contentent pas d'améliorer la flu-

idité du sang mais peuvent aussi accélérer la sédimentation des cellules. Le taux de sédimentation des érythrocytes (en anglais ESR pour erythrocyte sedimentation rate) est un test pathologique non spécifique fréquent dans le cadre des maladies inflammatoires du corps humain [17, 18]. Puisque les tubes de tests hématologiques ESR ne sont pas standardisés, l'ESR a été étudié en fonction du diamètre du tube. Cela a mené à trouver qu'une augmentation de ce diamètre entraîne une augmentation de la vitesse de sédimentation des RBCs. Dans certaines études cliniques, l'ESR est directement corrélé avec la concentration de protéine C réactive [1, 191]. Ce travail montre, par les mesures de sédimentation et la microscopie confocale, que cette corrélation est un artéfact, très certainement induit par une concentration élevée de fibrinogène. Ces résultats sont publiés dans la référence [78].

Cette double caractérisation par sédimentation et microscopie confocale a aussi été utilisée pour analyser les géométries des zones d'interaction des RBCs agrégés par l'ajout de Dextran ou de fibrinogène. Des zones de contact plates à faible énergie d'interaction et des interfaces courbes à forte énergie ont ainsi pu être révélées. Ce résultat pourrait avoir des conséquences sur la stabilité et le comportement des groupes de cellules en écoulement. Cet effet a été comparé à un processus de flambage, publié dans la référence [77]. Les mesures directes des énergies d'interaction par microscopie à force atomique ont mené à des résultats similaires ainsi qu'à une discussion sur l'influence de la viscosité sur ce type de mesures.

L'origine de l'agrégation des globules rouges reste incertaine. Il existe deux modèles permettant de l'expliquer. D'une part, il y a la théorie de la déplétion qui implique une pression osmotique colloïdale engendrée par les macromolécules, générant les structures en rouleaux [143]. D'un autre côté, la théorie de pontage prévoit l'adsorption des macromolécules à la paroi cellulaire et ainsi une possible adhésion entre cellule comme origine de la formation des rouleaux [133]. Ces deux modèles sont confrontés aux résultats expérimentaux de ce travail et sont discutés en donnant une approche nouvelle, combinant ces deux modèles, dans une nouvelle théorie combinée, issue de la physique des colloïdes [70].

Après une introduction des outils biologiques utilisés, des modèles théoriques et des dispositifs expérimentaux, les résultats expérimentaux de ce travail seront présentés selon une échelle décroissante des mesures : dans un premier temps les mesures macroscopiques, avec les études rhéologiques et de sédimentation, puis les mesures microscopiques comprenant l'évaluation des énergies d'interaction et enfin une discussion des modèles de déplétion et de pontage.

Einführung (deutsch)

Bereits in der Antike hatte der griechische Philosoph Heraklit erkannt, dass $\pi\acute{\alpha}\nu\tau\alpha \rho\acute{\epsilon}\tilde{\iota}$ (panta rhei) "alles fließt". Hier bezieht sich Heraklit auf das Sein, was bezogen auf "Der Krieg ist der Vater aller Dinge", einer Veränderung unterliegt, wobei er meint, dass der Konflikt zwischen den Extremen des Lebens, wie z.B. Tod und Leben, gute

Zeiten und schlechte Zeiten usw., wesentlich für unser Sein sind. Offensichtlich ist das Sein auch der Fokus in Shakespeare's Hamlet "Sein oder nicht Sein: Das ist die Frage!". In der Naturwissenschaft kann dies auf rheologischen Fragen übertragen werden, wie z.B. "Wie fließt eine Flüssigkeit; Newtonsch oder nicht-Newtonsch?", "Aggregation oder keine Aggregation?" und "Depletion oder Bridging?". Da die Antwort darauf einen Teil unseres Seins betrifft, ist die Erklärung des Seins folglich eine Schlüsselfrage der Naturwissenschaft.

Verglichen mit der Antike, in der eine Klassifizierung der Naturwissenschaften nicht direkt erörtert wurde, d.h. Physik, Biologie, Medizin etc., wird die Wissenschaft heutzutage mehr und mehr interdisziplinär. Die Fragestellungen sind relativ komplex und daher erfordern die Erklärungen fortgeschrittene sowohl numerische und experimentelle Methoden als auch Konzepte aus verschiedenen Wissenschaftsbereichen [179].

Eine solch komplexe Frage, welche der Untersuchung durch Vielzahl von Wissenschaften bedarf, ist der Mechanismus der Blutkoagulation. Auf der einen Seite ist diese notwendig für die Wundheilung und auf der anderen Seite kann sie in pathologischen Fällen Thrombosen mit weitreichenden medizinischen Folgen verursachen. Der Prozess der Koagulation hängt von vielen Parametern und Interaktionen ab. Beispielsweise besteht ein "roter Thrombus" aus einer großen Menge roter Blutzellen und Blutplättchen, die in einem Fibrinnetzwerk eingeschlossen sind. Fibrin ist ein Protein, dass über die Koagulationskaskade aus Fibrinogen gebildet wird. Obwohl die Blutplättchen für die Bildung von Thromben wichtig sind, kann die Interaktion roter Blutzellen nicht vernachlässigt werden. Hinzu kommt, dass rote Blutzellen im normalen Blutfluss aufgrund von Proteinen und Antikörpern, z.B. Fibrinogen und Immunglobuline, aggregieren. In diesem Fall ähnelt ihr Gesamtaussehen einer Geldrolle, weshalb diese auch Rouleaux genannt werden, wie in Abb. 1.1 (b) dargestellt ist. Künstlich können sie durch die Zugabe von makromolekularen Plasmaexpandern, z.B. Dextran oder Hydroxyethylstärke (HES) erzeugt werden. Anfänglich aggregieren einzelne rote Blutzellen mit erhöhter Makromolekülkonzentration bis sie ein Maximum bei der Konzentration c_1 erreichen, wie in Abb.1.1 (a) und (b) zu sehen ist. Eine weitere Erhöhung der Konzentration führt zur Disaggregation und bei c_2 sind keine Aggregate mehr beobachtbar. Zur Vereinfachung wird dieses Phänomen in dieser Arbeit als "bell-shape" bezeichnet. Im Gegensatz hierzu zeigen menschliche Proteine eine lineare Aggregation roter Blutzellen bei ansteigender Proteinkonzentration.

Solche reversiblen Aggregate oder Gruppierungen werden in vivo fortlaufend geformt und zerbrechen aufgrund von Scherspannungen in Venen und Kapillaren. Bei geringen Scherraten aggregieren mehr Zellen, was die Blutviskosität erhöht, während das Auseinanderbrechen der Rouleaux bei hohen Scherraten eine verringerte Blutviskosität zu Folge hat (Scherverdünnung). Dieser Effekt ist seit mehreren Jahrzehnten bekannt und wurde in dieser Arbeit weiter untersucht, um ein besseres Verständnis für den Einfluss der Aggregation roter Blutzellen auf den Blutfluss zu erhalten [56]. Diese Resultate wurden in [79] publiziert.

Darüber hinaus führt die Aggregation roter Blutzellen nicht nur zu einem Anstieg der Viskosität, sondern auch zu einer gesteigerten Sedimentationsrate der Zellen. Die Blutsenkung (ESR) ist ein klassischer unspezifischer Test für entzündliche Erkrankungen im menschlichen Körper [17, 18]. Da die Blutsenkungsröhrchen pathologischer Untersuchungen nicht standardisiert sind, wurde die ESR in Abhängigkeit des Röhrchendurchmessers untersucht, was zu dem Ergebnis führte, dass ein vergrößerter Röhrchendurchmesser zu einer höheren Sedimentationsgeschwindigkeit führt. Einigen medizinische Studien korrelieren die ESR direkt mit dem C-reaktiven Protein [1, 191]. Mit Sedimentation und Konfokalmikroskopie wurde gezeigt, dass dies ein Artefakt ist, welches wahrscheinlich durch eine erhöhte Fibrinogenkonzentration hervorgerufen wird. Dieses Ergebnis wurde in [78] publiziert.

Eine Kombination aus Sedimentation und Konfokalmikroskopie wurde genutzt, um Interaktionszonen aggregierter roter Blutzellen, die durch Dextran und Fibrinogen hervorgerufen wurden, zu untersuchen. Flache Interaktionszonen wurden für geringe Interaktionsenergien, während deformierte Interaktionszonen für große Interaktionsenergien gefunden wurden, was eventuell eine Konsequenz für das Verhalten von Aggregaten roter Blutzellen im Fluss haben könnte. Diese Verhalten wurde in Zusammenhang mit einem “buckling”-Prozess gebracht und publiziert [77]. Eine direkte Messung der Interaktionsenergien mit Atomkraftmikroskopie führte zu einem ähnlichen Ergebnis und einer Diskussion über den Einfluss der Viskosität auf solche Messungen.

Der Ursprung der Aggregation roter Blutzellen ist nach wie vor unklar. Es gibt zwei Theorien, die koexistieren. Einerseits besteht die Depletion-Theorie, die den kolloidosmotischen Druck der Makromoleküle als den wesentlichen Grund für die Aggregation ansieht [143]. Andererseits postuliert die Bridging-Theorie, dass eine Adsorption der Makromoleküle an den Membranen der roten Blutzellen und daher eine mögliche Adhäsion zwischen den Zellen der wesentliche Grund für die Aggregation der Blutzellen ist [133]. Diese Modelle wurden mit Experimenten verglichen und ein neuer Ansatz für eine kombinierte Theorie, abgeleitet von der Kolloidphysik, wird dargestellt [70].

Nach der Einführung der verwendeten biologischen Materialien, theoretischen Modelle und des experimentellen Aufbaus ist diese Arbeit von makroskopischen zu mikroskopischen Untersuchungen strukturiert: Beginnend mit Rheologie und Sedimentation über mikroskopische Untersuchungen der Interaktionsenergie zweier roter Blutzellen werden am Ende Experimente vorgestellt, die sich auf die Frage “Depletion oder Bridging?” beziehen.

1.2 Literature overview

The phase separation of red blood cells (RBCs) was already noticed by the ancient Greek [68] and the connected problem of the sedimentation rate of blood was first described by Biernacki over one century ago [30]. Nowadays, it is still used by clinical research and diagnosis as an unspecific marker for inflammatory diseases in the human body [1, 17, 18, 76, 101, 157, 163]. This sedimentation rate is often directly correlated with the concentration of the C-reactive protein (CRP) [1, 6, 35, 45, 62, 75, 101, 157, 185, 190, 191, 197]. It was found that the CRP is not the origin of the increase in sedimentation rate [78], but, that it was most probably connected to the elevated fibrinogen concentrations [4, 45, 124, 125, 128]. Fibrinogen was identified in 1960's as a cause of the red blood cell aggregation [133, 132] and therefore an increasing fibrinogen concentration leads to an increase in sedimentation rate [54]. Nowadays, it is known that elevated fibrinogen concentrations as well as the clustering of red blood cells can cause thrombosis and similar agglomerates [11, 109, 144, 145]. After noticing that polysaccharides such as dextran provoke the clustering process as well, these effects were extensively investigated by several authors over three decades [47, 51, 55, 57, 60, 111, 124, 159, 179]. Dextran was for a long time used as a plasma expander for humans after the loss of large amounts of blood, it is still used in veterinary medicine [41] and there is no prohibition to use it in human medicine. A similar molecule that is widely used as a plasma expander in human medicine is hydroxyethyl starch (HES) [121, 131], which is seen critical since 2013 for both human and veterinary medicine [2, 71, 195, 158]. The significant difference with fibrinogen is that dextran and HES cause the red blood cells to aggregate until reaching a critical macromolecule concentration beyond which the RBCs start to disaggregate back to single cells for high polysaccharide concentrations. This phenomenon is known since the 1970's and in this work called bell-shape behavior [26, 47, 53, 52, 79]. One determining factor in macromolecules induced clustering processes seems to be the hydrodynamic radius that is inhibiting the aggregation below ca. 4 nm, while the above ca. 4 nm the RBC aggregation is induced [13, 63].

The origin of the rouleaux formation is still unclear. Two models coexist: The depletion theory introduced in 1958 [14] identifies the osmotic pressure of small colloids in the surrounding solution as the main reason for the attractive forces between larger particles. In the case of RBCs the small colloids correspond to macromolecules and the larger colloids correspond to the cells [26, 143]. On the other hand, the bridging theory was introduced in 1966 [133]. In this process a physisorption of macromolecules onto the cell membranes can connect two cells. The adhesion of both fibrinogen [48] and dextran [55, 52, 60] was demonstrated experimentally, identifying bridging as the reason for RBC aggregation. Nevertheless, both explanations were not aware of the fact that the overlap concentration of e.g. dextran [104, 116] could play a role in such systems [5, 50, 81, 167] and that a temperature increase could cause the system to switch from depletion to bridging [74]. In addition, it was shown theoretically that both phenomena can coexist in the same system at

the same temperature [70]. Consequently, they are not excluding each other. The bell-shape can be explained with all models, whereby none of them describes the fact that a changing shape of RBCs to e.g. stomatocytes leads to less aggregation affinity [161, 163]. Not only the change in shape could influence the interactions between RBCs. The interactions can influence the shape as well.

Changes of isolated membrane shape induced by artificial surfaces in contact with cells were characterized [172]. For freestanding capsules a similar change in shape was attributed to buckling instabilities [61, 114]. Theoretical [182, 200] and experimental [187] investigations showed a significant dependency of the interfacial membranes on the interaction energy or the kind of macromolecules. Nowadays, more advanced techniques allow the analysis of such systems with confocal microscopy [135, 136, 137, 146, 148, 154, 160, 194]. This leads to the possibility of quantifying such shape changes without parasitical contacts with substrates and compare it to numerical simulations [77].

Another technical development, the atomic force microscopy [46, 80, 134], uses the contact deformation of cantilevers to investigate very small forces down to 10^{-18} N [31, 102, 103, 122, 177]. It allows e.g. to measure the deformation of single dextran molecules induced by stretching [164] and the adherence force of fibrinogen onto RBCs [48]. Furthermore, the interaction energy between two RBCs [180, 179] can be investigated using single cell force spectroscopy [92] as well as the local mechanical properties of cells like cancer cells or RBCs [58, 134]. Due to the fact that the elasticity is measured locally by an AFM the results can be quite disposed from each other and differ from other techniques like optical stretchers or micropipetts that are measuring a global elasticity [21, 67]. Using the latter technique, it was already shown that RBC can produce long tethers [28, 96, 97, 98, 99] which could influence the aggregation behavior of the cells as well [119]. These clustering processes and the RBCs themselves are the main factors influencing blood viscosity.

Rheological investigations over the last half century describe the complex flow behavior of red blood cells [10, 12, 44, 57, 127, 132]. For instance, it is known that the shear-thinning of blood and suspensions containing RBC aggregates are mainly induced by a break-up of rouleaux [7, 72, 83, 170] and the elastic deformation of the cells [56]. Despite these intensive investigations there are still many open questions regarding e.g. the normalization of rheological data in order to divide RBC induced and suspending phase induced viscosities [79] as well as the yield stress of blood and red blood cell suspensions [155]. The yield stress itself is controversially discussed anyhow [22, 23, 39, 69], since it appears difficult to measure it directly. Therefore, many methods were proposed over the years to approximate it [32, 49, 93, 123]. In particular, regarding such rheological questions the sedimentation of suspended particles can influence the results significantly [69]. Even if the effect is well known since ancient times as mentioned above the origin of the differences in sedimentation velocity of RBCs are still not well understood.

Some investigations show disagreements with others, quantitative analyses of the

shape of contact zones and the buckling phenomenon they involve were still missing and there is still the open question of the origin of aggregation is depletion or bridging. In this contact, this work clarifies the correlation between CRP and ESR, and investigates the dependency of the interaction energy between two RBCs from the surrounding viscosity using an AFM. The quantitative consequences of the bell-shape behavior of aggregation versus macromolecular concentrations are studied in different situations and with different methods. Finally, the normalization of rheological data and the yield stress is discussed. Moreover, hints and new ideas are given to explain the origin of RBC aggregation.

2 Materials and methods

Abstract

In this chapter, the composition of blood is explained by focusing on red blood cells (RBCs) and their membrane. The two classic models for the aggregation of RBCs are summarized, which is followed by an approach of a combined model. The utilized experimental devices are explained, i.e. confocal microscopy, rheology and atomic force microscopy as the main used setups. UV/Vis spectroscopy and surface acoustic waves are briefly discussed. In the end, specific (preparation) techniques and protocols are depicted.

Résumé

Dans ce chapitre, la composition du sang est décrite avec une attention particulière pour les globules rouges (RBCs) et leur membrane. Les deux modèles classiques de l'agrégation des RBCs sont résumés suivis par la description d'un modèle les couplant. Les principales techniques expérimentales, i.e. la microscopie confocale, la rhéologie et la microscopie à force atomique, sont décrites. La spectroscopie UV-Visible et les ondes acoustiques de surface sont ensuite brièvement abordées. Ce chapitre se finit par une description des techniques spécifiques et des protocoles de préparation d'échantillons.

Kurzzusammenfassung

In diesem Kapitel werden die Bestandteile des Blutes bezogen auf rote Blutzellen (RBCs) und deren Membranen erklärt. Die beiden klassischen Modelle für die Aggregation roter Blutzellen werden erläutert, was durch einem Denkansatz für ein kombiniertes Modell ergänzt wird. Die verwendeten experimentellen Geräte werden erklärt, d.h. Konfokalmikroskopie, Rheologie und Atomkraftmikroskopie als die primär verwendeten Messinstrumente. UV/Vis Spektroskopie und akustische Oberflächenwellen werden kurz diskutiert. Zuletzt werden spezifische Präparationstechniken und Protokolle eingeführt.

2.1 Blood, red blood cell aggregation introduction and theoretical background

2.1.1 Blood and red blood cells

Blood carries oxygen and nutrients to the tissues as well as waste products to the organs, which are removing them from the body. Blood consists of red blood cells (RBCs, erythrocytes), white blood cells (WBCs, leukocytes), platelets (thrombocytes) and plasma as illustrated in fig. 2.1. By volume 40-50% of human blood is constituted of RBCs, while just 0.5 % are WBCs and platelets. The cellular part of the blood is called hematocrit. The remaining plasma is composed of 93% water that carries ions as well as nutrients and 7% proteins [17].

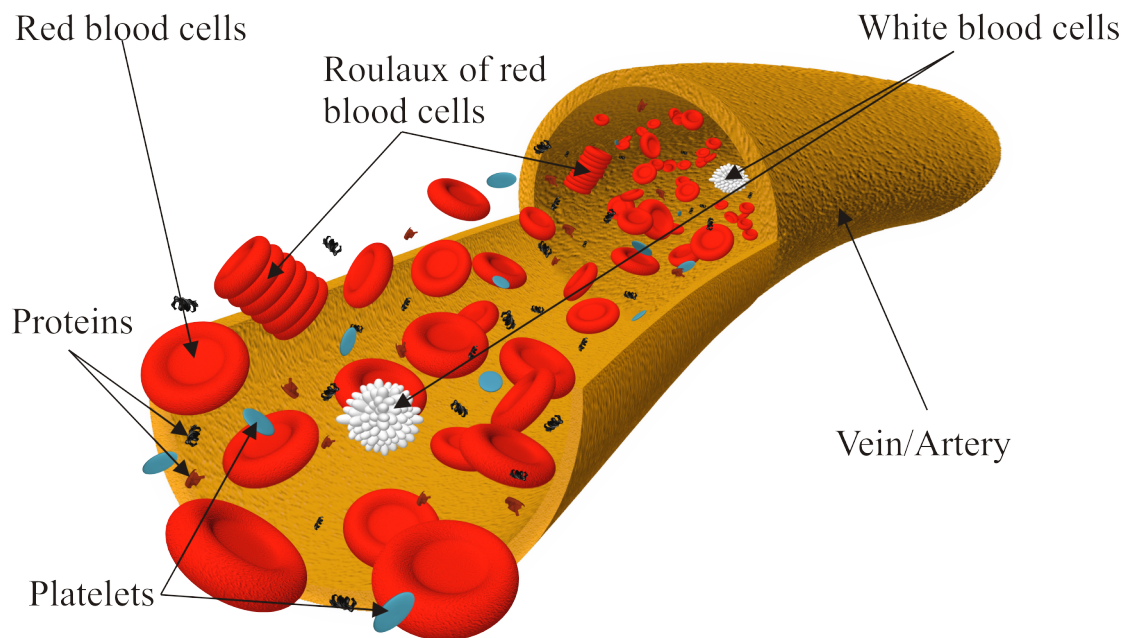


Figure 2.1: Blood consists beside (aggregated) RBCs of the plasma (several proteins etc.) and the buffy coat (mainly white blood cells and platelets). The single components are just an illustration and the concentrations differ from the reality.

In vitro blood separates after sedimentation due to density differences into three parts: plasma, buffy coat (contains platelets and WBCs) and RBCs as shown in fig. 2.2. This method is widely used to separate RBCs from the other blood components by centrifugation.

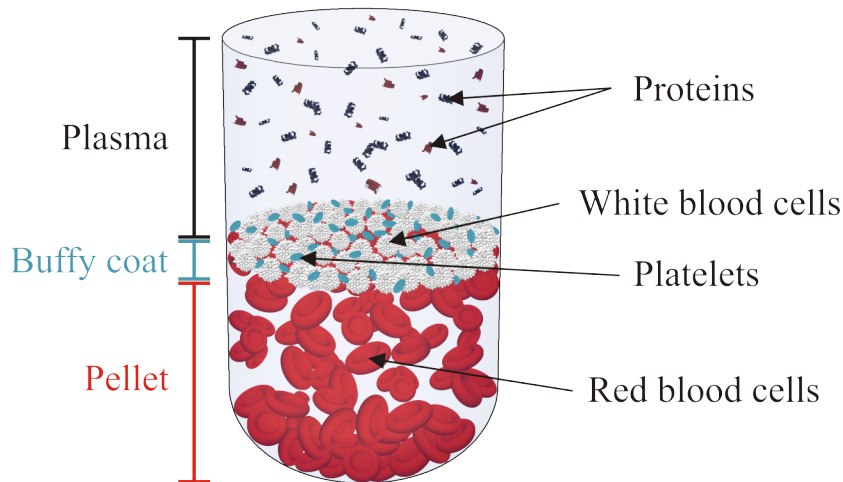


Figure 2.2: Sedimentation of blood in vitro leads to a separation between plasma, buffy coat and red blood cells. The single components are just an illustration and the concentrations differ from the reality.

The RBCs carry hemoglobin that is able to bind oxygen in the respiratory organs and release it to the tissues. In comparison to many other cells, human RBCs are relatively simply designed because of the absence of many cell organelles such as nuclei, endoplasmic reticula and golgi apparatus. Therefore, they are often used as model system in order to answer several questions regarding plasma membrane permeabilities and rather biophysical questions [188, 173, 198].

Normal mature red blood cells show a biconcave disc-like shape (so called discocyte) with a mean diameter of 7.5-8 μm and a height between 1.5 μm (in the middle) and 2-2.5 μm (close to the edges) as illustrated in fig. 2.3 (a). The surface area is assumed to be 140 μm^2 for a volume of 90 fl [8, 198]. Depending on tonicity, pH or cationic lipid-soluble drugs discocytes can change in vitro their shape to a cup-like RBC, so called stomatocytes as depicted in fig. 2.3 (b). It is assumed that this results from volume increase induced by hyponic environments and an extension of the inner leaflet of the membrane. In vivo stomatocytes have been reported as a result of liver diseases with a significant relation to alcohol excesses. If the surrounding solution of the RBC is hypertonic in comparison to normal blood plasma a discocyte can change to an echinocyte shape, which has 10-30 short blunt spicules (see 2.3 (c)). In vivo such a change can have several reasons as cardiopulmonary bypasses or decompression phase after diving. In vitro such a change is often related to fatty acids, incubation, drugs and many more [18]. One very important reason for the discocyte-echinocyte change in vitro is the so called glass effect: If RBC are in contact with an artificial surface such as glass or plastic materials they can change their shape to an echinocyte. The reason for this effect is still not understood, but one argumentation correlates it with static electricity [66]. In contrast, if the surrounding solution is hypotonic in comparison to normal blood plasma, the discocyte can

change via a stomatocyte into a spherocyte shape, which is comparable to a sphere and shown in fig. 2.3 (d). Beside the hypotonic environment this shape is most probably due to an abnormality of the cytoskeleton with a destabilization and loss of membrane parts [17]. It was reported as a direct result from cell damages (e.g. by heating the RBCs) or snake venom [18]. Both echinocytes and stomatocytes can lead to a spherocyte shape in hypotonic environments [198] and are known not to stack well into rouleaux [161, 163]. All explanations of rouleaux formation support this hypothesis (see 2.1.3).

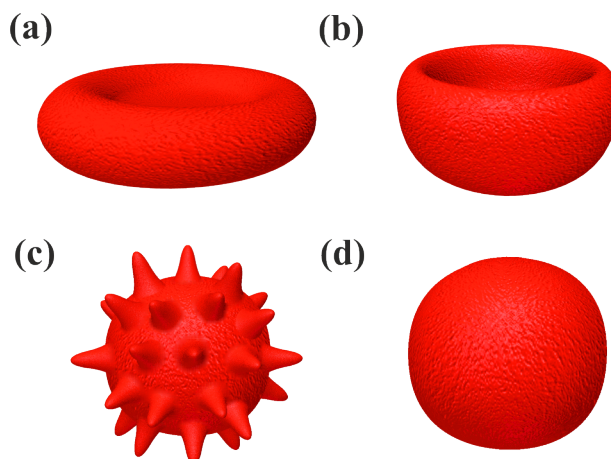


Figure 2.3: A discocyte (a) can change its shape to a stomatocyte in a slight hypotonic environment (b) or to an echinocyte shape in an hypertonic environment in contact with glass or similar (c) or to a spherocyte shape in e.g. an hypotonic environment (d).

The red blood cell membrane consists of 19.5% water (w/w), 39.6% proteins, 35.1% lipids and 5.8% carbohydrates, which is believed to be similar in most animal RBCs [152, 198]. The glycocalyx (an outer covering of the cell membrane) of an RBCs is mainly built of carbohydrates and glycolipids with an height of ca. 5-10 nm [129]. The carbohydrates contain a large amount of sialic acid that is a negatively charged sugar, which is most probably the main reason for the net negative charge of RBCs under physiological conditions. Thanks to this net negative charge the cells are prevented from aggregating if no other aggregating factor, such as proteins, is present. The widely accepted Fluid-Mosaik model describes the membrane as a double lipid-layer with attached and embedded proteins [174]. Taken this lipid bilayer and the underlying spectrin network into account the cell membrane has a thickness of 40-50 nm and exhibits a resistance to compression at around 20-25 nm [91, 65] as illustrated in 2.4. The spectrin network is a cytoskeleton which is responsible for the elastic properties. Beside the double-lipid layer itself these properties are necessary for passing capillaries which are smaller than the RBC diameter [3].

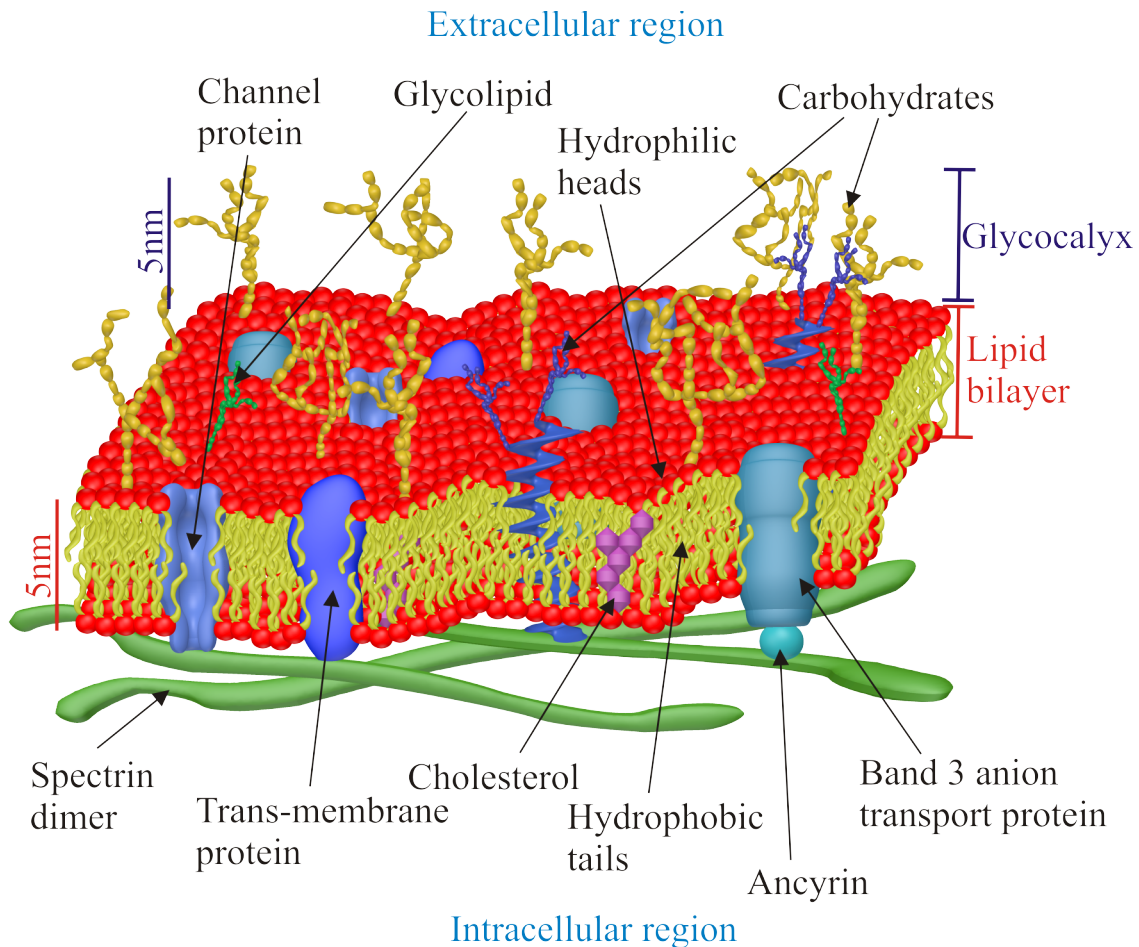


Figure 2.4: The red blood cell membrane formed out of a double lipid layer, several proteins, the glycocalyx and an underlying spectrin network.

Two types of RBC proteins are known: Membrane proteins are (non-)covalently bound to the proteins connected to the spectrin network. Integral or transmembrane proteins are embedded into the membrane due to their hydrophobic tails and consequently they can take on transport and receptor functions. RBCs involve more than 300 proteins including 105 integral membrane or transmembrane proteins. Of the latter ca. 25% are assumed to specify the blood group antigens [151, 140, 65].

Aggregation and coagulation of red blood cells

Macroscopically, there are two processes which should be separated from each other: Blood coagulation and red blood cell aggregation.

Blood coagulation (also known as blood clotting) is a complex process involving many reactions and many participating players. In general, every human has already observed it when e.g. cutting a finger. At the wound, blood starts to clot

and form a film which is closing the wound. This film is called coagulum in the extravascular system, while in the intravascular system it is called thrombus. Both involve RBCs, WBCs and platelets which are stabilized by a network of fibrin (a protein built from fibrinogen via the coagulation cascade). In brief, the coagulation is induced e.g. by a damage of the vessel wall, which leads to an activation of the thrombocytes. This means that coagulation factors (enzymes etc.) are involving the cellular fractions of blood and lead finally to a coagulum or thrombus (this process is called coagulation cascade) [179, 126]. Platelets play the most important role in such a process, but RBCs are embedded in thrombi formations (e.g. red thrombi). As shown by Kaestner and co-worker [109] the signaling cascade can involve an active participation of RBCs. Moreover, several publications showed that extracellular calcium can enter the RBCs after the activation process of the platelets, which shows in the end that the red blood cell adhesion could take part in the coagulation process as well [178, 144, 145, 107]. Therefore, understanding red blood cell aggregation without any activation could be an important factor for blood coagulation as well.

The clustering or aggregation process of RBCs is the main topic of this thesis. Red blood cell aggregation is a process in which the cells stay in their normal shape under physiological conditions. Aggregation means that the RBCs form a so-called rouleau which appears similar to a stack of coins due to adhesion forces between the cells, as shown e.g. in fig. 1.1. In vivo it is induced by proteins or antibodies such as fibrinogen, immunoglobulin G, immunoglobulin M etc., all of which having a hydrodynamic radius larger than 4nm. Macromolecules smaller than 4 nm have been shown to inhibit RBC aggregation [13]. Moreover, it can be induced by polysaccharides like dextran or HES on which the next chapter will focus [26].

2.1.2 Macromolecules

In this chapter the main macromolecules used in the presented work are discussed. Starting with the two plasma expanders dextran and hydroxyethylated starch (HES) the two proteins fibrinogen and C-reactive protein will be briefly discussed. All of these macromolecules (except CRP, see 3.3 and [78]) are known to be actively involved in the aggregation and sedimentation processes of RBCs (see chapter 3.2 and [45]).

In medicine, hypovolaemic patients (the decrease of blood volume, e.g. caused by an accident with the loss of blood) are given colloidal suspensions to expand the plasma volume. Typically, they can be administered from 15% of total blood volume loss. Some of them have a hyperoncotic effect which means that water diffuses from the extracellular regions to the “colloids”, which enhances the total blood volume even more (such as dextran 40 kDa [131]). All plasma expanders have a colloidal osmotic pressure similar to that of blood plasma [37]. A vast enzymatic degradation (typically within hours) eliminates them from the body via the kidneys. Albumin, gelatin, HES and dextrans are commonly used to expand blood plasma.

Dextran is a polysaccharide elaborated enzymatically by bacteria of the genus *Leuconostoc mesenteroides* and is available in molecular masses from 10 to 50,000 kDa. At a physiological pH of 7.4 it is neutrally charged and e.g. dextran 70 kDa has an hydrodynamic radius of 5.8 nm [86]. Since 1947, a 6% solution (or 60 mg/ml) of dextran 70 kDa was worldwide used as a plasma expander. The effect on blood volume stays for around five hours. After the introduction of dextran 40 kDa in 1961 10% solutions were used as a plasma expander and for their inhibition of RBC aggregation [63]. The effect on blood volume stays for one to three hours. In one out of 4500 patients both dextran 70 kDa and dextran 40 kDa are known to create severe anaphylactoid reactions, which can lead to death [131]. Therefore, dextran is not commonly used anymore as a plasma expander in human medicine, but they are still widely used in veterinary medicine due to low cost [41]. Interestingly, both were for a long time used to reduce the risk of thrombosis, thanks to the fact that the total plasma volume is enhanced [156]. In contrast, their impact on blood coagulation is well known, why the use should be limited [131]. The same argument is valid for HES.

HES is a branched natural polymer of amylopectin (typically build of 70-80% starch and 20-30% polysaccharides) and it is available from 70 kDa to over 450 kDa. Its hydrodynamic radius is about 6 nm at a molecular mass of 130 kDa and a negative surface net charge [71]. It is commonly used at 130 kDa as a plasma expander [121] and provided e.g. by the company Fresenius SE & Co. KGaA [108]. For this purpose 6% is the most common concentration, while it is also available in 3 and 10%. The effect on the blood volume stays for around one hour. It is limited to 1.5-2.5 liters per day due to renal tubular blockage induced by a drastic viscosity increase of the urine. Anaphylactoid reactions are observed in less than one of 16000 patients [131]. Hence, in the clinical use it is favorable to dextrans, even if the PRAC (Pharmacovigilance Risk Assessment Committee) of the European Medicines Agency recommended to deprive the marketing authorization for products including HES in 2013 [158].

Fibrinogen is a plasma protein with a molecular mass of 340 kDa and an hydrodynamic radius of 10.95 nm [13]. The dried molecule has a rod-like shape with a total length of ca. 47.5 nm and ca. 0.8-1.5 nm in diameter. At both ends fibrinogen has nodules of ca. 5-6.5 nm in diameter, while one is larger than the other [90]. For healthy humans the fibrinogen concentration is between 1.5 and 3 mg/ml, while it can increase up to 7 mg/ml for pregnant women [4] and even more for inflammatory diseases. Such elevated fibrinogen concentrations can cause thrombosis [11]. In physiological conditions it has a net negative charge [130], which is distributed heterogeneously with mainly negative charges at the ends and positive charges in the coiled-coil regions (the middle part) as depicted in fig. 2.5 (a) from [149].

CRP is an acute-phase protein and can be imagined as a ring of five subunits and has an hydrodynamic radius of 4.8 nm, a molecular weight between 135 and 140 kDa with a molecular weight of 23 kDa for each of the five subunits/monomers [117]. The

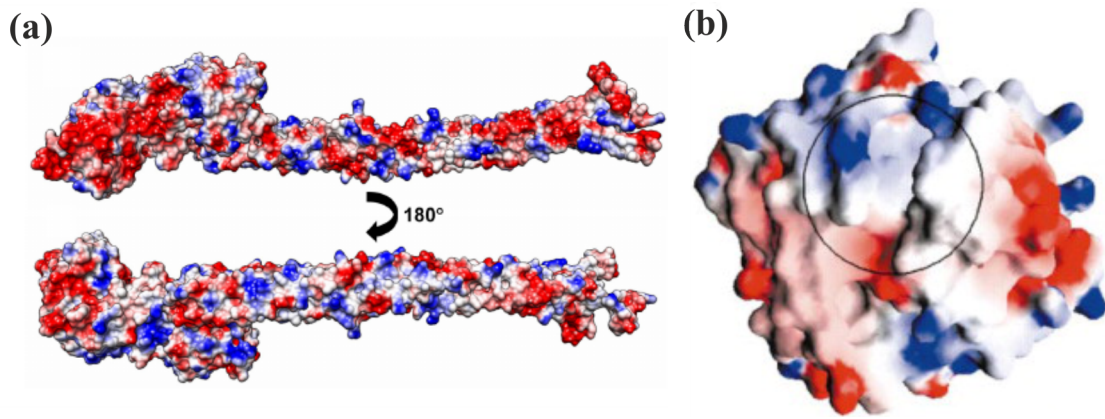


Figure 2.5: Electrostatic potential surface diagram of (a) a fibrinogen monomer from [149] and (b) C-reactive protein from [186]. Negative charges are marked in red, positive charges are marked in blue.

net charge in physiological conditions is neutral while the inner part of the “ring” is negatively charged [186, 189] and the outer parts are depicted in fig. 2.5 (b). It is known and used in hemograms as an unspecific marker for inflammatory diseases. The normal value for healthy humans is 3-10 mg/l, while a value above 200 mg/l indicates strong infections. CRP values between 10 and 200 mg/l are associated with virus infections, bacterial infection or active inflammations. In medicine it is appreciated as an indicator, because the CRP value is strongly increasing (within hours) after the inflammation/infection [35].

2.1.3 Bridging and Depletion

Since the beginning of the last century it is known that human RBCs tend to form clusters, which appear like stacks of coins and are therefore named rouleaux [53, 54, 68]. In vivo and at rest such rouleaux consist of two RBCs to several hundred RBCs forming a network. Under physiological conditions in vivo, the applied shear forces can break clusters into single cells, which is one reason for the shear thinning behavior of blood [170]. This aggregation process shouldn't be confused with the process of coagulation. Aggregation is a reversible process induced by macromolecules (e.g. fibrinogen, immunoglobulin G, immunoglobulin M etc.), while blood coagulation is induced by a change from fibrinogen into fibrin (via the complex coagulation cascade) that forms a network in order to entrap platelets and RBCs [43]. Both effects can encourage thrombi formations, that may lead to serious diseases or death.

Between fibrinogen and plasma expanders (HES, dextran) there is one important difference: With an increasing fibrinogen concentration the number of RBC clusters is increasing. In contrast, with an increasing dextran or HES concentration the number of RBC clusters reaches a maximum. A further increase of the concentration leads to decrease of the number of aggregated RBCs. The resulting aggregation versus concentration curve therefore has a bell-shape.

For both plasma expanders and fibrinogen the reason for aggregation itself is not fully understood [183]. Since the middle of last century two explanations were coexisting: The depletion theory and the bridging model. While the depletion theory makes use of a purely colloidal effect, the bridging model involves physisorption of the macromolecules onto the RBC membranes. This chapter focuses on the qualitative explanation of both models. In addition a speculation of the combination of both models will be introduced, which is called here "Bridletion".

2.1.3.1 Bridging

First mentioned by Merrill in 1966 [133] fibrinogen was assumed to have the capacity to bind to RBCs and form rouleaux. This idea was taken up by many authors such as Chien [53], Brooks [42], Swenson [183] and some more [24, 175] for the case of dextran. Most theoretical works make use of the so called "stretched spring" models, where the dextran is assumed to be slightly stretched in between the RBCs. In the most recent work of Bagchi [16] a "stretched spring" model similar to the one of Skalak [175] was proposed and led to an aggregation force per unit length \underline{f}_{agg} of the cell membrane:

$$\underline{f}_{agg} = k_b (l - l_0) n_b \frac{x}{l} \quad (2.1)$$

where k_b is the spring constant, l is the stretched bond length, l_0 is the unstretched bond length, \underline{x} is the distance of the cells and n_b is the bond density defined by the reaction equation

$$\frac{\partial n_b}{\partial t} = 2 \left[k_+ \left(n - \frac{n_b}{2} \right)^2 - k_- n_b^2 \right] \quad (2.2)$$

where n representing the density of cross-linking molecules on each cell. The forward and reverse reaction rate coefficients k_+ and k_- are given by the correlations:

$$k_+ = k_+^0 \exp \left[-\frac{k_{ts} (l - l_0)^2}{2K_B T} \right], |\underline{x}| = l < l_t \quad (2.3)$$

$$k_- = k_-^0 \exp \left[-\frac{(k_b - k_{ts}) (l - l_0)^2}{2K_B T} \right] \quad (2.4)$$

where k_+^0 and k_-^0 are the rate coefficients in equilibrium, k_{ts} is the transition spring constant and l_t is the distance below which the bond formation is initiated (here it is assumed to be 1.2 times the unstretched length of the macromolecule l_0).

Such a model can explain the increasing aggregation of RBCs with increasing macromolecule concentration, but not the decrease after reaching a maximum (bell-shape). In this model it is assumed that both aggregated cells contribute an equal number of molecules to the bond formation. Intuitively it is obvious that the maximum interaction force will be reached, if 50% of the surface area of each cell is covered by macromolecules, because 50 % of the surface have free binding sites as depicted in fig. 2.6. Assuming that the macromolecules cannot interact with themselves due to steric interactions (respectively form bridges) a 100% coverage of the cell surfaces would lead to no interaction, because no free binding sites exist. Due to the fact that the coverage of the cells would be continuously increasing with increasing macromolecule concentration the interaction energy between the cells would increase up to 50 % coverage, while it would decrease from 50 to 100 %. Consequently, the bell-shape can be explained with such a bridging model.

One open question is how fibrinogen, dextran and HES can bind to the RBCs. On the one hand, there can be a specific binding where a specific part of the macromolecules binds to a specific protein on the RBC. On the other hand, parts of the macromolecule could bind to several proteins or the cell membrane itself e.g. induced by Van-der-Waals-forces, called unspecific binding as illustrated in fig. 2.7 (b). For fibrinogen a specific binding to an unknown receptor of the RBCs could

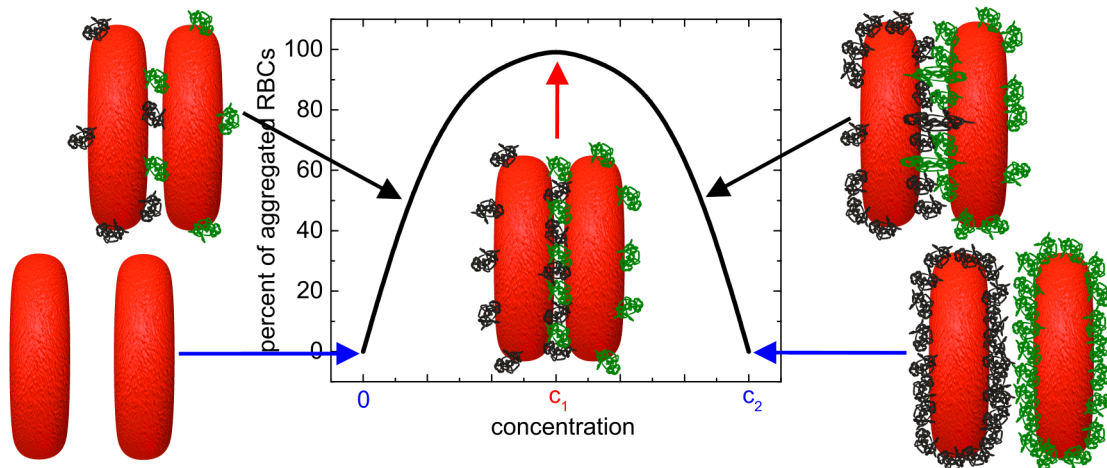


Figure 2.6: If no macromolecules are present RBCs don't aggregate as depicted in the most left image. If 50 % of the surfaces of two cells is covered by macromolecules 50 % of the surfaces is uncovered and therefore the aggregation, i.e. the interaction energy is at the maximum (middle image). If 100 % of both cell surfaces is covered by steric-interacting macromolecules no free binding sites exist and the cells can't aggregate (most right image). Cells in between (upper left and right image) represent the intermediate state between maximum and minimum interaction energy. Macromolecules mainly adhered to the right cell of the cell pair are marked in green, while macromolecules mainly adhered to the left cell of the cell pair are marked in black.

occur (see fig. 2.7 (a)), which is most probably related to the $\alpha_{IIb}\beta_3$ integrin by comparison with the well-known platelet interaction with fibrinogen via this receptor as shown by Carvalho and co-workers [48]. For dextran and HES the OH-groups seem to be the most reasonable binding sides for an unspecific binding to unknown binding sites on RBCs [60].

There is no final proof for the bridging theory regarding the clustering process of RBCs. Even if an adsorption onto the RBCs is shown the depletion effect can't be excluded as the primary effect as explained in chapter 2.1.3.2 and 2.1.3.3.

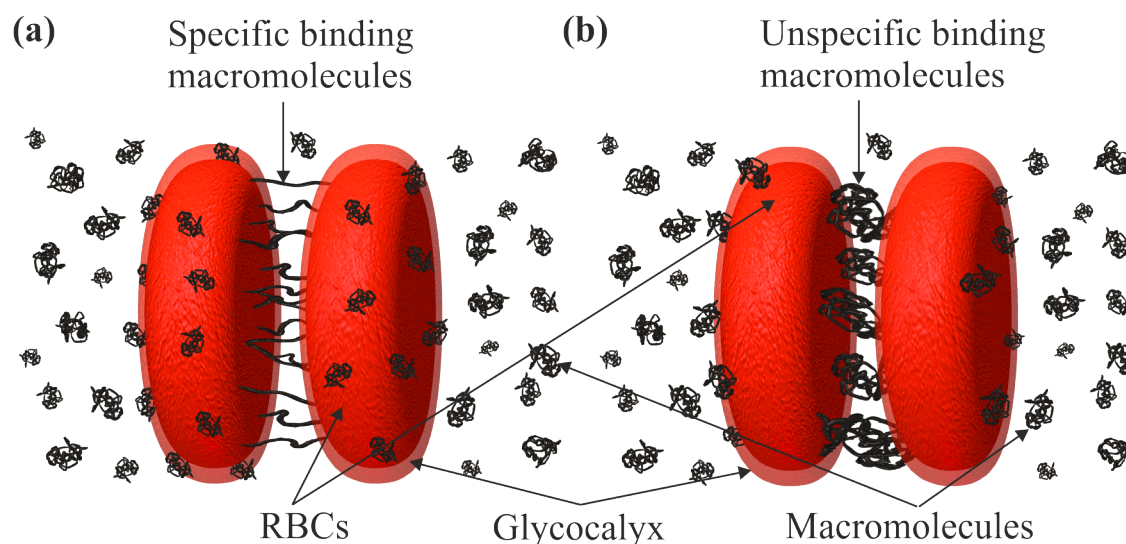


Figure 2.7: A specific binding to proteins of macromolecules (black) between two red blood cells (red) (a) could be unspecific if no membrane proteins are involved (b). The glycocalyx is marked slightly red. Different sizes of macromolecules indicating the presence of imperfect macromolecules.

2.1.3.2 Depletion

Asakura and Oosawa were introducing the depletion theory first in 1958 [14]. Here two large plates or two large spheres are considered in a medium of much smaller rigid spheres, that could be represented by macromolecules. The center of mass of the smaller spheres cannot enter a volume around the plates/large spheres, which has the size of the radius of the smaller spheres and is called depletion layer. If those layers overlap the so called “forbidden areas” appear. In such areas no smaller spheres or macromolecules are presented anymore, which leads to an decrease of free volume and therefore an increase of the entropy. Hence, an attractive force between the large plates/spheres appears, that is illustrated in fig. 2.8 (a) for spheres. This force is proportional to the osmotic pressure of the smaller spheres [14].

The model was taken up by Neu and Meiselman and applied to RBC aggregation [143]. Here the smaller particles are represented by spheres which have 1.4 times the radius of gyration of e.g. dextran molecules in order to respect the fact that the macromolecules are compressible near the interfaces, which was applied to the depletion theory by Vincent [192] and derived from de Gennes [81]. In addition, the presence of the glycocalyx of RBCs is taken into account in the sense that macromolecules can penetrate the glycocalyx between adhering cells and cancel out the attractive effect induced by the outer molecules if the osmotic pressure of the latter is high enough as illustrated in fig. 2.8 (b). This leads to an attractive

interaction energy of

$$w_D = -2\Pi \left(\Delta - \frac{d}{2} + \delta - p \right) \quad (2.5)$$

where d is the separation distance between the cells, δ is the thickness of the glycocalyx and p is the penetration depth. The osmotic pressure Π of the bulk polymer concentration is derived from the virial equation up to the second virial coefficient B_2 , which leads to

$$\Pi = \frac{RT}{M_2} c_2^b + B_2 (c_2^b)^2 = -\frac{(\mu_1 - \mu_1^0)}{\nu_1} \quad (2.6)$$

where R is the gas constant, T the absolute temperature, M_2 is the molecular weight of the polymer, c_2^b is the bulk polymer concentration, μ_1 is the chemical potential of the solvent in the polymer solution, μ_1^0 is the chemical potential of the solvent in the polymer free solution and ν_1 is the molecular volume of the solvent.

The depletion layer thickness Δ is derived from Vincent [192] and based on the equilibrium between compression energy and osmotic forces by assuming that the surfaces (respectively RBC surfaces) are not able to absorb macromolecules, which leads to

$$\Delta = -\frac{\Pi}{2D} + \frac{1}{2} \sqrt{\left(\frac{\Pi}{D}\right)^2 + 4\Delta_0^2} \quad (2.7)$$

in which Δ_0 is the depletion thickness for vanishing polymer concentrations and fixed to 1.4 times the radius of gyration and D is a function of the bulk polymer concentration given by

$$D = \frac{2k_B T}{\Delta_0^2} \left(\frac{c_2^b N_a}{M_2} \right)^{\frac{2}{3}} \quad (2.8)$$

where k_B is the Boltzmann constant and N_a the Avogadro constant.

The knowledge about the interaction of the glycocalyx with macromolecules being very limited, one can assume a penetration depth of the following form:

$$p = \delta \left(1 - \exp \left(-\frac{c_2^b}{c_2^p} \right) \right) \quad (2.9)$$

where c_2^p is the penetration constant of the polymer in the solution and δ is assumed to be independent of the bulk polymer concentration. Additionally it is assumed that neither the fact that the local osmotic pressure of the glycocalyx is influencing the penetration [193] nor that the osmotic pressure of the bulk polymer concentration can lead to a collapse of the macromolecules [106] is assumed.

Taken into account the net negative charge of the RBC glycocalyx by an isothermal charging process the electrostatic repulsion can be calculated as

$$w_E = \frac{\sigma^2}{\delta^2 \varepsilon \varepsilon_0 \kappa^3} \begin{cases} \sinh(\kappa\delta) (\exp(\kappa\delta - \kappa d)) & , d \geq 2\delta \\ (2\kappa\delta - \kappa d) - \exp(-\kappa\delta) \sinh(\kappa\delta - \kappa d) - \sinh(\kappa\delta) \exp(-\kappa d) & , d < 2\delta \end{cases} \quad (2.10)$$

where ε is the relative permittivity of the solvent, ε_0 is the permittivity of vacuum, σ is the surface charge density and κ^{-1} is the Debye length which is small compared to both the cell to cell distance d and the thickness of the glycocalyx δ . This assumption allows to use the superposition of the potentials of the two RBCs.

Finally, the total interaction energy of two aggregated RBCs is considered to be

$$w_T = w_D + w_E \quad (2.11)$$

This theory leads to the first explanation for the bell-shape behavior. Nevertheless, the end of the bell-shape, where the macromolecular concentration is so high that RBCs do not aggregate, is at around 40 mg/ml for the case of dextran 70 kDa by approximating the experimental data of Buxbaum [47]. Chien [52] already showed experimentally that the bell-shape for dextran 80 kDa ends at around 80 mg/ml with an aggregation peak at 40 mg/ml. In addition, all data presented in this thesis show that the bell-shape for dextran 70 kDa ends at around 120 mg/ml while the maximum aggregation appears at 60 mg/ml. Hence, there are discrepancies in the experimental results. That would be explained by limitations of the theoretical model of Neu and Meiselman [143]. Some ideas for these discrepancies are given in the following discussion.

First, as depicted in several publication of Pathak [5, 50, 167] the pH, the concentration, clustering processes in between the macromolecules etc. play an important role for protein solutions, which could be applied to macromolecules such as dextran. Therefore, as it was already partly done in the study of Neu and Meiselman [143] macromolecules can most often not be assumed to be hard spheres. It is unclear if this applies to dextran also. This has to be taken into account for the aggregation of

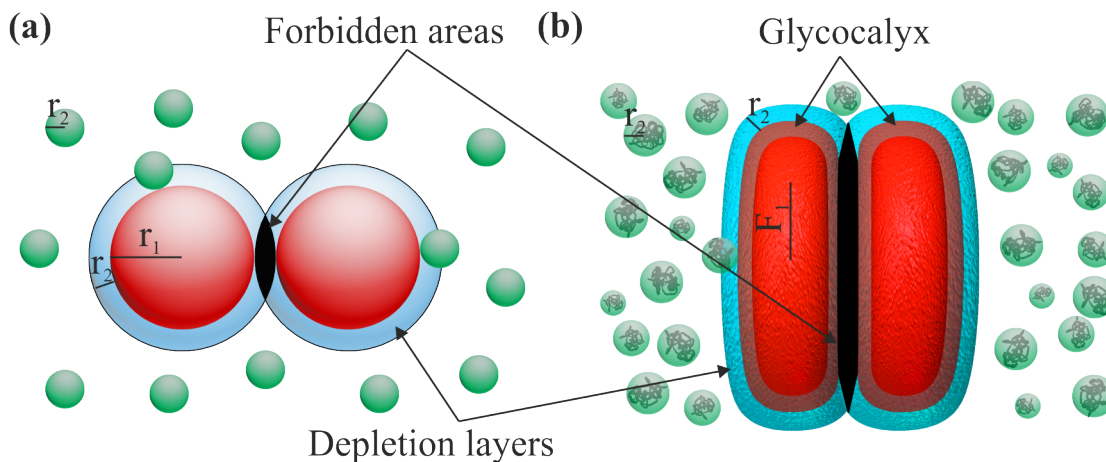


Figure 2.8: (a) The depletion of large spheres (marked in red) induced by small spheres (marked in green). The depletion layer is shown in blue and the forbidden areas are illustrated in black. (b) The depletion is changing by changing the sphere shape to a RBC shape. Small and greater green balls are indicating the presence of imperfect macromolecules, which do not have all the same size.

RBCs induced by fibrinogen as well due to the fact that it is a protein with several charges including a net negative charge in physiological conditions.

Second, in the theory of Neu and Meiselman [143] the function D depends on the molecular weight and the bulk polymer concentration, which is only valid for vanishing polymer concentrations. For moderately dilute solution where polymer concentration is not vanishing, but small enough for the coils of polymers to be studied according to de Gennes' theory [81], the theory of Vincent [192] can be applied. Here, the overlap concentration c^* has to be taken into account. If the bulk polymer concentration c exceeds c^* , the system's behavior could be influenced significantly. According to de Gennes, concentrations higher than c^* could lead to entanglement of the polymer chains that form a transient network [81]. For dextran 70 kDa the overlap concentration was shown to be around 20 mg/ml [116]. This could influence many factors of the theory of Neu and Meiselman [143] such as the osmotic pressure, the penetration depth, the radius of gyration etc. One can find that 20 mg/ml is the overlap concentration, but this concentration is not changing the "true molecular mass" or the "true radius of gyration" and hence it is not changing the system significantly. These two parameters change at three times the expected overlap concentration, i.e. 60 mg/ml, which was shown by Ioan and co-workers [104]. Consistently, the concentration that could affect the system significantly is 60 mg/ml. Nevertheless, a penetration into the glycocalyx is obviously happening taken the work of Pathak [167] into account. The huge challenge is to find out how strong such a penetration is influencing the aggregation of RBCs in contrast to the influence of the overlap concentration and the "true molecular mass" and the "true radius of gyration". This is as valid for dextran as it is for fibrinogen with the main question

why no bell-shape exists in the case of fibrinogen. Most probably the answer at a pH of 7.4 could be that fibrinogen and RBCs are net negatively charged, which should be investigated further.

Third, if there is an adsorption of macromolecules on the RBCs the presented formulas are not valid anymore. This fact will be explained in the following chapter 2.1.3.3.

Nevertheless, coming from the experimental point of view a simplified system with particles (on which dextran cannot adsorb) instead of RBCs could help to understand if depletion is a valid explanation for RBC clustering. Such an experiment was already performed by Badaire and co-workers [15]. Here SU8 particles of cylindrical shapes and on average half the diameter of RBCs were chosen to investigate a pure depletion effect. The particles had a density of 1.2 g/cm^3 which is slightly larger than the averaged density of RBCs with 1.14 g/cm^3 [82]. Using dextran 70 kDa at a very low concentration of $8 \text{ }\mu\text{g/ml}$ the authors showed that the SU8's are forming stable rouleaux within 24-48 hours. Dextran was showed not to adsorb to the particles, following a method similar to the sedimentation method presented in this work (see chapter 3.1.3) and therefore bridging effects can be excluded, which led the authors to the assumption that a pure depletion force is acting. In contrast, the aggregation of RBCs happens much faster as shown in [52] and in the present thesis on timescales which are far below 5 min (see chapter 3.2). Time scales in the order of one or two days [15] could be related to the very low dextran concentrations in comparison to the work of Chien [52], in which ca. 10,000 times higher concentrations were used. Nonetheless, if the illustrated experiment were performed with the concentrations valid for RBC aggregation and the time scale were still in the range of days it would be very challenging to argue that depletion is the main factor of RBC aggregation, because the clustering should happen within minutes.

2.1.3.3 “Bridletion”

In the two chapters above two different theories for the aggregation mechanism were illustrated. If a macromolecule can adsorb onto a substrate as a colloid, a dish or a RBC both theories should be taken into account. Here a speculation about the combination of both theories for RBC aggregation is developed that was not shown in this way in previous studies, called “bridletion”.

In several publications the adsorption of dextran molecules on RBCs was evidenced [52, 55, 60]. Recently, it was found using AFM that fibrinogen can be assumed to bind to RBC membranes [48]. Consequently, it is assumed that different macromolecules can adsorb onto the RBCs. As depicted by Fanatoni and co-workers [70] a depletion and bridging can co-occur in a colloidal system of large and small spheres by changing the concentration of the smaller spheres. Applied to RBCs it suggests that the addition of a small amount of macromolecules can lead to a coexistence of bridging and clustering. If the surface area of the RBCs is covered

by 50% of macromolecules then the bridging force would reach its maximum as illustrated in fig. 2.9 (b). Increasing the macromolecular concentration to a 100% coverage of the RBC surface area and assuming that the macromolecules cannot form bridges between themselves, the surface of the cells is passivated, which leads to a non-aggregating RBC suspension as depicted in fig. 2.9 (c). Increasing the concentration of macromolecules after this passivation of the surface further a depletion could occur. This is due to the fact that the adsorbed macromolecules don't belong to the bulk polymer concentration, which is inducing the depletion forces as shown in fig. 2.9 (d). Taken the overlap concentration c^* into account a further increase of the concentration could lead to a disaggregation of the depleted RBCs again. The consequence would be a double bell-shape behavior. The first bell-shape is due to the percent of coverage of the RBC surfaces by macromolecules, while the second bell-shape would occur due to depletion in combination with the overlap concentration of the macromolecules. However, such a behavior was never observed experimentally. Going further the step of 100% coverage is not even necessary, because a depletion could already occur while the RBCs are linked via macromolecular bridges. Consequently, such a system would include bridging and depletion at the same time. The question in such a case is: What is the primary effect, depletion or bridging?

To make it even more complicated one very important parameter was not taken into account yet: the temperature. As shown by Feng and co-workers [74] in a system of TPM-, polystyrene- and silica particles in combination with PEO, dextran or nanoparticles, depletion effects happen at low temperatures (36° C), while bridging is favored at high temperatures (82°C). The investigated polymers are known not to adsorb onto these particles at low temperatures (up to 36°C). The interaction energies of bridging are $2 k_B T$, around four times higher than the depletion interaction energies of $0.5 k_B T$. One difference between depletion and bridging is revealed by the interparticle distance, which is low for depletion (close to zero) and high for bridging (in the range of the radius of gyration of the macromolecules). Consequently, for RBC aggregation the temperature could change the balance between the fundamental mechanics of aggregation. Taking into account that RBCs are more complex than the used particles, one could assume that a crossover between depletion and bridging is happening at much lower temperatures than applied in the work of Feng and co-workers.

In summary, it was shown in several publications that macromolecules can adsorb to RBCs [48, 52, 55, 60]. If a polysaccharide as dextran can bind to one RBC it can bind to another one as well, because of the repeated monomers. As a consequence, bridging cannot be excluded, if an adsorption onto the RBCs was shown. On the other hand, depletion can never be excluded, because of the osmotic pressure of the macromolecules. The formula of Neu and Meiselman [143] can be modified in a more defined model: First, the true molecular mass and radius of gyration induced by the overlapping of macromolecules should be taken into account. Consequently,

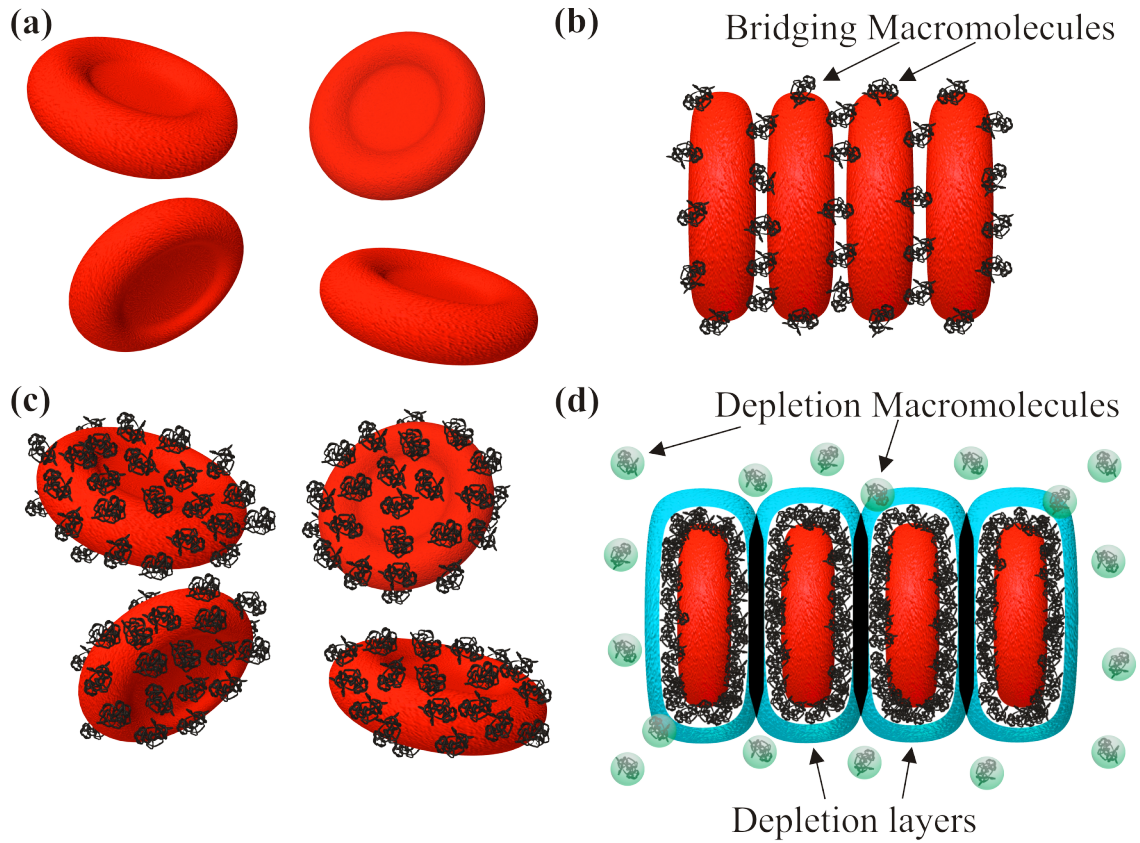


Figure 2.9: Red blood cells (a) could adsorb macromolecules which leads to bridging (b). By a further increase of the macromolecule concentration the cells could be fully covered by those molecules and can't bridge anymore, if the macromolecules can't adhere to themselves (c). Increasing the molecule concentration even more a depletion layer can appear, which leads again to an aggregation of the red blood cells (d).

the molecular mass of the equations 2.6 and 2.7 becomes a function that depends on concentration. Second, even if the bridging effects are low at low temperatures they have to be taken into account, which leads to an additional term. Third, the effect of temperature seems to be very important, as it could influence the relative impact of bridging and depletion. Those three facts leads at least to the following formula for the interaction energy:

$$w_{agg} = \begin{cases} w_E + w_{D1} + w_B & , T < T_{crit} \\ w_E + w_{D2} + w_B & , T > T_{crit} \end{cases} \quad (2.12)$$

where T_{crit} is the temperature at which the system is changing the primary effect of the RBC aggregation, w_{D1} and w_{D2} are the depletion interaction energies for low and high temperatures. They are implying the fact of the overlap concentration,

which will change the formulas, cause they are directly related to the molecular weights that are changing beyond the overlap concentration (respectively a change in true molecular mass). w_B is the bridging interaction energy, which results from the direct integration along \underline{x} of \underline{f}_{agg} (see chapter 2.1.3.1 for definitions). Below the critical temperature $w_{D1} \gg w_B$ and w_B can be neglected and therefore w_{D1} represents the main attractive interaction energy and consequently the system is dominated by depletion forces. Above the critical temperature $w_{D1} \ll w_B$ and w_B represents the main attractive interaction energy and therefore the system is dominated by bridging effect. In the ideal case of low temperatures bridging is neglected and if one ideally neglect depletion for high temperatures the system can be approximated to

$$w_{agg} = \begin{cases} w_E + w_D & , T \ll T_{crit} \\ w_E + w_B & , T \gg T_{crit} \end{cases} \quad (2.13)$$

In addition, the fact that RBCs can create more tethers (see chapter 5.5) in the presence of dextran should be taken into account as well as the change in stiffness of the RBCs by adding dextran (see chapter 3.5.1) that could change the aggregation behavior. In this work a change of shape for RBCs from discocytes to stomatocytes is assumed for high dextran and HES concentrations. If it were confirmed by future work, this would change both the depletion and bridging theory for this specific case, because a change in shape is not included in the theoretical descriptions.

2.2 General techniques

2.2.1 Confocal microscopy

In this chapter the pioneering ideas for the development of confocal microscopes is briefly introduced. Afterwards, the technical realizations of point scanning and spinning disk microscopy are explained leading to three dimensional reconstructions and the very basic mathematical descriptions.

2.2.1.1 General introduction

In 1927, Berek realized that the spread out-of-focus light is one important parameter in microscopy which should be minimized [27]. In order to do so 30 years later the principle of confocal microscopy was invented by Minsky [136]. Due to technical issues it took Minsky until 1988 to set up the first confocal microscope [137]. Here, the normal light source is replaced by a point light source, which was realized in the original microscope by a pinhole in front of a zirconium arc lamp. Focused by an objective into the specimen the passed-through light was again focused by a second objective to a second pinhole, hence the name con-focal. The second pinhole reduces the out-of-focus light. Finally, the light falls to a photo detector that is translating the signal into an image point. This method is imaging a single-point of the specimen, which is not very useful. To create an image of the whole specimen the entire stage, to which the specimen was fixed, needed to be moved. This method is very slow and susceptible for vibrations. With the work of White [194] this technique was improved by moving the illumination instead of the stage across the sample (so called beam-scanning), which created an enormous interest for biological applications [148, 160]. Nowadays, with the progress in laser technology, objectives, computers and fluorescent labeling the confocal microscopy improved significantly. Two main types of confocal microscopes are commercially available: The (multi-)point scanning and spinning disc confocal microscopes, which will be introduced in the following paragraph.

2.2.1.2 Point scanning and spinning disk confocal microscopy

The point scanning confocal microscopy (PSCM) is based on the original idea of such a microscope with the improvements explained below. By adding a dichromatic beamsplitter the specimen does not have to be placed in between the lenses, which makes it easier to handle especially for biological samples. This technique is called epi-illumination and illustrated in fig. 2.10 (a). Laser light is focused by an objective lens to the pinhole that creates a bright focused point source. This light is reflected by a dichromatic beamsplitter and collected at the condenser lens to a laser spot (in reality this spot is a double-cone that has an expansion of ca. 750x250 nm,

depending on the specific setup) onto the fluorophore labeled specimen. Due to the excitation the fluorescent dye emits light of a larger wavelength than the excitation laser, which passes the dichroic mirror after the condenser lens. The objective lens is now focusing the emitted light onto the second pinhole (with the same focus as the first pinhole), which forwards it to the detector and blocks the out-of-focus light. The detector is typically a photomultiplier tube (PMT) or a high-sensitive hybrid detector (HyD), which combines the benefit of vacuum tubes with the one of semiconductor silicon avalanching techniques. Therefore, HyDs provide a higher dynamic range and a higher contrast as PMTs and were introduced into commercial confocal microscopy by Leica [135]. In order to create an whole image the laser spot is moved across the specimen line by line with e.g. with galvo mirrors or a resonant scanner (which is in fact a vibrating mirror) as illustrated in fig. 2.10 (c). The image itself is reconstructed by the software. Often such microscopes are called line scanning microscopes (LSCM) as well, if they are used for scanning a single line. This technique is relatively slow, because every single point has to be scanned and in order to increase the image quality several line scans and images become averaged [148, 160].

Another confocal technique is increasing the scanning velocity enormously using a Nipkow-disk. This invention goes back to Nipkow in 1884, who wanted to convert an optical image into an electrical signal [146]. He used a perforated wheel with a spiral pattern array, the so called Nipkow-disk. Spinning such a disk leads to a change of the small sampled areas. The design of the Nipkow-disk was modified by Petrán and co-workers [154] including multiple spiral patterns in a single disk. One design of spinning disk confocal microscopes (SDCM) was introduced by Yokogawa Electric Corporation of Japan. Here two coaxial aligned disks fulfill the effect of a lens and a pinhole as illustrated in fig. 2.10 (b). In such a confocal microscope the laser beam passes first the lens disk. This is a glass disk with Fresnel microlenses on the top, which focus the beams. After passing the dichromatic beamsplitter the light crosses the Nipkow-disk and becomes focused onto the specimen by the condenser lens. The fluorophore labeled specimen emits photons of longer wavelength than the excitation wavelength laser. Emitted light is passing the condenser lens and is focused towards the Nipkow-disk acting as a pinhole. Now, the light becomes reflected by the dichromatic beamsplitter and focused on a CCD or CMOS camera by the objective lens. If both disks rotate synchronously (at typical velocities of 1,800 to 10,000 rpm) several lines are scanning the specimen, which will be expressed pixel per pixel on the camera. The characteristic scanning patterns are illustrated in fig. 2.10 (d). For typical exposure time such spinning disk microscopes can reach frame rates of more than 20 fps, which is much faster than for point scanning microscopes where one image can take several seconds depending on the resolution and scan speeds (the exception is if one is interested in a single line of the sample, because here the point scanners reach 8,000-10,000 lines per second). Due to lower peak laser power on each point of the sample SDCM decreases photobleaching (loss of

fluorescence due to illumination) and toxicity (due to free radicals which could lead to cell death) in comparison to the PSCM. In spinning disk systems the image quality can be blurred due to pinhole size, which can be optimized for a given numerical aperture objective, and because crosstalking effects between different laser beams is possible. This problem was already minimized by Yokogawa with increasing the distance between the pinholes of the disk. Nevertheless, with both techniques 3D images can be produced by scanning the sample in z-direction (the direction parallel to the laser beam).

For 3D imaging one plane of the specimen is imaged in this manner. Afterwards either the stage or the lens is moved up- or downwards e.g. with piezo motors. At this position a second scan is performed etc., which is illustrated for six scans in fig. 2.11 (a). This results in a stack of images as depicted in fig. 2.11 (b). Such a stack of images can be used to reconstruct a 3D image with e.g. the software Imaris that was used in this work for all 3D reconstructions. Two classical renderings are used frequently: A side view image creates the view from the top of the sample and two side views as shown in fig. 2.11 (c). The second rendering method is a 3D surface rendering, which is resulting in a digital 3D object that can be turned ad libitum and illustrated in fig. 2.11 (d) for one point of view. Depending on the setup, the z-resolutions can be around 600 nm based on x63, NA 1.4 oil immersion objective [160].

Confocal imaging can be performed in transmission and reflecting mode using non-fluorescent materials. However, for biological applications fluorescein labeled samples have the big advantages to increase the contrast signal, decrease the out of focus light even more and specificity (special areas can be labeled without labeling other parts e.g. actin with TexasRed and the membrane with FITC).

In order to collect most of the emitted photons one important factor is the numerical aperture of the objective lens. The numerical aperture is a dimensionless number which describes the maximum angle at which the system can emit or accept light. It is defined as

$$NA = n \cdot \sin \Theta \quad (2.14)$$

where n is the refractive index of the medium (e.g. air, water, oil) and Θ is the the half angle of the light cone entering or emitting the objective. This number is important, because it has a direct proportional influence on the resolution d :

$$d = 0.61 \cdot \lambda \cdot NA \quad (2.15)$$

where λ is the wavelength of the light. Moreover, it has a quadratic dependency of the depth of field Z that describes which areas of an image are in focus:

$$Z = n \cdot \lambda \cdot NA^2 \tag{2.16}$$

Consequently, a higher numerical aperture leads to higher z-resolution [160].

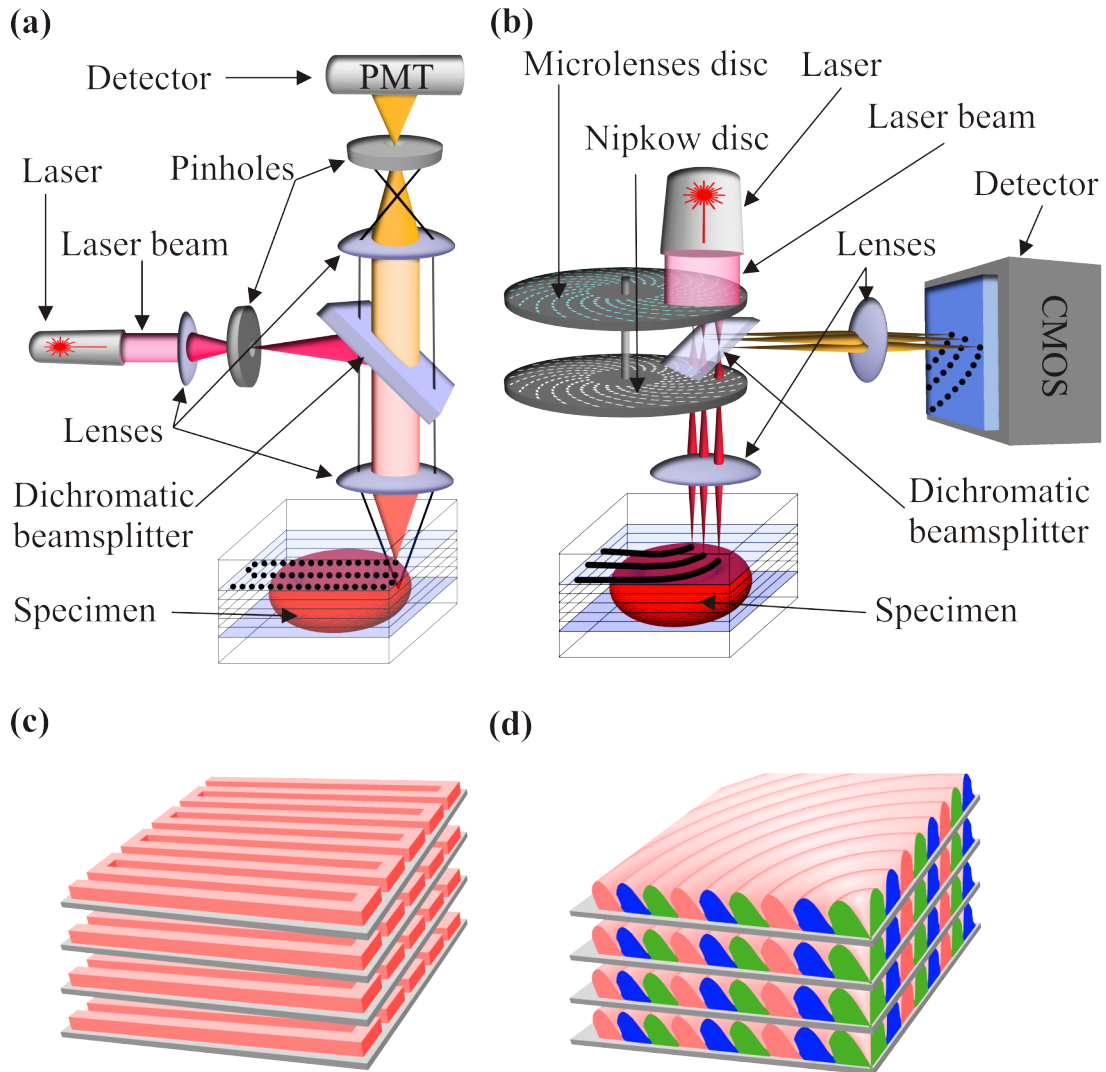


Figure 2.10: A point scanning confocal microscope (a) scans the entire probe point by point and line by line (c). Out of focus light is marked in black. A spinning disc confocal microscope (b) scans the whole probe (d) using parallel curved lines (parallel scans are marked with the same color).

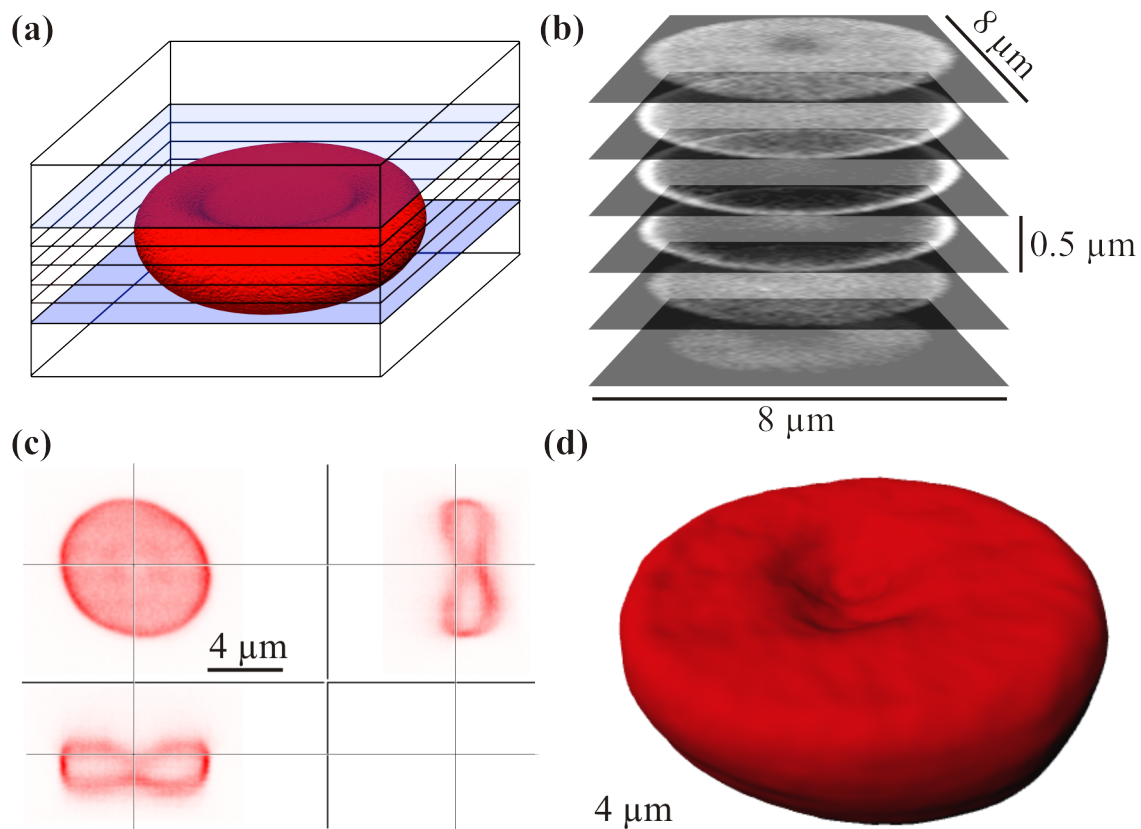


Figure 2.11: A confocal microscope is able to scan several areas in z -direction (e.g. from the bottom to the top of a sample, as shown here for a discocyte RBC) (a), which leads to a stack of images, where each image is representing one area in z -direction (b). In order to get a 3D view one can have a look to the reconstruction of the stacks from the side (c) or reconstruct the specimen by setting a surface threshold (d).

2.2.2 Rheology

The word ‘‘rheology’’ was derived from the ancient Greek words $\rho\acute{\epsilon}\omega$ and $\lambda\omicron\gamma\acute{\iota}\alpha$, which means loosely translated ‘‘The study of flow’’. In this specific chapter $\pi\acute{\alpha}\nu\tau\alpha\ \rho\acute{\epsilon}\tilde{\epsilon}\tilde{i}$ will be transferred to the flow behavior of RBCs. In section 2.2.2.1 it is briefly explained how shear is influencing classical fluid systems. The rheological setup is illustrated in section 2.2.2.2. In section 2.2.2.3 a description of how blood can change its rheological behavior due to shear stresses is given. In section 2.2.2.4 the basic principles of a yield stress will be introduced briefly.

2.2.2.1 General introduction

Fluids can be classified as *compressible* or *incompressible* and whether their viscosity does not change applying a shear stress (*non-Newtonian*) or the viscosity changes applying a shear stress (*Newtonian*) as depicted in fig. 2.12 (b). In order to keep it simple here it is sicked to incompressible fluids and no turbulent flow behavior. The Navier-Stokes-equation is reduced to

$$0 = \rho \underline{f} - \nabla p + \eta \nabla^2 \underline{v} \quad (2.17)$$

where ρ is the density of the fluid, \underline{v} the velocity vector, \underline{f} the outer force per mass unit, p the pressure and η the shear viscosity.

Making several assumptions the Navier-Stokes-equation can solve the probably most simple experiment in rheology: Assuming a fluid in between two parallel plates of the area A , while one of them is moved with the force F and the velocity $V_x = v_x(y) = v_x(d)$ as illustrated in fig. 2.12 (a) the shear viscosity can be derived to be

$$\tau_{xy} = \frac{F}{A} = \eta \dot{\gamma}_{xy} \quad (2.18)$$

Here a linear flow profile $v_x(y) = V_x y = d$, which leads to a constant shear rate $\dot{\gamma}_{xy} = V_x/d =: dv_x(y)/dy$ and consequently proportional to $\tau_{xy} = F/A$ is assumed.

The stress tensor (depicted in 2.12 (a)) has nine components divided into three stress and six shearing components. Assuming the tensor to act on a single fluid element it has to be symmetric and tracefree for incompressible fluids. Therefore, several components are equal $xy=yx$, $xz=zx$, $yz=zy$ and the normal stresses are defined by $N_1 = \tau_{xx} - \tau_{yy}$ and $N_2 = \tau_{zz} - \tau_{yy}$. In the case of a Newtonian fluid all components τ_{ii} become equal to zero.

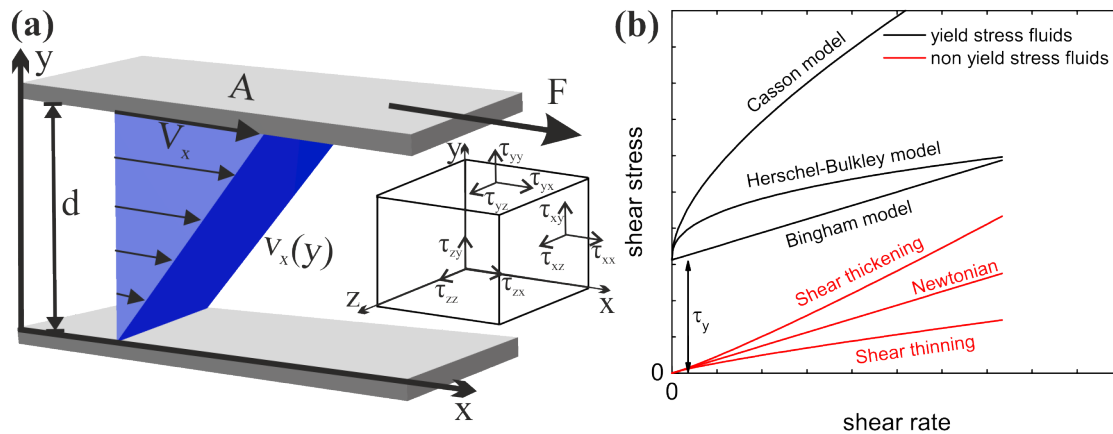


Figure 2.12: Unidirectional shearing of a small volume element (here strongly magnified) with a linear velocity profile and constant shear rate for Newtonian fluids (a). The dependency of the shear stress on the shear rate differ for Newtonian, shear thickening and shear thinning fluids (red). The three basic approximation models for yield stress fluids (Bingham, Herschel-Bulkley and Casson model) are depicted in black (b) and discussed in chapter 2.2.2.4.

For viscoelastic and Non-Newtonian fluids (called complex fluids as well) τ_{xx} can't be taken equal to τ_{yy} , which would lead to $N_1 = 0$ [150] as illustrated in fig. 2.13. Here, the elastic ingredients such as polymers or RBCs become deformed due to the applied shear stresses. Hence, the fluid becomes anisotropic due to shear stresses [34].

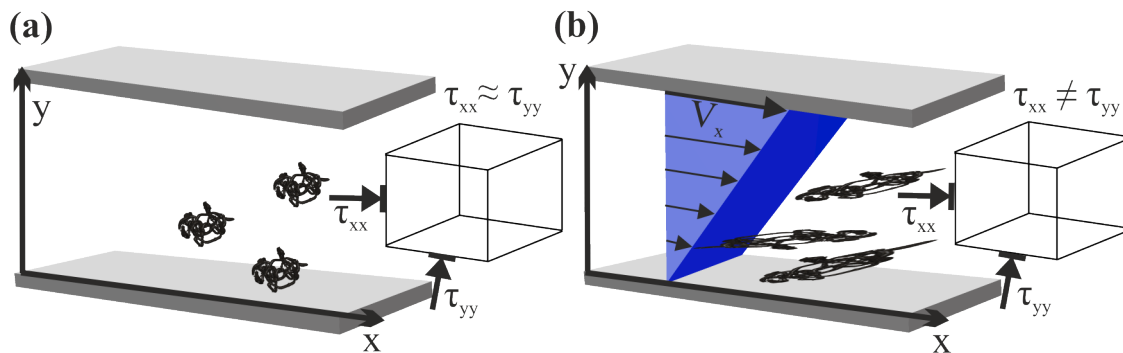


Figure 2.13: In rest or at low shear rates polymers are coiled (a). At high shear rates the polymers get stretched, which leads to an anisotropy of the fluid (b).

Those basic principles are applied in commercial rheometers to characterize a huge number of fluids [44, 76, 141, 168].

2.2.2.2 Rheometer MCR 702

Well-established devices to measure parameters of Newtonian and complex fluids are rotational steady shear rheometers. The principle idea, which was established in 1968, is the use of two coaxial mounted geometries (e.g. plate-plate, cone-plate and Taylor-Couette) with a gap between them, which can be filled with the fluid. One or both geometries are connected to an electric motor, which is most commonly an alternating current drag-cup motor (DC-motor) with an air bearing mounted axle to reduce frictions. For most rheometers the applied motor current is translated to the torque M on an axle, while the resistance of the sample allows the upper geometry only to rotate at a certain speed (the bottom geometry is held at rest). In combination with an optical angular detector this speed can be measured and fed back into a control loop to maintain the desired angular velocity. Due to the fact that the applied shear stress is used this method is called “controlled stress” (CS). In contrast, if the rotor speed is controlled, the resistance of the sample results in a viscosity depending torque, which can be measured by an additional torque sensor, i.e. a torque transducer. Due to the fact that the applied shear rate is used this method is called “controlled rate” (CR) [171].

In 1995, brushless DC-motors, which are called “electronically commutated synchronous motors” (EC), were introduced for commercial rheometers as depicted in fig.2.14.

The big advantage in comparison to a DC-motor is that the rotor consists of permanent magnets, while the stator uses coils to create torque via the induced current. That leads to a combination of CR- and CS-rheometers, which increases the accuracy and range to a minimum torque of 5 nNm and minimum controlling angular deflections as low as 50 nrad in the case of the manufacturer AntonPaar Germany [147]. Here the AntonPaar MCR702 with two EC-motors was applied: In the case of a TC geometry the outer cylinder, driven by the lower EC-motor, is set to apply a certain shear stress/rate, while the inner cylinder, coupled to the upper motor acting as a torque transducer, is used to measure the torque exerted on the fluid. Based on the fact that a water temperature control (as usual, if one geometry is fixated) is not available for this system and that all measurements were performed at room temperature (23 ± 0.5 °C measured by a peltier system) the provided air cooling system was not used in order to minimize drying effects of the RBC dispersions for this work.

In the case of a cone-plate geometry with small angles α the laminar fluid flow is approximately constant, which leads to an easy calculation for the shear stress, if the torque is known:

$$\tau = \frac{3M}{2\pi R^3} \quad (2.19)$$

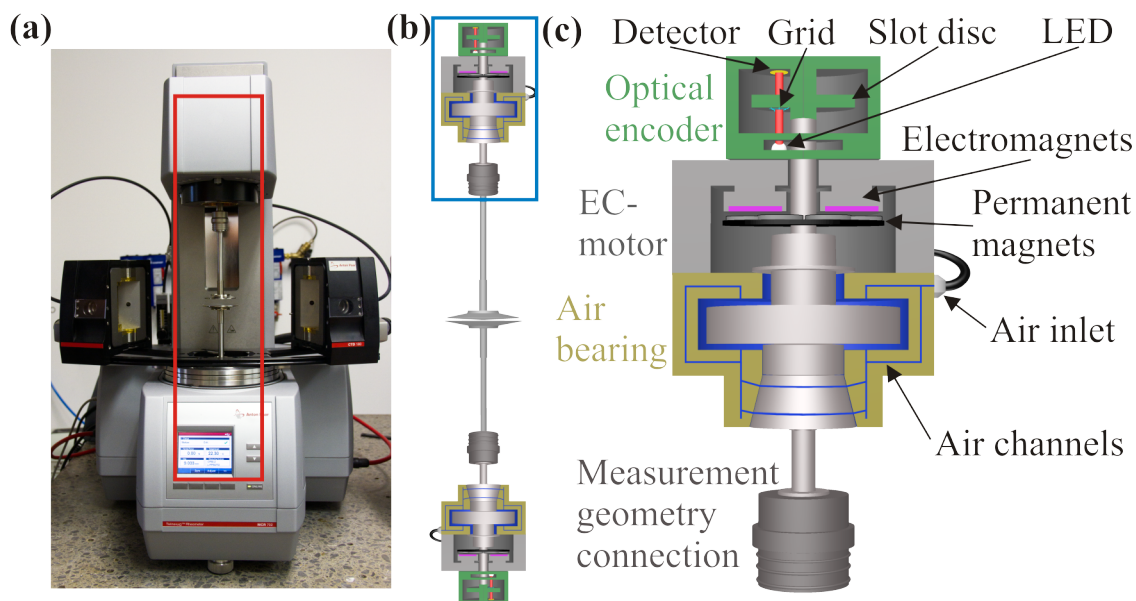


Figure 2.14: The AntonPaar MCR702 (a) is equipped (red rectangle, magnified in (b)) with two EC-motors (b) while a single motor (blue rectangle, magnified in (c)) is equipped with an optical encoder and an air bearing (c).

where τ is the shear stress, M is the torque and R is the radius of the cone as depicted in fig. 2.15 (a). In the case of a Taylor-Couette system the shear stress can be calculated with simplifying the Navier-Stokes equation to:

$$\tau = \frac{1 + \vartheta^2}{2\vartheta^2} \frac{M}{2\pi LR_I^2} \quad (2.20)$$

where $\vartheta = R_O/R_I$ is the radius ratio in which R_O is the radius of the outer cylinder, R_I the radius of the inner cylinder and L the gap length.

In conclusion, a rotational shear rheometer, which operates in a CR mode, can be e.g. used for determining the shear stress at a constant shear rate. In a standard scanning protocol the shear rate is increased or decreased in small steps. The resulting data can be depicted by the apparent viscosity, which, in the case of a laminar flow, is:

$$\eta(\dot{\gamma}) = \frac{\tau(\dot{\gamma})}{\dot{\gamma}} \quad (2.21)$$

where η is the viscosity and $\dot{\gamma}$ is the shear rate.

If the rheometer operates in a CS mode it can be e.g. used for determining the shear rate at a constant shear stress, which leads in a standard scanning protocol and the

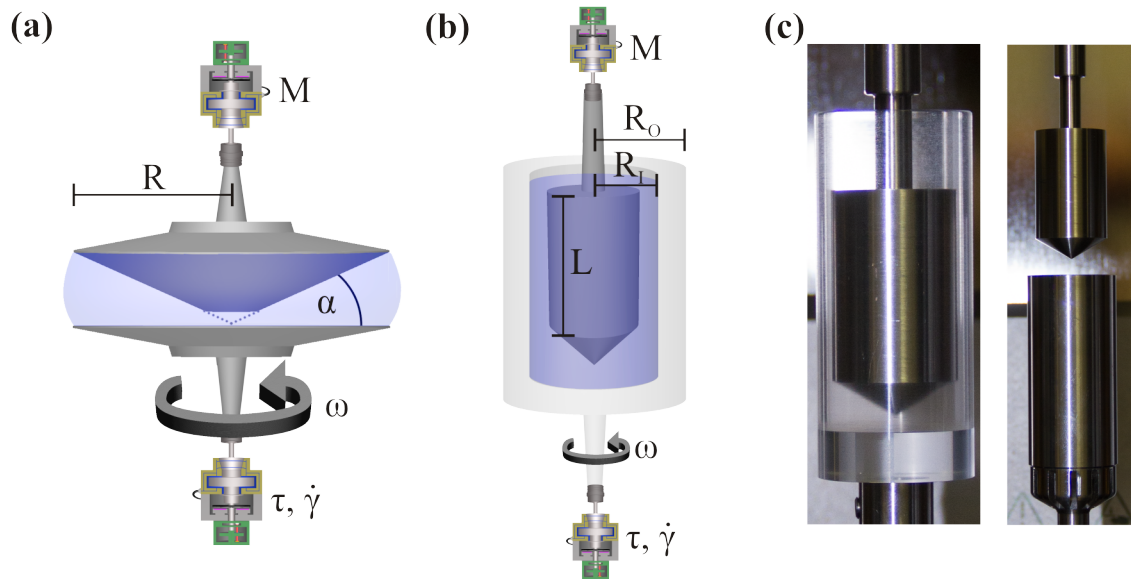


Figure 2.15: A cone-plate geometry (a) in comparison to a Taylor-Couette geometry (b), which has a significantly higher measurement position (c, left) and is realized with stainless steel (c, right). The inner diameter of the outer cylinder is 22 mm.

case of a laminar flow to the apparent viscosity:

$$\eta(\tau) = \frac{\tau}{\dot{\gamma}(\tau)} \quad (2.22)$$

For all measurements a cone-plate or Taylor-Couette geometry in SMT (separate motor transducer) mode was used. Meaning that the shear rate or shear stress was given by the lower motor, while the upper one detected the resulting shear stress or shear rate.

2.2.2.3 Flow dependency applied to red blood cells

The shear thinning behavior of blood [155, 7] is caused by two effects: A rouleaux break-up leads to a strong shear thinning and the cells become orientated as well as elastically deformed at high shear rates, which lead to a slight shear thinning [56, 127]. Blood contains many proteins (see 2.1.1), which cause the RBCs to form reversible aggregates in rest or at low shear rates comparable to adding dextran solutions to the RBCs [128]. Shearing such a suspension leads to a break-up of most aggregates that is followed by an elastic response and orientation in the flow direction of the cells up to approximately 100 s^{-1} as illustrated in fig. 2.16. Theoretically this was shown by Fedosov and other [72, 7] as well as experimentally by Chien and others [56, 155, 83]. For higher shear rates the cells deform to stomatocytes and polylobed cells [118].

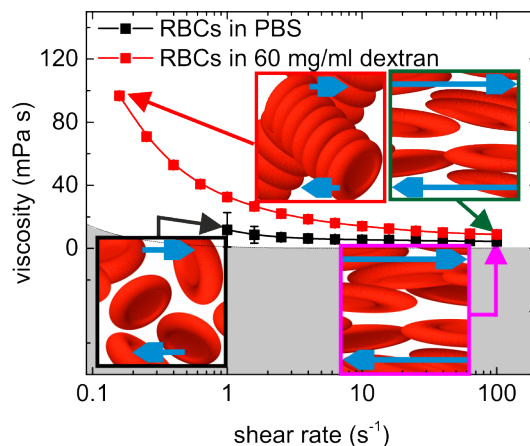


Figure 2.16: The shear thinning behavior of RBCs within the resolution limit of the rheometer MCR702 using the CC20 geometry (gray). If the RBCs are suspended in the buffer solution (black frame) the slight shear thinning behavior is caused by an elastic deformation and an orientation of the cells in flow direction (pink frame). If the RBCs are suspended in a 60 mg/ml dextran solution strong clustering appears resulting in a high viscosity (red frame). During shearing (indicated by blue arrows) most of the rouleaux break up and the cells become deformed elastically (green frame), which leads to a strong shear thinning behavior. The higher viscosity for the red curve at 100 s^{-1} is caused by the viscosity of dextran. Lines are there to guide the eye.

Due to the RBCs gel-like (network-forming) behavior at high macromolecular concentrations (see chapter 3.2) blood and RBC suspensions can show a yield stress as summarized by Picart and co-workers [155]. The yield stress concept (the stress at which a fluid starts to flow) is widely discussed, but mainly accepted. However, it is an idealization and accurate measurements indicate that it does probably not exist [23, 22]. To shorten the whole discussion: Does it flow always or is it really a solid? Both questions are in the end related to time and measurements accuracy. Consequently, the question if a yield stress is existing can't be answered. Nevertheless, it is a useful concept to understand the properties of fluids if the measurements are performed in the same way. The yield stress will be discussed in the following paragraph.

2.2.2.4 Yield stress

If one observes the behavior of everyday fluids like e.g. ketchup, mayonnaise or toothpaste is striking that they don't flow while being in the bottle or tube at a shear rate of zero. By increasing the shear rate to a certain value (i.e. shaking the bottle or pressing the tube) one can put it on the plate or toothbrush etc. The value at which the solid or fluid starts to flow is called the yield stress. Therefore, the

yield stress is defined as the shear stress below the fluid behaves like an (elastic) solid and above like a (complex) liquid [123, 138].

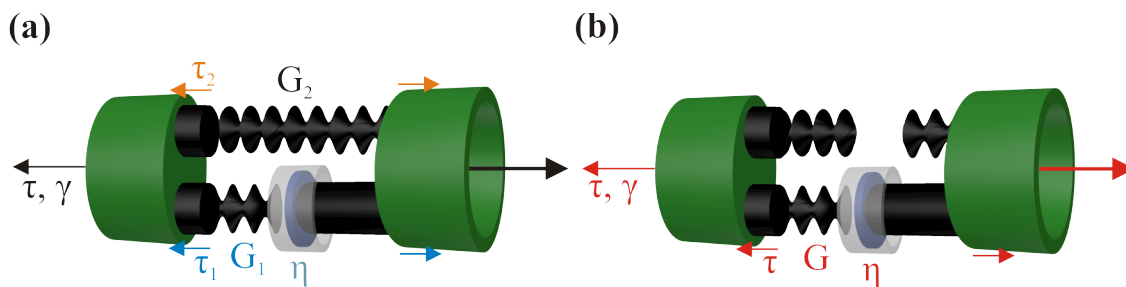


Figure 2.17: The linear Zener model represents a gel (a), which transfers to a viscoelastic fluid represented by the Maxwell model after the yield stress point (b).

A principal idea is to use the standard linear solid model (Zener model) for a gel while the fluid behaves as a solid and the Maxwell model while it behaves as a viscoelastic fluid, because of the absence of the Young's modulus of the upper spring G_2 as illustrated in fig. 2.17. This model couldn't be proven experimentally, yet. Several other models have been proposed to describe the yield stress [89]. However, direct evidence of a yield stress is still missing and falling sphere experiments failed the model. Hence, theoretical models of the yield stress have to be taken with care. Several methods exist to determine the yield stress experimentally, which are explained in detail in [123] and briefly summarized in the following.

To name the main methods: 1. A stress ramp. The applied shear stress starts low and is increased until a peak in viscosity is reached. The corresponding stress to this viscosity is the yield stress.

2. An oscillatory amplitude sweep. The yield stress can be defined as the point where the elastic modulus G' has the same value as the viscous modulus G'' or where G' starts to decrease. If depicting the viscosity vs shear stress for an oscillatory measurement the crossover of the tangent of starting and decreasing region is the yield stress.

3. Extrapolation: The traditional method is to extrapolate the shear stress from measured data at greater than zero shear by applying an empirical model. This was done in this thesis. An extensive overview of that models is given in [162]. The main three models that are applied for this method are illustrated in fig. 2.12 (b) and explained in the following:

The **Bingham model** was introduced by Bingham in 1922 [32]. The fluid is assumed to behave as an solid below the yield stress and starts to flow at the minimum shear stress. The according formula is

$$\sigma = \sigma_0 + \eta_B \dot{\gamma} \quad (2.23)$$

where σ_0 the minimum shear stress and η_B is the Bingham viscosity, which can't be taken as a real viscosity because it describes only the Newtonian portion of the data.

The **Herschel-Bulkley model** was introduced by Herschel and Bulkley in 1926 [93]. It describes a non-Newtonian yield stress fluid, in which the strain of the fluid is related with the stress. The according formula is

$$\sigma = \sigma_0 + K\dot{\gamma}^n \quad (2.24)$$

where σ_0 is the yield stress, K is the consistency, a constant, and n is a specific index for the Herschel-Bulkley model, which describes the degree of shear-thinning or -thickening.

The **Casson model** was introduced by Casson in 1959 [49]. This model is comparable to the Bingham model while all components are taken to the power of 0.5, which makes it more reasonable for the transition of a Newtonian to complex fluid behavior. The according formula is

$$\sqrt{\sigma} = \sqrt{\sigma_0} + \sqrt{\eta_c \dot{\gamma}} \quad (2.25)$$

where σ_0 is the yield stress, η_c is the Casson viscosity which depends on a high shear rate viscosity (without turbulences). This model is widely used to describe RBC suspensions, e.g. blood [155]. Therefore, it is also the main model used in this work (see chapter 3.1.2).

2.2.3 AFM

2.2.3.1 General introduction

The atomic force microscope was introduced in 1986 by Binnig and Gerber [80], who were demonstrating a resolution limit of 10^{-18} N with a lateral resolution of 30 Å and a vertical resolution of 1 Å in air. This was creating the possibility to resolve single atoms. The basic idea is to use a reflecting cantilever in combination with a laser and a four quadrant photo-diode that can measure the deformation of the cantilever induced by contact with the sample or the substrate due to a position shift of the laser measured. Piezo electric motors move the cantilever in z-direction (perpendicular to the microscope dish that is defined as x-y direction) until it is in contact with the sample leading to a deflection of the cantilever. This deflection is measured by a position shift of the laser onto the photo diode as illustrated in fig. 2.18 (c). The result is force-distance curve, while the distance is given by position of the piezo motors and the force by the deflection as depicted in fig. 2.18 (d). By calibrating the cantilever the photo-diode signal is translated to a force as explained in the following chapter. In addition, keeping a constant deflection the cantilever can be moved in x-y direction over the probe in order to scan the sample surface in three dimensions if the constant force is controlled by the piezo motors that provide the z-resolution. Nowadays, AFMs can be used in liquids, which offers several advantages for biological applications and cell physics. Nevertheless, this technique is very challenging in many matters that could lead to severe issues regarding single cell force spectroscopy (SCFS) or atomic force microscopy (AFM) applications.

2.2.3.2 Calibration

To obtain the force exerted by the sample on the cantilever, instead of the position measurements on the photodiode, the system has to be calibrated every time a cantilever is mounted on the AFM. In order to calibrate the cantilever one has to align the laser with the tip area of the cantilever. By adjusting the mirror the laser spot exposes the photo-diode, which can be measured as an absolute photoelectric voltage, and its position on the photodiode can be measured by the voltage difference between the different quadrants of the diode, as shown in fig. 2.18 (a). The cantilever is driven by piezo(electric) motors. The aim of the calibration is to correlate the laser signal with the piezo motors in order to be able to apply and measure a certain force exerted at the tip of the cantilever. Therefore, two calibration steps are necessary: The sensitivity calibration transfers the voltage signal into a voltage per nanometer (movement of the piezo motors) signal. The spring constant calibration transfers the V/nm signal into a Newton per nm signal.

The sensitivity calibration is rather straight forward and shown in fig. 2.18 (c) and (d): The movement of the piezo motors approaches the cantilever onto a very stiff

(compared to the cantilever) substrate (black extend curve), which leads to a deformation of the cantilever and consequently to a user-defined shift of the maximum detected voltage (here 3V). After the retraction (red retract curve) one approximate the linear range of either the retract or the extend curve with a linear function (blue line). The inverse slopes (“optical lever sensitivity”) correlates the change in voltage ΔV with the cantilever deflection Δz and therefore with the piezo movement as shown e.g. in [122]. Using the relation $s = \frac{\Delta z}{\Delta V}$ Hutter [102] showed with a mainly geometrical approach that the forces can be measured by

$$F = \frac{k_0 \Delta y}{\cos^2 \alpha} = \frac{k_0 s \Delta V}{\cos^2 \alpha} \quad (2.26)$$

where k_0 is the correction factor (see below) and α is the angle (for JPK AFMs it’s typically 10°) between the cantilever and its mounting axis (respectively the substrate, if it is perfect horizontal).

The spring constant calibration is most commonly based on a so called thermal noise calibration [46], which was introduced by Hutter and Bechhoefer in 1993 [103]. Using the equipartition theorem for an ideal spring the Hamiltonian is quadratic dependent on $\frac{k_B T}{2}$, where k_B is the Boltzmann constant and T the temperature. Due to the fact that the geometry of the cantilever plays an important role the approximation of the thermal noise in the vertical direction $\langle y^2 \rangle$ can’t simply replace the denominator of the Hamiltonian. Therefore, Butt and Stark [46, 177] were using the eigenmodes of the cantilever, which are induced by thermal energy (e.g. Brownian motion). A further calculation by Hutter [102] based on the equipartition theorem leads to the correction factor for a tip-less cantilever by using the fundamental mode of the cantilever:

$$k_0 = \frac{16}{3} \cdot \frac{k_b T}{s^2 P} \cdot \cos^2 \alpha \cdot \left(\frac{\sin \alpha_1 \sinh \alpha_1}{\alpha_1 (\sin \alpha_1 + \sinh \alpha_1)} \right)^2 = 0.8174 \cdot \frac{k_b T}{s^2 P} \cdot \cos^2 \alpha \quad (2.27)$$

where P is the voltage noise power measured by the integration over the Lorentz approximation of one mode as depicted (and magnified in the inset) in fig. 2.18 (b) for the second mode. $\alpha_1 = 1.8751$ is a parameter, which depends on the amplitude of a certain vibration mode and was calculated for the first ten modes by Butt and Jaschke [46]. If one is using the second mode (as shown in fig. 2.18), the prefactor 0.8174 is changing to 0.251, because α_1 gets replaced by $\alpha_2 = 4.6941$. Using a cantilever with a tip, an additional torque has to be taken into account which leads to the force

$$F = \frac{k_0 s \Delta V}{\left(1 - \frac{3D}{2L} \tan \alpha\right) \cos^2 \alpha} \quad (2.28)$$

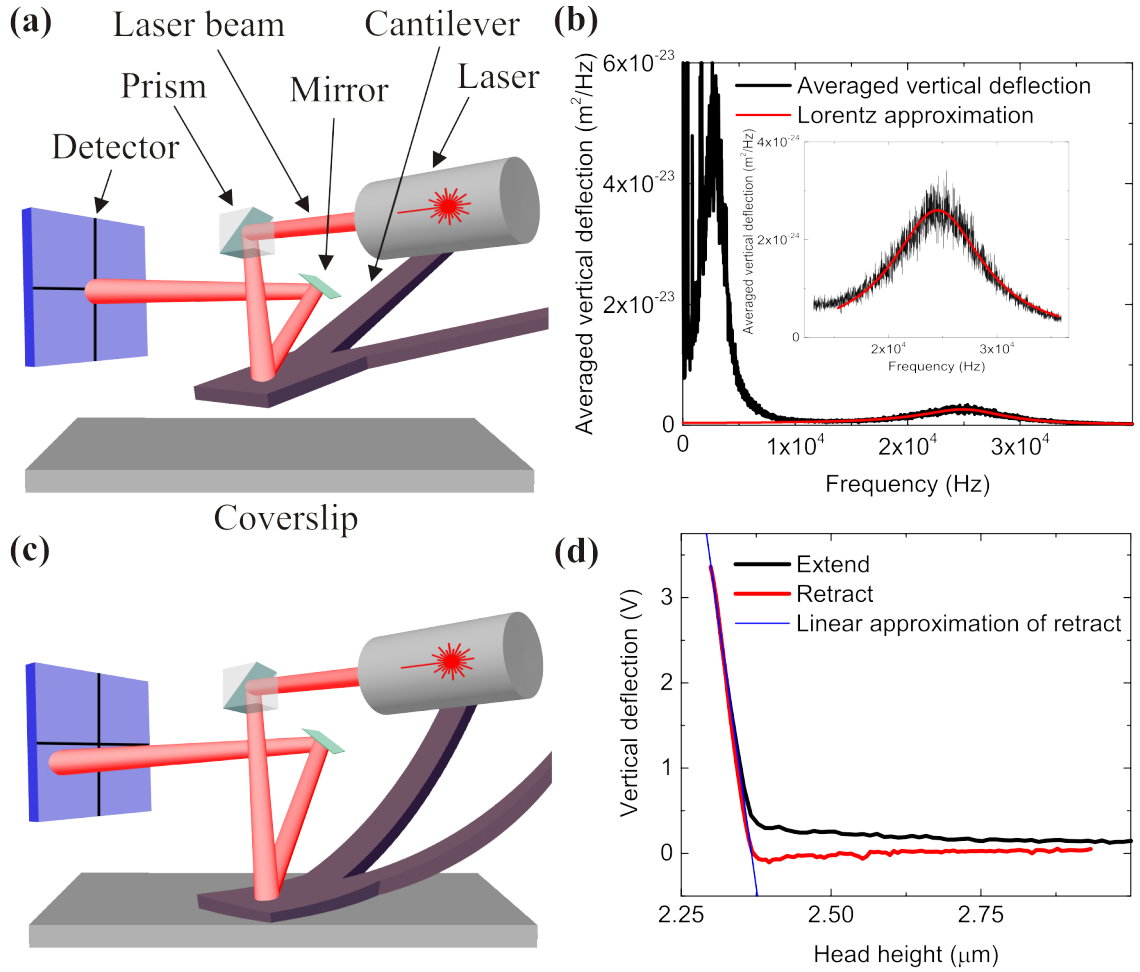


Figure 2.18: Main components of the AFM (a) with no contact of the cantilever with the substrate, which is used for the measurement of the sensitivity (b). The cantilever in contact with the substrate (c) leads to a significant change in vertical deflection, which is used for the measurement of the spring constant (d).

where D is the height of the tip and L is the length of the cantilever. For the fundamental mode this is resulting in the correction factor

$$k_0 = 0.8174 \cdot \frac{k_b T}{s^2 P} \cdot \left(\frac{1 - 3D \tan \frac{\alpha}{2L}}{1 - 2D \tan \frac{\alpha}{L}} \cdot \cos \alpha \right)^2 \quad (2.29)$$

where the prefactor has to be exchanged as in 2.27, if the second mode is used.

2.2.3.3 Elasticity models

In 1896 Hertz [94] showed that an elastic deformation of two elastic bodies leads to a deformation in shape and size of those bodies. Expanding this observation further by using contact equilibrium energy in combination with attractive forces of the two bodies led to a modified formula of this problem [105] as shown in fig. 2.19 (a). This research resulted finally in a correlation between the force of indentation and the Young's modulus of the surface, which is known as the "Hertz approximation":

$$F_{Hertz} = \frac{4}{3} \cdot \frac{E_S}{1 - \nu_S^2} \cdot \sqrt{R_T} \cdot \delta^{\frac{3}{2}} \quad (2.30)$$

where F_{Hertz} is the force applied to the surface, E_S is the Young's modulus, ν_S is the Poisson ratio, R_T is the radius of the tip of a paraboloid and δ in the indentation depth.

Using elementary mathematical methods Sneddon [176] solved the problem to penetrate an elastic body with a non-elastic cone, which lead to the so called "Sneddon approximation":

$$F_{Sneddon} = \frac{\pi}{2} \cdot \frac{E_S}{1 - \nu_S^2} \cdot \tan(\alpha) \cdot \delta^{\frac{3}{2}} \quad (2.31)$$

where α is the angle between the middle axis and the surface of the cylinder as depicted in fig. 2.19 (b).

Considering the non-axisymmetric problem of a regular four-sided pyramid Bilodeau [31] took the contact area and the normal stress by maximization of the indenting force into account, which is shown in fig. 2.19 (c). This leads to final formula, which JPK is using for the data analysis for pyramidal indenters:

$$F_{Bilodeau} = 0.7453 \cdot \frac{E_S}{1 - \nu_S^2} \cdot \tan(\alpha) \cdot \delta^2 \quad (2.32)$$

If the used pyramid (tip) is not quadratic regarding the base area as depicted in 3D in fig. 2.20 (a), the angle α is not clearly defined. As a consequence of the detailed 3D view, there are three different angles between the tip of the pyramid and the sharp sides for the MLCT cantilevers from Bruker: $\beta = 25^\circ$, $\gamma = 15^\circ$ and $\varepsilon = 17.5^\circ$.

Due to the fact that there was no theory found about a pyramid like this in our analysis an angle of 18.75° was used. This is the result of averaging the four existing angles of this pyramid-like tip (while ε is used twice).

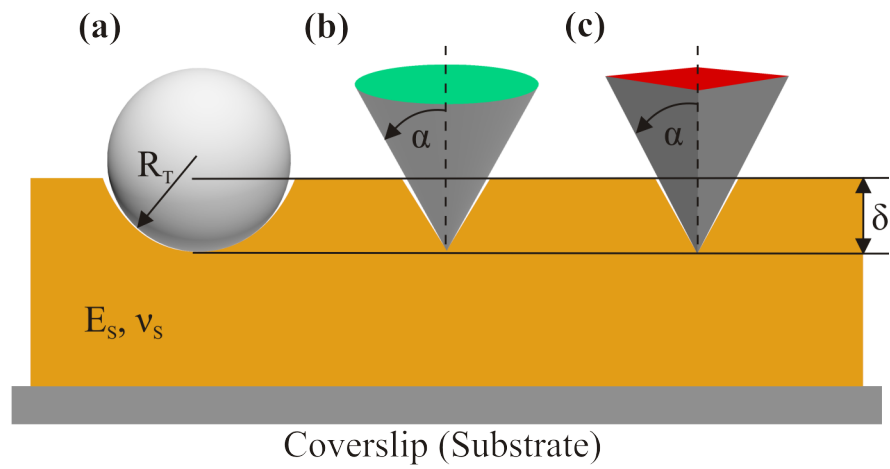


Figure 2.19: The indentations into an elastic body (orange) of (a) the tip of a paraboloid, (b) a cone and (c) a quadratic pyramid.

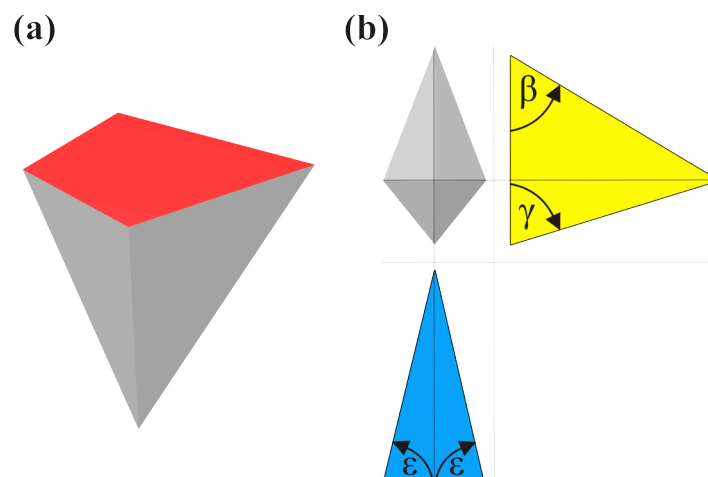


Figure 2.20: The used cantilever tip in 3D (a) is shown from the side views (b).

2.2.4 UV/Vis Spectroscopy

Light spectroscopy is a technique based on the fact that atoms are able to absorb, emit or scatter light with a certain likelihood. If a photon of the energy $h\nu$ (where h is the Planck's constant and ν is the frequency) hits an atom it can reach an excited state. This process is called absorption. The returning to a lower state with the emission of a photon is called inelastic scattering. In the case that the energy of the photon is too low to excite the atom an elastic scattering appears. Processes like absorption, elastic and inelastic scattering are rather complex and theoretically described in several publications via quantum mechanics [19, 59, 38, 84, 181, 120].

These effects are used to measure spectra, which are representing the relation between energy (typically in the sense of absorption) and the wave lengths of light. These measurements are typically performed with a spectrometer. In such a device the light of e.g. a xenon flash lamp is split into its spectral colors while a slit is creating a single wave length (monochromator). The light reaches the detector after passing through the sample that is typically in a glass or plastic cuvette. Depending on the spectrometer the control measurement (no probe) is performed in advance ("single beam spectrometer") or in parallel to the sample measurement ("dual beam spectrometer") as depicted in fig. 2.21 for the used UV/Vis photospectrometer Genesys 6 (Thermo Spectronic, Waltham, MA, USA). UV/Vis (ultraviolet/visible) in this context is related to the applicable wavelengths that are 190 nm to 1100 nm for this specific instrument and therefore in the ultraviolet or UV (ca. 200 -380 nm) and visible or vis (ca. 380 - 800 nm) range of light.

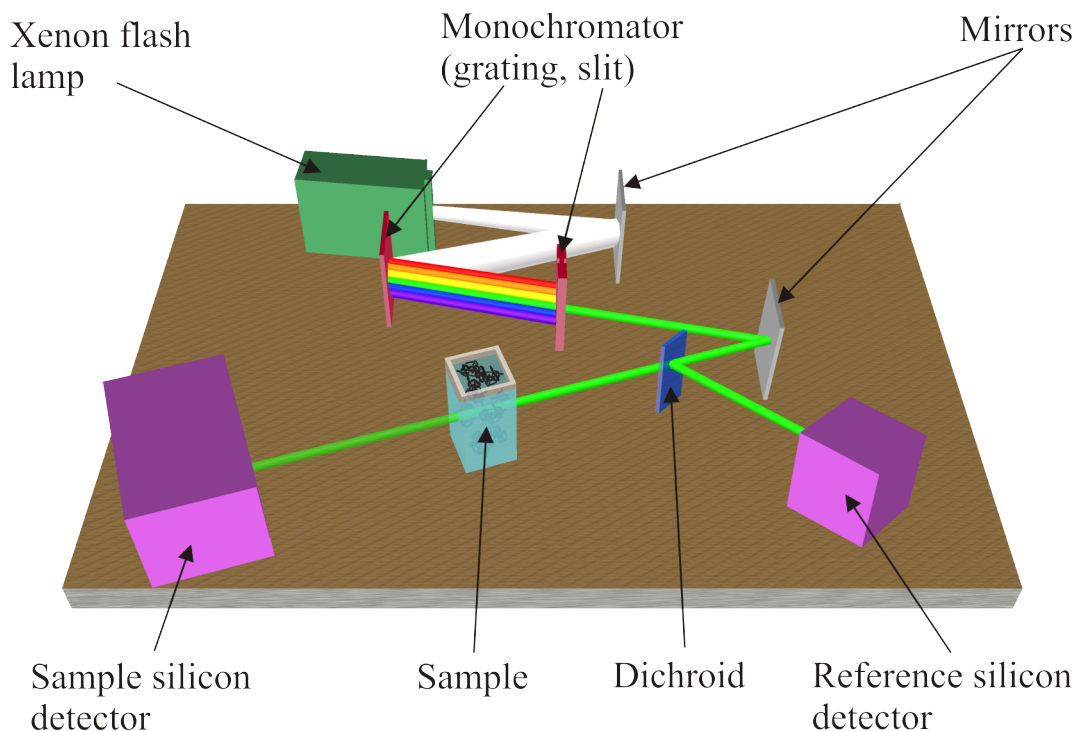


Figure 2.21: The setup of a dual beam spectrometer includes a light source whose light is reduced to a single wave length by a monochromator. A dichroic mirror is splitting the beam into one that is passing the probe and reaching the sample detector and one that is directly reaching the reference detector.

Depending on the optical properties of a probe the absorption and consequently the spectrum at a certain wave length range differs from zero. With such a spectrum one can e.g. determine the concentration of macromolecules in solution by knowing the concentration dependency on the absorption. This process is described by the Lambert-Beer's law

$$E_{\lambda} = \log \left(\frac{I_0}{I_1} \right) \propto c \quad (2.33)$$

in which E_{λ} is the extinction (as a measure for the absorbance), I_0 is the intensity of the light before passing the sample, I_1 is the intensity of the light after passing the sample and c is the concentration of e.g. the macromolecules in the solution. In practice one can e.g. measure several macromolecular concentrations and correlate a specific wavelength to its value of absorption per concentration [19, 120]. In the end, knowing the absorption leads to the knowledge of the concentration.

As an example in the case of potentially adsorbed macromolecules onto the RBCs the concentration of macromolecules in the supernatant after the sedimentation of

RBC would change as illustrated in fig. 2.22, which can be measured with e.g. UV/Vis spectroscopy.

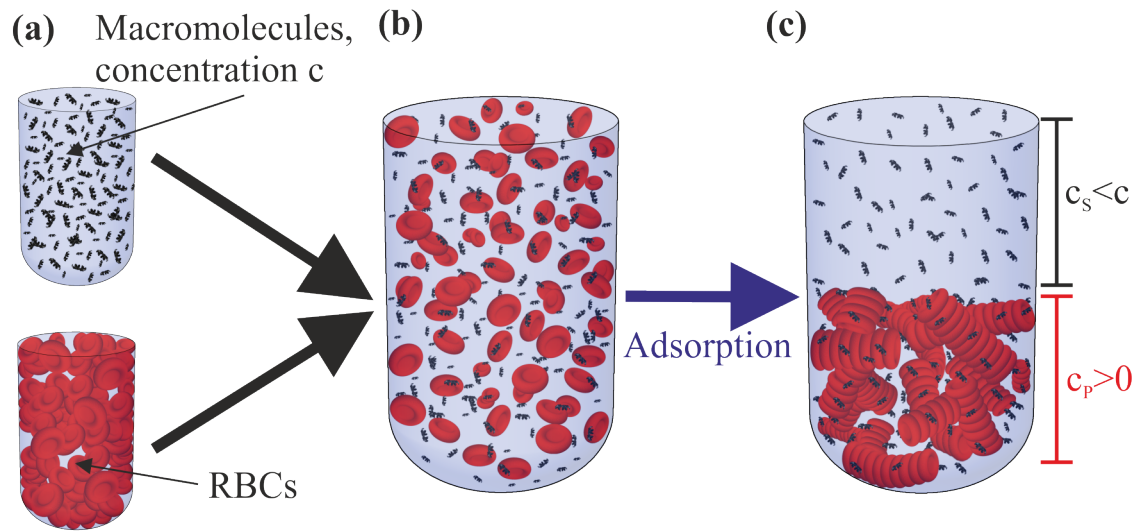


Figure 2.22: If 45 % RBCs and macromolecules of a concentration c (a) are mixed with 55 % macromolecule solutions (b) it could lead to a sedimentation where the macromolecules are adsorbed to the RBC (c). The concentration of the supernatant is indicated by c_s while the concentration of the pellet is indicated by c_p .

2.2.5 Surface acoustic waves (SAW)

The fundamentals for surface acoustic waves (SAW) were developed by Pierre Curie and Paul-Jacques Curie describing the piezoelectric effect as well as by John William Strutt describing the principle of a surface acoustic waves at the end of the 19th century. The SAW is an acoustic and mechanical wave that is spread linearly onto a piezoelectric material (for SAW e.g. lithium niobate is commonly utilized). Practically, this is realized with biosensors that convert an electrical signal (such as a radio frequency) via the input interdigital transducer (IDT) into a polarized transversal wave which is propagated onto the piezoelectric material. This wave is again converted via the output IDT into an electrical signal that is measured. As illustrated in fig. 2.23, the wave itself is not spread over the whole piezoelectric material, but it forms a rather thin guiding layer that can be in the range of several microns in height an length [87, 113, 153, 169].

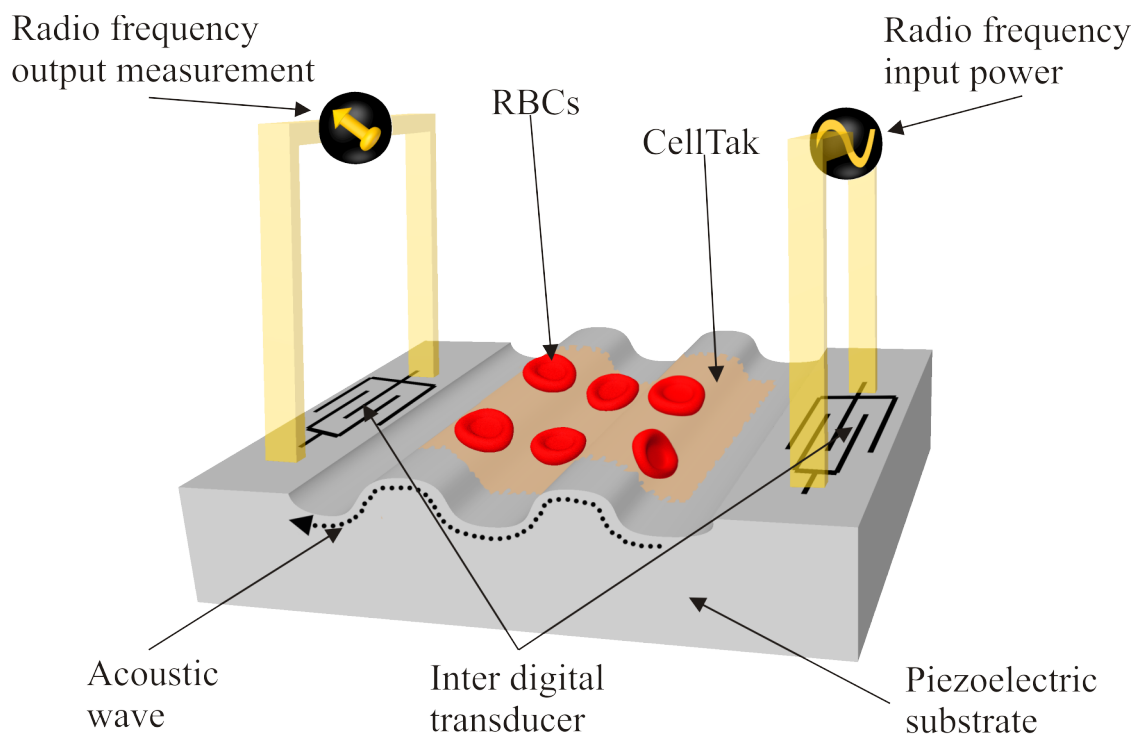


Figure 2.23: The SAW setup includes the in- and output IDT as well as the piezoelectric material on that the acoustic wave is transversally propagated. RBCs adhered to the cell-adhesive “CellTak” are taken as an example for a biofilm.

Connecting this system with any medium leads to a change in phase and amplitude of the wave. If parts of the medium such as macromolecules or antibodies bind to the surface of the piezoelectric material the wave is disturbed and the change in phase and amplitude can be measured as depicted in fig. 2.24 (b) for the example of

adhered RBCs to the substrate. Practically, the medium can be changed because of the combination with a flow chamber in which the setup is embedded. Changing the medium to one that is preferred by the macromolecules or antibodies in comparison to the substrate or e.g. RBCs the molecules are detached as shown in fig. 2.24 (c). This procedure results first in an increased phase/decreased amplitude and as soon as the medium is flowed over the substrate the phase decreases while the amplitude increase until reaching the initial condition (if all macromolecules or antibodies are detached).

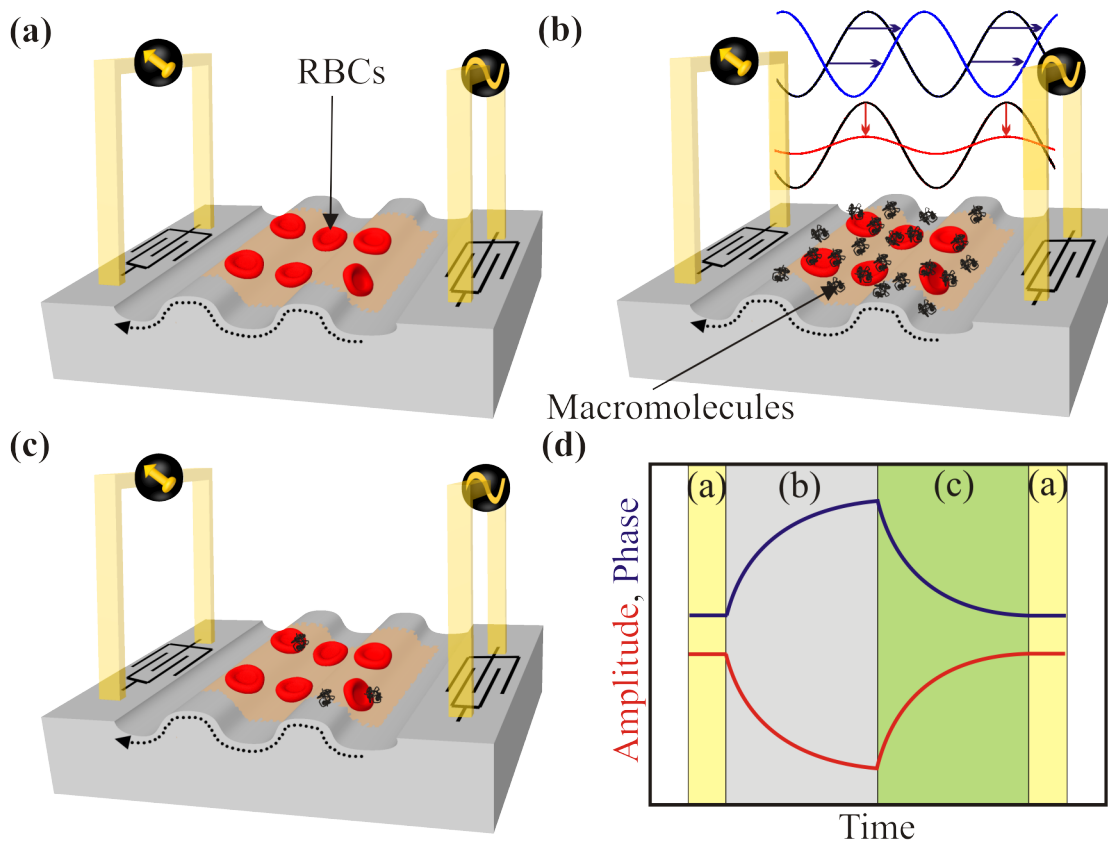


Figure 2.24: A surface acoustic wave (a) is changing its phase if e.g. a macromolecule adhere to the biological substrate and its amplitude if e.g. the substrate becomes more flexible (b). This behavior is (fully or nearly) reversible if the molecules don't have an severe effect on the substrate (c), which can be shown in relation to the time (d). Colored areas are directly related to the letters of these figure.

As a consequence of the surface acoustic waves a change in phase can be directly related with a change in mass and a change in amplitude can be directly related with a change in flexibility of the attached molecules or RBCs. With an increasing frequency (nowadays frequencies in the range of 500 MHz are possible) the resolution

can theoretically reach 10^{-15} g in mass change, which makes the device suitable for even rare binding events [165].

SAW measurements were performed with the SAW samX biosensors. The producer SAW instruments (GmbH, Bonn and Munich, Germany) was overtaken by NanoTemper (NanoTemper Technologies GmbH, Munich, Germany) that creates a SAW instrument called Seismos NT.X based on the samX technique. The gold based biosensor chips have now five independent (at the time of measurement there were eight) flow channels that could be utilized for independent measurements.

2.3 Measurement techniques and preparation protocols

2.3.1 Sedimentation measurements

The sedimentation of RBCs is directly related to the clustering process of RBCs [26]. Therefore, the erythrocyte sedimentation rate (ESR) was quantified in some measurements to characterize the RBC aggregation and their influence on the sedimentation. In order to control the clustering process washes RBCs (compare chapter 2.3.3) were added to macromolecular solutions without the addition of human plasma. Two methods were occupied to measure the sedimentation of RBCs: DSLR-imaging and UV/Vis spectroscopy at $23\pm 0.5^\circ$ C.

DSLR-imaging was performed with the commercial DSLR-camera Canon EOS 550D with a EF-S 18-200 mm lens (Canon, Tokyo, Japan). The RBC suspensions were filled into different sedimentation tubes or the cuvettes 170-QS (Hellma Analytics, Muellheim, Germany). Imaging was performed between one and three hours by taken a picture typically every 5 min.

UV/Vis spectroscopy was performed with the spectrometer Genesys 6 (Thermo Scientific, Waltham, MA, USA) at 940 nm, which is approximately the adsorption wavelength of hemoglobin. Three suspensions were filled into three 170-QS cuvettes, while one cuvette were always filled with the reference solution (i.e. the solution in which the RBCs were suspended). These four measurements were performed in parallel every minute.

2.3.2 Microscopical aggregation index

The microscopical aggregation index (MAI) was already introduced for RBCs by Chien and Jan [52] and overtaken by Kiesewetter [112]. The MAI is a measure how many cells are aggregated. After a 5 min sedimentation time an microscopic image is taken and the number of aggregated cells is related to the total number of cells. For the experiments presented in this work a control sample was left at rest for 5 min at 37° C under the microscope before an image was taken. Control sample refers here to a Ringer solution (0.5 % human serum albumin, pH adjustment to 7.4 and dextran added in the same concentration as the test sample) in which 1 % RBCs are suspended. The same procedure was performed with the test sample (e.g. 1 % RBCs in a 20 mg/ml dextran solution). Chien and Jan defined the MAI as the number of cellular units (a single non-aggregated cell as well as an aggregate counts as one cellular unit) per unit area of the control sample which is divided by the total number of cells for the test sample. This means that the MAI of Chien is a comparison between the RBC aggregation in a modified (Ringer solution) to an unmodified solution (test sample). Being interested in the relative number of aggregated cells here the MAI is defined without taken a control sample into account. Thus, for all aggregation conditions (several concentrations and different macromolecules) the total number of aggregates N_{agg} was divided by the total number of cells N_{cells} per image and therefor the MAI is defined as

$$MAI = \frac{N_{agg}}{N_{cells}} \quad (2.34)$$

which means that if the MAI is e.g. 0.5 that 50 % of the cells are aggregated. In order to increase the statistics the whole image (typically approximately 144x144 μm) was taken as the “unit area”. The probability of collision events for RBCs and therefore for the increase for the probability of clustering is dependent on the cell concentration. Here 10 % RBCs are used (see appendix fig. 5.10), which leads to a total number between 400 and 600 cells per image depending on the viscosity of the concentration of macromolecules, because all images were taken after 5 min and the sedimentation rate depends on the macromolecular concentration. In addition, this is closer to the physiological condition of approximately 45 % hematocrit than lower hematocrit concentrations though a very high cell concentration regarding microscopical investigations. All measurements were performed at a room temperature of $23 \pm 0.5^\circ \text{C}$ in a suspension of three components: PBS as buffer, macromolecules and RBCs. The membranes of RBCs were labeled with CellMask (TexasRed). A cell was counted as a part of the cluster if the the membranes were optically not distinguishable over a range of at least 3 μm . The MAIs of at least three images, which were taken after 5 min for all concentrations, were averaged.

2.3.3 RBC preparation

Blood was drawn from donors by either a needlestick into the finger or by a needlestick into the vein and filled into EDTA tubes (S-Monovette; Sarstedt, Nümbrecht, Germany). The first method results in a total volume of 1-10 μl (this wide range is reasoned by the position of the needlestick, the temperature, coagulation behavior etc.). The second method results in a total volume of 9-126 ml (9 ml is the filling level of one tube and here a maximum of 14 tubes was drawn at one day). In order to separate the plasma and the buffy coat from the RBCs (pellet, which contains 20 % of plasma as well) the blood was centrifuged at 704 g for 3 min. Plasma and buffy coat were carefully removed. The same amount as removed was replaced by PBS, intermixed carefully by hand and centrifuged again. This procedure was repeated three times in order to reduce the protein concentration by a factor of ca. 650. The pellet itself contains ca. 80% RBCs, which was determined with a spun hematocrit centrifuge (see next chapter). Small amounts of blood ($< 10 \mu\text{l}$) were centrifuged with the centrifuge 5415C (Eppendorf AG, Hamburg, Germany). Large amounts of blood ($> 10 \mu\text{l}$) were centrifuged with the Z326K (Hermle Z326K, Hermle Labortechnik GmbH, Wehingen, Germany).

The RBCs were stored at 4 °C. All measurements were performed within four hours after blood drawing. The only exceptions were rheological measurements where a huge amount of blood was needed. For this purpose the RBCs were stored for at least eight hours. Cross-checks after a storage of 24 to 36 hours leads not to a significant change regarding the results.

2.3.4 Hematocrit concentration of the pellet

A centrifugation with 704 g for 3 min leads to a RBC pellet which consists of approximately 80% RBCs and 20% plasma or PBS. Those values were determined with the spun hematocrit centrifuge (ZFA (centrifuge); OSC.tec, Erding, Germany) at 10000 and 15000 g for 10 min using capillary tubes (1.2 mm diameter, 10 cm height) by measuring the height of the supernatant by eye with a mm-scale.

2.3.5 Osmolality

The osmolality is a measure for the osmotic pressure. Therefore, the osmolality for most of the used solution was measured by the vapor pressure osmometer VAPRO (Wescor VAPRO Model 5520; Wescor Inc., South Logan, UT, USA). A solute-free paper disc became wetted with 10 μl of the solution. The whole measurement took 80 s per sample.

2.3.6 Filtering of fibrinogen and used macromolecular concentrations

Fibrinogen from human plasma (Sigma-Aldrich, St Louis, IL, USA) as provided by Sigma Aldrich contains approximately 40% salt (15% sodium citrate and 25% sodium chloride), which is most probably used to stabilize the protein long-term. High amounts of those salts has a significant influence on the RBC shapes. In order to use pure fibrinogen it was necessary to remove the salt from the protein. Adding 120 mg fibrinogen to 3 ml distilled water the solution was ultrafiltrated with a 10 kDa filter (Vivaspin Turbo 4; Satorius AG, Goettingen, Germany) at 3500 g for 1 hour by removing the salt and adding approximately 2 ml of PBS to the upper fibrinogen part depicted in fig. 2.25. This procedure was repeated at least 10 times. The remaining protein solution was freeze-dried (over 12 hours), resuspended into PBS immediately and measured within 12 hours after freeze-drying. The osmolality of the resulting fibrinogen solution was in the order of PBS (+/- 5%) for all measured concentrations, called “saltfree”.

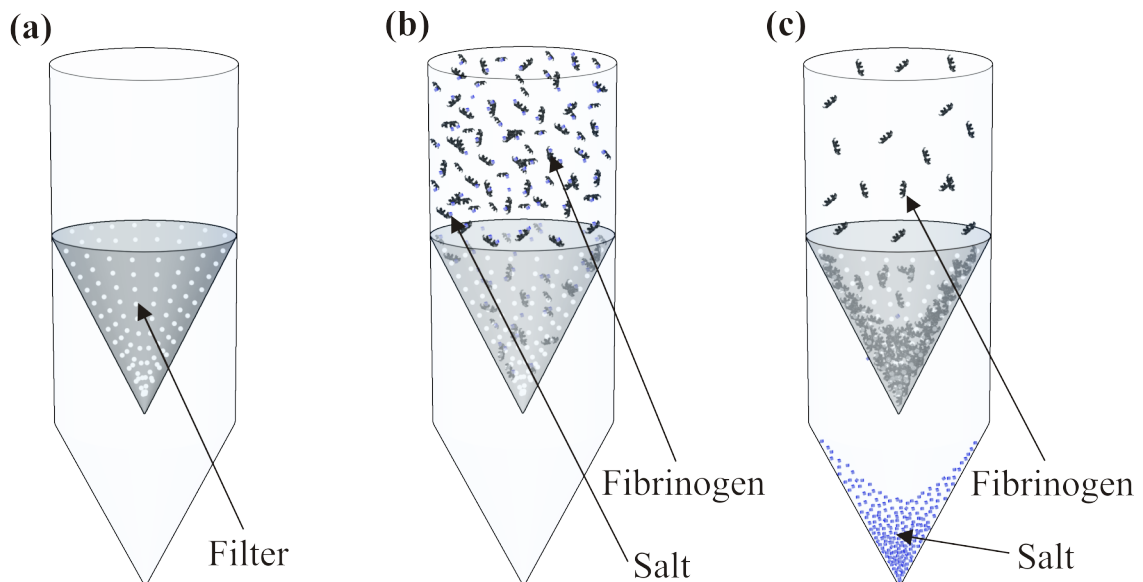


Figure 2.25: On top of the filter inside a 15ml Vivaspin tube (a) the fibrinogen as provided by Sigma Aldrich dissolved in H_2O was added (b). After one centrifugation procedure some salt diluted in distilled water remains on the bottom of the 15 ml tube, while the fibrinogen can't pass the 10 kDa filter (c). The lost volume was replaced by H_2O and after mixing the procedure was repeated at least 10 times (one hour between the addition of H_2O).

Fibrinogen and all other macromolecular solution were prepared in a non-molar way that means: The amount of macromolecules A_u was weighted and one ml of PBS was

added. This leads to the label A_u mg/ml. In contrast, some publications are using a molar way to create their solutions. It means that the amount of macromolecules A_m was weighted and that much PBS was added until the volumetric flask reaches the measuring line (that marks the volume of e.g. 1ml). Due to the fact that this method is based on the human eye accuracy in combination with a cone formation due to capillary effects the non-molar way of preparation was used. In order to compare both ways the density of the molar way was measured and compared to the non-molar way as depicted in fig. 5.9. The result is that for both fibrinogen and dextran the molar way leads to a ca. 4% higher concentration in comparison to the non-molar way.

2.3.7 Cell-Tak functionalization protocol

In order to fixate RBCs to dishes, cantilevers etc. Cell-Tak (BD Cell-Tak adhesive; BD Biosciences, Bedford, MA, USA) was used. It is a formulation of “polyphenolic proteins” that are extracted from the marine mussel *Mytilus edulis*.

Instead of the so called hand-spreading method (coating with the pure Cell-Tak, which is rinsed after ca. 20min with water and ethanol) here the adsorption method was used for all measurements. First, one have to mix e.g. 10 μ l of Cell-Tak, 285 μ l of sodium bicarbonate (0.1 M at a pH of 8.0) with NaOH (1N), which have to be added immediately before coating. Second, one have to append the solution to the substrate (wells, dishes etc.) or the parts one want to coat (e.g. cantilevers) to the solution. Third, waiting for min. 20 min and rinse either the substrate or the parts with distilled water and possibly PBS (as it was done with the cantilevers for AFM experiments) leads to the resonance effort. According to the manufacturer the coated parts can be stored up to two week at 2°-8° C [33]. Nevertheless, for the presented measurements all coatings have been performed immediately before the experiments begun (less than one hour).

2.3.8 BSA coating protocol

Due to the fact that RBCs show a strong interaction with plastic and glass surfaces with a significant change in shape (e.g. from discocytes to echinocytes) [66] is was necessary for some measurements (e.g. cell-cell adhesion and contact zones) to coat the wells/dishes with BSA (Bovine, Serum Albumin; Sigma-Aldrich, St Louis, IL, USA) in order to minimize those effects. Therefore, 1 mg BSA was solved into 1 ml of PBS (phosphate-buffered solution; Life Technologies, Waltham, MA, USA). This solution was added to the substrate for an incubation time of 30 min. After removing the solution and rinsing with PBS the wells/dishes were dried either by air pressure (for cell-cell adhesion measurements) or by a 10 min incubation time at 37° C (for contact zone measurements).

2.3.9 CellMask protocol

In order to visualize RBCs with e.g. a confocal microscope it is necessary to label the cells with a fluorescein dye. CellMask (Life Technologies, Waltham, MA, USA) deep red (649/666 nm) are amphiphilic molecules with a lipophilic part for membrane loading and hydrophilic dye that is negatively charged [184].

0.1 μl of CellMask were added to 200 μl of RBC which were diluted into 1 ml of PBS (for needlesticks into the finger). After the addition of 0.1 μl of CellMask to the suspension the incubation time was set to 10 min. Washing the suspension three times with PBS leads to stable stained (regarding confocal imaging) RBCs between 60 and 90 min. Nevertheless, with time the dye diffuses into the solution due to its hydrophilic part.

2.3.10 Overview of main devices and consumables

Notation	Number	Manufacturer
AFM CellHesion module	200	JPK instruments
AFM NanoWizard module	3	JPK instruments
Centrifuge	5415c	Eppendorf
Centrifuge	Z326K	Hermle
Cuvette	170-QS	Hellma Analytics
Microhaematocrit Centrifuge	XC-2001	premiere
Leica TCS point scanning microscope	SP5	Leica Microsystems
Rheometer	MCR 702	AntonPaar GmbH
UV-Vis spectrometer Genesys	6	Thermo Spectronic
VAPRO vapor pressure osmometer	5520	Wescor Inc.
Yokogawa spinning disk scanner unit	CSU-W1	Yokogawa Electric Co.

Table 2.1: Overview of the main devices.

Notation	Number	Amount	Manufacturer
BSA	SLBN2104V	10 g	Sigma Aldrich
Cell-Tak cell and tissue adhesive	354240	100 μ l	BD Biosciences
CellMask Plasma Membrane Stain	C37608	100 μ l	Life Technologies
Human C-reactive protein 1mg/ml	031567	500 μ l	Academy Biomedical Co.
Dextran from Leuconostoc Mesenteroides wt 64,000-76,000	SLBL9703V	100 g	Sigma Aldrich
FITC-dextran: Fluorescein isothiocyanate-dextran av. wt 70,000	BCBP1019V	100 mg	Sigma Aldrich
FITC-dextran: Fluorescein isothiocyanate-dextran av. wt 2,000,000	BCBK4227V	1 g	Sigma Aldrich
Fibrinogen from human plasma 50-70% protein	SLBK3747	5 g	Sigma Aldrich
Fibrinogen from human plasma AlexaFluor 488 conjugate	1701953	5 g	Life Technologies
HES	B05AA07	500 g	Fresenius Kabi
PBS	10010-31	1 l	Life Technologies
BLOOD	-	entire ca. 6.25 l	self-made
Cantilever MLCT	-	10 pcs	Bruker AFM probes
Cantilever MLCT-O10	-	10 pcs	Bruker AFM probes
uncoated 60 μ -dish, 35mm, low	80131	60 pcs	Ibidi
EDTA tubes K3E	6030211	50 pcs (9 ml)	Sarstedt
μ -slide 18-well treated	140922/3	15 pcs	Ibidi
Vivaspin Turbo 4 10kDa	1601008VS	25 pcs (15ml)	Satorius AG

Table 2.2: Overview of the main consumables.

3 Results

3.1 Rheology and sedimentation

RBCs are the main cellular component of blood and are responsible for the peculiarities of blood viscosity. In order to understand how blood is flowing the aggregation of RBCs was controlled by the addition of dextran to a buffer solution, which leads to well defined experimental parameters without the variability of plasma between different samples. The rheology of such a complex mixture is influenced by the aggregation effect as well as the viscosity of the surrounding solution (suspending phase). So as to separate these effects a normalization is necessary, which is performed in literature by dividing the measured viscosity by the viscosity of the stock solution (i.e. the viscosity of the suspending dextran solution before suspending the RBCs in it). The adsorption of macromolecules onto the RBCs modifies the viscosity of the suspending phase and therefore that effect has to be taken into account performing a normalization of such rheological data.

The bell-shape behavior of RBC viscosity as a function of the dextran 70 kDa concentration is investigated with a classical shear rheometer. The normalization of the data depends on the amount of dextran adsorbed to the cells. It is shown that the position of maximum of the bell-shape curve increases with increasing viscosity of the suspending phase. This indicates that the (dis)aggregation processes are a result of hydrodynamic interactions, which can be suppressed by high hematocrit suspensions of ca. 80%.

The yield stress is the stress at which a fluid starts to flow. Blood and red blood cells are assumed to be yield stress fluids [155]. An issue with yield stress measurements is that the yield stress can be only extrapolated, i.e. not measured directly, because one cannot determine a viscosity at a shear rate of zero with the present techniques. Therefore, the shear stress in dependence on the shear rate can be measured from a low shear rate range to the lowest resolution limit of e.g. a commercial rheometer and the resulting curve is approximated and extrapolated to a shear rate of zero, which is called “extrapolation method”. Hence, yield stress measurements with the classical extrapolation methods leads to the assumption that the yield stress is depending on the resolution limit of the rheometer that could finally indicate a non-existing yield stress for infinite resolution limits. Nevertheless, it is assumed to be a useful concept, because it mirrors the bell-shape behavior of the flow dependency measurements.

RBCs in solution sediment which can influence the rheological data significantly. Hence, the sedimentation rates of RBCs in dextran solutions were measured in order to determine timescales over which rheological measurements can be made without significant influences of sedimentation effects. In addition, the bell-shape was shown for blood sedimentation similar to the clinical blood sedimentation with the statement that the sedimentation rate is increasing with the diameter of the sedimentation tubes.

3.1.1 Separation of the clustering induced viscosity from the suspending phase viscosity

As measured by e.g. Maeda [127] the shear thinning behavior of blood is mainly caused by the reversible rouleaux break-up due to shear stresses. In this work, to control aggregation processes, washed (see chapter 2.3.3 for details) red blood cells were suspended in solutions of sundry dextran concentrations (see chapter 2.3.6 for details). In order to create a 45% hematocrit suspension 4400 μl of the RBC-pellet (that contains ca. 80% RBCs and ca. 20% buffer solution after a centrifugation for 3 min at 704 g) were added to 3600 μl of stock solution. Viscosity measurements were performed with two different protocols. The “up” protocol consists of first a pre-shearing at 100 s^{-1} for one minute and second a shear rate ramp including 16 logarithmic steps between 0.1 and 100 s^{-1} , in which every step was fixed to 30 s followed by an averaging time of 25 s for data acquisition. The “down” protocol is constituted of the same parameters as the “up” protocol with the different that 21 logarithmic steps between 100 and 0.01 s^{-1} are applied. To minimize the effect of the sedimentation of RBCs in suspension the CC20 Taylor-Couette geometry (outer radius of the inner cylinder: 10 mm, inner radius of the outer cylinder: 11mm) was chosen with a slight overfilling by ca. 1 cm in order to keep the cell concentration constant at the measurement position of the inner cylinder (cells can sediment from the top to the reservoir at the bottom, compare fig. 2.15 (b)). The sedimentation rate at rest for this system does not reach the measurement position of the inner cylinder within the time scale of 9 min for the “up” protocol and 11.5 min for the “down” protocol as depicted from the sedimentation measurements in fig. 3.14. Using the AntonPaar MCR702 in SMT mode (the motor connected to the outer cylinder applies the shear rate while the motor connected to the inner cylinder is measuring the stress) the shear thinning for the “up” and “down” protocol at room temperature of $23 \pm 0.5^\circ \text{ C}$ for at least three measurements with RBCs of different donors is shown in fig. 3.1 (a) and (c).

The slight viscosity increase for the “up” protocol at the lowest shear rates can be attributed to the pre-shearing and the fact that the flow field will not decrease immediately with a lower shear rate, while the pre-shearing is not affecting the system that much using the “down” protocol. Here a slight increase of viscosity for low shear rates in comparison to a stronger increase at higher shear rates appears at

the resolution limit. However, for a better comparison the data sets were analyzed in the shear rate range of the “up” protocol. The viscosities for different shear rates were plotted for seven dextran concentrations. This leads to a non-monotonic bell-shape like behavior at least for low shear rates as illustrated in fig. 3.1 (b) and (d) for the “up” and “down” protocol. Especially, for high concentrations of dextran, the bell-shape is not well pronounced which can be related to the relatively high viscosity of the stock solution (e.g. approximately 7 mPa s for 120 mg/ml dextran without RBCs). Consequently, the aggregation effects of the RBCs need to be separated from the viscosity effects of dextran. Classically, this is performed by normalizing with the stock solution viscosities, which is valid only as long as macromolecules do not adsorb onto cell membranes.

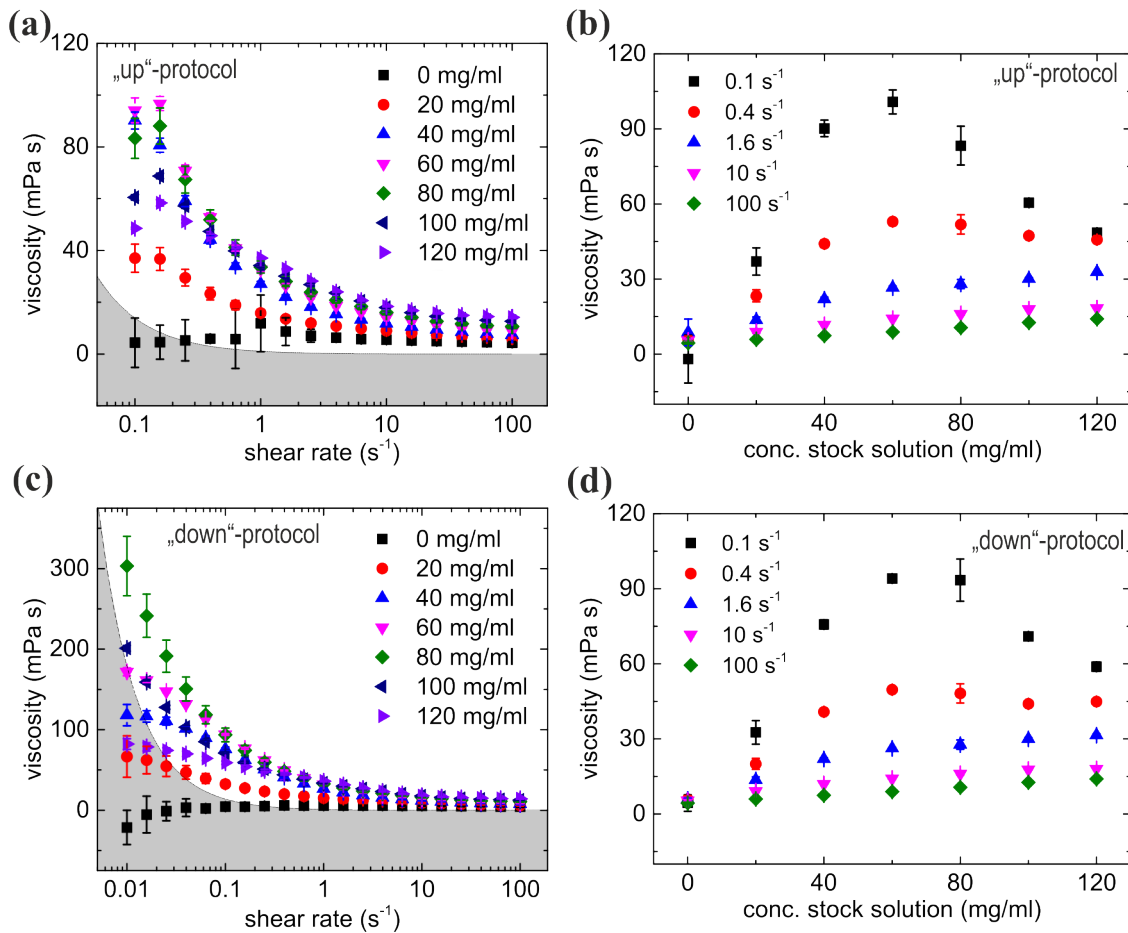


Figure 3.1: The viscosity of RBC-dextran suspensions for different dextran concentrations. (a) represents the “down” protocol and (b) represents the “up” protocol. Gray areas are the measured resolution limit of the MCR702 (with 20% tolerance, compare fig. 5.1). Respectively, in (b) and (d), the viscosities at a given shear rate for different dextran concentrations are depicted. Error bars indicate the standard deviation of at least three measurements.

If macromolecular adsorption onto RBCs is taken into account, the concentration of the suspending phase c_s after the sedimentation of RBCs will be lower than the concentration of the stock solution c as illustrated in fig. 3.2. Therefore, this influence on the viscosity of suspending phase was measured in the following way: 45% hematocrit suspensions for several dextran concentrations were created. After one hour of sedimentation the suspension was centrifuged at 704 g for 3 min in order to reduce the remaining number of RBC inside the supernatant. Pellet and suspending phase were carefully divided, the viscosity of the supernatant was measured and compared to the viscosity of the stock solution. As a control the same procedure was performed for 36% hematocrit suspensions.

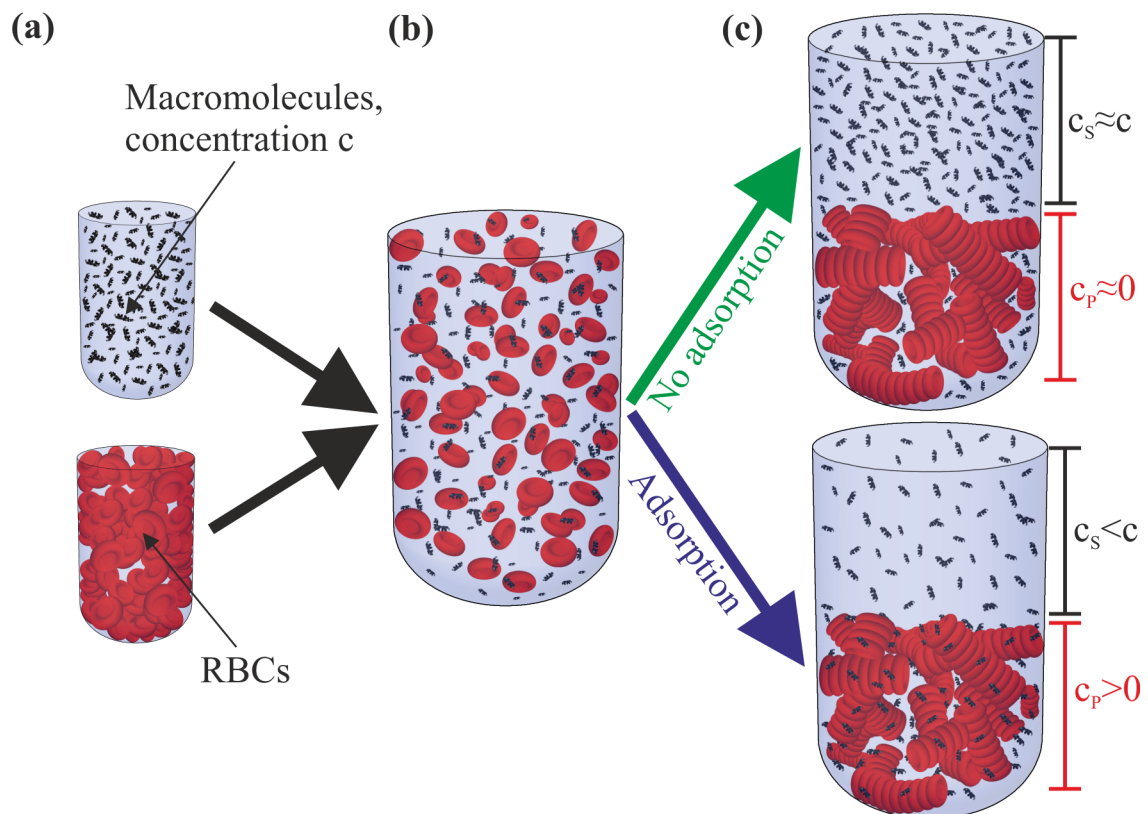


Figure 3.2: If 45 % RBCs and macromolecules of a concentration c (a) are mixed with 55 % macromolecule solutions (b) it could lead either to a sedimentation where no macromolecules are actively involved which would be the case of no adsorption (c, upper graphic) or it could lead to a sedimentation where the macromolecules are adsorbed to the RBC (c, lower graphic). The concentration of the supernatant is indicated by c_s while the concentration of the pellet is indicated by c_p .

For measurements of the stock solutions, suspending phase solutions and the pellet (see below) the CP50/2° geometry (cone plate with a radius of ca. 25 mm and

a cone angle of 2°) was used, because of low required fluid amounts (ca. 1 ml in comparison to ca. 7.5 ml for the TC-geometry) and negligible sedimentation effects of the macromolecules within the time scale of the “up” protocol. Owing to the Newtonian behavior of pure dextran solutions without RBCs the “up” protocol was performed and the apparent viscosity at 100 s^{-1} was taken as the viscosity for stock solution and supernatant. It was found that the viscosities for the stock solution and for both suspending phases (at 36% and 45% hematocrit) can be described with an empirical power law

$$\eta(c) = \eta_0 + \eta_1 e^{bc} \quad (3.1)$$

in which $\eta(c)$ is the apparent dextran 70 kDa viscosity at 100 s^{-1} , c is the concentration of the macromolecules and η_0 , η_1 and b are approximation constants as depicted in fig. 3.3 (a). The higher viscosity of the suspending phase at 36 % hematocrit indicates less adsorption onto the RBCs, which is expected due to the smaller overall RBC surface area. As illustrated in fig. 3.3 (b), around 8 % of the dextran molecules for 36 % hematocrit and around 12 % of the dextran molecules for 45 % hematocrit are adsorbing to the RBCs. Restrictively this result has to be taken with care because the macromolecules themselves can sediment as it was shown for fibrinogen in chapter 2.3.6. For dextran, the centrifugation time was only three minutes at 704 g and validation measurements have not show a significant influence of stratification, but this may depend on the position where the supernatant is sampled from the centrifugation tube (here it was always the middle height of the supernatant).

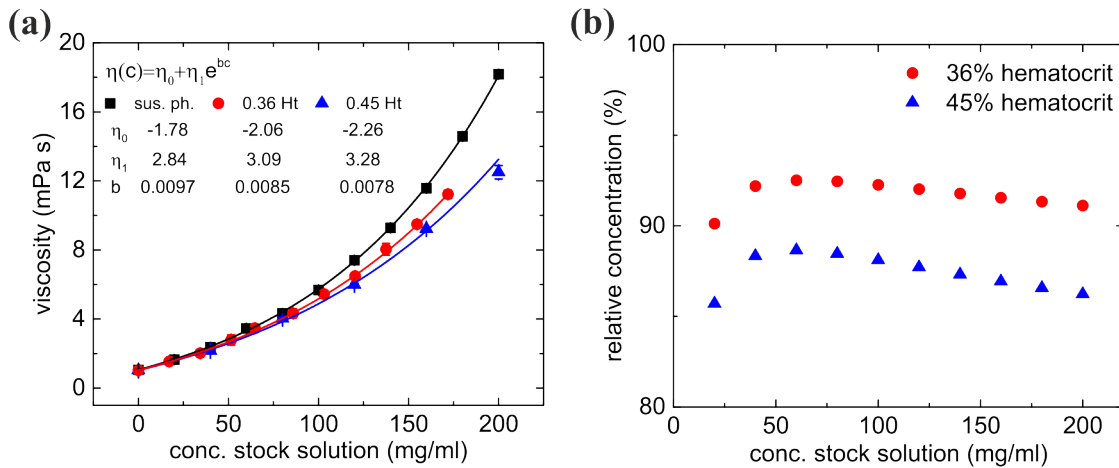


Figure 3.3: Viscosity measurements of the supernatant of a 45 % and 36 % RBC-dextran suspension after sedimentation (a) and relative concentration in dependency on the concentration of the stock solution (b).

Using the viscosities of the suspending phase for 45% hematocrit, the data of fig. 3.1 (b) and (d) can be normalized in the classical way. This leads to a pronounced bell-shape behavior as depicted in fig. 3.4 (a) and (c) for “up” and “down” protocol in relation to the concentration of the stock solution. Owing to the fact that the concentration of dextran in the suspending phase is changing with the amount of RBCs, the concentration of dextran in the supernatant can be calculated from equation 3.1 for the parameters of the suspending phase in combination with the parameters of the supernatant, which is a new way of normalizing. This leads again to pronounced bell-shape behavior with a shift in absolute viscosities as well as a shift in dextran concentration as shown in fig. 3.4 (b) and (d) for the “up” and “down” protocol compared to the classical normalization approach. Nevertheless, the qualitative curve shape appears similar, but the position of the maximum of the bell-shape, i.e. the viscosity of the suspending phase, shifting with shear rate as illustrated in fig. 3.6. Consequently, there seems to be still an underlying kinetic of (dis)aggregation processes while shearing that is probably affected by both interaction energy and macromolecule concentration.

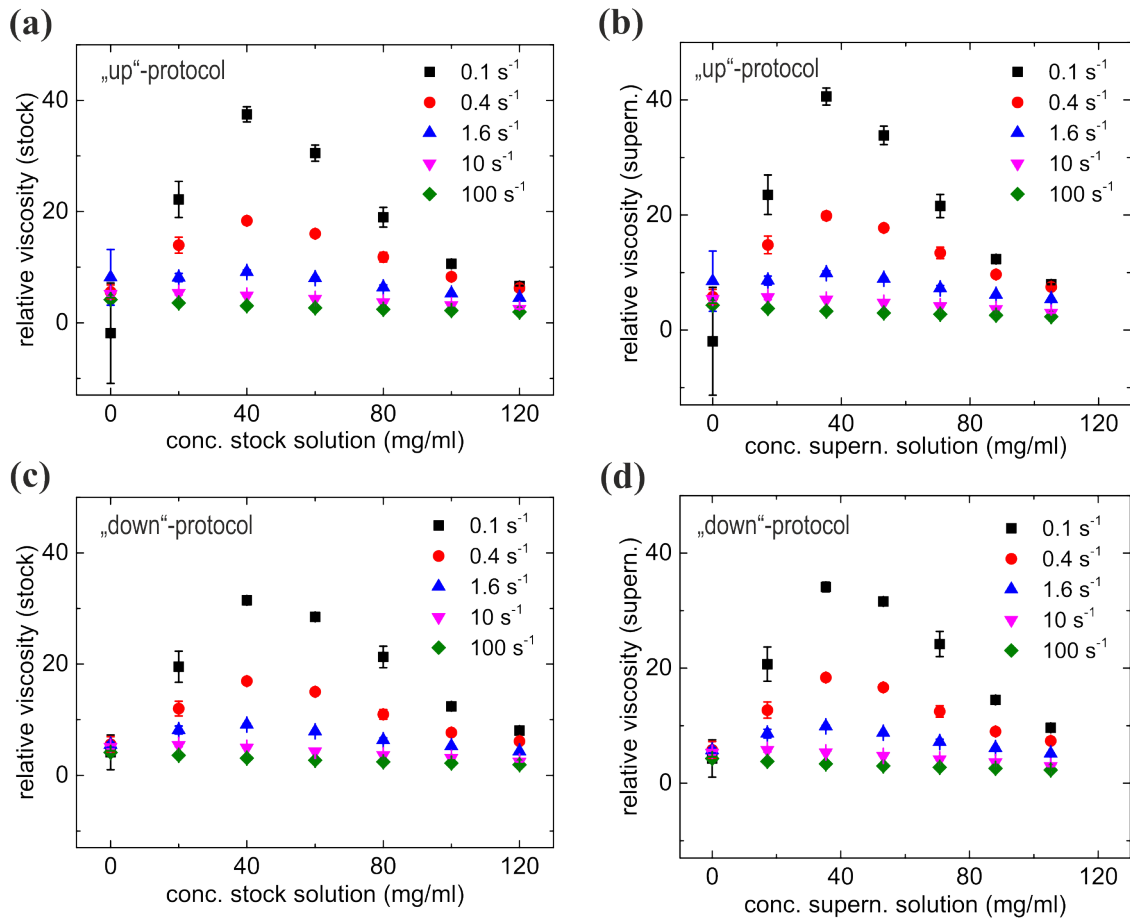


Figure 3.4: Relative viscosities of RBC-dextran suspensions for different shear rates with the (a) stock and (b) supernatant viscosities using the “up” protocol and (c) stock and (d) supernatant viscosities with the “down” protocol [79].

In order to minimize the effects of hydrodynamic coupling the pellet of RBCs with just 20% remaining suspending phase after sedimentation was measured with the “up” protocol. Again, a strong shear thinning behavior is observed with much higher viscosities as depicted in fig. 3.5, while the bell-shape is not that pronounced for high dextran concentration, which is similar for 45% hematocrit suspensions (compare fig. 3.1). This is most probably related to the fact that the remaining suspending phase concentration act as a lubricant in between the cells.

For a comparison of different methods the position of the maximum vs. the shear rate is shown in fig. 3.6. The positions of the maxima of normalized bell-shapes show a strong dependency on the shear rate as explained above. In contrast, the maximum position of bell-shape for the pellet is not affected by the shear rate, which indicates that the high cellular volume fraction is suppressing all kinetic effect transmitted by the flow field as well as minimizing viscosity effects of the suspending phase.

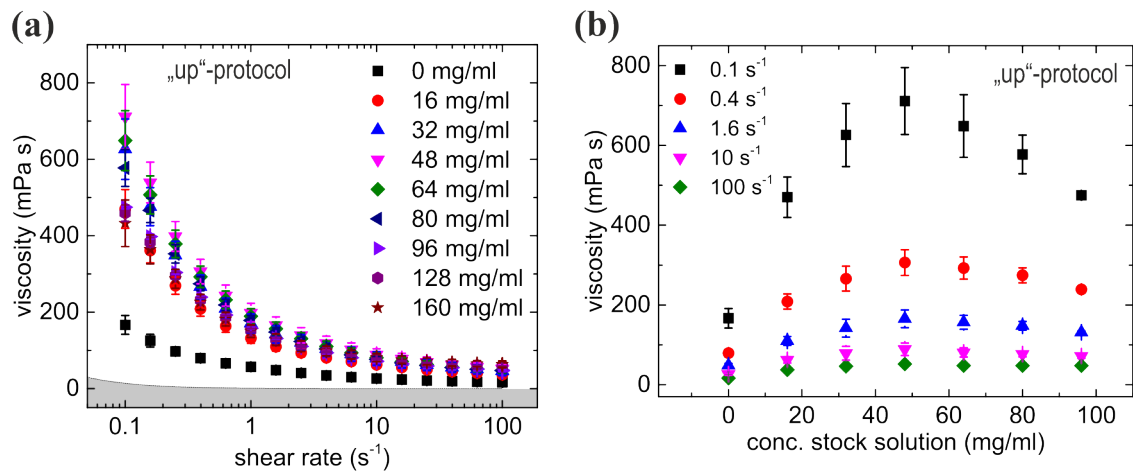


Figure 3.5: The viscosity of the pellet for different dextran concentrations using the “up” protocol (a). Gray areas are the measured resolution limit of the MCR702 (with 20% tolerance, compare fig. 5.1). Respectively, in (b) the viscosities at a given shear rate become related to the dextran concentrations. Error bars represent the standard deviation of at least three different measurements.

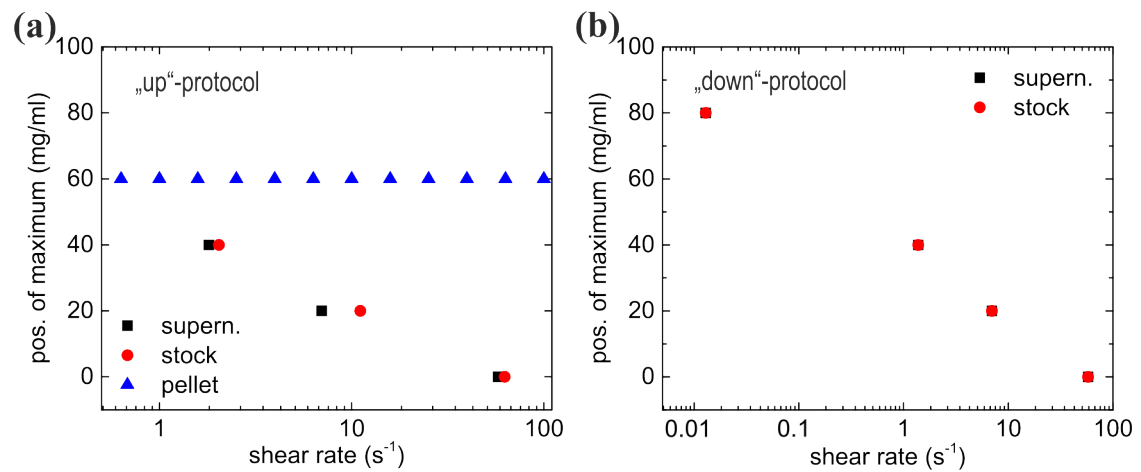


Figure 3.6: The position of maximum of normalized bell-shaped graphs, for the normalization with the stock solution and with the supernatant solution for both protocols (a) “up” and (b) “down”. In (a) the position of the maximum for the pellet is shown as well.

Summary of the normalization of rheological data in a system where macromolecules can be adsorbed

A robust protocol was presented in order to separate the effects of RBC aggregation from the suspending phase viscosity. The plasma expander dextran can be adsorbed by the RBCs and hence the supernatant viscosity should be used for a proper normalization of the rheological data. Finding that the position of the bell-shape maximum depends on the shear rate, an underlying kinetic effect is suspected, which leads to the investigation of the rheological behavior of the pellet. For the latter the position of maximum is independent on the shear rate at 60 mg/ml, which is in good agreement with all following bell-shapes using other methods (except single cell force spectroscopy due to other influences). These results are potentially applicable to colloidal and biological systems that show adsorption effects of the macromolecules in the suspending phase. From the physiological point of view, a plasma expander that does not induce secondary was not found yet. Dextran was used for a long time as a plasma expander for humans that is nowadays changed to hydroxyethyl starch (HES), which has a similar molecular structure [2, 131]. Even if HES is regraded as safe in comparison to dextran it is recommended to only use it for patients with no other diseases [195] and it shows similar adsorption and aggregation effect on RBCs (see chapter 3.2 and 3.6.1). Therefore, the rheological properties could be very similar to the ones of dextran. Hence, the presented results could influence the understanding of the rheological consequences using dextran and similar plasma expanders. This was published by Flormann and co-workers [79].

Résumé sur la normalisation des données de rhéologie pour un système dans lequel les macromolécules peuvent s'adsorber

Un protocole robuste de séparation des effets d'agrégation des RBCs sur la viscosité de la phase suspendue a été présenté. Le succédané de plasma Dextran peut s'adsorber sur les RBCs et de fait la viscosité du surnageant doit être utilisé comme facteur de normalisation des données rhéologiques. Le résultat de la dépendance du taux de cisaillement sur la position du maximum de la courbe en cloche semble impliquer un effet cinétique sous-jacent. Ceci a mené à une étude du comportement rhéologique du culot. Pour ce dernier, la position du maximum est indépendante du taux de cisaillement à 60 mg/mL, ce qui est en accord avec toutes les courbes en cloches obtenues par d'autres méthodes (exception faite de la spectroscopie sur cellule unique soumise à d'autres facteurs). Ces résultats pourraient être applicables à d'autres systèmes colloïdaux ou biologiques soumis à des effets d'adsorption de macromolécules dans la phase suspendue. D'un point de vue physiologique, aucun succédané de plasma sans effets secondaires n'a été trouvé. Le Dextran est utilisé depuis longtemps dans les plasmas humains et est de nos jours remplacé par l'hydroxyéthylamidon (HES), dont la structure moléculaire est similaire [2, 131]. Bien que le HES soit considéré comme sûr, il reste recommandé uniquement dans

le cas où le patient ne souffre d'aucune autre pathologie [195] et a montré des effets d'adsorption et d'agrégation similaires sur les RBCs (voir chapitre 3.2 et 3.6.1). Ainsi, ses propriétés rhéologiques pourraient être très semblables à celles du Dextran. En conclusion, les résultats présentés dans cette section pourraient être utiles à la compréhension des conséquences rhéologiques de l'utilisation du Dextran ou de succédanés similaires. Ceci a été publié par Flormann et collaborateurs [79].

Zusammenfassung der Normierung rheologischer Daten in einem System, in dem Makromoleküle adsorbieren können

Es wurde ein robustes Protokoll präsentiert, um die Aggregationseffekte roter Blutzellen von der Viskosität der suspendierenden Phase zu separieren. Der Plasmaexpander Dextran kann an roten Blutzellen adsorbieren und daher sollte die Überstandsviskosität für eine korrekte Normierung rheologischer Daten verwendet werden. Das Resultat der Abhängigkeit des Glockenkurvenmaximums lässt eine zugrunde liegende Kinetik vermuten, was zur rheologischen Untersuchung des Bodensatzes führt. Für letzteres ist die Position des Maximum unabhängig von der Scherrate bei 60 mg/ml, was gut mit allen anderen Methoden, die in einer Glockenkurve resultieren, übereinstimmt (ausgenommen Einzelzellkraftmikroskopie aufgrund anderer Einflüsse). Diese Ergebnisse sind möglicherweise auf kolloidale und biologische Systeme anwendbar, die Adsorptionseffekte von Makromolekülen in der suspendierenden Phase zeigen. Vom physiologischen Gesichtspunkt aus wurden bisher noch keine Plasmaexpander gefunden, die zweiteres nicht hervorrufen. Lange Zeit wurde Dextran als Plasmaexpander für Menschen genutzt, was heutzutage durch Hydroxyethylstärke (HES) ersetzt wird, welches eine ähnliche Molekularstruktur hat [2, 131]. Obwohl HES im Vergleich zu Dextran als sicher erachtet wird, wird es nur für Patienten ohne andere Krankheiten empfohlen und zeigt ähnliche Adsorptions- und Aggregationseffekte bezogen auf rote Blutzellen [195] (vergleiche Kapitel 3.2 und 3.6.1). Daher könnten die rheologischen Eigenschaften sehr ähnlich denen des Dextrans sein. Folglich könnten die präsentierten Resultate das Verständnis der rheologischen Konsequenzen bei der Verwendung von Dextran oder ähnlichen Plasmaexpandern beeinflussen. Dies wurde von Flormann und Mitarbeitern publiziert [79].

3.1.2 The yield stress of aggregated red blood cells

There is a huge discussion in literature if the yield stress as a general concept for real fluids exists or not, which is summarized in [39]. In a brief manner, on the one hand the argumentation is that a yield stress fluid is a fluid that flows with time and that maybe the measurement accuracy is just too low to measure the effects [22, 23]. On the other hand yield stress fluids are assumed to be (viscoelastic) solids and do not flow at rest [57, 155]. One main issue seems to be the definition for the yield stress as one specific shear stress, because by assuming a network of aggregated RBCs the stress required to initiate the flow can be much higher than the stress to maintain it reasoned by the fact that the microstructures have to break down first [39]. Avoiding a too deep discussion about the existence of the yield stress Picart and co-workers [155] presented an intensive study about the yield stress of whole blood as a function of the surface roughness of the rheological geometries for hematocrits between 54% and 75%. Below a shear rate of 0.1 s^{-1} rough surfaces show higher yield stress values than smooth surfaces. Nevertheless, these authors were not showing real yield stress data, cause the shear stress value of 0.001 s^{-1} was taken as a good measure for the yield stress value. Even if the used rheometer was theoretically able to resolve such low shear rates at the given viscosities the theoretical resolution limit can differ significantly from the measured one even for today's high resolution rheometers (compare fig. 5.1). Hence, such low shear rates at medium hematocrits like 54% have to be taken with care.

However, inspired by their work, the yield stress was measured using the classical extrapolation method as a function of the aggregation, controlled by the dextran concentration. From the experimental data of the “down” protocol (see above) the shear stress was calculated and plotted against the shear. This allows e.g. approximations with the Bingham or Herschel-Bulkley model. As depicted in fig. 3.7 (a) and (b) the Herschel-Bulkley model approximates the data much better than the Bingham model, which is induced by the fact that the Bingham model is a linear approximation model (compare equation 2.23) describing a Newtonian behavior while the Herschel-Bulkley model describes a power law model for yield stress systems (compare equation 2.24). Empirically, the Casson model (compare equation 2.25) seems to be the most valid one for blood and RBC suspensions [57, 132]. This is due to the fact that the physical model is based on the reversible rod-like aggregation of particles at low shear rates and a successive break-up at high shear rates [10]. Regarding the aggregation of RBCs this model is definitely the most favored one in this context. Therefore, the square root of the shear stress has to be plotted against the square root of the shear rate and can be then linearly approximated as depicted in fig. 3.7 (c). Within the error bars, the Casson model shows a good agreement with the data.

A new idea for measuring the yield stress could be to apply a specific shear stress value and measuring the viscosity over time. If the rheometer is at some point not able to measure a viscosity within the time scale of 20 min (free chosen time) it

means that the measurement is either out of the resolution limit (i.e. viscosities below 0 mPa s are measured) that is limiting the yield stress anyhow or it means that the fluid returns to the solid-like state (respectively viscosities above 0 mPa s are measured). By applying several stresses one can find both regimes (flow or no flow measurable). Between the last flow value and the first no flow value, the measureability of the yield stress can be assumed as depicted for 60 mg/ml dextran in tab. 3.7 (d). This method has two significant issues that remain to be solved: The sedimentation of the RBCs can lead to a pseudo yield stress explained by the increasing RBC concentration at the lower part of the cylinder, and the setup of the MCR702 is yet not able to resolve in SMT mode the same shear stress values at the inner (measured stress in SMT mode) and outer cylinder (applied shear stress in SMT mode).

Surprisingly this analysis leads for all models to a bell-shape behavior as illustrated in fig. 3.8. It is conspicuous that the bell-shape is less pronounced for the same method with the utilized protocol. The “down” protocol is adding the range of 0.01 to 0.1 s⁻¹ and therefore more respect is given to the lower shear rate values. Nonetheless, if the technical resolution becomes better will the bell-shape becomes lesser pronounced or will it completely disappear? From the latter it would follow that the yield stress does not exist for such a system. Taking the Casson model as the most valid one for RBC suspensions, the results are magnified and compared to the new introduced “resolution vs. flow” method. Due to the fact that the resolution vs. flow method is by definition determining either a yield stress or the resolution limit it is obvious that the yield stress is almost directly measured instead of extrapolated. In the end, this method leads to a very slight bell-shape behavior that could be approximated with a straight line as well. Assuming that the method is valid to determine the yield stress one could believe that it does not exist for this system. On the other hand if it exists, the classical Casson approximation results in a bell-shape behavior for the yield stress in the expected range [155].

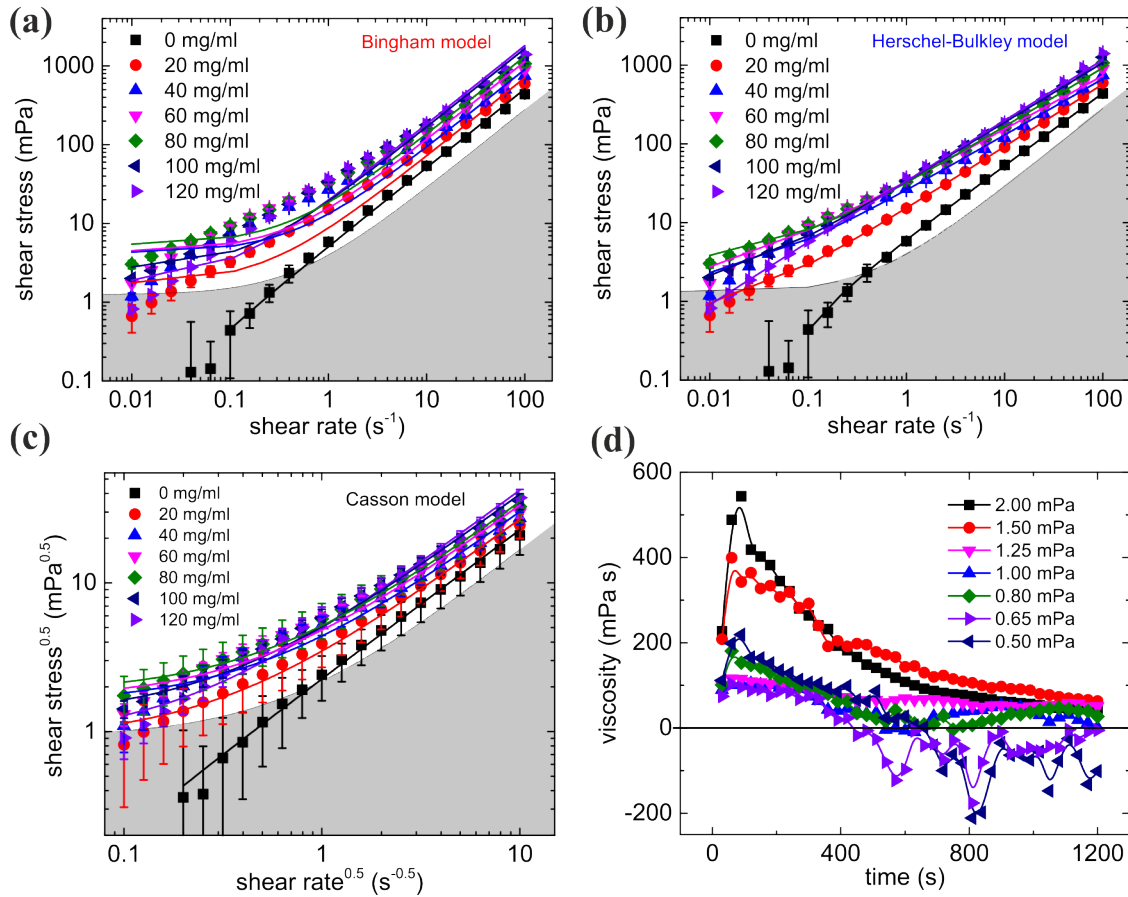


Figure 3.7: The three common model to approximate a yield stress are the Bingham model (a), the Herschel-Bulkley model (b) and especially for RBC suspensions the Casson model (c), which are shown for RBC-dextran suspensions by varying the dextran concentration. Additionally, a new idea for measuring the yield stress on the example of 60 mg/ml shows either a flow or at some point no flow anymore. Exact approximation values are depicted in table 5.1. The applied shear stresses are shown here. Gray areas are the measured resolution limit of the MCR702 (with 20 % tolerance, compare fig. 5.1).

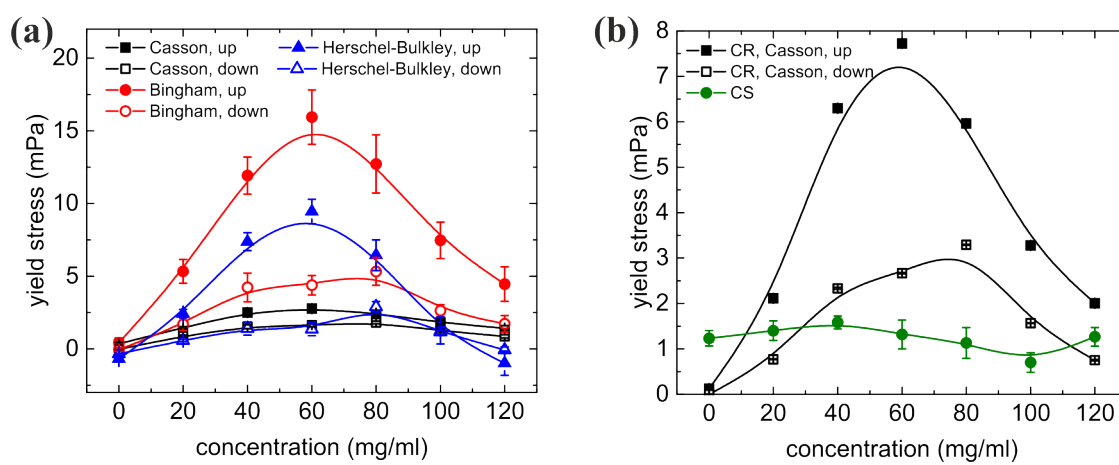


Figure 3.8: The yield stress extrapolated by all three classical yield stress models (a) and compared to the new introduced resolution vs. flow method (b).

Summary of the yield stress of aggregated red blood cells

The existence of the yield stress in general is controversially discussed [22, 23, 39]. Nevertheless, the yield stress of dextran-induced RBC clusters was extrapolated via classic approximation methods, finding that the yield stress is decreasing with an increasing resolution limit, which could lead to the conclusion that it does not exist. Due to the fact that the resolution limit is a determining factor and that the results are mirroring the bell-shape behavior (see above) it was taken at least as a useful concept in the ongoing study presented here. For full blood, this was already done indirectly by Picart and co-workers [155] using the stress at the lowest measured shear, which is in fact not the yield stress as it is theoretically defined.

Résumé sur la contrainte seuil des globules rouges agrégés

L'existence d'une contrainte seuil est généralement discutée de manière controversée [22, 23, 39]. Néanmoins, la contrainte seuil des amas de RBCs induits par adsorption de Dextran a été extrapolée par des méthodes d'approximation classiques. Il a été trouvé que cette contrainte décroît lorsque la limite de résolution augmente, ce qui tend à montrer qu'elle n'existe pas. Puisque la limite de résolution est un facteur déterminant et que les résultats reflètent le comportement « en cloche » (voir plus haut), ce nouveau concept a été pris en compte dans la suite de ce travail. Pour le sang non reconstitué, Picart et collaborateurs [155] avaient déjà pris ce concept en compte en utilisant la contrainte au cisaillement le plus faible, ce qui n'est pas la contrainte seuil telle qu'elle est théoriquement définie.

Zusammenfassung der Fließspannung aggregierter roter Blutzellen

Die Existenz der Fließspannung wird kontrovers diskutiert [22, 23, 39]. Nichtsdestotrotz wurde die Fließspannung von Dextran induzierten Aggregaten roter Blutzellen mit Hilfe klassischer Annäherungsmethoden extrapoliert, wobei gezeigt wurde, dass die Fließspannung mit erhöhter Auflösungsgrenze abnimmt, was zu dem Schluss führen könnte, dass die Fließspannung nicht existiert. Aufgrund der Tatsache, dass die Auflösungsgrenze ein determinierender Faktor ist und dass die Resultate die Glockenkurve widerspiegeln (siehe oben), wurde es als sinnvolles Konzept einer laufenden Studie präsentiert. Für Blut wurde dies bereits indirekt von Picart und Mitarbeitern unter Verwendung der Fließspannung als der geringsten Scherspannung untersucht [155], was faktisch nicht die Fließspannung ist, wie sie theoretisch definiert ist.

3.1.3 The sedimentation of aggregated red blood cells

Dealing with blood rheology has one significant issue: the sedimentation of the cells could influence the measurement result. The theoretical description of sedimentation is rather complex [166]. Nevertheless, experimental studies with rigid fibers at concentrations less than 1% show that they can orient in the direction of gravity and increase the sedimentation velocity by clustering [88, 95]. On the other hand if the concentration becomes too high the mean velocity decrease again, which is most probably a consequence of the rigidity of the fibers. This results cannot be directly applied to RBCs, but the orientation in the direction of gravity could be a reasonable explanation as well as the increasing local mass due to aggregation processes. Here, it was focused on the sedimentation rate in order to determine the potential influence on the rheological data. In addition, a bell-shape behavior was found and a dependence of the sedimentation rate on the diameter of the used tubes.

In pathological studies, the erythrocyte sedimentation rate (ESR) is used to determine unspecific inflammatory states. The clinical determination of the ESR works straight forward: blood is filled into a tube and the ESR is measured after one hour in mm by eye. The diameters of the used tubes are unstandardized, which could lead to differences in absolute ESRs. Such experiments were performed with RBC-dextran suspensions of different dextran concentrations at 45 % hematocrit in tubes of different diameters as depicted in fig. 3.9 for a tube diameter of 25 mm at different times and dextran concentrations. Dextran was used to compare the results directly with the rheological results and in order to focus on the controlled aggregation of RBCs. The RBC clustering is the main reason for a potential increase of the ESR clinically induced by inflammatory diseases in the body that leads to an elevated fibrinogen concentration and therefore to an increasing RBC aggregation [26, 45, 163].

All measurements were performed for at least three healthy donors at room temperature of $23 \pm 0.5^\circ \text{C}$. Every five minutes an image was taken with a commercial DSLR camera (EOS 550D with a EF-S 18-200 mm lens; Canon, Tokyo, Japan) with 18 MP resolution. The obtained images were analyzed by taking the number of pixels of the filling level as 100% and measuring the number of pixels for the sedimentation front at the lowest part of the fluid cone. The results for four different diameters between 1.15 mm (glass tube) and 25 mm (the three other filled heights were performed in plastic tubes) for different dextran concentrations are illustrated in fig. 3.10.

Inspired by the clinical ESR test where sedimentation rates can be related to the aggregation level of RBCs, the sedimentation of RBCs was related to the concentration of dextran, which leads for all diameters and analyzed times (except 0 h) to a very pronounced bell-shape behavior as shown in fig. 3.11. It is remarkable that for all smaller diameters the sedimentation of RBCs in PBS is negligible while it is

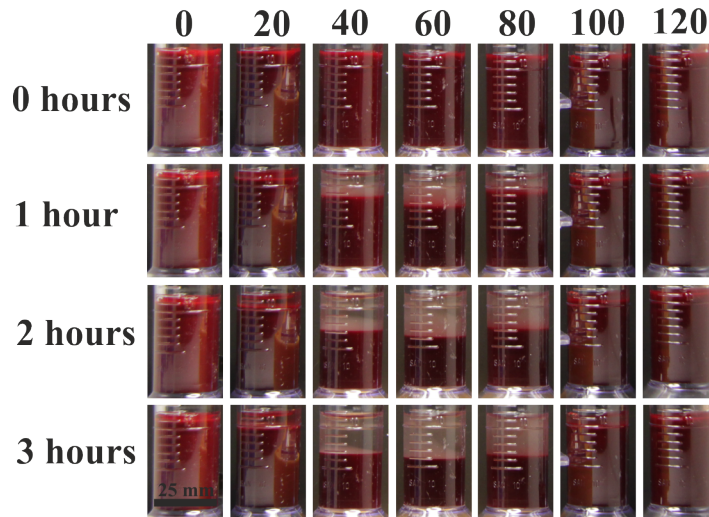


Figure 3.9: Image of cell sedimentation for different times at all investigated dextran concentrations (indicated in mg/ml at the first line) at a tube diameter of 25 mm. With increasing time a bell-shape behavior is clearly visible due to a strong sedimentation in the middle part (40-80 mg/ml), while a low sedimentation at the outer parts (0, 20, 100 and 120 mg/ml).

not for 25 mm, which undergoes confinement effects and large scale velocity fluctuations. At this diameter it is most probably a consequence of the high viscosity at 120 mg/ml that the sedimentation value of PBS differs from the one at 120 mg/ml.

In order to quantify the difference between the diameters of the tubes the maximum position of most bell-shapes at 60 mg/ml was chosen as the value with the most significant effect due to the highest aggregation rate of RBCs (as it will be shown in the following chapters). The overall tendency within the standard deviations shows an increasing sedimentation of RBCs with an increasing tube diameter by ca. 30% between 2.4 mm and 12 mm as shown in fig. 3.12. The diameter 1.15 mm of the glass tube shows slightly more sedimentation than 2.4 mm (plastic tube) that is maybe related to different surface properties. Hence, wall-slip or adherence effects could potentially influence the measurements. Nevertheless, the increasing sedimentation rate in combination with the knowledge that the diameter of clinical sedimentation tube is unstandardized leads to the conclusion that the clinical ESR values cannot be directly compared without taken into account the diameter of the sedimentation tubes. On the other hand, it is the only way to compare different clinical studies since the sedimented suspensions are more undefined than the measuring system, but the absolute values of clinical ESRs have to be taken with care. In addition, these measurements can be used for many rheological issues regarding RBC-dextran suspensions to quantify the influence of sedimentation in the system.

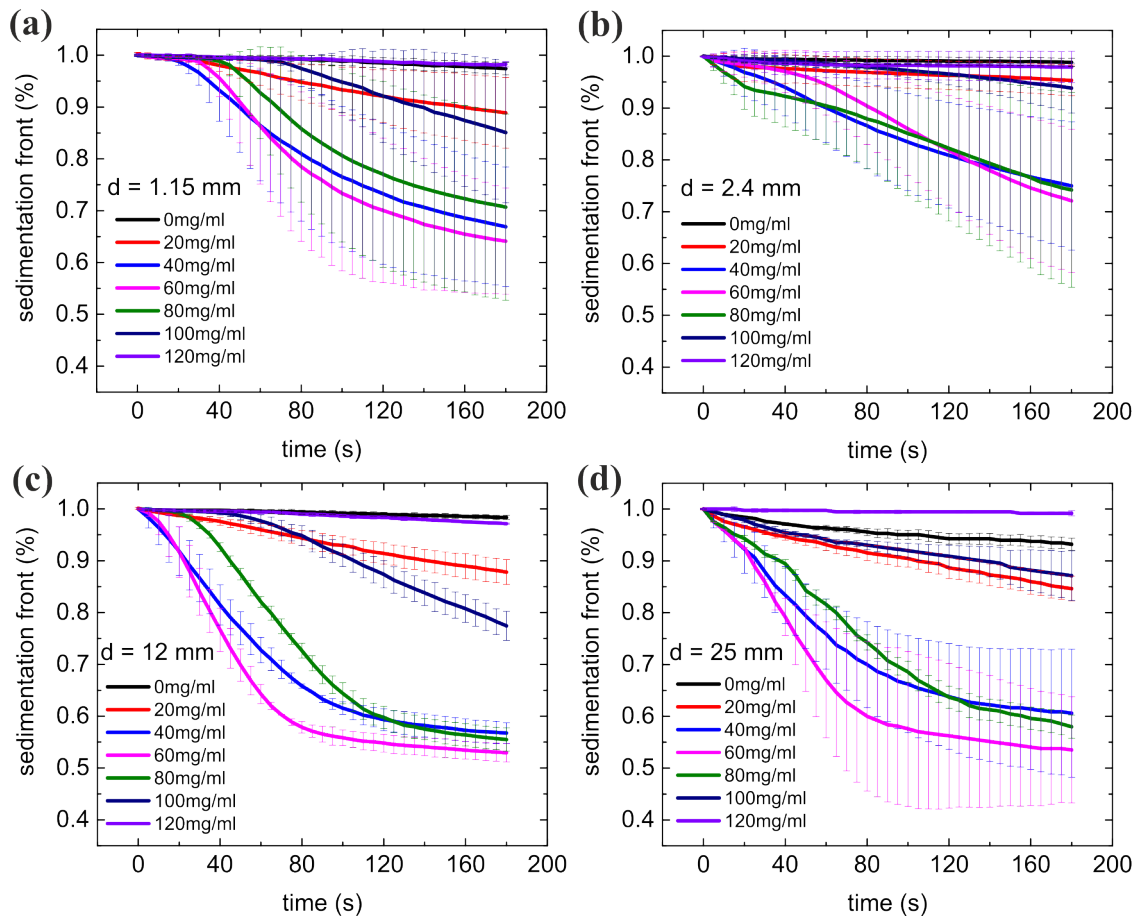


Figure 3.10: Position of the sedimentation front in % of filling levels in dependence on the time for the used dextran concentrations at different tube diameters. Error bars are representing the standard deviation of measurements for at least three healthy donors. Lines are there to guide the eye.

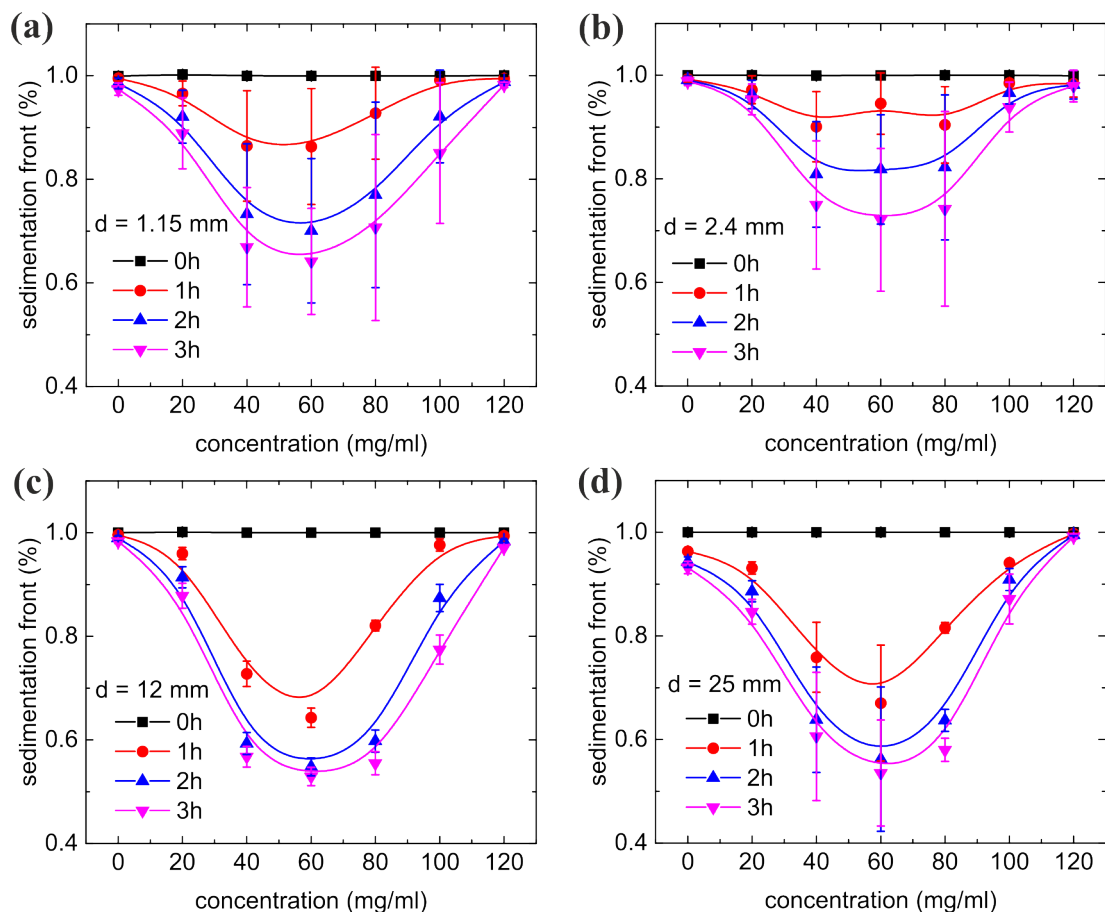


Figure 3.11: The sedimentation of RBC in dependency on the dextran concentration for tubes with the diameters 1.15 mm (a), 2.4 mm (b), 12 mm (c) and 25 mm (d) at different times. 25 mm reflects directly fig. 3.9. Error bars are representing the standard deviation of measurements for at least three healthy donors. Lines are there to guide the eye.

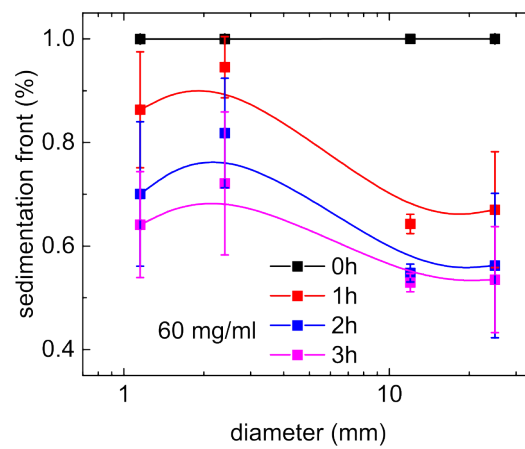


Figure 3.12: Sedimentation of the maximum sedimentation at 60 mg/ml dextran for different times. Error bars represent the standard deviation of measurements for at least three healthy donors. Lines are there to guide the eye.

With this knowledge the sedimentation of the more complex rheological system are probed. Therefore, the outer steel cylinder was replaced by a manufactured acrylic glass cylinder. Even if it was observed with this and known from the literature [69] that a RBC or similar suspensions get mixed up by an applied shear rate the quantification of this effect was important to exclude sedimentation effects for the performed measurements. Using the “up” or “down” protocol no sedimentation was visible at all. Being conservative as possible no shear rate was applied to the system which leads to a slight sedimentation as illustrated in fig. 3.13.

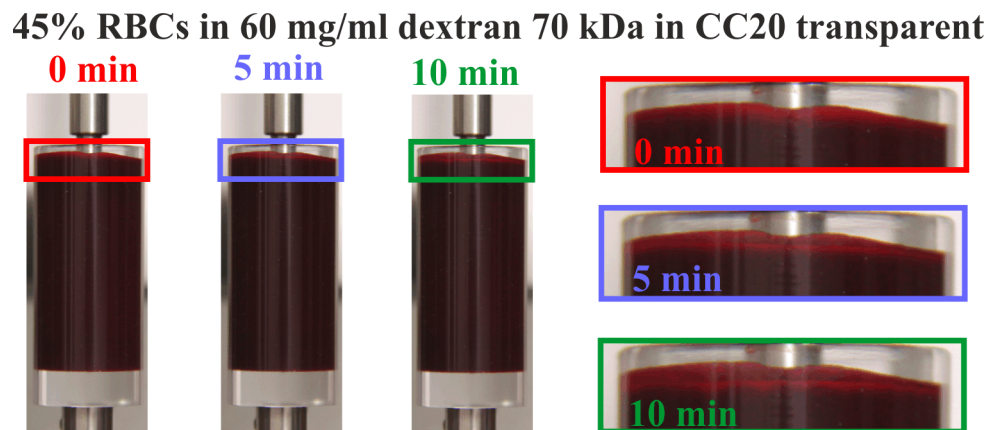


Figure 3.13: Sedimentation of 45 % hematocrit in a 60 mg/ml dextran 70 kDa solution for three different times using a transparent CC20 geometry. Magnifications are marked in the same colors.

Performing the measurements at a room temperature of $23 \pm 0.5^\circ \text{C}$ for 10 min for at least three healthy donors leads a slight bell-shape behavior as illustrated in fig. 3.14. Nevertheless, the maximum of the bell-shape is around 97 % that means by an used overfilling of slightly less than ca. 1 cm the Taylor-Couette geometry should be 100 cm in height to affect the presented measurements (while the real height is ca. 10 cm). Consequently, the sedimentation of RBCs does not seem to affect the rheological investigations above at all.

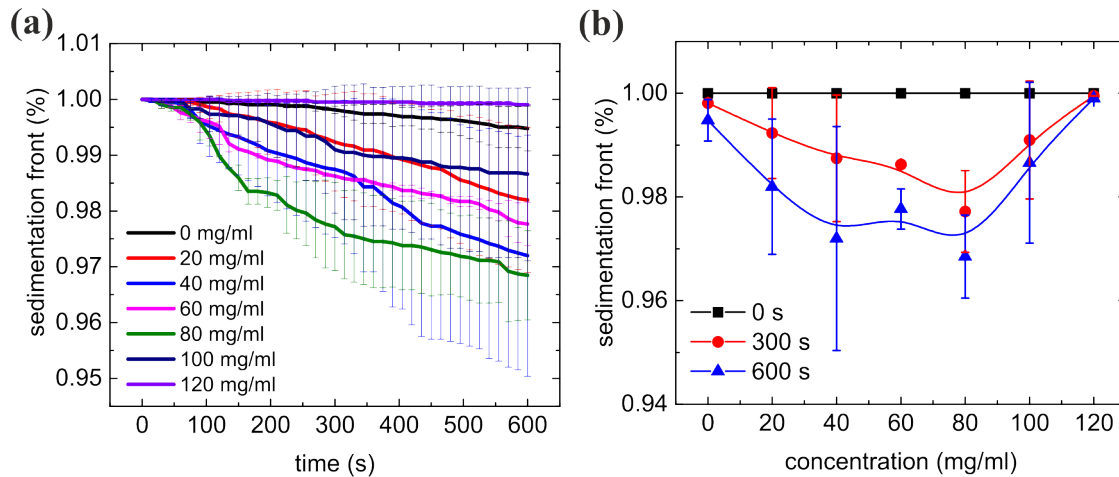


Figure 3.14: Measurements become not affected by sedimentation due to ca. 1 cm overfilling (100 % equals ca. 10 cm)

Summary of the sedimentation of aggregated red blood cells

From the pathological point of view the blood sedimentation is a widely used un-specific method to identify inflammatory diseases in the human body [1, 17, 18, 76, 101, 157, 163], which is induced by the aggregation of RBCs [26, 45, 163]. In such pathological investigations the diameter of the sedimentation tubes is unstandardized. It was presented that an increasing diameter of the sedimentation tubes increases the sedimentation rate. Hence, it is fraught with problems to compare the quantitative data of clinical studies with each other without knowing the diameter of the tubes. In addition, it was shown that the controlled aggregation of RBCs using dextran leads to a bell-shape behavior, which is in great agreement with all other performed measurements of this work leading to a bell-shape (except single cell force spectroscopy due to other issues). Furthermore, the sedimentation of RBC does not influence the rheological data presented above.

Résumé sur la sédimentation des globules rouges agrégés

D'un point de vue pathologique, la sédimentation du sang est une méthode non spécifique couramment utilisée pour identifier des maladies inflammatoires du corps humain [1, 17, 18, 76, 101, 157, 163], qui sont dues à une agrégation des RBCs [26, 45, 163]. Pour ces mesures pathologiques, le diamètre des tubes utilisés n'est pas standard. Il est montré ici que le taux de sédimentation augmente avec la taille du tube. La comparaison de données quantitatives cliniques semble donc particulièrement difficile dans ce contexte de méconnaissance du diamètre de tube. En outre, il est montré que l'agrégation contrôlée des RBCs par le Dextran entraîne un comportement en cloche, ce qui est en très bon accord avec toutes les autres mesures de ce travail montrant un tel comportement (exception faite de la spectroscopie sur

cellule unique soumise à d'autres facteurs). Enfin, la sédimentation des RBCs n'a pas d'influence sur les données de rhéologie présentées plus haut.

Zusammenfassung der Sedimentation aggregierter roter Blutzellen

Aus pathologischer Sicht ist die Blutsenkung, welche unter anderem durch die Aggregation roter Blutzellen hervorgerufen wird [26, 45, 163], eine weit verbreitete unspezifische Methode, um entzündliche Erkrankungen im menschlichen Körper zu indentifizieren [1, 17, 18, 76, 101, 157, 163]. Bei solchen medizinischen Untersuchungen sind die Durchmesser der Sedimentationsröhrchen nicht standardisiert. Es wurde gezeigt, dass die Sedimentationsrate mit steigendem Durchmesser der Sedimentationsröhrchen steigt. Daher ist es problematisch die quantitativen Daten klinischer Studien untereinander zu vergleichen, falls der Sedimentationsröhrchendurchmesser nicht bekannt ist. Ergänzend wurde gezeigt, dass die kontrollierte Aggregation roter Blutzellen durch Dextran zu einem Glockenkurvenverhalten führt, was gut mit allen anderen durchgeführten Messungen, die zu einer Glockenkurve führen, übereinstimmt (ausgenommen Einzelzellkraftmikroskopie aufgrund anderer Sachverhalte). Darüber hinaus beeinflusst die Sedimentation roter Blutzellen nicht die rheologischen Daten, die oben präsentiert wurden.

3.2 Microscopical aggregation index investigations

The principle of the method of the microscopical aggregation index (MAI) as a measure of the quantity of aggregated RBCs is presented in chapter 2.3.2. In this work it was measured for the five different macromolecular suspensions: 10 % RBCs in dextran 70 kDa, HES 130 kDa, fibrinogen as delivered by SigmaAldrich, washed (i.e. saltfree) fibrinogen and C-reactive protein. Microscopical imaging for different concentrations of dextran and fibrinogen are depicted in fig. 3.15 (a). Fibrinogen as delivered by sigma contains approximately 15% of sodium citrate and ca. 25% of sodium chloride (referred here as “fibrinogen with salt”). Due to the fact that salt has a significant influence in osmolality (see chapter 3.6.2), a strong change in RBC shapes (see fig. 5.11 (c)) and therefore a significant influence in the aggregation behavior (explained below), it is necessary to filter the salt out of the fibrinogen solution, which was realized by the method described in chapter 2.3.6. The resulting pure protein is named “Fibrinogen saltfree” as illustrated in fig. 3.15 (a). Moreover, fibrinogen with salt, dextran 70 kDa, HES 130 kDa and CRP were investigated as shown in 3.15 (b), while CRP is illustrated at physiological concentrations that are very low (up to 0.25 mg/ml) and do not show a significant influence on the MAI. CRP is only shown for comparison in fig. 3.15 (a) and discussed in detail in the following chapter 3.3. The related images can be observed in fig. 5.11.

Dextran, HES and fibrinogen with salt show a bell-shape behavior. Saltfree fibrinogen leads to a strong RBC aggregation without any bell-shape behavior.

Starting with fibrinogen containing ca. 40% of salt as delivered by Sigma Aldrich the protein induces a bell-shape. Investigations of the pure salt effect on RBC (see fig. 5.11 (c)) shows that high salt concentrations lead to a strong deformation of RBCs due to the hypertonic environment in combination with an approximately three times higher osmolality in comparison to the buffer solution (see chapter 3.6.2). Consequently, the effect of high salt concentrations leads to a disaggregation of the RBCs either due to shape deformation or due to cell rupture. In contrast to dextran and HES, the pure protein (fibrinogen saltfree) at 60 mg/ml leads to no bell-shape behavior and to a stronger aggregation of RBCs in comparison to the other investigated macromolecules, because it is the only one that creates a membrane deformation that leads to strong curvatures (with apparent angles near 90°), which requires more bending energy than an aggregation with just slight shape changes, as depicted in fig. 3.15 (a) second row at 60 mg/ml. Higher concentrations of fibrinogen were investigated for lower hematocrit concentrations in order to investigate RBC interaction shapes of doublets (see chapter 3.4) which would lead to an MAI of one up to 160 mg/ml (data are not shown here due to the changed hematocrit).

The reason for the non-bell-shape behavior of saltfree fibrinogen is most probably the net negative charge of the fibrinogen [130] in combination with the net negative charge of RBCs [17, 18] or a remaining discocyte shape in contrast to dextran

and HES for which the shape seems to change to a stomatocyte shape (compare e.g. 3.15 (a), 120 mg/ml dextran). For the depletion model the repulsive forces of protein-protein and protein-RBC interaction can lead to a higher or no overlap concentration or to an absence of the penetration into the glycocalyx. In the context of the bridging theory, at 60 mg/ml one could be still in the regime where the surface coverage of the RBCs is around 50%, which would lead to strong clustering. Bridging itself is in principle possible because the charge distribution of the RBC surface is heterogeneous. This is highly speculative because it would mean that the surface coverage of the RBCs is nearly constant including free binding sites between ca. 20 mg/ml and 60 mg/ml. The possible reasons for the bell-shape behavior are discussed in detail in chapter 2.1.3.

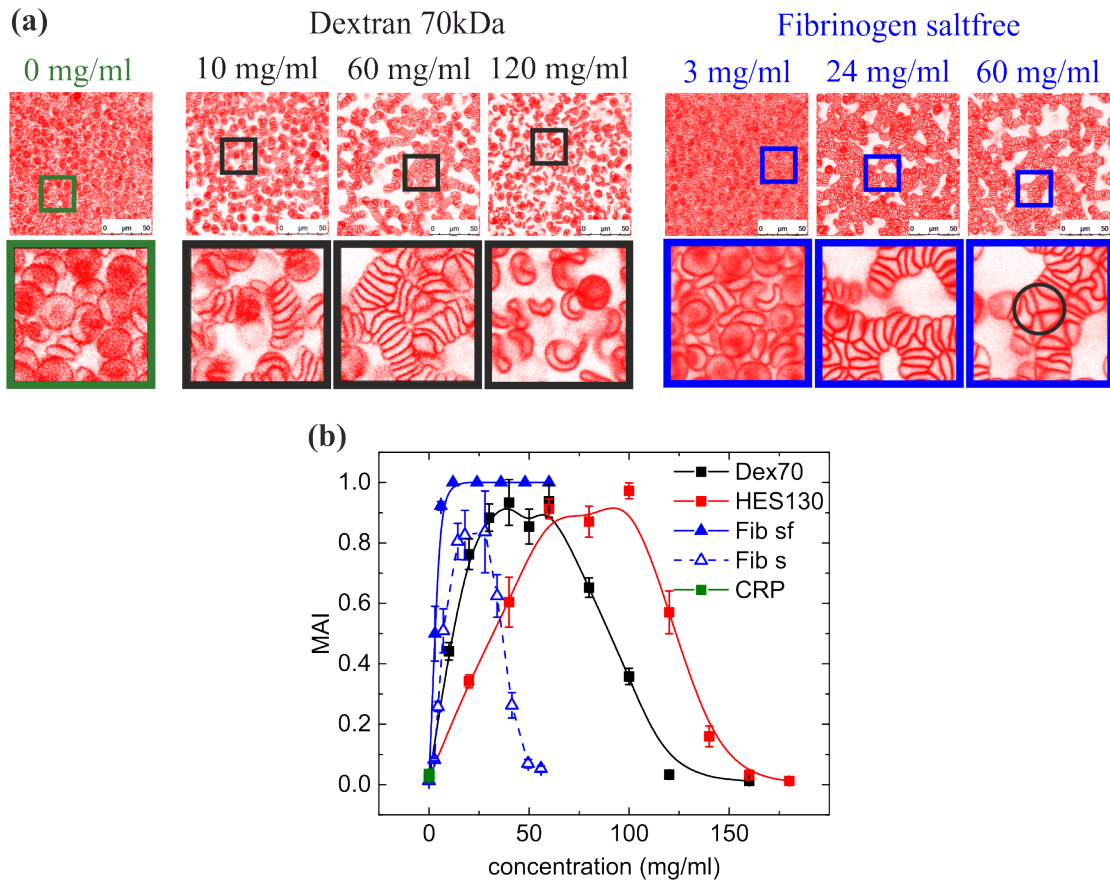


Figure 3.15: Microscopic imaging of dextran 70 kDa and saltfree fibrinogen for different concentrations in the first row and magnifications in the second row. Contacts at 90° angles of the cell membranes for saltfree fibrinogen are marked with a black circle (a). Microscopical aggregation indices for dextran 70 kDa (black curve), HES 130 kDa (red curve), saltfree (filtered) Fibrinogen (blue, filled triangles), Fibrinogen as delivered by Sigma Aldrich with approx. 40% salt (empty triangles) and C-reactive protein (green). Error bars represent the standard deviation of measurements for at least three healthy donors. Lines are guides to the eye (b).

Summary of the microscopical aggregation index investigations

The MAI leads to a bell-shape behavior for both dextran and HES. In the case of dextran the peak position and right foot of the bell-shape occurs at significant larger concentrations than measured by Chien [52], which could be related to the temperature difference (Chien: 37° C, here: 23° C). For HES no data for comparison were found. One remarkable fact is the change in RBC shape for high dextran and HES concentrations. In both images (fig. 3.15 (a) at 120 mg/ml dextran and fig. 5.11 (b) at 160 mg/ml HES) many RBCs appear as stomatocytes. This shape is known to have a low aggregation affinity similar to spherocytes [17, 18, 163, 161]. The reason for the influence of these shapes on the aggregation is not well understood.

A bell-shape behavior depends on the macromolecules. For all of them that show a bell-shape behavior, the shape of many RBCs is changing to stomatocytes. This fact was never taken into account by the theoretical models of aggregation and could be involved in the the bell-shape behavior. Hence, it should be included in the theoretical models, because it would change the total contact area and therefore the forbidden areas and the total areas for a potential bridging.

Résumé sur les mesures d'indice d'agrégation microscopique

Le MAI (pour microscopical aggregation index, en anglais) a pour résultat un comportement en cloche pour le Dextran et le HES. Dans le cas du Dextran, la position du pic et le retour sur la ligne de fond à droite sont observés pour des valeurs de concentration plus hautes que celles mesurées par Chien [52], ce qui pourrait être expliqué par une différence de température de mesure (Chien : 37°c, ce travail : 23°c). Pour le HES, il n'a pas été possible de trouver d'autre étude pour comparer les résultats. Il est intéressant de remarquer que les RBCs changent de forme pour les plus fortes concentrations de Dextran et de HES. Dans les deux images (fig. 3.15 (a) à 120 mg/ml de Dextran et fig. 5.11 (b) à 160 mg/ml des HES), beaucoup de RBCs ont une forme de stomatocytes. Cette géométrie est connue pour avoir une faible affinité d'agrégation comme dans le cas des sphérocytes [17, 18, 163, 161]. La raison de l'influence de ces formes sur l'agrégation n'est pas bien comprise. Un comportement en cloche dépend du type de macromolécules. Pour toutes celles entraînant un comportement en cloche, les RBCs adoptent une forme de stomatocytes. Cet effet n'a jamais été pris en compte dans les modèles théoriques de l'agrégation et pourrait être impliqué dans le comportement en cloche. Ainsi, il faudrait le prendre en compte dans les modèles car cela changerait la surface de contact totale et donc les zones dans lesquelles un pontage potentiel pourrait survenir.

Zusammenfassung der Untersuchungen zum mikroskopischen Aggregationsindex

Der MAI führt zu einem Glockenkurvenverhalten für Dextran und HES. Im Fall von Dextran befindet sich das Maximum und der rechte Bereich der Glockenkurve an signifikant höheren Konzentrationen als von Chien gemessen [52], was auf den Temperaturunterschied zurückzuführen sein könnte (Chien: 37° C, hier: 23° C). Für HES wurden keine vergleichbaren Daten gefunden. In beiden Bildern (Abb. 3.15 (a) bei 120 mg/ml Dextran und Abb. 5.11 (b) bei 160 mg/ml HES) erscheinen viele rote Blutzellen als Sphärozyten [17, 18, 163, 161]. Diese Zellform ist bekannt für ihr schlechtes Aggregationsverhalten. Der Grund für den Einfluss dieser Form noch nicht ausreichend erforscht.

Ein Glockenkurvenverhalten hängt von den verwendeten Makromolekülen ab. Für alle, die ein Glockenkurvenverhalten zeigen, ändert sich die Form der roten Blutzellen zu Stomatozyten. Dieser Aspekt wurde in den theoretischen Modellen nicht berücksichtigt und könnte eine Rolle für das Glockenkurvenverhalten spielen. Daher sollte dieser in den theoretischen Modellen Verwendung finden, weil er die absolute Kontaktzone und daher die verbotenen Bereiche und die absoluten Bereiche für ein potentiell Bridging ändern würde.

3.3 C-reactive protein influence on the RBC aggregation

The erythrocyte sedimentation rate (ESR) is a widely used method to identify inflammatory diseases in patients. The method itself is rather straight forward as already explained and investigated in chapter 3.1.3. Nevertheless, a brief recapitulation is given at this point: After drawing blood is filled in a tube and one measures the velocity of the sedimentation front in mm/h. It is known that the ESR is directly related to the clustering process of RBCs [26]. Consequently, a high ESR implies an increased aggregation of RBC.

In several medical publications, the acute phase C-reactive protein is assumed to enhance the sedimentation rate of red blood cells [1, 6, 62, 75, 101, 157, 185, 190, 191, 197]. There the CRP values were measured and correlated directly with the ESR. In order to give a better overview of these measurements they were summarized in a meta-analysis in fig. 3.16. All of these investigations are clinical studies where blood was drawn from several patients with different diseases and the amount of CRP in the plasma as well as the ESR were determined. Due to the fact that the ESR is performed in plasma which contains several other ingredients, e.g. fibrinogen, it is questionable if the increase of CRP is responsible for the increasing ESR.

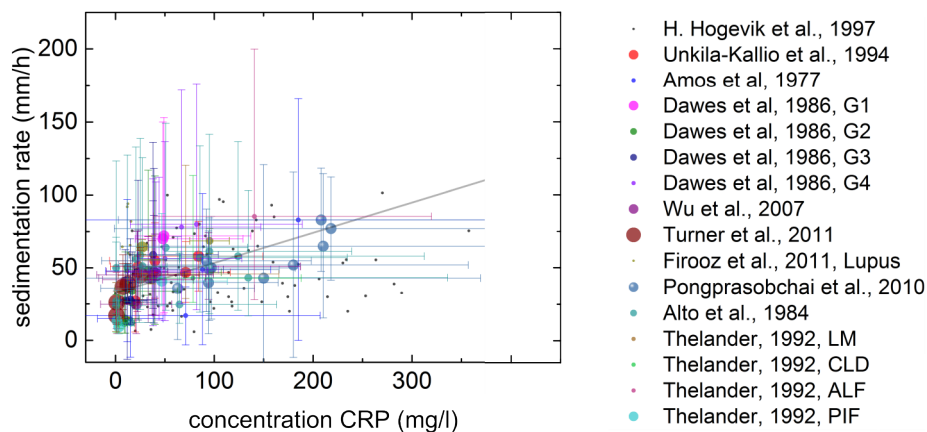


Figure 3.16: Meta-analysis of several medical publications regarding the correlation between CRP concentration and ESR. Shortcuts are indicating the illness. The size of the measuring points is correlated with the number of patients (large: high number, small: low number). Error bars are either standard errors or standard deviations depending on the publication. The linear approximation (gray line) gives the overall tendency to guide the eye.

In the following it will be shown with ESR and MAI that the CRP concentration at physiological conditions does not influence the aggregation process of RBC and

therefore not the ESR (under controlled conditions, i.e. a suspension of RBCs, PBS and CRP where no plasma is involved). The correlation between CRP and ESR is most probably caused by the fact that the fibrinogen level increases at the same time as CRP levels [78].

The fundamental methods of the sedimentation investigations is explained in chapter 2.3.1 and briefly recapitulated: The first approach is to observe the sedimentation of RBCs in PBS instead of plasma with several amounts of CRP at room temperature ($23\pm 0.5^\circ\text{C}$) as done by the medical researchers in plasma. Those investigations were performed with a commercial DSLR camera in combination with 120 μl RBC suspensions in 170-QS cuvettes. The result clearly shows that the RBC sedimentation rate does not increase within physiological CRP concentrations (0 - 0.25 mg/ml) as depicted in fig. 3.17.

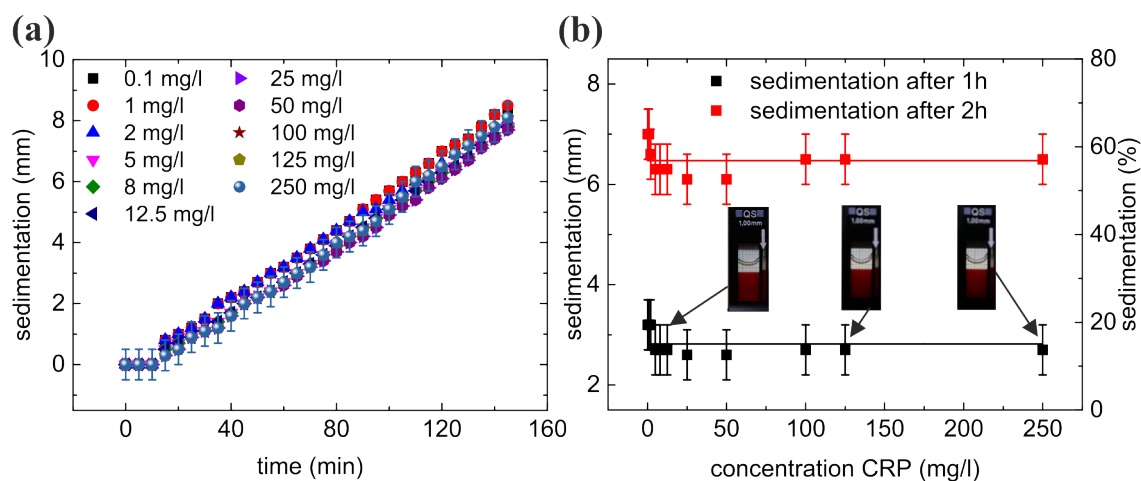


Figure 3.17: The sedimentation front (indicated with “sedimentation”) of washed RBC in PBS with the addition of several CRP concentrations in dependence on the time (a). No concentration dependency can be observed within the error bars (b). Line are there to guide the eye and images to are related to (from left to right) 0.0001 mg/ml, 0.125 mg/ml and 0.25 mg/ml of CRP. Error bars represent the standard deviations of at least three healthy donors.

The same measurements were performed with the spectrometer Genesys 6 (Thermo Scientific, Waltham, MA, USA) at a wavelength of 940 nm. Including a positive control with fibrinogen as delivered by Sigma Aldrich in physiological ranges the result indicates the same as above and is illustrated in fig. 3.18 (b). Due to the fact that the time of the inflection point represents a measure for the rapidity of the sedimentation, it is shown in fig. 3.18 (c and d) that it does not change for different CRP concentrations, but strongly changes with the concentration of fibrinogen as delivered by Sigma Aldrich.

Moreover, the MAI for RBC in presence of CRP is not indicating an aggregation process at all as it is visible in fig. 3.18 (a). There the MAI is in the range of the

3.3 C-reactive protein influence on the RBC aggregation

one of PBS, which is most probably influenced by “pseudo-aggregates” which means that the cell membranes of two cells are not distinguishable due to the fact that the RBCs are lying side-by-side without a real interaction.

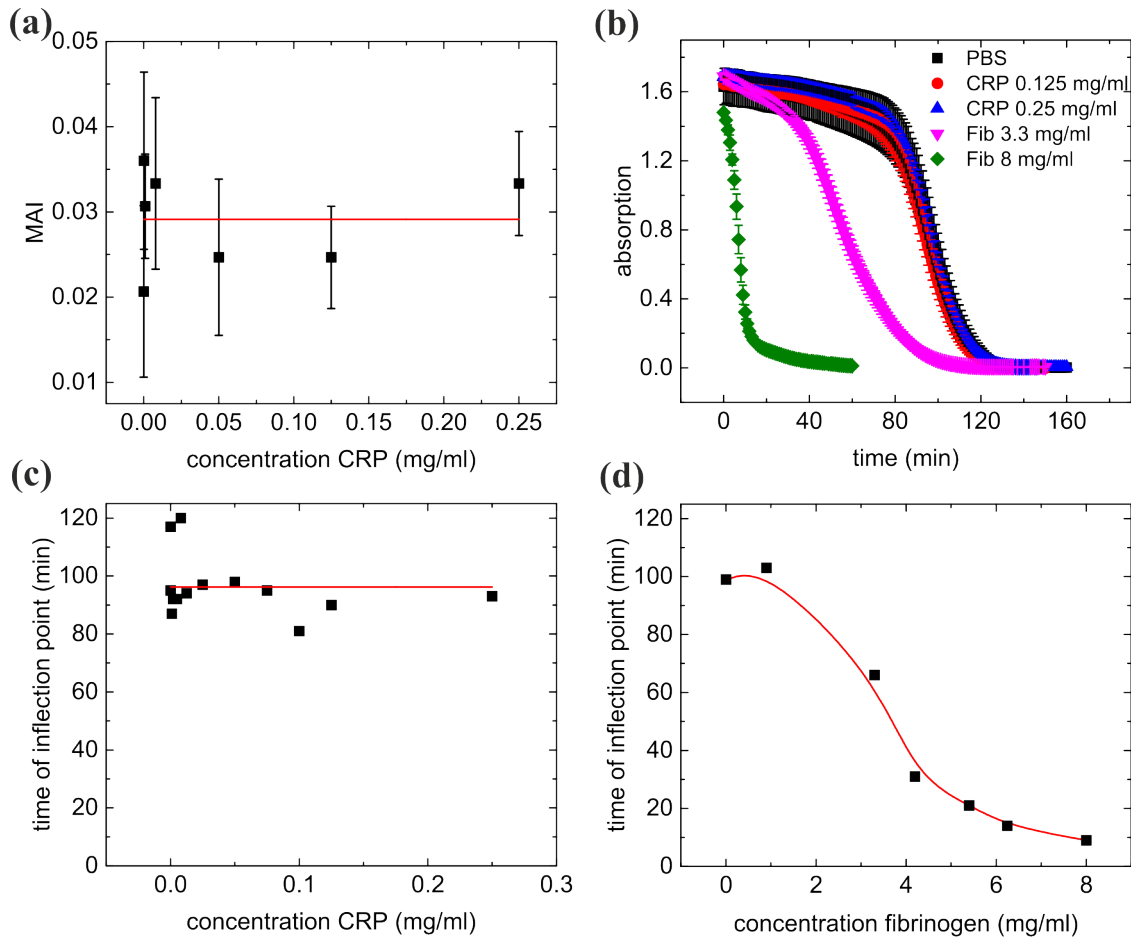


Figure 3.18: MAI shows no significant increase of the RBC aggregation in the presence of CRP (a). Sedimentation measurements performed with an UV-Vis spectrometer show a rapid sedimentation of RBCs for the presence of fibrinogen and no effects for CRP compared to PBS (b). The analysis for the time of the inflection point confirms this result (c and d). Red lines are there to guide the eye and error bars represent the standard deviation of at least three measurements of three healthy donors.

In addition, CRP does not influence the calcium channels of the RBCs (as it is the case for dextran and fibrinogen as well; see fig. 5.16), which could have had an influence on the aggregation behavior.

Summary of the C-reactive protein influence on RBC aggregation

Following this study, there seems to be no relation between the physiological concentration of CRP and the aggregation of RBCs as suggested by many authors [1, 6, 62, 75, 101, 157, 185, 190, 191, 197] via the ESR that is dependent on the clustering process [26]. Referring to the clinical studies, it means that the increase of the ESR correlated to the CRP concentration is most probably due to a concurrence with elevated fibrinogen or other protein levels (antibodies as IgM or IgG could play a role as well). Regarding clinical studies, the CRP-ESR correlation was performed with ill patients which could influence the RBCs in a way that they maybe change their aggregation behaviors that could be easily checked by the presented MAI. From the theoretical point of view the CRP is assumed to have an hydrodynamic radius of 4.8 nm, which is quite close to the limited expected radius (4 nm, see [26]) that can have influences on the RBC aggregation and therefore to the ESR. Additionally, the physiological concentrations of CRP are about 1000 times lower than the concentrations of fibrinogen (or HES and dextran in the case of plasma expanders), which leads again to the assumption that CRP in physiological concentrations is not influencing the clustering process or ESR as it was published by Flormann and co-workers [78].

Résumé sur l'influence de la protéine C réactive sur l'agrégation des globules rouges

Par ce travail, il ne semble pas y avoir de relation entre la concentration physiologique de protéine C réactive (en anglais C-reactive protein, CRP) et l'agrégation des RBCs alors que de nombreux auteurs [1, 6, 62, 75, 101, 157, 185, 190, 191, 197] l'ont suggéré par la dépendance du taux de sédimentation sur le processus d'agrégation [26]. Si l'on s'en réfère aux études cliniques, cela signifie que l'augmentation de l'ESR corrélé à la concentration en CRP est très probablement due à un fort taux de fibrinogène ou d'autres protéines simultanément (des anticorps tels que les immunoglobulines M ou G pourraient jouer un rôle). Par rapport à ces études cliniques, la corrélation ESR-CRP a été mesurée sur des patients malades, ce qui pourrait avoir un effet sur les RBCs dans la mesure où ces dernières pourraient avoir des propriétés d'agrégation différentes. Cela serait aisément être vérifiable par une mesure du MAI. D'un point de vue théorique, on estime le rayon hydrodynamique de la CRP à 4,8nm ce qui est assez proche de son rayon physique attendu (4nm, voir [26]) et cela pourrait donc avoir un effet sur l'agrégation des RBCs et donc sur l'ESR. De plus, les concentrations physiologiques de CRP sont environ 1000 fois moins élevées que celles en fibrinogène (ou en Dextran ou HES dans le cas de sang reconstitué), ce qui, encore une fois, renforce l'hypothèse que la CRP n'a pas d'influence sur l'agrégation et donc sur l'ESR, ainsi que Flormann et collaborateurs l'ont publié [78].

Zusammenfassung des Einflusses des C-reactiven Proteins auf die Aggregation roter Blutzellen

In dieser Studie scheint keine Relation zwischen physiologischen CRP Konzentrationen und der Aggregation roter Blutzellen zu bestehen, wie von vielen Autoren mit Hilfe der ESR, die vom Aggregationsprozess abhängt [26], vermutet wurde [1, 6, 62, 75, 101, 157, 185, 190, 191, 197]. Bezugnehmend auf klinische Studien bedeutet dies, dass die erhöhte ESR, welche mit der CRP Konzentration korreliert wurde, sehr wahrscheinlich auf einen erhöhten Fibrinogenspiegel oder die Erhöhung anderer Konzentrationen von Proteinen (Antikörper wie IgM oder IgG könnten auch eine Rolle spielen) zurückzuführen ist. Im Fall von medizinischen Studien wurde die CRP-ESR Korrelation mit kranken Patienten durchgeführt, was einen Einfluss auf die roten Blutzellen im Sinne einer Änderung des Aggregationsverhaltens haben könnte, was mit dem vorgestellten MAI einfach zu überprüfen ist. Vom theoretischen Gesichtspunkt aus wird der hydrodynamische Radius von CRP mit 4,8 nm angenommen, was sehr nahe an dem Radius (4 nm, siehe [26]) liegt, der Einfluss auf die Aggregation roter Blutzellen und daher auch auf die ESR hat. Hinzu kommt, dass die physiologische Konzentration von CRP etwa 1000 mal kleiner ist als die Konzentration von Fibrinogen (oder HES und Dextran im Fall von Plasmaexpandern), was erneut zu der Annahme führt, dass CRP den Aggregationsprozess oder die ESR nicht beeinflusst, wie von Flormann und Mitarbeitern publiziert wurde [78].

3.4 Interaction zones of RBCs

Many studies investigated the interaction between cells or vesicles and artificial flat and solid surfaces [115, 172]. In these studies buckling is observed, which is characterized by a failure mode resulting from a compressive stress that is higher than the compressive stress the material can resist. Consequently, the material is deformed which can occur for cell membranes as well. For freestanding capsules and vesicles buckling was observed as well, induced by osmotic pressure, shear forces, asymmetric lipid distributions [25, 61, 114, 142, 196]. For dead RBCs buckling like instabilities, especially S-shapes (see below), have been showed in 1987 by Tilley and co-workers using TEM [187], but were never quantified or analyzed for the case of living RBCs. Two decades later the variety of RBC interaction zones was shown theoretically by minimizing the free energy of the membranes and varying the interaction energy by Svetina and Zihelr [200, 182]. In their work, the interaction zones of RBC doublets mainly depend on the dimensionless adhesion strength γ and the reduced volume $\nu = 3V\sqrt{4\pi}S^{-3/2}$ in which V is the enclosed volume and S the surface of the membrane. Physiologically, the reduced volume varies with the age of the cells. Due to the dispersity of RBCs in a given sample it is most likely that in an aggregate of two RBCs the reduced volumes of the cells differ from each other. In this study performed three dimensional observations of such RBC doublets in vitro (see fig. 3.19 (b)) appear very similar to the theoretical predictions as illustrated in fig. 3.19 (a).

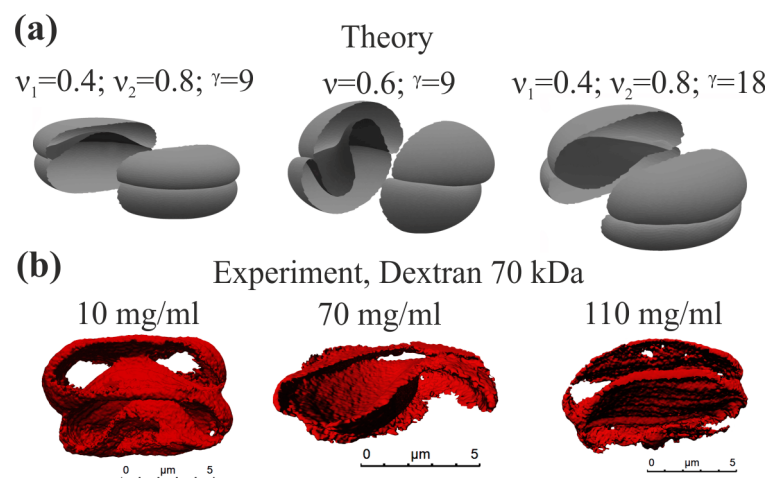


Figure 3.19: Three dimensional adhered RBCs in relation to the adhesion strength and reduced volume theoretically observed by Svetina and Zihelr from [182] (a) and in relation the interaction energy varied by the dextran concentration for RBC in contact with the microscopy dish (b). From left to right the interaction zones are called: male-female, strong sigmoid or S and low sigmoid or S.

Inspired by the work of Svetina and Zihelr the interaction zones of RBCs were

investigated by varying the interaction energy via the dextran or fibrinogen concentration.

3.4.1 Doublets

For experimental observations, the RBCs were labeled with CellMask (see chapter 2.3.9) and 0.2 % of them were added to the macromolecular solution. After mixing the suspension by hand 20 μl were appended to one well of the “ μ -slide 18-well treated” (Ibidi GmbH, Munich, Germany). Directly afterwards, the position about 50 μm above the bottom of the well in z-position of the confocal microscope SP5 II (Leica Microsystems, Wetzlar, Germany) was adjusted. An doublet (an aggregated pair of two cells) entering the 50 μm -zone was imaged immediately during sedimentation in a fast imaging mode. Due to the rotation during sedimentation the statistics of the presented study is limited to 30 interaction zones per concentration, for which the evaluation was performed in an orientation in which the interaction zones were clearly visible without rotation effects. Therefore, approximately 200-300 cell pairs were measured per concentration in order to reach this premise. With this method it was ensured that the cells are not in contact with any artificial surfaces. All measurements were performed at $23\pm 0.5^\circ\text{C}$. Following the investigations of Svetina and co-workers [200, 182] they were named parachute, sigmoid- or S- and male-female shape. Parachute shapes are defined by all interaction zones and outer zones having a convex shape with the constraint that one of the non interacting surfaces is allowed to have a concave shape, otherwise they were taken as a male-female shape. A male-female shapes was defined as rather flat non interacting zones with a bulge for the interacting zones. Flat interaction zones were taken into this category as well. Sigmoid shapes correspond to cases where the curvature of the interaction zone shows a change of concavity (i.e. two bulges). Typical images for RBC doublets in a dextran 70 kDa solution are shown in fig. 3.20.

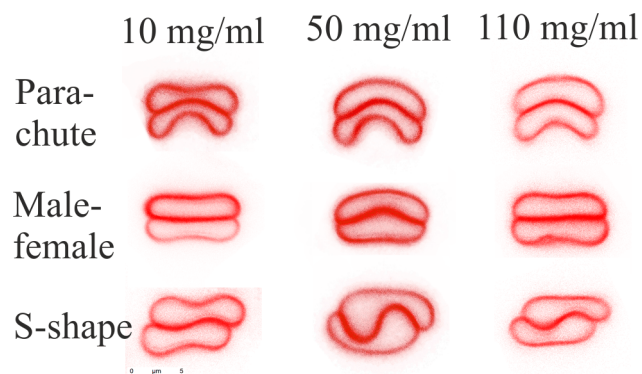


Figure 3.20: Overview of the observable doublets by varying the dextran concentration exemplary.

As it is obvious for the S-shape the interaction zones of the RBC are strongly bent in the middle for the middle dextran concentration of 50 mg/ml (and expected high interaction energies), while the interaction zone is just weakly deformed at the low and high dextran concentration where the interaction energy is assumed to be low. In addition, it can be clearly seen that for all concentrations all cell shapes can be observed which is most probably due to the variation of reduced volume induced by using all cell ages. The rather low statistics of 15 or 30 cell pairs in the presented study that is a consequence of the strong required definition for analyzing doublets. All error bars concerning the interactions zones of RBCs represent the standard errors. This has to be taken with care, because the real distribution of the results is not known [20], but this constraint was accepted to give a better overview of the main results.

In addition, the cells were allowed to touch the well which leads to the formation echinocytes. For these data just 15 cells per concentration were analyzed, since attached doublets are typically oriented perpendicular to the observation direction, i.e. the interaction zones were not visible. In only approximately one out of 50-100 doublets the interaction zone was visible. Representative images of the visible interaction zones are illustrated in fig. 3.21 (b). As already explained, fibrinogen as delivered by SigmaAldrich contains ca. 40 % of salt. Therefore, both “salty” and “saltfree” fibrinogen were measured while the latter was filtered as explained in chapter 2.3.6 and shown for RBC doublets in 3.21 (a) and (c). Comparing both set of images, the RBCs for the salty fibrinogen seem to be deflated with increasing fibrinogen (respectively salt concentration), which is most probably leading to the fact that nearly no aggregates are observed above 60 mg/ml. In contrast, saltfree fibrinogen shows no volume difference of the RBCs but strong interaction up to 160 mg/ml (higher concentrations were not measured because the fibrinogen does not dissolve well). Hence, the salt concentration does not just influence the shape (as illustrated in fig. 5.11 (a)) but also the aggregation behavior.

Numerical simulations, summarized here, were performed by Othmane Aouane using vesicles with a bilayer membrane enclosing an inner fluid and surrounded by an outer fluid with a different viscosity than the inner fluid. Simulations were restricted to 2D because it was shown that 2D and 3D have the same essential features [9, 73, 110]. The boundary integral method is based on solving the Stokes equation [9]. For the presented numerical results the interaction energy was varied between 0 and $27 \mu\text{J}/\text{m}^2$, the reduced area between 0.4 and 0.65 and the curvature energy was fixed to $\kappa_B = 4 \cdot 10^{-19}\text{J}$. In order to compare the results simulations were performed for pairs of vesicles with similar reduced volume and by varying the interaction energy (modeled by a Lennard-Jones like potential) as depicted in fig. 3.21 (d). A more detailed explanation of the numerical simulation is given in [77], where slight parachute shapes were observed by changing the curvature energy to $\kappa_B/4$ and changing the reduced areas to 0.4 for one vesicle and to 0.55 for the other vesicle.

The interaction zones were clarified according to their shapes. For saltfree fibrinogen

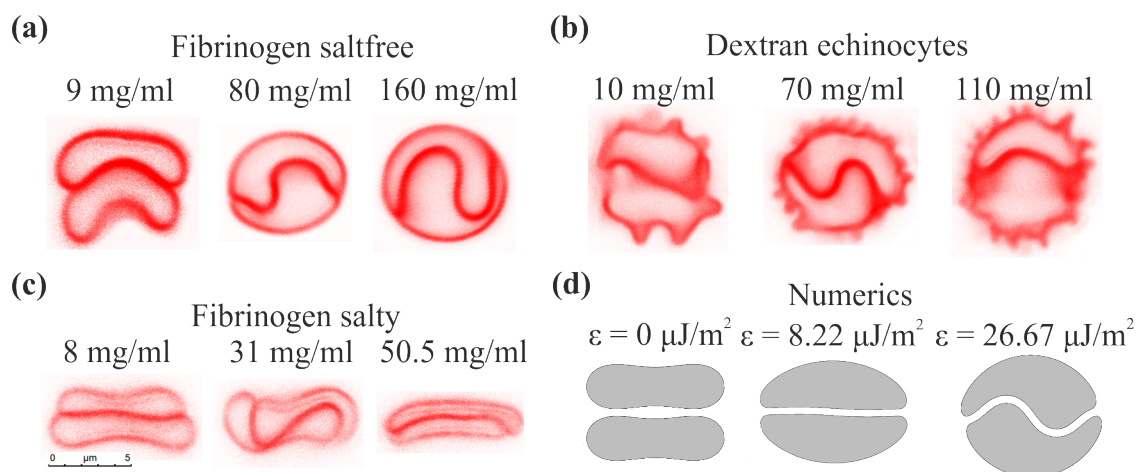


Figure 3.21: Observed RBC doublet shapes for saltfree fibrinogen (a), salty fibrinogen (c) and dextran while here the echinocyte shape was created by the glass effect (b) and numerics for the same reduced areas of 0.65 by varying the interaction energies (d).

just parachutes are observed at the middle physiological concentration of 3 mg/ml, while at 40 mg/ml just male-female and S-shapes with a preference to the latter were observed. For 160 mg/ml nearly only sigmoid shapes were observed as shown in fig. 3.22 (a). In contrast, the changing shape of RBCs as a function of the salty fibrinogen concentration leads to a clear bell-shape behavior with many sigmoidal shapes at the middle fibrinogen concentration, and less S-shapes at the low and high fibrinogen concentrations as illustrated in fig. 3.22 (b). Dextran shows a similar behavior under the same conditions with a strongly increased parachute shape prevalence at concentrations higher than 110 mg/ml as depicted in fig. 3.22 (c). Allowing the doublets to touch the artificial surface as it is the case for echinocytes due to the glass effect no parachutes are observed at all while the bell-shape behavior is similar to the one of RBCs during the sedimentation in dextran, whereas parachute shapes are replaced by male-female shapes.

In order to quantify these shapes the interaction zones were approximated by an heuristically chosen sinus function, whose amplitude was taken as a measure for the quantification of interacting zones as shown in fig. 3.23 for both doublets and clusters that will be explained below.

Regarding the numerics the reduced area (the equivalent of reduced volume for the simulated 2D case) influences the amplitude of interaction zones significantly as illustrated in fig. 3.24 (a). Hence, the most stable and probably most physiological one ($\tau_1 = 0.6$ and $\tau_2 = 0.65$) was chosen to compare it with the experiments as it is depicted in fig. 3.24 (b) for doublets of discocytes during free sedimentation

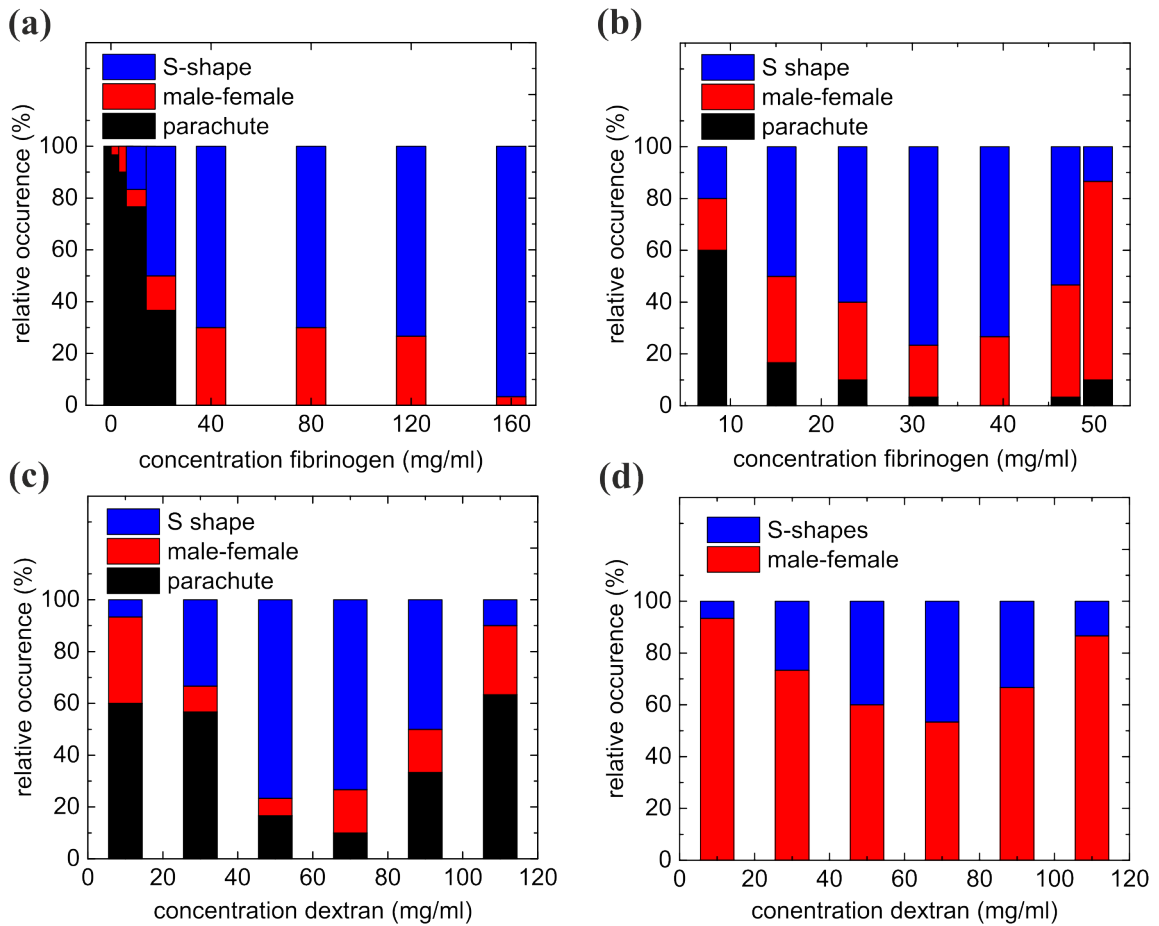


Figure 3.22: RBC doublet contact zone distribution for saltfree fibrinogen (a), salty fibrinogen (b), dextran discocytes (c), dextran echinocytes (d).

and echinocytes attached to the artificial plastic surface. Numerical data are shown a mirrored bow by the $22.5 \mu J/m^2$ value, assuming that the interaction energy decreases linearly after the bell-shape maximum. Even if the simulations are not perfectly fitting with the experiments yet they show an increase of amplitude with an increasing experimental amplitude/interaction energy that leads to a qualitative agreement. A correspondance between the interaction energy scale and the dextran concentration scale can be found by comparing simulations with $\tau_1 = \tau_2 = 0.6$ and experiments, and matching the interaction energy so that the maximum amplitude of deformations are about the same as shown in fig. 3.24 (d). The error bars represent the minimum and maximum interaction energies of the numerical results derived from the experimental standard errors. They are very high, because the aggregation of RBCs seems to involve a buckling process indicated by the bifurcation in fig. 3.24 (a), which leads to slight amplitude change at high interaction energies as illustrated in 3.24 (a) and therefore to a wide range of possible amplitudes within the standard errors of the experimental data. Nevertheless, even here a slight bell-shape behavior

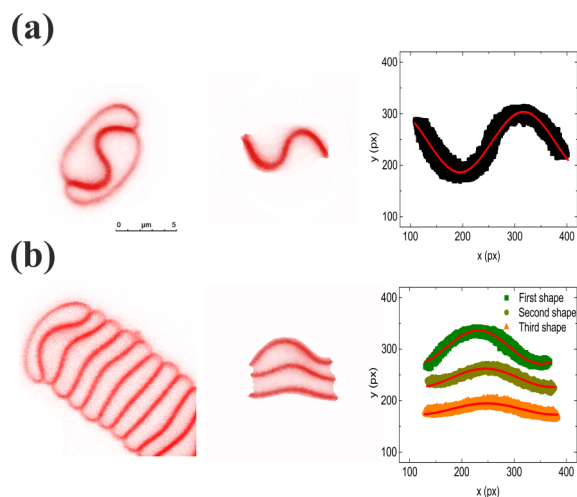


Figure 3.23: Procedure of analyzing RBC doublet (a) and clusters larger than seven single cells (b) was performed by reducing the images to interaction zones (second column) and approximating the pixels with a sinus function.

is discernible by assuming that the interaction energy is zero at 0 and 120 mg/ml for dextran as well as for 60 mg/ml salty fibrinogen.

The buckling process itself was analytically described by Thomas Podgorski [77]. Therefore, the shape of one cell of an RBC doublet is supposed to consist of two semi-circular cups with the radius R , a straight curvature line L_1 and a sinusoidal curvature line L_2 with the amplitude A as depicted in fig. 3.25 (a). This leads to the mathematical description of interaction zone

$$y(x) = AL_1 \sin\left(\frac{2\pi x}{L_1}\right) \quad (3.2)$$

where $-L_1/2 < x < L_1/2$. The interaction energy is given by the expansion at the order of four in A :

$$E_i = -\epsilon L_1 \left(1 + \pi^2 A^2 - \frac{3}{4} \pi^4 A^4\right) \quad (3.3)$$

in which ϵ is the interaction energy per unit length. The curvature energy of the system is concentrated in the circular caps E_{b1} and the deformed contact zone E_{b2}

$$E_{b1} = \frac{2\pi\kappa}{R} \quad (3.4)$$

$$E_{b2} \simeq \frac{8\pi^4 A^2 - 20\pi^6 A^4}{L_1} \quad (3.5)$$

where $\kappa = 4 \cdot 10^{-19}$ J is the membrane stiffness. Consequently, the total energy $E = E_i + E_{b1} + E_{b2}$ depends on A , R and L_1 that are related via the constant area S and the constant perimeter L described by

$$S = \pi R^2 + 2RL_1 \quad (3.6)$$

$$L = 2\pi R + L_1 \left(2 + \pi^2 A^2 - \frac{3}{4} \pi^4 A^4 \right) \quad (3.7)$$

Rescaling the interaction energy to $\beta = \epsilon L^2 / \kappa$ leads to clear bifurcation of the amplitude A as illustrated in fig. 3.25 (b). A more detailed explanation of this analytical model is given by Thomas Podgorski [77].

In clinical researches clusters much larger than two cell are observed. In this perspective, clusters larger than 6 cells per RBC aggregate were also investigated regarding their interaction zone changes.

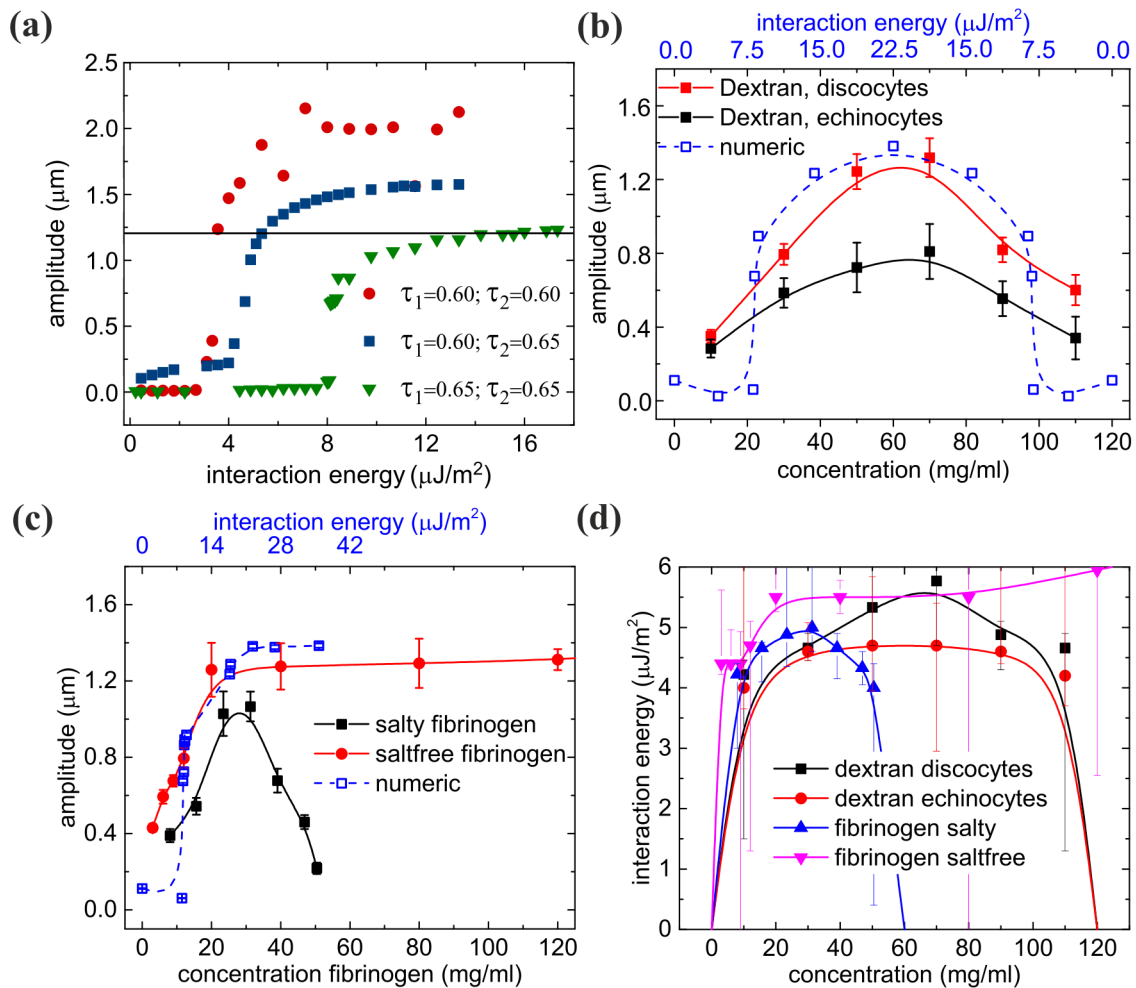


Figure 3.24: Numerical simulations performed by Othmane Aouane [77] (a), dextran amplitudes compared to $\tau_1 = 0.65$ and $\tau_2 = 0.65$ (b), fibrinogen amplitudes compared to $\tau_1 = 0.65$ and $\tau_2 = 0.65$ (c) and the interaction energy in relation to the concentration for $\tau_1 = 0.60$ and $\tau_2 = 0.65$. Error bars represent the standard errors of 15 doublets for echinocytes and 30 doublets for all the other of at least three healthy donors. Thin error bars in (d) represent the minimum and maximum interaction energies within the standard errors of the experimental data compared to the numerical amplitudes. Lines are there to guide the eye.

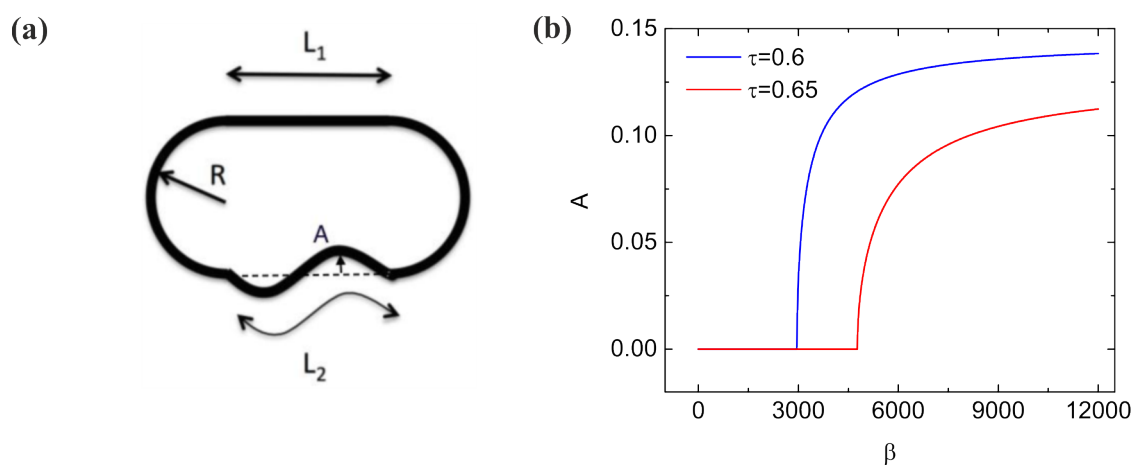


Figure 3.25: The parameters of analytical investigations performed by Thomas Podgorski [77] (a) lead to a bifurcation of the amplitude A of the changed interaction zone in depending on the rescaled interaction energy β for two reduced areas (b).

3.4.2 Clusters larger than six cells per aggregate

Red blood cell aggregates in this chapter are defined as aggregates of RBC that contain at least seven single RBCs. A concentration of 0.4 % of RBCs is chosen and images were directly taken after the clusters were sedimented on the bottom of the well coated with 1 mg/ml BSA as described in chapter 2.3.8. Only linear aggregates that are not connected to other aggregates from the side were analyzed, because such a connection influences the interacting zones as depicted in fig. 5.11. It was found that only the first three interaction zones (seen from the end cell of the cluster) respond to a change of interaction energy (respectively dextran concentration), while the others do not as illustrated in fig. 3.26 (a) and (c). This is in good agreement with numerical simulations performed by Othmane Aouane [77] as depicted in fig. 3.26 (b) for different interaction zones at the same reduced areas of $\tau = 0.6$. Hence, the first three interaction zones were analyzed as shown in fig. 3.24 (b). These interfacial shapes can differ significantly for a given dextran concentration, which is most probably due to the uncontrolled reduced volumes (respectively cell ages).

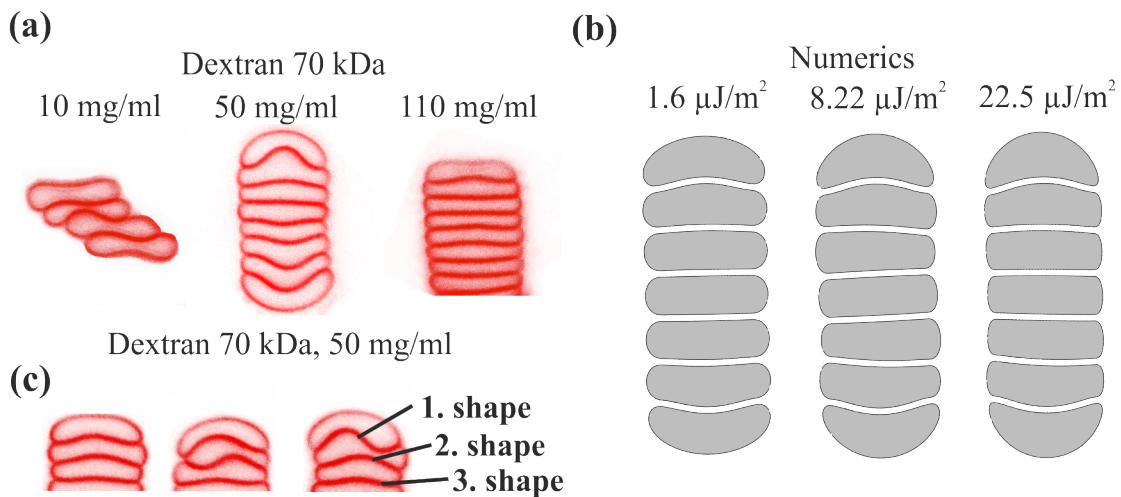


Figure 3.26: Exemplary images for clusters larger than seven cells (except for 10 mg/ml) for three dextran concentrations (a). At 10 mg/ml all observed aggregates contain four cells or less, cause no larger ones were observed. Only clusters of four cells were analyzed. The variation of the first three interaction zones for one dextran concentration can be severe (c), which was not observed by numerical simulation performed by Othmane Aouane [77] for different interaction energies at the same reduced areas of $\tau = 0.6$ (b).

Nevertheless, they can be analyzed in the same way as the doublets were (see fig. 3.23 (b)). In this case, no parachute shapes were observed at all which is most probably due to the interaction of several involved cells and the interactions with an artificial plastic surface, which could influence the results as well. S- and male-female shapes were counted similar to the case of doublet as depicted in fig. 3.21

(a). The amplitudes of the first shape are close to the amplitude of echinocyte doublets. They are in good agreement with the numerical results as well as the second interaction zones. In the case of the third interfacial shape, experiments slightly differ qualitatively in comparison to the numerical results, but strongly as far as amplitudes are concerned which is most probably due to the fact that many pixels per vertical line (a given thickness of the interaction zones induced by the fluorescence based technique) are analyzed per concentration for the experimental case while just one pixel is relevant for the numerical results.

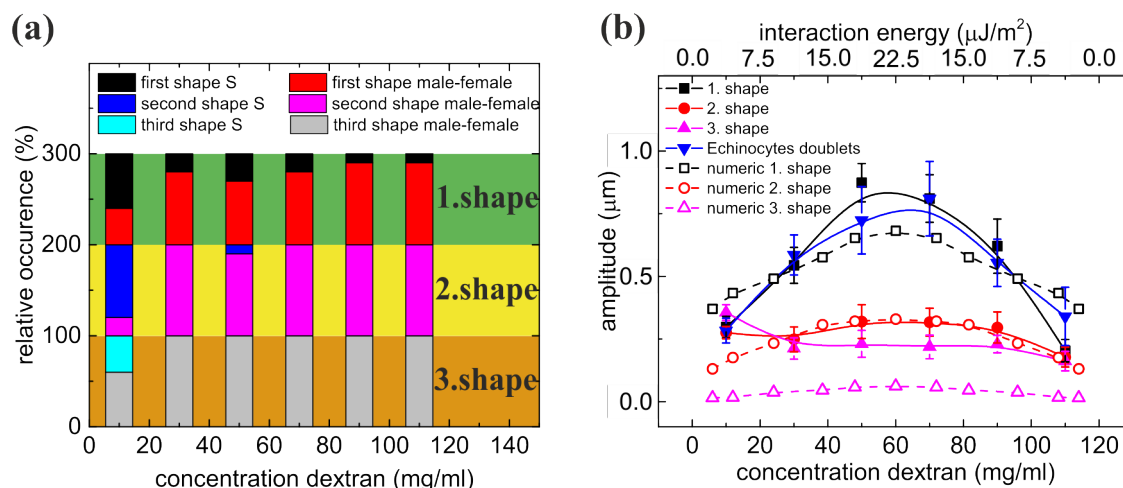


Figure 3.27: Distribution of the first three interaction zones within a rouleau that consists of at least seven single RBCs. Only S- and male-female shapes were observed (a). Amplitudes of the first three interfacial shapes in dependence on the dextran concentration. For comparison data for echinocyte doublets are shown as well as numerical results for clusters of exact 7 cells and the same reduced volumes. Error bars are indicating standard errors.

In order to measure the interaction energy between two RBCs directly single cell force spectroscopy was used in the following chapter.

Summary of the interaction zones of RBCs

The aggregation of RBCs was induced by the human protein fibrinogen as well as by the plasma expander dextran. For increasing interaction energies the contact zone of two cells change from a rather flat surface (male-female) to a buckling induced sigmoid shape as predicted by Svetina and Zihlerl [182, 200]. While the S-shape was already found by Tilley [187] for several macromolecules, the transformation from the additional observed parachute via the male-female to the sigmoid is shown here first experimentally, and was published in [77]. A comparison to numerical simulations indicates a buckling instability that was characterized to a analytic

model [77]. Characterizations of larger clusters resulted in the observation that only the first three interaction zones at the two ends are clearly deformed, whereas the other cells of the cluster show flat interfacial zones. A comparison to aggregates under pathological conditions would be very interesting.

Résumé sur les zones d'interaction entrée globules rouges

L'agrégation des RBCS a été induite par du fibrinogène humain ou par du Dextran. En augmentant l'énergie d'interaction, les zones de contact entre deux cellules ont évolué depuis une surface quasi plane (mâle-femelle) vers une forme sigmoïde créée par flambage, ainsi que cela a été prédit par Svetina et Zhierl [182, 200]. Alors que la forme en S a déjà été observée par Tilley [187] pour plusieurs types de macromolécules, la transformation de la forme en parachute additionnelle en sigmoïde avec un intermédiaire mâle-femelle a été observée expérimentalement pour la première fois dans ce travail, ce qui a donné lieu à une publication [77]. Une comparaison avec des simulations numériques montrent une instabilité de flambage qui a été caractérisée par un modèle analytique [77]. La caractérisation des amas plus importants a montré que seules les trois premières interfaces de contact à chaque extrémité sont déformées alors que le reste des cellules de l'amas conservent une interface plane. Il serait intéressant de comparer ces résultats à des agrégats obtenus dans des conditions physiologiques.

Zusammenfassung der Interaktionszonen roter Blutzellen

Die Aggregation roter Blutzellen wurde durch das menschliche Protein Fibrinogen und den Plasmaexpander Dextran hervorgerufen. Für steigende Interaktionsenergien verändert sich die flache Kontaktzone zwischen zwei Zellen (male-female) zu einer S-förmigen, die durch Buckling induziert wird, was von Svetina und Zihlerl vorhergesagt wurde [182, 200]. Während die S-Kontur bereits von [187] für verschiedene Makromoleküle gefunden wurde, wird die Umwandlung der beobachteten Fallschirmform via der Male-female-Form zu einer Sigmoidalform, hier zum ersten Mal experimentell gezeigt, was in [77] publiziert ist. Ein Vergleich mit numerischen Simulationen legt eine Buckling-Instabilität nahe, was mit einem analytischen Model charakterisiert wurde [77]. Untersuchungen größerer Cluster resultierten in der Beobachtung, dass nur die ersten drei Interaktionszonen an den beiden Enden deutlich deformiert werden, während die anderen Zellen des Clusters flache Interaktionszonen zeigen. Ein Vergleich zu Aggregaten unter physiologischen Bedingungen wäre sehr interessant.

3.5 AFM

This AFM chapter is giving an overview of two ongoing studies. In the first chapter the influence of dextran on the RBC deformability will be presented by using an AFM with a pyramidal indenter. The second chapter is focused on the issues of single cell force spectroscopy (SCFS) to investigate aggregation forces by using two RBCs in mechanical contact with the result of a bell-shape that is influenced by viscosity effects.

Therefore, two types of cantilevers are used: the SCFS was performed with V-shape cantilevers without an indenter, named MLCT-O (see fig. 3.28 (a) and (c)). All elasticity measurements were performed with a pyramidal indenter, named MLCT (see fig. 3.28 (b) and (d)). Both are manufactured by Bruker (Bruker AFM probes, Camarillo, CA, USA). For SCFS and elasticity the softest cantilevers “C” were used.

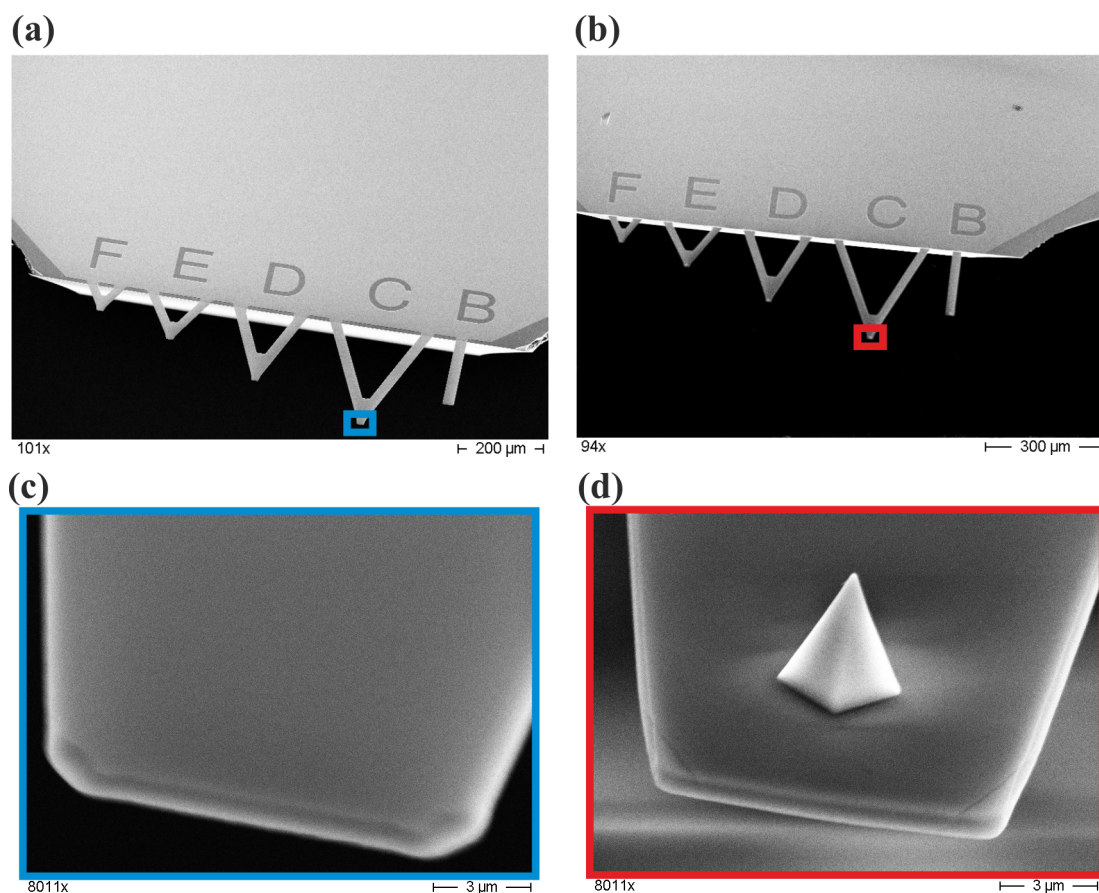


Figure 3.28: Scanning electron microscopy (SEM) enables the high resolution imaging of the MLCT-O (a) and MLCT (b) cantilevers (Bruker). The magnification is marked with blue squares for MLCT-O (c) and with red rectangles for MLCT (d) cantilevers.

3.5.1 Elasticity

Indicated by surface acoustic wave measurements (see 3.6.1) the RBCs seem to become softer in the presence of dextran, while their stiffness is not changing by adding fibrinogen. In order to determine the Young's modulus of RBCs a wide range of measuring tools exists, e.g. micropipets, optical stretchers, AFMs etc. while some measure a local (e.g. AFM) and others a global elasticity (e.g. micropipets). The existing measured values are in a range from 100 Pa [134, 21, 67] to ca. 2,000 Pa [58] depending on the used measuring tool and the way of analyzing the data.

The sensitivity of the AFM technique makes it a good candidate to quantify the change of stiffness of RBCs by changing the dextran concentration. As already depicted by Ciasca and co-workers [58] making use of an AFM leads to an estimation of a local and not a global elasticity of the RBCs as depicted for the setup used in the present work in fig. 3.29 (a) for the entire cell, for all measured moduli and for the region of interest (lower Young's moduli appear at the highest regions of the discocyte close to the edges) in fig. 3.29 (b). Here a 16x16 pixel surface scan of a discocyte RBC was performed by scanning from the bottom left corner to the top right corner. The setpoint was 1 nN and the velocity was 0.5 $\mu\text{m}/\text{s}$. One can observe by an increasing cell-diameter in the upper part of the scan (which was not the case compared to the cell shape investigated by light microscopy) that the measuring errors become more frequent. This is most probably due to the fact that the more often the tip of the cantilever is puncturing the cell the higher is the chance of pulling tethers out of the cell membrane. Such tethers can stick to the cantilever and consequently they can create measuring errors as briefly explained in chapter 5.5.

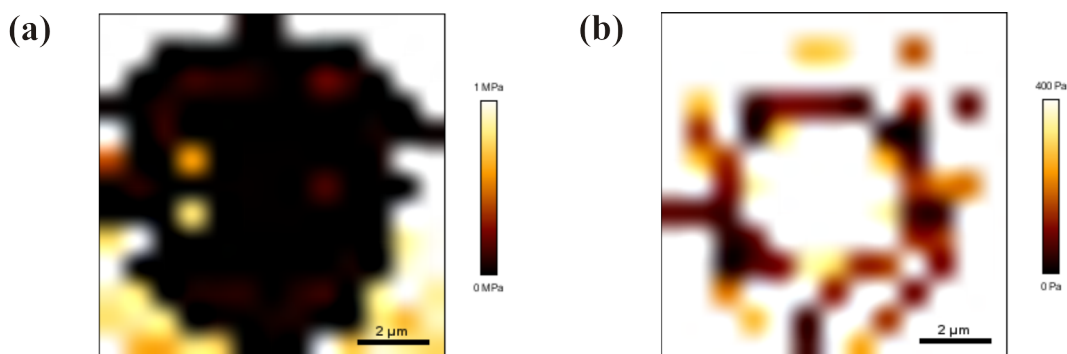


Figure 3.29: Illustration of the different Young's moduli of a RBC performing an AFM scan. The RBC, which has a much lower Young's modulus than the substrate, is marked in black for a color code up to 1 MPa (a). Assuming that the local Young's modulus of a RBC close to the edges is around 400 Pa as maximum the same cell as in (a) is shown with a color code up to 400 Pa (b).

In this study the highest region of the RBCs (around max. 2.5 μm , which is close to

the edge of the RBC; see fig. 3.29 (b)) was chosen without using a scan combined with an indentation force of 1 nN using a velocity of 0.5 $\mu\text{m/s}$ in order to be as conservative as possible, following Ciasca and co-workers [58]. This leads to a wide range of measurement results depending on the position of the cantilever regarding the RBC, which are presented in fig. 3.30. It is assumed that some represent the substrate due to the high deformability in the middle part of the RBCs, which is thinner than the outer parts of the cell and therefore it could be very flexible and probably not in contact with the substrate ((c) and (d)). This could lead to the fact that the cantilever is in contact with the substrate before the cell is elastically responding. Making use of the method to employ, just the parts of the edges of RBCs show a lower Young's modulus as shown in fig. 3.30 ((e) and (f)). Using exactly the same measurement method after adding dextran the response of the cell is a much lower Young's modulus (shown in (a) and (b)).

Around 15 measurements per cell were taken by choosing the one which fulfills the fact that it was taken close to the edge. In this way 20 measurements per cell of the same donor and the same dextran concentration were performed to show that the Young's modulus of this RBC region is decreasing with an increasing dextran concentration. The same method shows that an increasing fibrinogen concentration does not change the Young's modulus of RBCs as depicted in fig. 3.31 for fibrinogen and dextran.

The method of using a setpoint force is probably puncturing the cell to the substrate, which could damage the cell significantly, is here not taken into account. If a tether could be seen optically by the deformation of a RBC the whole measurement was not taken into account. A discussion of the results is given at the end of chapter 3.5.

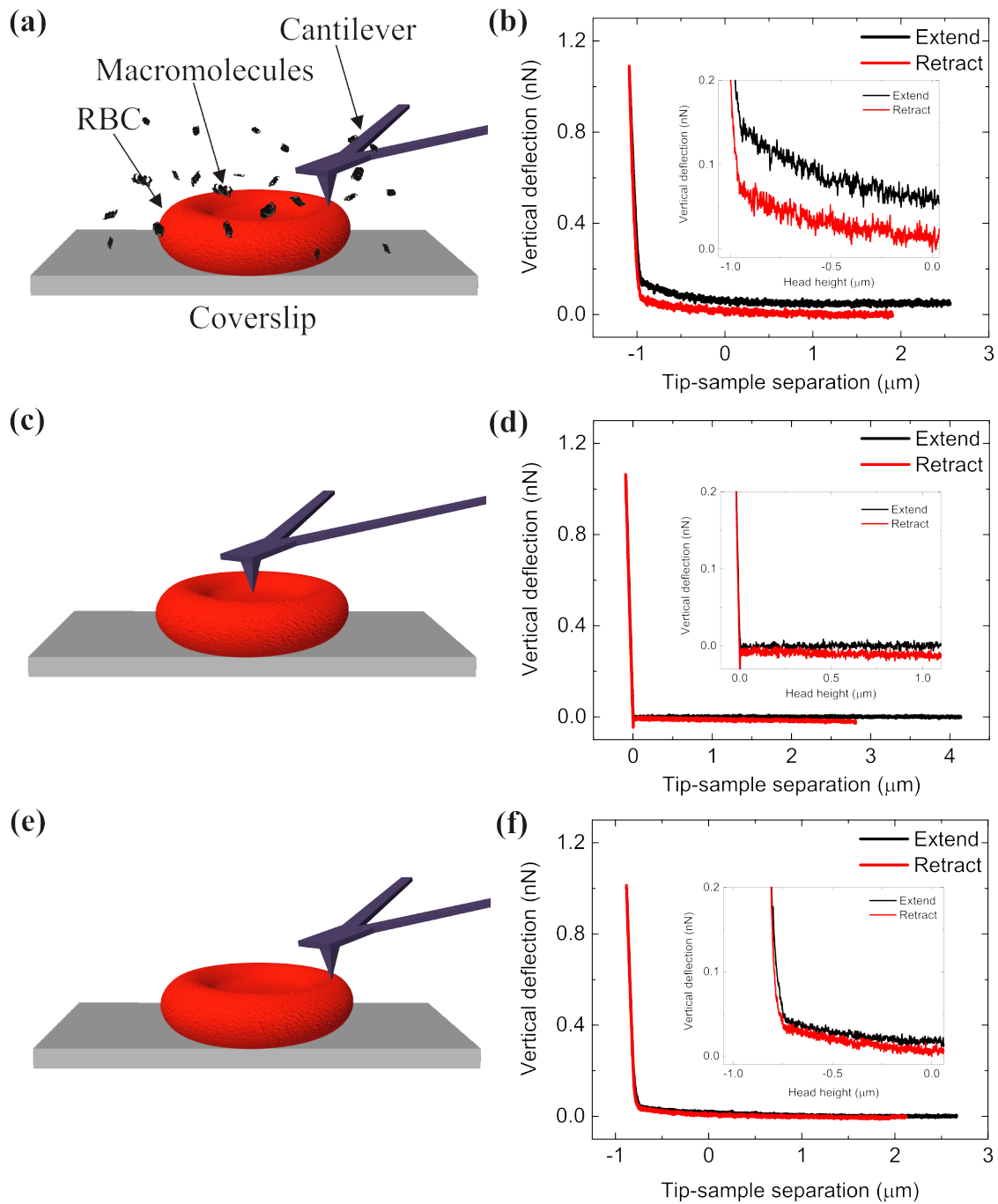


Figure 3.30: Matching the valid area of measurement on RBC when dextran 70 kDa (at 60 mg/ml) is present (a) it leads to a “soft” curve while the inset is showing the magnification of the approximated area (b) as for all other representations in this figure. If the RBC is surrounded by PBS (c) and it’s not matched properly the cantilever (respectively the AFM) feels the substrate which leads to a very high Young’s modulus (d). If the RBC is matched properly with PBS in the surroundings (e) the resulting curve leads to moderate Young’s modulus (f).

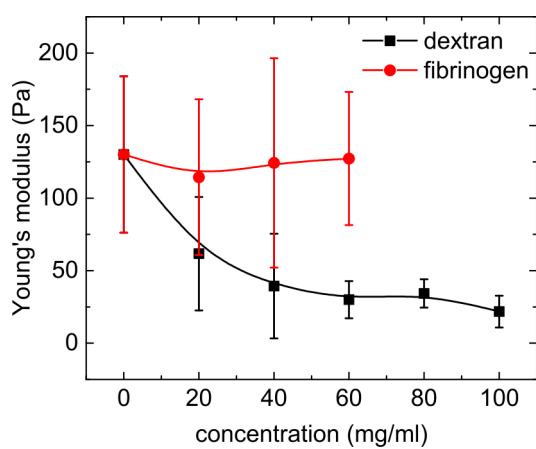


Figure 3.31: The Young's moduli of RBCs by using a MLCT cantilever (Bruker) for an increasing fibrinogen and dextran concentration. Error bars representing the standard deviation of at least 20 different cells. Lines are there to guide the eye.

3.5.2 Cell-Cell adhesion

In order to quantify the interaction energy of two aggregated RBCs, single cell force spectroscopy (SCFS) using an AFM was used [92]. In this capture the concentration dependency of RBC aggregation on dextran 70 kDa regarding maximum force, interaction distance and interaction energy will be presented at the cellular level. While finding that the contact time (up to 30 s) seems to play a subordinated role, the velocity of approach and retract seems to play a major role mainly due to viscosity effects of the surrounding solution. A careful comparison to previous studies [180] shows this as well. This study [180] was the main motivation for the SCFS experiments in the presented work, because the retraction force-distance curve, while separating the two cells via the cantilever from each other, shows an interaction force over long interacting distances (close to 20 μm) as depicted in fig. 3.32 (a) from [180]. In addition, the resulting bell-shape for dextran 70 kDa ends at approximately 45 mg/ml, which is not the case for all presented experiments in this work as it was shown above.

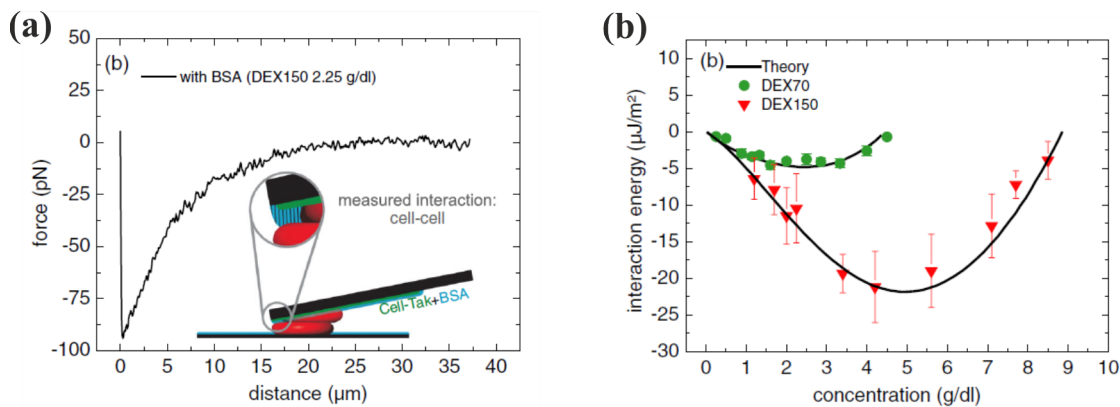


Figure 3.32: The force-distance curve while retracting the cantilever of two “adhered” cells for the case of dextran 150 kDa (a) leads to a bell-shape behavior regarding the interaction energy in dependency on the macromolecular concentration for both dextran 70 kDa and dextran 150 kDa. Measurements were performed by Patrick Steffen and published in [180].

In conclusion, on the one hand a velocity was found, which leads to a bell-shape behavior that differs from [180]. On the other hand, one should be aware that such measurements are extremely challenging regarding the parameter settings under the assumption that the measurements themselves are possible, which is still questionable. Therefore, the quantitative results (especially at high dextran concentrations) have to be taken with care.

Preparation

RBCs were recovered by a needlestick and prepared in the explained way (see chapter 2.3.3). The cantilever was prepared with Cell-Tak in order to be able to glue a cell onto the cantilever as depicted in chapter 2.3.7. The used dishes (Ibidi uncoated 60 μ -dish, 35mm, low, Ibidi GmbH, Martinsried, Germany) have the characteristic that RBCs stick well to them and most of the cells stay in their discocyte shapes over hours. Being capable of “catching” a cell with the cantilever it was necessary to coat a very small area with BSA as explained in chapter 2.3.8. Here a droplet of ca. 1 μ l of a 1 mg/ml BSA solution was used.

Protocol

After the calibration of the MLCT-O cantilever (Bruker) in the explained way of chapter 2.2.3.2 three droplets of 0.5 % (v/v) of RBCs were added directly onto the BSA-prepared dish and 1 ml of PBS was added immediately. Letting the RBCs sediment for approximately 5 min the AFM with the cantilever was placed on top of the sample. From this time one has ca. 3 min to catch a cell before the BSA, which is resolved partly into the PBS, which can passivate the Cell-Tak on the cantilever that much that the adherence of a RBC onto the dish is stronger than the adherence onto the cantilever. A cell was “caught” with a setpoint force of 2.5 nN, a velocity of 5 μ m/s using a contact time of 10 s. While the cantilever was in contact with the cell it was moved by hand slightly (approximately 2 μ m/s) in the x-y-direction (z-direction is here defined as the direction perpendicular to the dish area, which is defined as the x-y-direction). According to this procedure the cell shows a strong echinocyte shape, which changes after a few minutes into a discocyte shape again. 0.5 ml of a 3 mg/ml BSA solution was added to the system by hand with a syringe connected to a perfusion chamber. This creates a surrounding BSA concentration of 1 mg/ml, which passivates the cantilever and the dishes partly in order to avoid losing the cell from the cantilever, if there is a contact to the dish by accident. Then the cantilever was moved not less than 200 μ m away from the BSA coated area (previously marked by a scratch into the dish) and a RBC in discocyte shape was searched. This was done as fast as possible by focusing on the cell, which was attached to the cantilever. If the cell was moving significantly away from its position on the cantilever during the motion of the cantilever the whole procedure was done again until the cell was assumed to be well attached. Using a distance of about 10 μ m between the cells the outer shapes of the RBCs were aligned concentrically by changing the focus of the light microscope with a 40 times magnification objective. Regarding the used setpoint force (maximum deflection of the cantilever) in [180] of 300 pN here the same one was chosen. At least three measurements for the velocities 0.1 μ m/s, 1 μ m/s and 5 μ m/s were performed. The contact times were varied from 0 s over 5s to 30 s for all of them. The cantilever with the attached cell was approaching the cell adhered to dish using different velocities. As soon as it

reaches 300 pN the cantilever position was fixed and one of the three different contact times were applied before retracting the cantilever. This procedure was performed always before adding the dextran solutions in order to be sure that the cells are well attached (if they were not well attached a strong movement of the RBCs was recognized and the whole procedure was performed from the very beginning) and that the results are comparable for PBS.

After this 1.5 ml of a doubled concentrated dextran solution (with 1 mg/ml BSA inside) was added to the sample in order to reach the nominal dextran concentration. Further measurements were performed for at least seven cells attached to the dish (without changing the cell on the cantilever) by the same protocol as explained above and illustrated in 3.33.

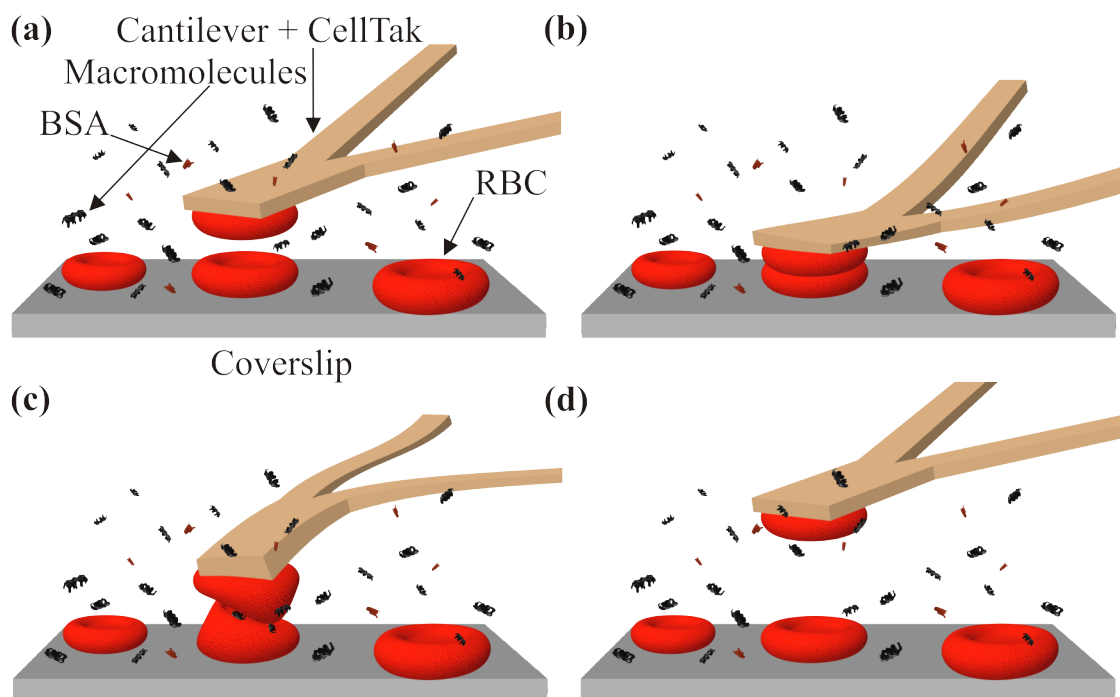


Figure 3.33: The AFM cell-cell adhesion measurement is performed by an approach with three different velocities (a) that leads to the contact of the two cells, while three contact times were used (b). Retracting the cantilever could lead to a deformation of the cells (c) and after the detachment of the RBC the cantilever should come to its approaching or no-contact position (d)

Exemplary data, data analysis and velocity

If the RBCs are aligned concentrically (see fig. 3.33 (b)) the resulting extend and retract data strongly depend on the velocity of the cantilever as depicted for a 40

mg/ml dextran solution as surrounding solution for the three applied velocities in fig. 3.34. Due to the fact that $0.1 \mu\text{m/s}$ will be chosen in the end of this chapter as the most reasonable velocity exemplary data for PBS instead of dextran are shown as well in (d). From those data the maximum interaction force is the absolute value of the lowest vertical deflection (e.g. approximately 250 pN, 50 pN, 15 pN and 20 pN in fig. 3.34 (a)-(d)). The interaction distance is the distance from 0 till the baseline is reached (e.g. approximately 20 μm , 3 μm , 1.5 μm and 1 μm in fig. 3.34 (a)-(d)). The interaction energy (depicted as gray areas) is calculated by the integration over the retract curve from 0 μm till the maximum interaction distance is reached (e.g. approximately 1396 aJ, 73 aJ, 16 aJ and 3 aJ in fig. 3.34 (a)-(d)).

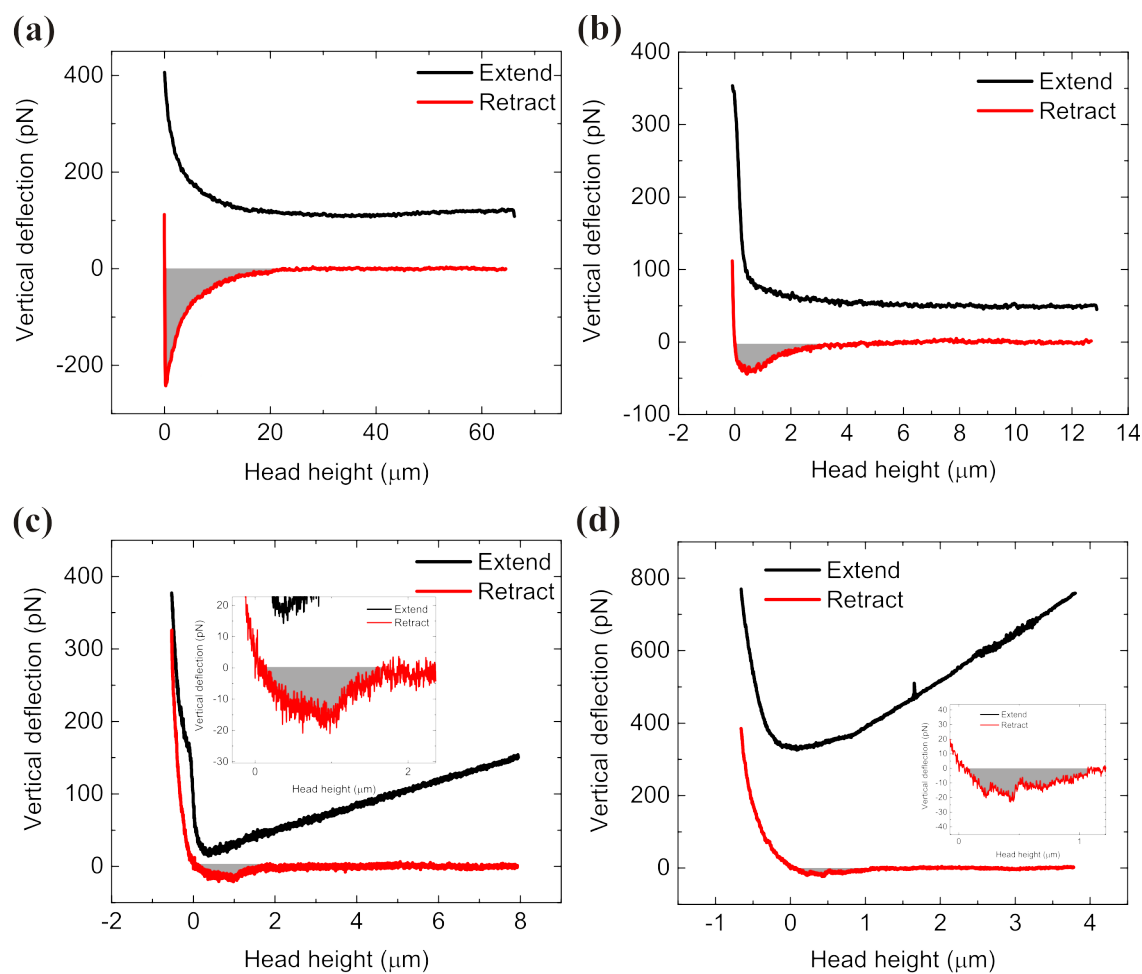


Figure 3.34: Exemplary data for 40 mg/ml dextran 70 kDa are shown for a contact time of 0 s with a velocity of $5 \mu\text{m/s}$ (a), 5 s with a velocity of $1 \mu\text{m/s}$ (b) and 5 s with a velocity of $0.1 \mu\text{m/s}$ (c). The SCFS for PBS is shown as a reference for a contact time of 30 s with a velocity of $0.1 \mu\text{m/s}$ (d). Insets in (c) and (d) show a magnification of the region of interest.

Obviously a decreasing velocity leads to a decrease of the three observed parameters (force, distance and energy), which is most probably caused by the viscosity of the surrounding solution. At the highest applied velocity of 5 $\mu\text{m/s}$ (see fig. 3.34 (a)) this effect is carried to extremes, because the retract curve is nearly the mirrored extend curve. The sharp transition from 0 μm to the other parts of the retract curve indicates that the cantilever deflection is mainly driven by viscosity effects instead of interactions between the two cells. Such interactions result in retract curves, which show a smooth retract curve as depicted in fig. 3.34 (b)-(d). Nevertheless, for the velocity of 1 $\mu\text{m/s}$ in a 40 mg/ml dextran-PBS solution it is assumed that the retract curve shows an overlay of viscosity and interaction effects, which will be explained below (see chapter 3.5.2).

If the RBCs are not matched concentrically (mismatched) as shown in fig. 3.41 the cell attached to the cantilever can interact with the Petri dish and the cell attached to the Petri dish can interact with the cantilever despite the partial BSA-passivation. The resulting raw data for PBS as surrounding solution are depicted in fig. 3.35 for a contact time of 0 s (a) and a contact time of 30 s (b) at a velocity of 5 $\mu\text{m/s}$. Two types of interactions are known for SCFS [92]: “Ordinary” unbinding events reasoned by the “glass effect” or/and the adhesive effect of the Cell-Tak on the cantilever, which can be recognized by short distance “jumps” in fig. 3.35. The second unbinding event is explained by the “glass effect” (the cell attached to the cantilever could bind to the petri dish) or/and the Cell-Tak on the cantilever (the cell attached to the petri dish could bind to the cantilever). Here tethers (parts of the double lipid layer of the membrane) are pulled out of the cell, which results in long distance interactions as shown in fig. 3.35 (b). Tethers are discussed more detailed in chapter 5.5. It is remarkable that in this specific SCFS experiment the contact time seems to play an important role for tether formations, cause for a long contact time (30 s) the interaction distance is by a factor of two larger than for 0 s. Nevertheless, results which are obtained when there is a mismatch of the RBCs were not analyzed and not taken into account for the SCFS experiment. Doing so, the contact time seems to have no influence as it is shown in the following chapter.

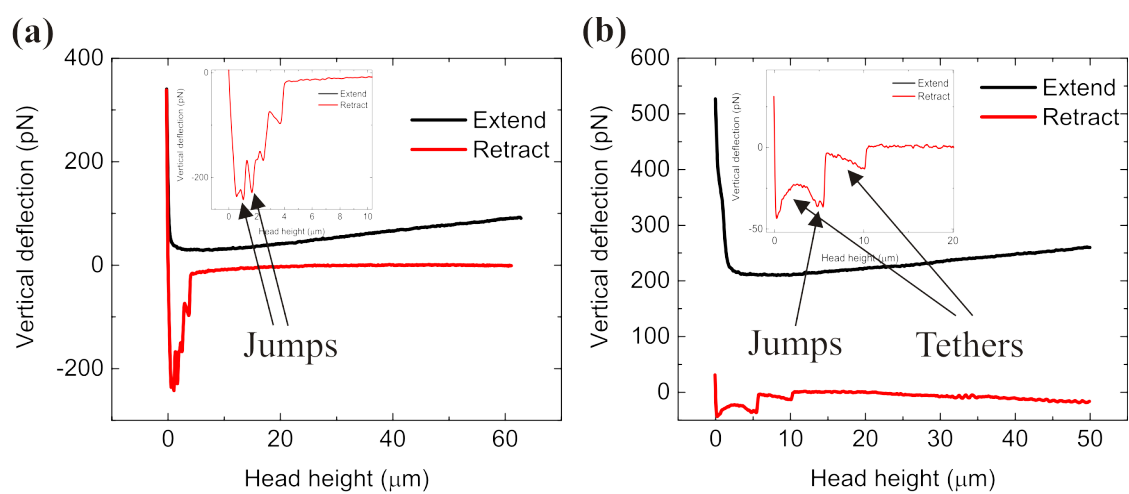


Figure 3.35: A mismatch of the RBCs in PBS at $5 \mu\text{m/s}$ leads to strong interaction forces at 0 s contact time (a) and can lead to strong tether formations at 30 s contact time with an increase of interaction distance by 100% (b) in comparison to (a).

Viscosity influence

Moving a cantilever in viscous media as e.g. dextran solutions, the viscosity can influence the vertical deflection and consequently the resulting interaction energy. If the experiment is performed as explained in chapter 3.5.2 one finds that an increasing interaction energy can be caused by the viscosity as depicted in fig. 3.36. The results for the maximum force and interaction distance show the same trend. As already mapped in fig. 3.34 (a) and (b) for 5 $\mu\text{m/s}$ and 1 $\mu\text{m/s}$ the extend and retract curves are pretty similar (mirrored on an horizontal line), which is driven by the viscosity. For high velocities and high concentrations of dextran (starting from 80 mg/ml) the RBCs were not in contact anymore, which was observed optically by the total absence of a cell deformation that is typical for the case of contact. This could be attributed to shielding effects, which means that the high viscous medium in between the cells become not pressed out of the intercellular volume before the cantilever reaches the maximum setpoint force. Consequently, the set contact parameters are reached before the RBCs are in contact. Therefore, for the further analysis only the lowest applied velocity of 0.1 $\mu\text{m/s}$ was taken into account.

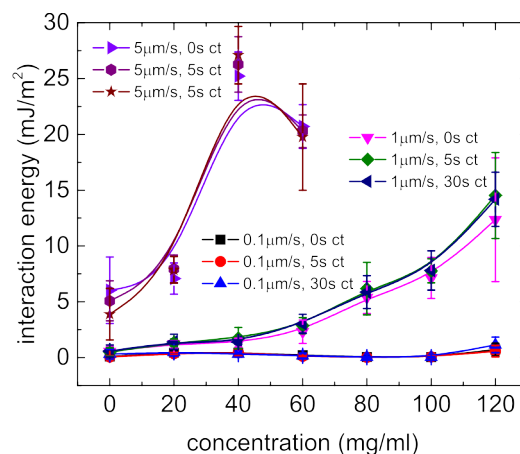


Figure 3.36: The interaction energy of SCFS versus on the dextran concentration by varying the extend/retract velocity from 0.1 over 1 to 5 $\mu\text{m/s}$ and the contact time (ct) from 0 over 5 to 30s. For high concentration of 80 mg/ml and more at 5 $\mu\text{m/s}$ the cells were not in contact anymore. Error bars represent the standard deviations of at least seven individual bottom cells using the same cell attached to the cantilever. Lines are there to guide the eye.

In order to isolate the pure viscosity effect from the cell-cell adhesion effect reference measurements with the same surrounding solutions (BSA and dextran 70 kDa in PBS) as for the SCFS experiments, but without RBCs, were performed as illustrated in fig. 3.37 (a). While the maximum forces are significantly higher, the interaction distances are in the same order as it was the case for SCFS as depicted in fig. 3.37 (b)

and (c). This leads to a higher interaction energy that is not depicted in relation to the area but as absolute values, because the interaction area of the cantilever with the petri dish is not known as shown in fig. 3.37 (d). This result allows the assumption that the interaction between the cantilever and the dish could be similar as the interaction between the two RBCs performing SCFS. Consequently, this method does not allow to separate the viscosity effect from the cell-cell adhesion effects, because of the adhesion between the cantilever and the Petri dish.

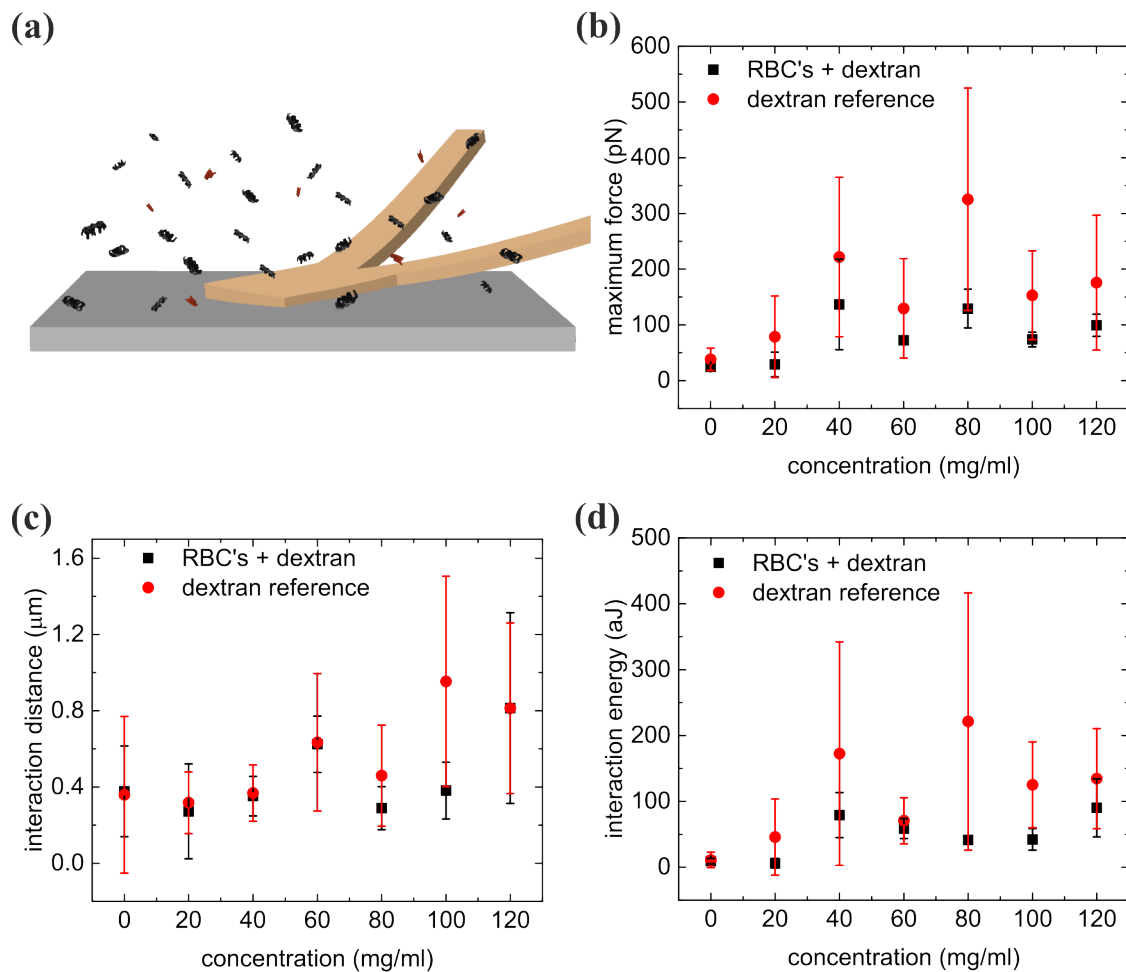


Figure 3.37: AFM measurements of the cantilever in BSA-dextran solutions without RBCs involved (a) compared with RBCs involved measurements for a velocity of $0.1 \mu\text{m/s}$ and 0 s of contact time. This leads to a higher maximum force (b), a comparable interaction distance (c) and a higher interaction energy for measurements without RBCs involved as a function of the dextran concentrations (d). Due to the high error bars (standard deviation) for dextran measurements without RBCs one can assume that the dextran reference leads to at least higher interaction forces and therefore to slightly higher interaction energies.

Glycerin-water mixtures were assumed not to influence the direct interaction between cantilever and Petri dish. These experiments were conducted following the same protocol as for SCFS. Knowing the viscosity of the used dextran solutions and the glycerin-water solutions (explained in fig. 5.8) one can translate the v/v concentration of glycerin-water into an equivalent dextran concentration. This leads to a direct comparison between the pure viscosity effect and the results of the SCFS. As depicted in fig. 3.38 (a), (b) and (d) with an increasing glycerin-water concentration the results stay constant up to a related dextran concentration of 80 mg/ml, where a slight increase is observed. This means that even at a velocity of 0.1 $\mu\text{m/s}$ a viscosity of approximately 4.3 mPa s (equivalent to 80 mg/ml dextran solution) has an influence on the measurements. The SCFS results (fig. 3.38 (a)-(c)) in a bell-shape behavior which ends around 80 mg/ml, while it is increasing again at 120 mg/ml. The observed bell-shape ends around 120 mg/ml usually, but not around 80 mg/ml. Possible explanations for this effect could be: First, as one can observe in fig. 3.38 (a) and (b) at 80 mg/ml the viscosity starts to play a role, since the maximum force and distance of the glycerin-water solution are increasing as well. Consequently, it seems most likely that the viscosity effects overcome the cell-cell interaction effects. Second, as depicted in fig. 3.34 (c) the interaction area and maximum force is in the order of the noise of the cantilever for the SCFS, which could lead to a suppression of cell-cell interactions by the noise of the AFM. Third, the error bars of the interaction distance for 80 and 100 mg/ml in fig. 3.38 (b) are by a factor of approximately four times smaller than the error bar up to 60 mg/ml. Additionally, the error bars and values for the interaction energy and maximum force are in the range of the glycerin-water ones. That leads to two consequences: First, a differentiation between cell-cell interaction and viscosity effects is not possible for 80 and 100 mg/ml, which is supported by the similar values of cell-cell interaction and the glycerin water reference. Second, assuming that shielding effects play a role for such high dextran concentrations the cells are potentially not in contact due to a too high approaching velocity, which is supported by the small error bars of the cell-cell interaction in comparison to the high error bars at lower concentrations.

These explanations are not supported by the very high values and error bars of 120 mg/ml for both interaction distance and maximum force. As a possible argument dextran seems to stabilize tethers between RBCs and the cantilever or the dish (see chapter 3.5.2). In addition, long tethers were observed between two or three RBCs (see chapter 5.5). At 120 mg/ml this effect could be so significant that no rupture of the tethers can be seen in the raw data or by eye. On the other hand, effects like this could happen for low dextran concentrations as well. Consequently, it is necessary to understand the tether formations in order to understand the SCFS data.

One could eventually overcome the noise level with a stiffer cantilever. A rectangular cantilever instead of an used V-shape cantilever would reduce the surface which interacts with the viscous surrounding medium, and consequently it could reduce

viscosity effects. Another option could be to reduce the velocity even further, which will be discussed in the next section.

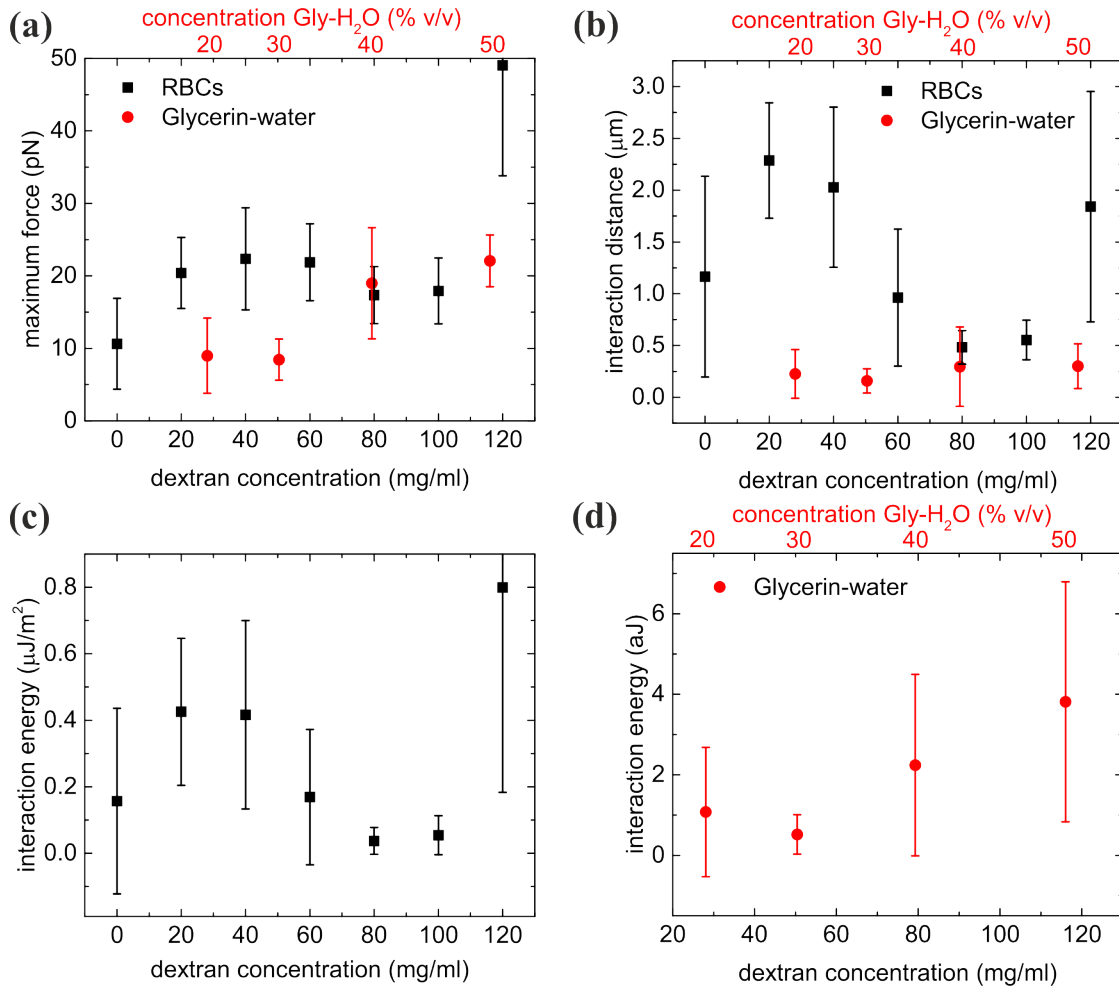


Figure 3.38: Comparison between the SCFS and the glycerin-water reference regarding the maximum force (a), interaction distance (b), interaction energy with taken the RBC contact area into account (c) and interaction energy for glycerin-water without taken any area into account because it is not known (d). Error bars represent the standard deviation of at least seven measurements. The exact values of the measured glycerin-water concentrations are given at the second x-axis and related to the dextran concentrations via the viscosity as depicted in 5.8.

Velocity influence

Velocities of $0.1 \mu\text{m/s}$ and higher were already discussed in the section 3.5.2 above. As depicted before for high concentrations of dextran or glycerin, viscosity plays an important role. Consequently, a glycerin-water mixture of 50%, which has approximately the same viscosity as 120 mg/ml of a dextran 70 kDa solution (see appendix fig. 5.8), was used to determine the velocity at which the pseudo-interaction between cantilever and Petri dish is negligible. Exemplary data for $0.04 \mu\text{m/s}$ are depicted in fig. 3.39 (a). The inset shows the magnification of the region, which could be potentially taken for approximation (marked in gray). For a velocity of $0.01 \mu\text{m/s}$ no interaction was observed. The sinus-like retract curve is based on a well-known effect: The laser of the AFM becomes reflected by the cantilever tip itself and by the sample. This leads to a constructive interference as depicted in the inset of fig. 3.39 (b). The phase of the resulting wave is in the order of two micrometers, which is approximately the double of the wavelength of the laser, making this explanation plausible. Due to the fact that for $0.01 \mu\text{m/s}$ no interaction driven by the viscosity could be observed this velocity is the favorable one for dextran concentrations up to 120 mg/ml (respectively 50% v/v glycerin-water).

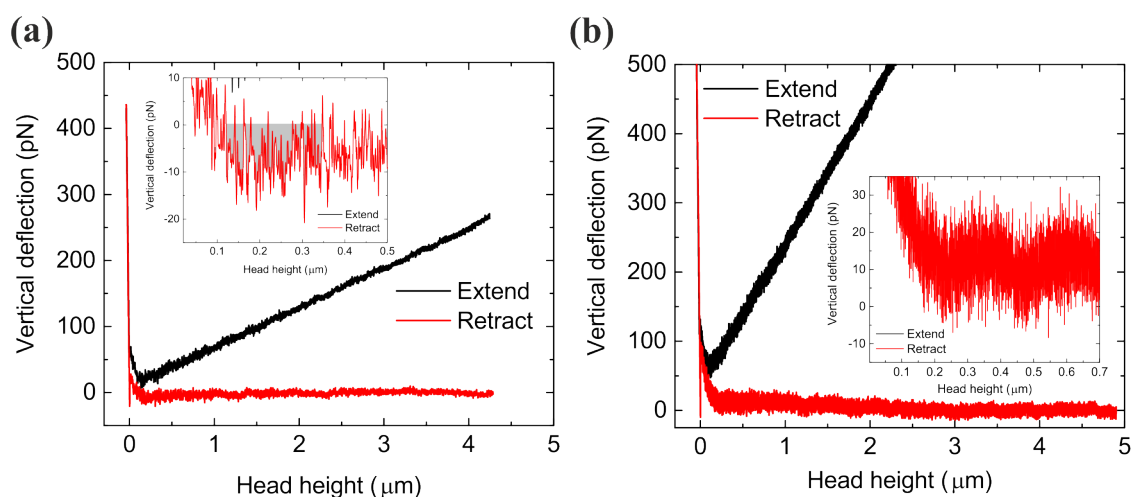


Figure 3.39: A 50 % v/v glycerin-water solution is used to measure the velocity dependency of the vertical deflection for $0.04 \mu\text{m/s}$ (a) and $0.01 \mu\text{m/s}$ (b). Both insets show the magnification of the retract curve in the potentially approximable range. Grey marked regions indicate possible integration areas.

The sharp peaks at the beginning of the retract curve (at around $0 \mu\text{m}$) are most probably due to electrostatic interactions between the cantilever and the dish.

SCFS was not performed for such low velocities, since the effect using $0.1 \mu\text{m/s}$ is already in the range of the noise. At a lower velocity at the same sampling rate the noise level will increase. This is potentially going to suppress the effect of the

cell-cell interaction. Consequently, this measurement setup seems not to be valid for this specific cell-cell interaction. The AFM was placed on top of an active damper, but effects of the surroundings cannot be excluded completely. Such an exclusion would be necessary to reduce the noise level. In summary, if these measurements are possible excluding the viscosity effect completely is still questionable.

3D analysis of the SCFS experiments

Using SCFS the cells could be deformed mechanically. The AFM was used in combination with the spinning disc confocal microscope (see chapter 2.2.1 for details) in order to relate the deformation of the cells with the force applied to them, which are ongoing investigations. The protocol was exactly the same as for the standard SCFS at 20 mg/ml dextran with two exceptions: First, the cells were labeled with CellMask before the SCFS protocol was applied. Second, the retract was stopped every micrometer in order to perform a z-scan with the spinning disk microscope. The results are illustrated in fig. 3.40. After the first retract of 1 μm with 0.1 $\mu\text{m}/\text{s}$ the image shown in fig. 3.40 (c) was taken. In the middle one can see the RBC pair from the top while the right and bottom image showing the side view of the RBC pair. At the bottom image the lower cell is in contact with the cantilever; at the right image the right cell is in contact with the cantilever. Here it is remarkable that two contact areas, i.e. two bulges, appear from one cell to the other. It seems that those are independent of the discocyte shape of the cell, as they are much closer to the axis of symmetry than to the edges. The 3D-reconstruction is depicted in fig. 3.40 (e). Here the cell pair has a height of approximately 5 μm . The further reconstructed area below the cell pair is a reflection of the upper cell on the cantilever axis. This effect happened as well for reflections onto the cantilever. A further retract by 3 μm leads to a break up of one contact area and a more significant deformation of the lower cell as shown in fig. 3.40 (d). This deformation can be seen clearly in the 3D-reconstruction (f). By retracting the cantilever fully the cell attached to the dish stayed in its deformed shape, which can't be explained for now. The whole measurement took ca. one hour, which is much longer than the SFCS measurements that were performed within several minutes for one cell pair. In addition, CellMask was not involved in the SFCS measurements. This issue remains an ongoing open question.

Performing this type of SCFS experiments there is a risk of mis-aligning the two cells, because of optical issues as e.g. the resolution limit of the microscope. This leads to a contact of the cell attached to the cantilever with the dish and a contact of the cell attached to the dish with the cantilever. It is shown in fig. 3.41 (a) graphically and in (c) as well as in (e) reconstructed in 3D. If the cantilever becomes now retracted tethers can be pulled out of the cells as depicted in fig. 3.41 (b) graphically and in (d) as well as in (f) reconstructed in 3D. The maximum visualizable distance in 3D was around 25 μm due to bleaching effects. Moving now the cantilever in x-y-direction

the cell attached to the dish shows a significant deformation of the cell in direction of the tether. This could be also used to quantify the maximum length of this specific tether without using a confocal microscope. The experiment was stopped when the cantilever reached the end of the dish while the tether did not break and has a length of around 1200 μm (see chapter 5.5). For comparison, a mismatch of cells in 0 mg/ml dextran leads to a break-up of the tethers within 1-5 μm and not 1.2 cm as it was the case for 20 mg/ml dextran 70 kDa. As a consequence, dextran seems to facilitate the formation of membrane tethers significantly over a long distance, which should be further investigated in order to understand the SCFS measurements better.

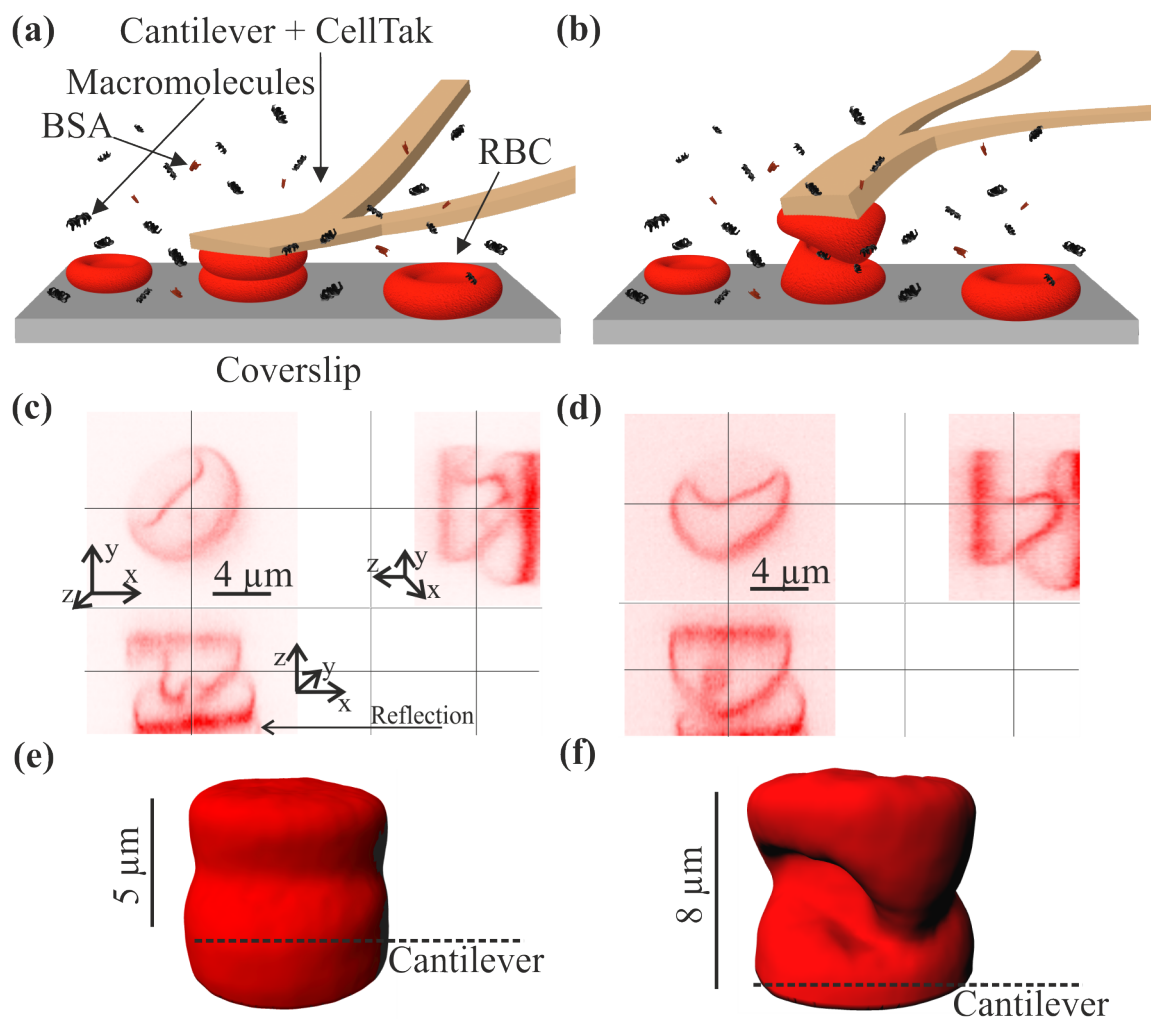


Figure 3.40: If the cells overlap properly (a) they could show a deformed shape while retracting the cantilever (b). In the 3D side view one can see that they match properly (c) and deform during the retraction of the cantilever (d), which is depicted in a 3D reconstruction in (e) for the matching and (f) for the retraction. The cantilever position could be illustrated in the 3D reconstructions, because of side view images and the knowledge that the cantilever encloses an angle of 10° with the dish.

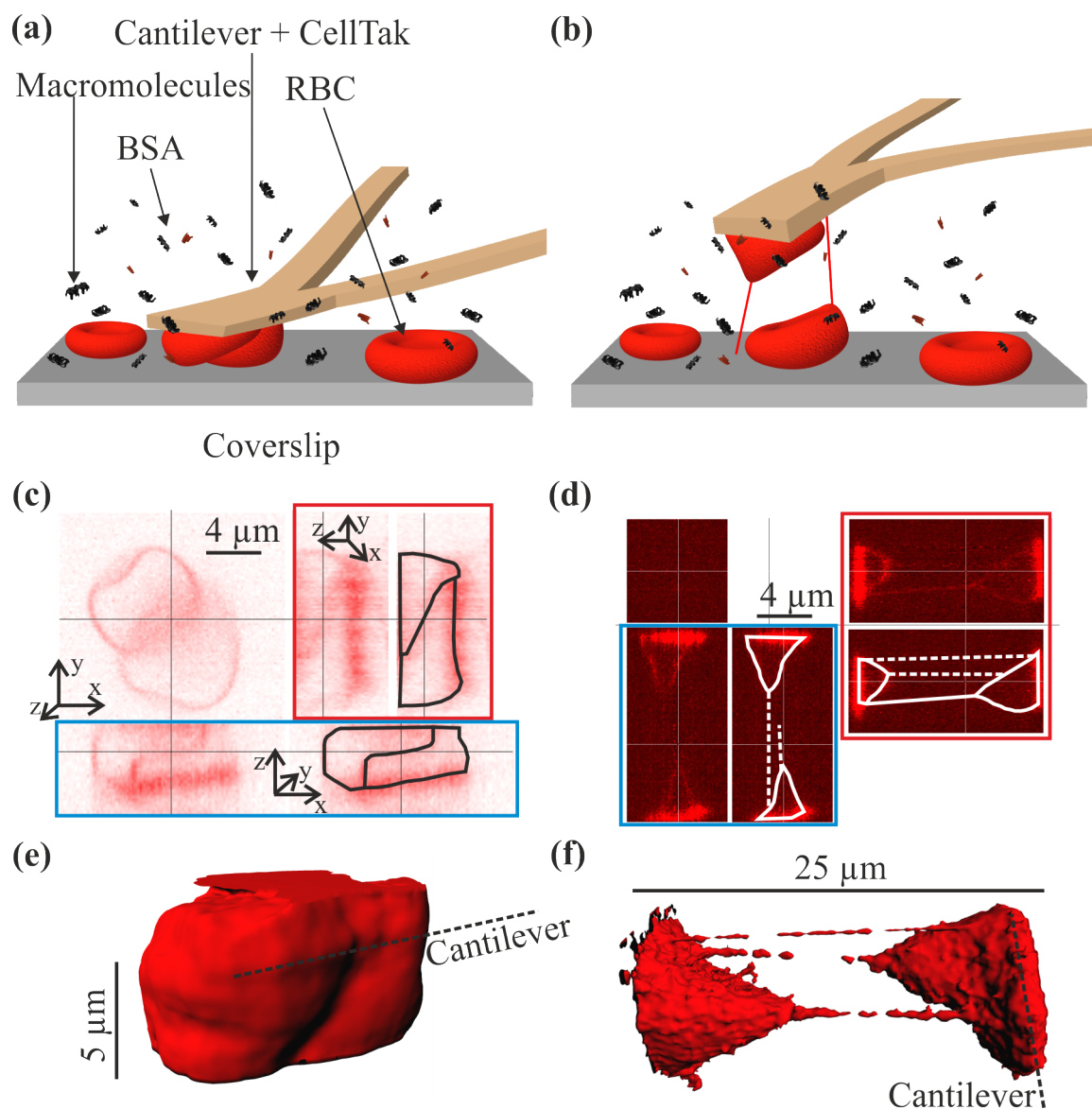


Figure 3.41: If the cells are not concentrically aligned (a) this could lead to an interaction between the upper cell and the coverslip or/and the lower cell and the cantilever (b). This happens as shown in the side view of the mismatch (c) and the retraction phase of the cantilever (d), while it is difficult to see the cell membrane in the original images due to bleaching effects. Therefore, the cell membranes are marked with black (c) and white (d) for a better visualization. The mismatch of the cells is depicted in (e) in a 3D reconstruction, while there is an mirroring by the cantilever of the cell which is attached to the cantilever. Consequently, the scale bar is showing the area that is including the cells (the part above the scale bar is the mirrored part). Retracting the mismatched cells by ca. $20\ \mu\text{m}$ that is taken by the cell itself only leads to a tether formation (f). The tethers are not touching the cells itself (even if it appears like this in the 3D reconstructions) but the coverslip and the cantilever, which is due to an over illumination of the cell-attached areas (d) and an over estimation of the threshold in case of the reconstruction (f).

Summary and discussion of the AFM experiments

In conclusion, it was shown that the local Young's modulus of RBCs decreases with an increasing dextran concentration. The presence of fibrinogen instead of dextran seems to have no influence on the local Young's modulus of RBCs.

The SCFS showed that the viscosity of the surrounding medium is affecting the maximum velocity of the cantilever, which should be used to obtain data that are not influenced by viscous effects, significantly. By using glycerin-water as a reference it was found that $0.01 \mu\text{m/s}$ seems to be the velocity at which a liquid with the viscosity of dextran 70 kDa (at 120 mg/ml with $\eta \approx 7.4 \text{ mPa s}$) has no influence on the measurement anymore. Due to the fact that the same measurements as the SCFS experiments with pure dextran solutions and without RBCs lead to a similar result, the effect of dextran onto two RBCs (see chapter depletion and bridging 2.1.3) could be the same as for the interaction between the cantilever and the dish. Nevertheless, the tendency of a bell-shape up to 80 mg/ml could be shown at $0.1 \mu\text{m/s}$ for cell-cell interactions in the presence of dextran and BSA. The absolute values of the interaction energy are very low and have to be taken with care, because the calibration factor (of JPK instruments) is just valid for rectangular cantilevers and could change for V-shape cantilevers, which were used in order to compare the data directly with Steffen et al. [180]. Moreover, no contact time dependency could be found. This results are nevertheless in excellent agreement with the results of Kern [111] by performing a very similar measurement with optical tweezers, which is a less invasive method.

The SCFS measurements were mainly driven by the fact that Steffen et al. [180] showed a bell-shape ending at around 45 mg/ml dextran. All measurements (except the AFM) of this thesis show that the bell-shape ends at ca. 120 mg/ml . This discrepancy is most probably due to the viscosity effect, because Steffen et al. measured the velocity at 25 mg/ml of dextran just down to $2 \mu\text{m/s}$. Here, a velocity of $0.1 \mu\text{m/s}$ was used, since all greater velocities show a mirroring effect for approach and retract, which is most probably due to the viscosity effect of dextran (already at 40 mg/ml). Moreover, the interaction energy seems to be independent of the setpoint force at [180], which is not possible due to the mirroring effect at the used $5 \mu\text{m/s}$. Last but not least, the contact time seems to play no role in the measurements presented in the manuscript at hand, while it does at [180]. The primary motivation of the presented results was to understand why the data of [180] differ from investigations like the microscopical aggregation index, rheology and sedimentation. The authors mentioned a possible relation between tethers and the high interaction length, which was shown to be an effect of the viscosity. In summary, it appears likely that Steffen and co-workers [180] measured mainly a viscosity effect and not a pure cell-cell interaction.

Finally, the 3D analysis of the SCFS experiment with a confocal microscope showed that the cells deform strongly and stay in their deformed shape (at least for minutes), if the measurement takes around one hour. In addition, there can be more than

just one contact area in between the cells while the retract phase of the cantilever. Tethers can be pulled out of the cell with this experiment in the presence of dextran easily. Due to the fact that the tethers are fluorescent in addition with the properties of the used dye CellMask it is obvious that those tethers are parts of the membrane as suggested in the literature [28, 96, 98]. With respect to the SCFS experiments the tethers can play an important role in this kind of experiments. Therefore, they have to be investigated carefully before claiming a clear result.

Résumé et discussion sur les mesures AFM

En conclusion, il a été montré ici que le module de Young local des RBCs décroît avec une concentration croissante de Dextran. L'utilisation de fibrinogène en lieu du Dextran ne paraît pas, en revanche, avoir d'influence sur le module de Young local des RBCs.

La spectroscopie de force sur cellule unique (en anglais Single Cell Force Spectroscopy ou SCFS) a montré que la viscosité du milieu environnant a un effet important sur la vitesse maximale du micro-levier, alors que ce dernier est censé donner accès à des mesures indépendantes de la viscosité. En utilisant un mélange eau-glycérol comme référence, il a été trouvé que pour un liquide ayant la viscosité du Dextran de 70 kDa (à 120 mg/mL avec une viscosité de 7.4 mPa.s), une vitesse de 0,01 $\mu\text{m/s}$ doit être utilisée pour s'affranchir de ces effets de viscosité. Puisque les mesures similaires aux mesures SCFS avec des solutions de Dextran pur et sans RBCs ont donné des résultats semblables, l'effet du Dextran entre deux RBCs (voir chapitre déplétion et pontage 2.1.3) pourrait être le même que dans le cas de l'interaction entre le micro-levier et la cuve de mesure. Néanmoins, un résultat tendant vers un comportement de courbe en cloche a pu être observé jusqu'à 80 mg/ml avec une vitesse de 0,1 $\mu\text{m/s}$ pour des mesures d'interaction cellule-cellule en présence de Dextran ou de BSA. Les valeurs absolues de l'énergie d'interaction sont très faibles et doivent être prises avec précaution car le facteur de calibration (des instruments JPK) n'est seulement valable que dans le cas de micro-leviers rectangulaire et peuvent être différents pour les micro-leviers en Y utilisés dans les données comparatives obtenues par Steffen et collaborateurs [180]. De plus, aucune dépendance avec le temps n'a pu être trouvée. Cependant ces résultats sont en très bon accord avec ceux de Kern [111] obtenus pour des expériences similaires avec une pince optique, une méthode moins invasive.

Les mesures SCFS étaient principalement motivées par le fait que Steffen et al. [180] ont montré une courbe en cloche se terminant aux alentours de 45 mg/ml de Dextran. Toutes les mesures de cette thèse (exception faite des mesures AFM) ont montré une courbe en cloche finissant plutôt vers 120 mg/ml. Cette différence provient très certainement des effets de viscosité car dans leur article, Steffen et collaborateurs ont utilisé, pour une concentration de 25 mg/ml, une vitesse de 2 $\mu\text{m/s}$. Dans notre cas, une vitesse de 0,1 $\mu\text{m/s}$ a été utilisée car toute vitesse supérieure entraîne un

effet de réflexion à l'approche et au retrait, provenant très certainement des effets de viscosité (et cela même à des concentrations de l'ordre de 40 mg/ml). De plus, dans [180], l'énergie d'interaction semble indépendante de la force de contact imposée ce qui ne paraît pas plausible en raison des effets de réflexion présents à la vitesse de 5 $\mu\text{m/s}$ utilisée. Enfin, le temps de contact ne semble jouer aucun rôle dans les mesures présentées dans cette thèse alors qu'il en a un dans [180]. La motivation première des résultats présentés ici était de comprendre pourquoi les mesures de [180] sont si différentes des résultats obtenus par les mesures de MAI, de rhéologie et de sédimentation. Les auteurs ont mentionné une très probable relation entre la pointe AFM et les grandes longueurs d'interactions, ce qui a été montré ici comme étant un effet de viscosité. En résumé, il semblerait que Steffen et collaborateurs [180] aient principalement mesuré un effet de viscosité et non une simple interaction cellule-cellule.

Enfin, les analyses 3D de SCFS couplée à la microscopie confocale ont montré que les cellules se déforment fortement et restent dans cet état déformé (au moins pendant plusieurs minutes) si la mesure dure environ une heure. De plus, plusieurs zones de contact peuvent coexister lors de la rétraction du micro-levier. Des tubes de cellules ont pu aussi être facilement étirés en présence de Dextran. Du fait que ces tubes soient fluorescent en présence du marqueur membranaire CellMask, il semble évident que ces tubes soient similaires aux tubes de membrane cellulaire décrits dans la littérature [28, 96, 98]. Dans le cadre des expériences de SCFS, ces tubes peuvent jouer un rôle important. Il conviendra alors dans le futur de caractériser de manière précise ces extensions de manière à éclaircir les résultats.

Zusammenfassung und Diskussion der AFM Experimente

Zusammengefasst wurde gezeigt, dass die lokale Elastizität roter Blutzellen mit steigender Dextranskonzentration abnimmt. Die Anwesenheit von Fibrinogen statt Dextran scheint keinen Einfluss auf die Elastizität roter Blutzellen zu haben.

Mit SCFS wurde gezeigt, dass die Viskosität des umgebenden Mediums die Maximalgeschwindigkeit des Cantilevers beeinflusst, was genutzt werden sollte, um Daten zu erhalten, die nicht signifikant von Viskositätseffekten beeinflusst werden. Unter Verwendung einer Glycerin-Wasser-Lösung als Referenz wurde 0,01 $\mu\text{m/s}$ als die Geschwindigkeit identifiziert, bei der eine Flüssigkeit von der Viskosität von Dextran 70 kDa (bei 120 mg/ml mit $\eta \approx 7.4 \text{ mPa s}$) keinen Einfluss auf die Messung mehr hat. Da dieselben Messungen wie die SCFS Experimente mit reinen Dextranlösungen und ohne rote Blutzellen zu einem ähnlichen Resultat führen, könnte der Effekt von Dextran auf zwei rote Blutzellen (vergleiche Kapitel 2.1.3) derselbe sein wie für die Interaktion zwischen Cantilever und Probenbehälter. Nichtsdestotrotz konnte die Tendenz zu einer Glockenkurve bis 80 mg/ml bei 0,1 $\mu\text{m/s}$ für Zell-Zell-Interaktionen bei der Anwesenheit von BSA gezeigt werden. Die Absolutwerte der Interaktionsenergie sind sehr gering und mit Vorsicht zu betrachten, da der Kalibrierungsfaktor (von JPK instruments) nur für rechteckige Cantilever valide ist und

sich für V-förmige Cantilever ändern könnte, die hier benutzt wurden, um die Daten direkt mit denen von Steffen et al. [180] zu vergleichen. Außerdem konnte keine Abhängigkeit der Kontaktzeit gefunden werden. Diese Resultate stimmen mit den Ergebnissen von Kern [111] bei der Durchführung einer ähnlichen Messung unter der Verwendung von optischen Pinzetten, was eine weniger invasive Methode ist, überein.

Die SCFS Messungen wurden wesentlich durch die Tatsache, dass die Glockenkurve von Steffen et al. [180] bei ca. 45 mg/ml Dextran endet, motiviert. Alle Messungen der hier vorgestellten Arbeit (ausgenommen AFM) zeigen ein Ende der Glockenkurve bei 120 mg/ml. Dieser Unterschied ist sehr wahrscheinlich auf Viskositätseffekte zurückzuführen, da Steffen et al. die Geschwindigkeit bei 25 mg/ml Dextran nur bis zu einem Minimalwert von 2 $\mu\text{m/s}$ gemessen haben. Hier wurde eine Geschwindigkeit von 0,1 $\mu\text{m/s}$ genutzt, da alle höheren Viskositäten einen Spiegel-effekt für Annäherung und Rückzug des Cantilevers zeigen, was sehr wahrscheinlich auf Viskositätseffekte von Dextran (bereits bei 40 mg/ml) zurückzuführen ist. Darüber hinaus scheint die Interaktionsenergie unabhängig von der Sollwertkraft bei [180] zu sein, was aufgrund der verwendeten 5 $\mu\text{m/s}$ nicht möglich ist. Zuletzt scheint die Kontaktzeit keine Rolle für die hier vorgestellten Messungen zu spielen während dies bei [180] der Fall ist. Die primäre Motivation der hier gezeigten Resultate war die Entwicklung eines Verständnisses für die Abweichung der Daten von [180] von Untersuchungen wie dem mikroskopischen Aggregationsindex, Rheologie und Sedimentation. Die Autoren nahmen eine mögliche Relation zwischen Tethers und den großen Interaktionsreichweiten an, was aufgrund der hier vorgestellten Resultate ein reiner Viskositätseffekt zu sein scheint. Zusammenfassend scheint es höchstwahrscheinlich, dass Steffen und Koautoren [180] hauptsächlich einen Viskositätseffekt und keine reine Zell-Zell-Interaktion gemessen haben.

Zu guter Letzt zeigte die 3D-Analyse der SCFS Experimente mit einem Konfokalmikroskop eine starke Deformation der Zellen und einen Verbleib dieser im deformierten Zustand (mindestens für einige Minuten), wenn die Messung selbst etwa eine Stunde dauert. Ergänzend kann mehr als nur eine Kontaktzone zwischen den Zellen während des Rückzugs des Cantilevers auftreten. Tethers können bei Anwesenheit von Dextran leicht aus den Zellen gezogen werden. Aufgrund der Tatsache, dass die Tether fluoreszent sind und der Eigenschaften des verwendeten Farbstoffs CellMask, ist es offensichtlich, dass diese Tethers Teile der Membrane sind, wie in der Literatur angenommen [28, 96, 98]. Bezugnehmend auf die SCFS Experimente können die Tethers eine wichtige Rolle für eine solche Art von Experimenten spielen. Daher müssen diese weiter untersucht werden, bevor ein klares Resultat gegeben werden kann.

3.6 Depletion versus bridging discussion

This chapter focuses on a variety of different experiments with the aim to develop a deeper understanding of the origin of RBC aggregation, i.e. if the primary effect is depletion or bridging. The effects of fibrinogen induced and dextran induced RBC aggregation into the models of depletion or bridging are discussed, with the final argument that depletion could be potentially proofed while this is much more challenging for bridging. Finally “bridletion” as an overlaying effect of bridging and depletion is proposed to explain the RBC aggregation with respect to both theories that are not excluding each other.

3.6.1 Adsorption of macromolecules

3.6.1.1 Surface acoustic waves

Eight flow channels were labeled with Cell-Tak (see chapter 2.3.7) that allows a good adherence of erythrocytes. The cells were prepared as explained in chapter 2.3.3. Afterwards, the pellet was mixed in the ratio 1:3 with PBS to prevent a potential channel blocking. First, PBS was flowed over all channels for 10 min to create a valid reference without anything attached except Cell-Tak. Second, erythrocytes (1:3 cells:PBS) were flowed through two channels for 3 min in order to let the cells adhere to the chip while two channels were kept without cells. In a third step, again PBS was flowed through all chips for 10 min in order to remove all non-adhered RBCs. Now, the first and lowest dextran 70 kDa concentration of 15 mg/ml (exact formulation see chapter 2.3.6) was flowed through all channels for 10 min. This was followed by PBS for 10 min before adding the next dextran concentration of 30 mg/ml etc. Two more dextran concentration of 60 and 120 mg/ml were applied to the same cells. All investigations were performed at 23° C with a flow velocity of 15 μ l/s while the phase and amplitude for both empty channel (just Cell-Tak) and the erythrocyte adhered channel were measured. A response of the acoustic wave only due to viscosity effects was measured, which was taken for each dextran concentration as the reference, called “empty (Cell-Tak)”. Therefore, the effective signal induced by the interaction between RBCs and the dextran molecules is basically the difference between the erythrocyte and empty channel as depicted in fig. 3.42.

The phase, a measure for the mass, increases with increasing dextran concentration, which leads to the assumption that the amount of dextran adhered to the RBCs increases with increasing dextran concentration. Moreover, the rapid decrease and the return to the baseline in phase by flowing PBS after dextran over the cells indicates that the dextran molecules are completely washed away from the cells by adding PBS within the resolution of the instrument as depicted in fig. 3.42 (a). The

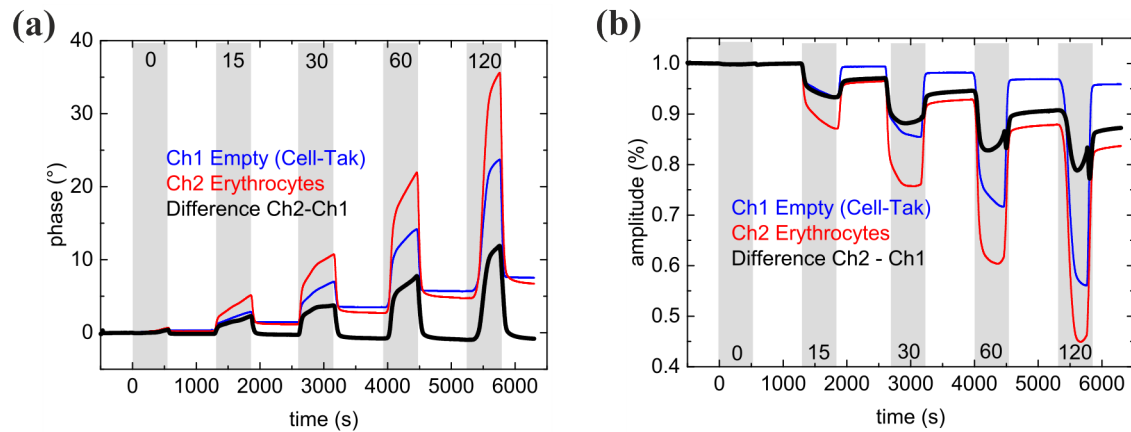


Figure 3.42: SAW measurements for dextran indicates a mass increase with dextran concentration shown by an increasing phase (a) while the flexibility of RBCs increase with the dextran concentration shown by a decreasing amplitude (b). Grey areas are indicating the added dextran concentration in mg/ml.

amplitude, as a measure for the flexibility, shows an increasing flexibility for increasing dextran concentrations, which leads to the assumption that the adhered dextran decreases the global Young's modulus. This observation is in good qualitative agreement with the local elasticity measurement performed by AFM (see chapter 3.5.1). Moreover, the addition of PBS does not induce a relapse to the amplitude baseline of 1. This indicates that the addition of dextran creates a non-reversible decrease of the Young's modulus within the observed time of 10 min for the PBS flow. Nevertheless, the slope of the amplitude during the addition of PBS shows a tendency towards the direction of the baseline, which could indicate that the process is not fully irreversible, but strongly depending on time. It is remarkable that the dextran molecules are fully removed from the cells by the addition of PBS as can be seen in the phase while the RBCs stay in a more flexible state for at least 10 min.

This leads to the final proposition that dextran acts on at least the double-lipid layer or the cytoskeleton, which have the main influence on cell stiffness [29, 85]. An adsorption of dextran molecules onto RBCs was clearly shown even though the binding seems not to be very strong, because the macromolecules can be removed easily within a relative short time.

In addition, the same measurements were performed with fibrinogen as delivered by Sigma Aldrich instead of dextran at the concentrations of 2, 4, 8, 15, 30 and 60 mg/ml. The empty channels show here a more significant signal than the erythrocyte channel, which indicates at least that potential binding or stiffness effects are much lower than for dextran or even not existing for low flow rates as 15 $\mu\text{l/s}$ as depicted in fig. 3.43.

Moreover, the chip was labeled with dextran 15 kDa as a control and dextran 70 kDa while the cells were flown over the chip instead of the other way around as

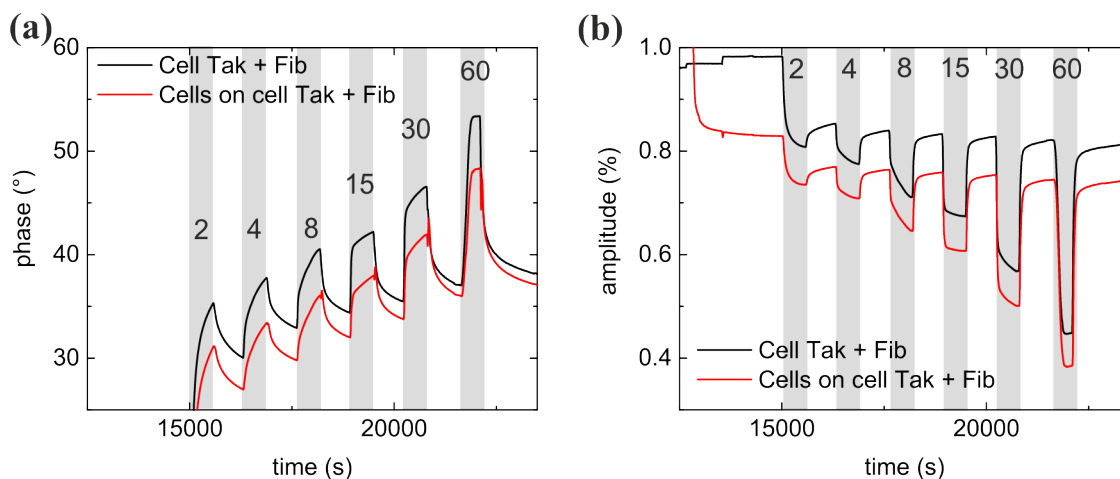


Figure 3.43: SAW results of the phase (a) and the amplitude (b) for RBC attached to the chip and fibrinogen flowed over. Reference signal (without cells) is higher than signal with cells. Grey areas are indicating the fibrinogen concentration in mg/ml.

discussed above. Additionally, an empty chip without any labeling was used as a reference. For both dextran 15 kDa and dextran 70 kDa the effect of the empty chip was much more significant, which means basically that the cells prefer to adhere onto the empty chip (respectively gold) than to the dextran molecules (data are not shown here). This supports the results of a low binding affinity of dextran to RBCs as explained above.

In summary, besides the elasticity effects it was shown that dextran 70 kDa can adhere to erythrocytes. Due to the fact that dextran is a polysaccharide it has repeated molecular units. Consequently, if dextran can adhere to one RBC it is highly probable that it can adhere to another cell and therefore form a bridge. In contrast, such effects couldn't be shown here for fibrinogen even if there are indications that it can bind to erythrocytes [48].

3.6.1.2 Spectroscopy and rheology

The adsorption of macromolecules onto RBCs is the basis of the bridging theory. Therefore, spectroscopic measurements were performed in the same way as the concentration of the supernatant was rheologically determined (see chapter 3.1.1), i.e. a measurement of different concentrations of the stock solution leads to a relation between adsorption and concentration that allows to determine the supernatant concentration as explained in chapter 2.2.4. The only difference was that the total filling of one sedimentation tube was approximately 1 ml for the spectroscopic measurements while it was approximately 8 ml for the rheological measurements. Exemplary data of the adsorption for different fibrinogen (as delivered by Sigma

Aldrich) concentration before and after sedimentation are shown in fig. 3.44 (a) for the chosen wavelength. From the concentration an estimation the total number and mass of the adhered macromolecules can be performed easily. The relation to the concentration is shown in fig. 3.44 (b) by approximating the data with the Freundlich isotherm [139]. Due to the fact that the number of adsorption sites layer is not known and it is not known if the the macromolecules can adhere in only one or more layers, adsorption isotherms like Langmuir and BET [139] were not used. Instead and in order to be as conservative as possible the Freundlich-isotherm were used as a comparable measure for the resulting data. Typically, the Freundlich approximation includes the fact that no adsorption saturation is reached or that the saturation pressure is relatively high. It is defined as

$$q = K_F \cdot c^{1/n} \quad (3.8)$$

where K_F is the Freundlich coefficient, n is the Freundlich exponent and q is the mass load that is defined here as the mass of dextran molecules adhered to one RBC divided by the mass of one RBC that was assumed to be 102.6 pg by using the density and volume of one RBC as presented in chapter 2.1.1. The qualitative Freundlich coefficient and exponent are summarized in table 3.1.

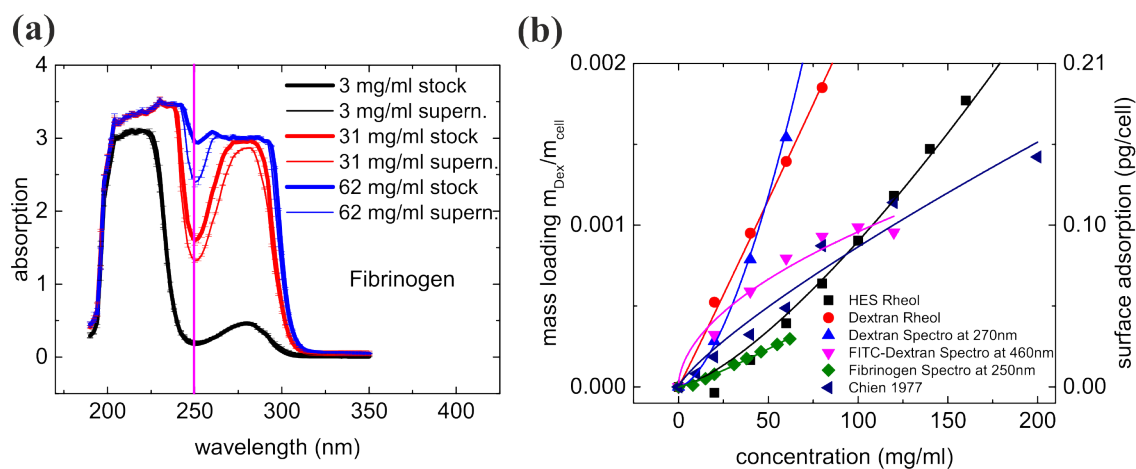


Figure 3.44: Exemplary data for the absorption spectrum of fibrinogen for stock solutions and the corresponding supernatant solution after adding 45% of RBCs (a). The mass loadings and surface adsorptions resulting from rheological and spectroscopic measurements are compared with the data from Chien [55].

The complete set of data which reaches even 1.23 pg/cell for the dextran spectroscopy (blue curve) can be considered in fig. 5.15 (a) while here only data up to

	HES r	Dex r	Dex s	FITC-Dex s	Fib s	Dex C ra
K_F	$1.62 \cdot 10^{-6}$	$21.12 \cdot 10^{-6}$	$1.92 \cdot 10^{-6}$	$84.65 \cdot 10^{-6}$	$2.23 \cdot 10^{-6}$	$21.12 \cdot 10^{-6}$
$1/n$	1.37	1.02	1.64	0.53	1.19	0.8

Table 3.1: Freundlich-coefficient and inverse Freundlich exponent for all data. “r” stands for rheology, “s” for spectroscopy and “ra” for radioactivity and “C” for Chien.

0.21 pg/cell are shown in order to compare them with the data of Chien taken in 1977 [55]. They performed a quite similar experiment with radioactive labeled dextran 70 kDa. Those data are in relatively good agreement with the ones presented here for FITC-labeled dextran 70 kDa (magenta curve) even if the isotherms differ. In contrast, dextran measured via the viscosity change (red curve) and dextran measured via the spectroscopic adsorption (blue curve) that are in relative good agreement to each other differ enormously from the data of Chien, as well as from the FITC-labeled dextran experiments. HES (black curve) rheological measured seems to adsorb not that good as dextran by comparing it with the rheological and spectroscopic measured dextran (not labeled). Surprisingly, Fibrinogen shows an adsorption as well that is significant lower than all other measurements, which could be attributed to the fact that fibrinogen molecules can sediment by themselves as it was used to wash fibrinogen (see chapter 2.3.6), which was not done for the adsorption measurements presented here. Such a sedimentation could lead to much higher artificial adsorptions. This could apply for all other measurements as well. Therefore, this data has to be taken with care, but nevertheless they give an indication of the number of adsorbed molecules, since the same measurement method allows a comparison between different macromolecules assuming that the sedimentation rate of the molecules itself is similar. Comparing rheology with spectroscopy is rather complicated, because of the total filling volume of the sedimentation tubes (ca. 1 ml for spectroscopic measurements and ca. 8 ml for rheological measurements). This could lead to lower adsorption values for spectroscopy induced by a much lower supernatant volume. In contrast, for the rheological investigations the macromolecules have to sediment through a volume of ca. 4 ml in EDTA tube (that is ca. 3-4 cm) at relative low g-forces of 704 g for 3 min. This problem applies for the data of Chien even much stronger, because the tubes were centrifuged at 35,000 rpm for one hour (g-forces are not given) which is definitely much more than 704 g and obviously much longer. Consequently, the rheological data seems to be more reasonable, but further investigations has to be made in order to reach similar results for rheology and spectroscopy. Especially, the concentration gradient has to be measured (here samples were tried to taken always from the half height of the supernatant).

For now, those data indicate that dextran is a potential candidate for bridging as the reason for RBC aggregation, while fibrinogen seems to adsorb weakly which could be induced by the sedimentation of the fibrinogen molecule itself and therefore it is

assumed to be a candidate for depletion. Regarding the SAW measurements and the relatively low adsorption (if there is any) here, fibrinogen seems to be a candidate for depletion as the reason for RBC aggregation. Even if the quantification of the adsorbed macromolecules is rather complex it is possible to show the existence of macromolecules in between aggregates as it will be explained in the following chapter.

3.6.1.3 Intercellular macromolecules

The adsorption of macromolecules onto RBCs was shown above as well as in several publications [60, 55]. Such an adsorption is a qualification for bridging as presented above, but not a sufficient condition. For this purpose it is necessary to show macromolecules in between the cells of an aggregate. Qualitatively, it was already shown by Chien [53] in electron micrographs of freeze-dried RBCs that the intercellular distance changes with the dextran size wherefore bridging was assumed. But it can be explained by the depletion theory as well because the overlap areas in the depletion theory depend on the hydrodynamic radius that is increasing with increasing molecular mass of the dextrans. Therefore, measurements were performed in order to image fluorophore labeled macromolecules in between cells. The setup is rather straight forward with the same conditions as for the MAI ($23 \pm 0,5^\circ \text{C}$, 5 min between adding the cells and imaging them at 10 % hematocrit) at 60 mg/ml FITC-dextran 70 kDa in a 1:100 mixture with normal dextran 70 kDa. The Yokogawa spinning disk was used with very high laser powers that could potentially lead to cell death. Nevertheless, a resulting image is shown in fig. 3.45.

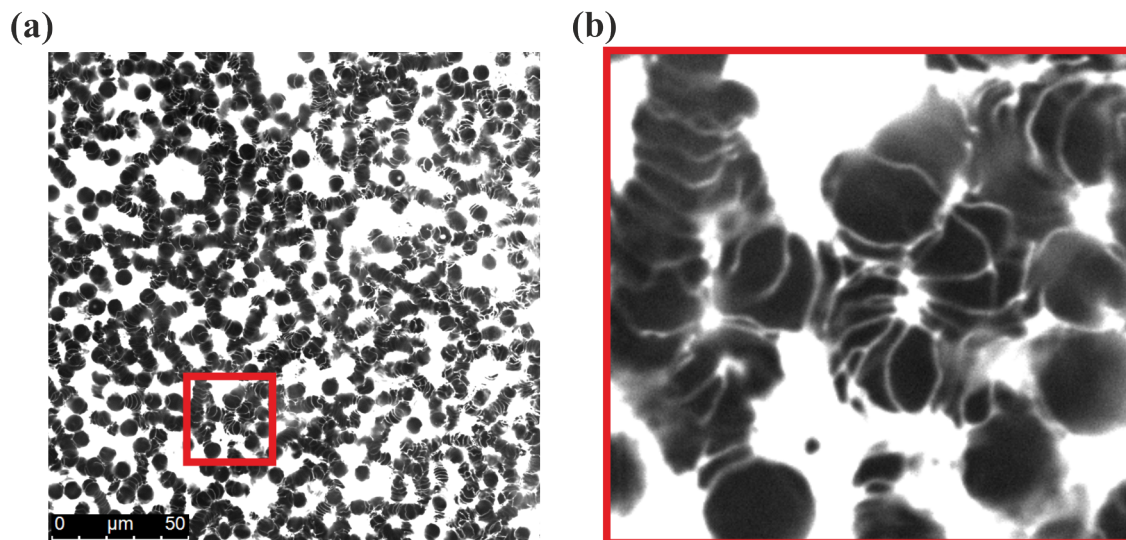


Figure 3.45: Aggregated red blood cells (black) with FITC-dextran (white) in between nearly all cells (a) and the magnification of the red square (b).

The RBCs appear slightly deformed most probably because of the high laser powers. Between nearly all aggregated cells (black) dextran is clearly visible in white. Consequently, dextran is again a candidate for bridging as the reason for RBC aggregation.

In a second experiment cell membranes were labeled with CellMask at the same 1:100 FITC-dextran:dextran mixture of 60 mg/ml and at a 1:1000 mixture of AlexaFluor fibrinogen with normal fibrinogen (as delivered by Sigma Aldrich) at 30 mg/ml. The lower ratio of mixture for fibrinogen is due to the fact that AlexaFluor fibrinogen at high concentrations is not easily soluble. The original idea for this experiment was to let the cells form aggregates and change the surrounding solution to PBS without inducing significant flows that would perturb the position of RBCs and remain aggregates as depicted in fig. 3.46 (a)-(c). If the main effect is bridging, the cells could remain in their aggregates, while they definitely should fall apart if depletion is the main effect. It turned out that both dextran and fibrinogen are not diffusing if the area of RBCs and dextran is approximately 1mm lower than the main flow area even by changing the whole volume 40 times. One solution for this could be to raise the position of the RBCs in z-direction in order to bring them closer to the surface. Nonetheless, it was possible to image the aggregated RBCs in both fibrinogen and dextran. In fig. 3.46 (b),(i) the RBC membranes are shown in black for the left image while dextran is shown in white on the right image (RBCs appear black). Even here by using lower laser powers than above, dextran is visible in between the rouleaux. Consequently, a bridging cannot be fully excluded. In contrast, fibrinogen at 30 mg/ml shows a slight deformation of the cells due to the contained salt as depicted in fig. 3.46 (b),(ii) left image where the cell membranes appear black. On the other hand, the right image shows RBCs in black and fibrinogen in white. It can be rarely seen between the aggregated RBCs which could be either accidental entrapments or a real formation of bridges. In the latter it cannot be explained for now why the cell do not adhere only at the fibrinogen areas at each other. Potentially, the amount of fluorescein fibrinogen should be increased as well as the laser power. Even if the entrapments are just accidentally happening bridging cannot be fully excluded, but it appears that depletion is more reasonable for fibrinogen thinking on the data presented above where no or only very low amounts of fibrinogen are adhering to the cells. Therefore, fibrinogen is more in favor to induce the RBC aggregation by depletion.

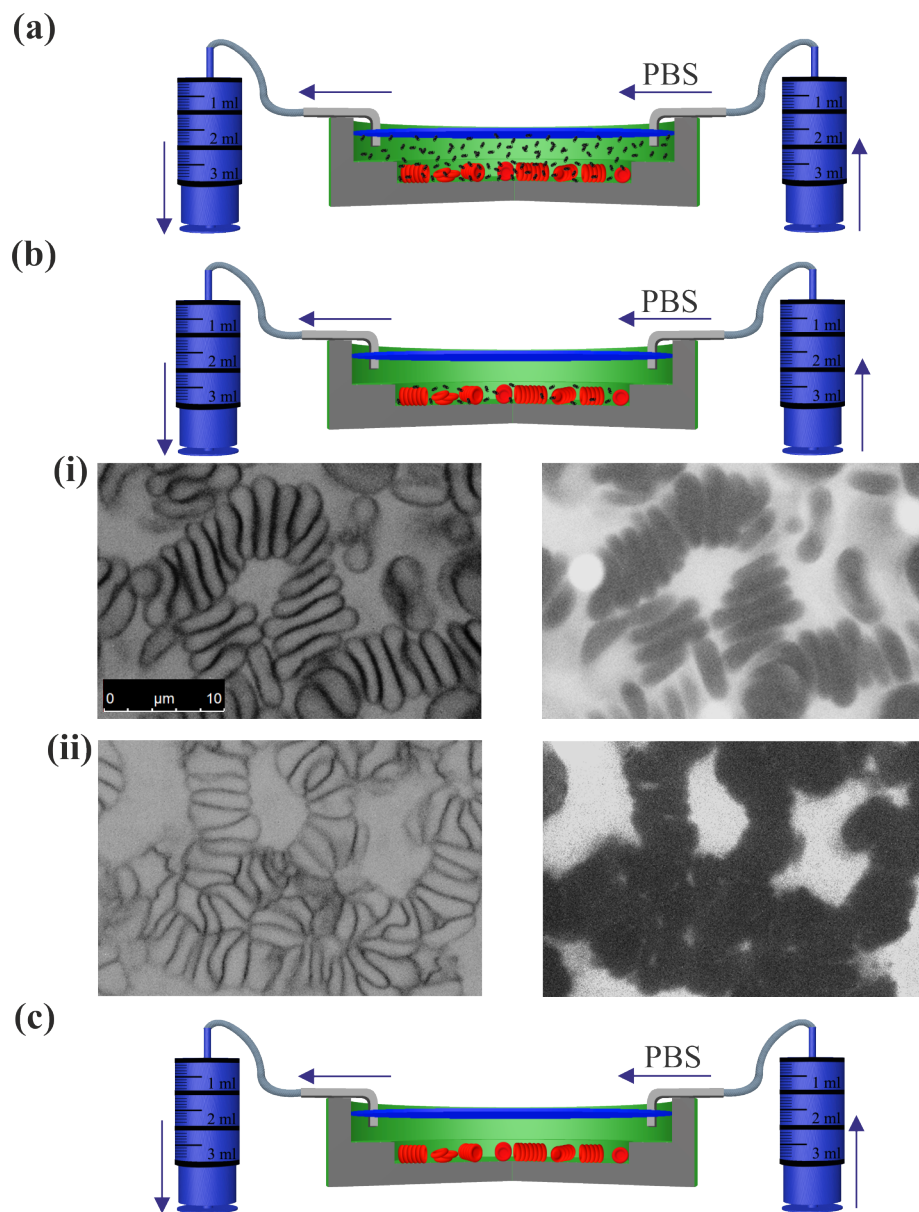


Figure 3.46: If RBCs are surrounded by a macromolecular solution (a) one can try to wash the macromolecules out with PBS (b) which could lead to the ideal case that no macromolecules are in the solution anymore (c). Images in (b) show RBCs labeled with CellMask in black (i) left as well as dextran shown in white on the right image while RBCs appear black. RBCs labeled with CellMask in fibrinogen solution are shown in black (ii) on the left image while fibrinogen is shown in white on the right image (cells appear black here).

3.6.2 Ghosts and macromolecules

Ghosts are basically red blood cells without hemoglobin, i.e. vesicles with connected proteins and an attached spectrin network. How the production process influences the RBC membranes, proteins and spectrin network is still unclear, because of many involved parameters especially the highly hypotonic environment. The manufacturing process includes the following steps: 750 μ l of RBCs were added to 30 ml of a 10 mOsmol mixture of 1:30 (PBS:H₂O dest.) and kept for 30 min on ice (no freezing). In this state the RBCs are expected to burst and the hemoglobin is relaxed in the suspending fluid (PBS:H₂O dest.). A centrifugation with 12,500 g for 45 min at 4° C led to a sedimentation of the open cell membranes and the supernatant became removed. Afterwards, 30 ml of the PBS:H₂O dest. mixture was added and the whole procedure was performed two more times. In the ideal case the ghosts are fully transparent due to the absence of hemoglobin. By increasing the temperature the open cell membranes are assumed to close fully to a spherical RBC membrane, and form called ghosts [36, 64, 100].

Due to the fact that the cell membranes are still intact one can label them with the membrane dye CellMask and image the ghosts with the Yokogawa spinning disk as depicted in fig. 3.47 (a). To these ghosts solutions of 40 mg/ml dextran 70 kDa, 40 mg/ml HES or 31 mg/ml fibrinogen as delivered by Sigma Aldrich (final concentration after the addition) were added as depicted in fig. 3.47 (b, c, d).

The result is highly significant, because for the polysaccharides the ghosts burst directly for dextran or shrink strongly for HES (within 30 s after the addition), while for the fibrinogen they stay in their shape and even form aggregates. Due to the fact that salty fibrinogen as delivered by Sigma Aldrich was used the difference in osmotic pressure could play a role. Therefore, the osmolality as a measure for the osmotic pressure was investigated with the the vapor pressure osmometer 5520 (Wescor Inc., Logan, UT, USA) as shown in fig. 3.48.

As it can be clearly seen the osmolalities of salty fibrinogen and the pure salt without fibrinogen rapidly increase with concentration due to the electrostatic repulsions of the ions. In contrast, filtered fibrinogen (saltfree), dextran and HES show a slight increase with increasing concentration while HES and dextran are nearly identical whereas the osmolality of saltfree fibrinogen show a little stronger increase that is most probably due to some remaining salt.

In such osmolality conditions the ghosts are bursting in dextran and HES and aggregate for fibrinogen with 40 % of salt. In contrast to the osmolality measurements the investigations of the ghosts were performed in distilled water, but only the base line (at 0 mg/ml) is expected to decrease using distilled water due to the primary effect of salt contained in PBS on the osmolality. Consequently, the bursting effect of the ghosts cannot be explained by an increasing osmotic pressure, because in

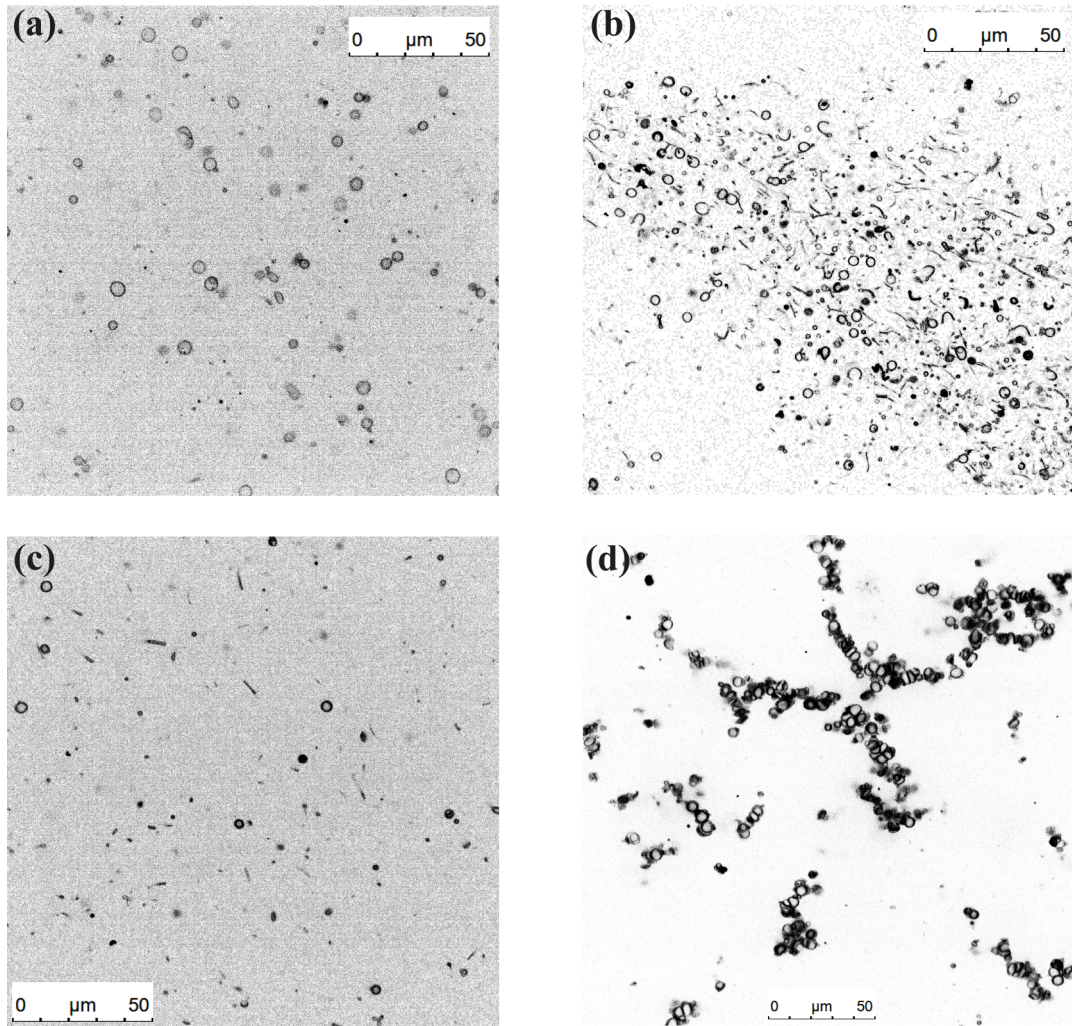


Figure 3.47: Measurements with ghosts in the presence of distilled water (a), dextran 70kDa at 40 mg/ml, HES at 40 mg/ml (c) and fibrinogen (salty) at 31 mg/ml (d) that were all solved in distilled water. RBC membranes are marked in black.

this case they should burst by the addition of fibrinogen (ca. the doubled osmotic pressure of PBS) and not by the addition of dextran or HES. As it was seen, the opposite is the case. For now, one explanation seems to be more reasonable: Dextran and eventually HES are strongly acting on the membrane and RBCs can stand this condition while ghosts not for an unknown reason. This leads again to the assumption that dextran and HES are possible candidates for the bridging theory as the origin for RBC aggregation. In contrast, adding (salty) fibrinogen leads to an aggregation of the ghosts, which means that it is highly probable that the effect of ghost aggregation is the same as for RBC aggregation. Assuming a bridging with a specific binding in case of fibrinogen it could simply mean the the production process of the ghosts does not eliminate the membrane protein that can potentially bind to fibrinogen. On the other hand a depletion interaction is possible as well.

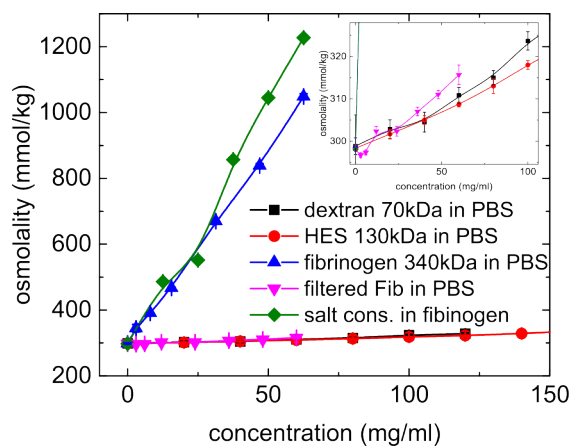


Figure 3.48: The osmolality for all used macromolecules in dependence on the concentration while the equivalent concentration of fibrinogen was used for the pure salt (green curve) that is typically attached to the protein. All macromolecules were solved in PBS. Error bars representing the standard deviation of at least three measurements. Lines are there to guide the eye.

Nonetheless, it is obvious that dextran and HES behave in a totally different manner from fibrinogen on the ghosts. Therefore, it is assumed that they behave differently on the RBCs while aggregation. Hence, both dextran and HES are not a perfect model system for fibrinogen.

3.6.3 Particle induced RBC aggregation

One issue regarding the depletion or bridging question is that both effects can co-exist. It is known that both dextran 40 kDa and poly(ethylene glycol) (PEG) 7.5 kDa inhibit the aggregation of RBCs, which is probably related to their hydrodynamic radius smaller than 4 nm, while a 10 kDa PEG even inhibits the clustering process of RBC in the presence of dextran 73 kDa [12, 13, 26, 51]. Additionally, it is known that silica particles can adhere well to RBCs while PEG-labeled silica particles adhere approximately four time less by observing the total adhered particles per cell with a confocal microscope as shown by [199]. In order to differentiate between depletion and bridging effects 5-7 nm custom made silica particles in PBS were compared to 5-7 nm custom made 7.5 kDa PEG-labeled silica particles (both from Nanocs Inc., New York, NY, USA). The silica particles were used as a model system for bridging while the PEG-labeled silica particles were assumed to have less bridging influence and the a similar osmotic pressure as necessary for a controlled depletion influence. The size of 5-7 nm was chosen because it is in the order of the hydrodynamic radius of dextran 70 kDa.

The cells were labeled with CellMask (see 2.3.9) and suspended into the colloidal suspensions of different particle amounts. Microscopical images at $23 \pm 0.5^\circ$ C in the confocal SP5 and MAI are shown in fig. 3.49. In addition, negatively charged gold particles in H_2O were investigated while the RBCs were imaged very fast due to the hypotonic environment as depicted in fig. 5.12. Aggregation of RBCs was observed for this system.

For both PEG-labeled silica particles and silica particles, the MAI increases rapidly with the concentration and decreases again for high concentrations with a stomatocyte-like shape of the RBCs. Even if the MAI for both appears similar there is one important difference at 0.75 %: RBC aggregates suspended in silica particles show a much more compact clustering and aggregation induced shape change. In contrast, PEG-labeled silica particles appear to cluster in large aggregates without significant shape changes due to aggregation. At the same time the cell shape slightly changes in an echinocyte-like direction, which is most probably caused by the PEG, because it is the only new parameter. This indicates a stronger interaction of RBCs for the silica particles and a lower interaction of RBCs for the PEG-labeled silica particles. By assuming the same osmotic pressures in both suspensions and therefore the same depletion interactions, the silica particles represent a strong bridging system while the PEG-labeled silica particles represent a weak bridging system regarding the total amount of adhered colloids onto the cells [199]. In addition, it was observed that both kinds of colloids tend to aggregate by themselves which makes the effective colloidal size hard to determine (ultrasonication was not leading to a complete break-up of the aggregates). Hence, measurements were performed directly after the particles arrived. Additionally, the measurements with negatively charged gold colloids of the same size were performed as mentioned above. The results of the gold particles are

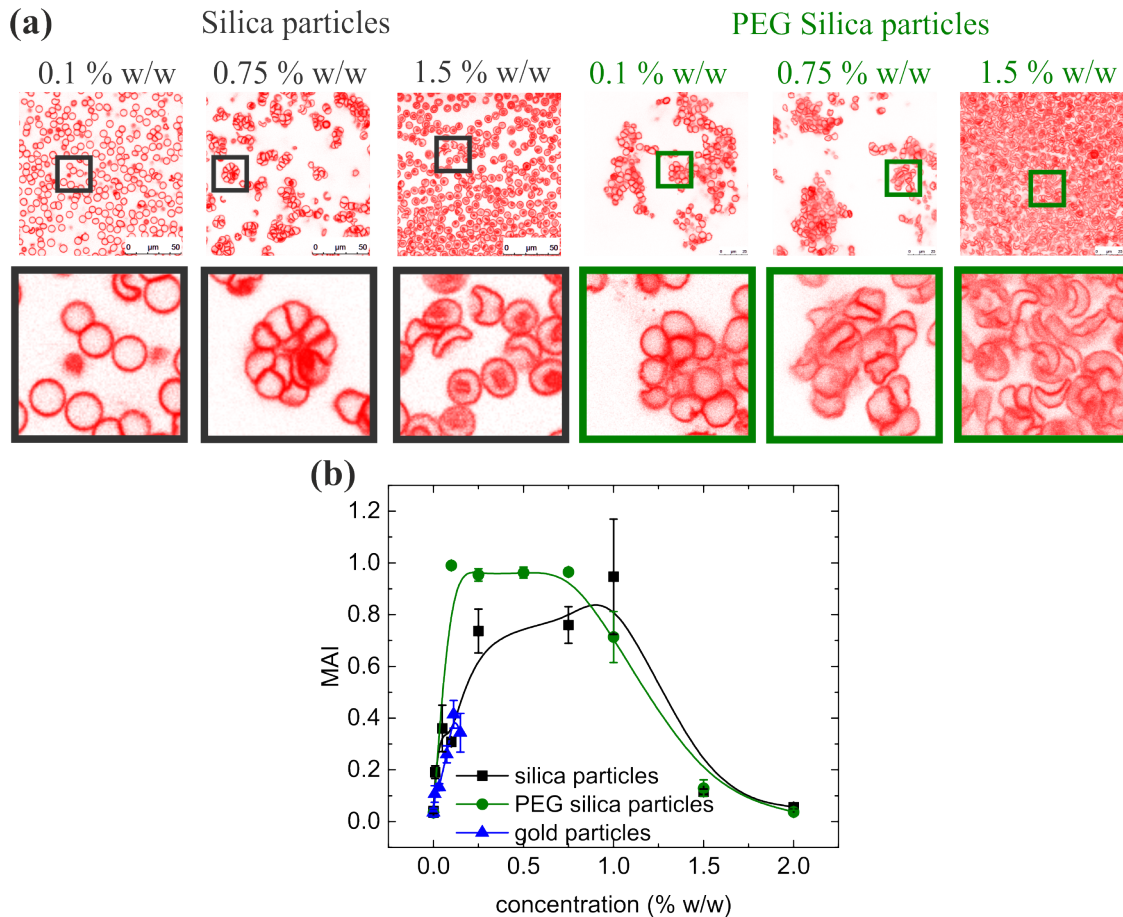


Figure 3.49: Microscopical images of silica and PEG-labeled silica particles where RBCs are marked in red (a) lead to a microscopical aggregation index in dependence on the concentration of particles (b).

in good agreement with both silica particles and PEG-labeled silica particles, which leads to the assumption, that the effective radius of the clusters of silica particles (much larger than 4 nm) are not influencing the RBC aggregation effect too much in the sense that no bell-shape would appear for the gold particles due to their negative charge (compared to negatively charged and whased fibrinogen). Consequently, it was shown that the RBCs can aggregate with a non-linear cluster shape induced by colloids. The effect seems to be mostly influenced by bridging interactions due to the adhesive behavior of silica and PEG-labeled silica particles onto RBCs [199]. This results do not explain the origin of aggregation regarding dextran or fibrinogen, but at least they show that bridging interactions can lead to RBC aggregation under the assumption that the PEG-labeling does not change the osmotic pressure of the colloidal system.

3.6.4 Single cell force spectroscopy induced cell deformation

Regarding the AFM experiments performed on top of the Yokogawa spinning disk microscope, a cell deformation was shown in chapter 3.5.2, fig. 3.40. In order to give a review of this a 3D reconstruction of this experiment is shown in fig. 3.50 where the cantilever is false color imaged in dark yellow and both RBCs are depicted in red.

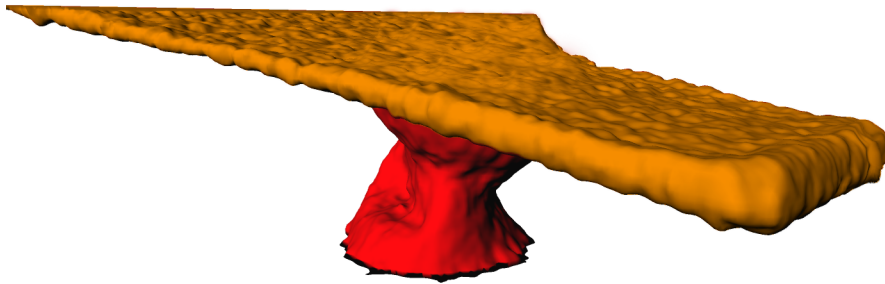


Figure 3.50: A 3D reconstruction of a cell (red, upper one) that is attached to the cantilever (dark yellow) while it is deforming itself slightly and a cell (red, lower one) attached to the coverslip (slightly marked in black).

Having in mind that bridging forces are in the order of four times higher than the depletion forces [74] in addition to the decreasing Young's modulus of RBCs in dextran solutions (see chapter 3.5.1) such a strong deformation is most probably due to bridging interactions. On the other hand, a depletion cannot be fully excluded and therefore this experiment does not resolve the the depletion versus bridging as one could might think seeing the data in chapter 3.5.2.

3.6.5 Summary of the depletion/bridging discussion

In order to compare the presented results 10 exemplary publications from the last decades are shown in table 3.2. It is obvious that the opinions differ enormously. While the results for dextran are balanced there is a tendency that fibrinogen is more in favor for bridging than for depletion, but the results do not claim to be comprehensive.

Publication	Method	Bridging		Depletion	
		Dex.	Fib.	Dex.	Fib.
Chien 1973 [53]	TEM	+	/	-	/
Chien 1977 [55]	Sedimentation	+	/	-	/
Maeda 1987 [128]	Aggregation velocity	/	+	/	-
Lominadze 2002 [125]	Fluorometric	/	+	/	-
Neu 2002 [143]	Theory	-	-	+	+
Pribush 2006 [159]	Conductivity	+	/	-	/
Badaire 2007 [15]	Colloids	-	-	+	+
Carvalho 2010 [48]	AFM	/	+	/	-
Steffen 2013 [180]	AFM	-	/	+	-
Lee 2016 [119]	Optical tweezers	/	+	/	-

Table 3.2: Summary of publications regarding depletion vs. bridging indications for dextran and fibrinogen with several methods over the years. Shown are the intentions of the authors and no interpretation if the conclusion is valid. Symbols are equivalent to the table 3.3.

In order to overview the indications for depletion and bridging the here presented results are summarized in table 3.3.

	Bridging		Depletion	
	Dex.	Fib.	Dex.	Fib.
SAW	+	-	-	+
Spectroscopy/Rheology	+	(+)	-	(-)
Intercellular macromolecules	+	(-)	-	(+)
Ghosts	(+)	(-)	(-)	(+)
Particle induced RBC aggregation	/	/	/	/
AFM	/	/	/	/

Table 3.3: Summary of depletion vs. bridging indications for dextran and fibrinogen with several here presented methods. “+” means “yes”; “-” means “no”; “(+)” means “yes, but with restrictions”; “(-)” means “no, but with restrictions”; “/” means “no statement”.

These measurements indicate a preference for fibrinogen to yield to depletion interactions while dextran is more preferred to yield to bridging interactions. In the end, the argumentation is mainly about the adsorption or non-adsorption of macromolecules. As depicted in chapter 2.1.3 by assuming a “bridletion” both effects can coexist and therefore it is not the question if the effect is depletion or bridging but the question is which effect is dominant by assuming an adsorption of macromolecules onto RBCs. Adsorption gives always the hint that bridging is involved which does

not exclude depletion at all (by assuming “bridletion”) while no adsorption clearly indicates depletion by the method of elimination. In summary, just indications are given here. Clear results are extremely challenging as explained.

There is one additional aspect regarding this discussion: The increase to a maximum of aggregation followed by its decrease for the plasma expanders and colloids, called here “bell-shape”. With both theories it can be explained and therefore with “bridletion” as well. As already mentioned in chapter 2.1.3 one important parameter is just implicit in the depletion or bridging theory, the overlap concentrations of macromolecules. Another aspect that was already mentioned is that for all macromolecules or colloids which show a bell-shape the RBC shapes change to stomatocytes. This cell deformation is well known to adhere very badly to other stomatocytes; hence it could directly influence the MAI as well as the sedimentation rate [161, 163]. If this is verified it would be absolutely necessary to include this cell shape transformation into the depletion and bridging theories, since it seems to be the only aspect that could justify the bell-shape behavior of RBC clustering processes from the experimental point of view.

Résumé de la discussion déplétion/pontage

Dans le but de comparer nos résultats avec ceux de la littérature, 10 publications considérées comme référence du domaine, publiées dans les dernières décennies ont été choisies et présentées dans le tableau 3.2. Il est évident en voyant cette comparaison que les opinions varient énormément. Alors que dans le cas du Dextran les résultats sont équilibrés, il semble y avoir une préférence pour le pontage plutôt que pour la déplétion dans le cas du fibrinogène. Cependant ces résultats n’ont pas la prétention d’être exhaustifs.

Dans le but de résumer les données de ce travail, ces dernières sont présentées dans le tableau 3.3.

Toutes ces mesures tendent à montrer qu’il y a une préférence pour le fibrinogène d’induire des interactions de déplétion alors que le Dextran serait plutôt engagé dans des interactions de pontage. Au final, la discussion de situe surtout autour de l’adsorption ou la non-adsorption des macromolécules. Ainsi que présenté dans le chapitre 2.1.3, en faisant l’hypothèse d’un modèle hybride de « pontlétion » (ou en anglais bridletion), les deux effets peuvent coexister. La question n’est donc plus de savoir si il est question de pontage ou de déplétion mais de savoir lequel de ces deux effets est dominant, en admettant qu’il y a adsorption des macromolécules sur les RBCs. L’adsorption donne toujours une indication de la possibilité de pontage mais cela n’exclut pas les interactions de déplétion (toujours dans l’hypothèse de pontlétion) alors que s’il n’y a pas d’adsorption, par élimination, la déplétion sera prédominante. En résumé, seules des tendances sont présentées ici. Comme expliqué dans ce chapitre, il est très difficile d’obtenir des résultats très tranchés.

Il reste une dernière partie pour cette discussion : l'augmentation de l'agrégation jusqu'à un maximum suivie par une décroissance des agrégats, le comportement de courbe en cloche obtenu pour les succédanées du plasma et pour les colloïdes. Puisque ce phénomène se comprend dans le cadre des deux théories il peut aussi être expliqué par la « pontlétion ». Ainsi que cela a déjà été mentionné dans le chapitre 2.1.3, un paramètre important est implicite dans les deux théories : les concentrations de recouvrement en macromolécules. Un autre aspect déjà mentionné est que toute macromolécules ou tout types de colloïdes impliquant un comportement en cloche induisent aussi un changement dans la forme des RBCs en stomatocytes. Cette déformation est connue pour avoir une mauvaise propriété d'adhésion sur les autre stomatocytes, cela pourrait donc avoir un impact direct sur le MAI ou sur le taux de sédimentation [161, 163]. Si cela était avéré vrai, il serait nécessaire d'inclure cette déformation cellulaire dans les théories de déplétion et de pontage puisque cela semble être le seul moyen de comprendre le comportement de courbe en cloche d'un point de vue expérimental.

Zusammenfassung der Depletion/Bridging-Diskussion

Um die präsentierten Ergebnisse zu vergleichen, wurden 10 beispielhafte Publikationen in Tabelle 3.2 zusammengefasst. Es ist offensichtlich, dass sich die Meinungen stark unterscheiden. Während die Resultate für Dextran ausgeglichen sind, zeigt sich eine Tendenz, dass Fibrinogen eher zu Bridging als Depletion führt, aber die Zusammenfassung hat keinen Anspruch auf Vollständigkeit.

Zur Übersicht sind die Indikatoren für Depletion und Bridging der hier vorgestellten Arbeit in Tabelle 3.3 zusammengefasst.

Diese Messungen weisen darauf hin, dass Fibrinogen eher zu Depletioninteraktionen, während Dextran eher zu Bridginginteraktionen führt. Im Wesentlichen basiert die Argumentation auf der Adsorption oder Nicht-Adsorption von Makromolekülen. Wie bereits in Kapitel 2.1.3 unter der Annahme von "Bridletion" gezeigt, können beide Effekte koexistieren und daher ist die Frage nicht, ob es sich um Depletion oder Bridging handelt, sondern die Frage ist, welcher Effekt unter der Annahme der Adsorption von Makromolekülen an roten Blutzellen überwiegt. Adsorption impliziert immer den Hinweis, dass Bridging involviert sein kann, was Depletion jedoch nicht ausschließt (unter der Annahme von "Bridletion"), während keine Adsorption aufgrund des Ausschlussverfahrens klar auf Depletion hinweist. Zusammenfassend werden hier lediglich Indikatoren vorgestellt. Wie bereits erklärt, sind klare Resultate wissenschaftlich noch nicht erreicht.

Es gibt einen weiteren Aspekt bezogen auf diese Diskussion: Der Anstieg zu einer Maximalaggregation gefolgt bei einem Abfall für Plasmaexpander und Kolloide, hier genannt "Glockenkurve". Mit beiden Theorien kann dieses Verhalten erklärt werden und daher auch mit "Bridletion". Wie bereits in Kapitel 2.1.3 erwähnt, ist die Überlappkonzentration von Makromolekülen nur implizit in beiden Theorien (Depletion

und Bridging) enthalten. Ein weiterer genannter Aspekt für Makromoleküle und Kolloide, die zu einer Glockenkurve führen, ist die Änderung der Erythrozytenform zu Stomatozyten. Diese Zelldeformation ist dafür bekannt, schlecht mit anderen Stomatozyten zu adhären; daher könnte dies den MAI und die Sedimentationsrate direkt beeinflussen [161, 163]. Sollte diese Deformation tatsächlich der Fall sein, wäre es absolut notwendig, dies in die Depletion- und Bridgingtheorie aufzunehmen, da es der einzige Aspekt sein könnte, der aus experimenteller Sicht für die Glockenkurve roter Blutzellen überprüfbar ist.

4 Summary and conclusion

Summary

In this work the adhesion of red blood cells (RBCs) is at the center of interest. In vivo these clustering processes could play a significant role in thrombi formations and in the coagulation of blood, while the aggregation of RBCs is responsible for the shear thinning behavior of blood. RBCs are the main part responsible for the blood viscosity. The aggregation of RBCs was provoked artificially by the addition of plasma expanders (dextran 70 kDa and HES 130 kDa) as well as human proteins (fibrinogen and C-reactive protein) in vitro. In the case of plasma expanders the aggregation of RBCs (i.e. rouleaux formation) increases with increasing concentrations of dextran or HES until reaching a maximum. A further concentration increase leads to a decrease of RBC aggregation. This behavior is here called “bell-shape”. Overall it was shown with several methods that this bell-shape reaches the peak at around 60 mg/ml dextran and not a complete disaggregation as suggested by others [45, 47, 143, 180].

Commercial rheology allows the quantification of shear dependent rouleaux break-up and their influence on the viscosity, which is well known since the last century. In order to separate viscosity effects of these break-ups from the viscosity of the surrounding dextran solutions a normalizing is necessary. The way of normalization for RBC suspensions was renewed in a way that is relevant for similar biological and physical systems. In this connection a bell-shape results that is in perfect agreement with the sedimentation rates of RBC-dextran suspensions by showing that the sedimentation does not influence the rheological data. The rheological results are published in [79]. The yield stress, i.e. the shear stress at which a fluid starts to flow, reflects these results as a useful concept.

Microscopy enables the observation of e.g. living biological probes as well as the investigation of RBC rouleaux formations. Using confocal microscopy the number of aggregated cells in comparison to the number of total cells per unit area leads either to a bell-shape behavior (for dextran and HES) or to an increasing aggregation for fibrinogen even at concentrations of 160 mg/ml. For CRP (C-reactive protein) at physiologically relevant concentrations no change in clustering was observed with increasing protein concentration. This means that the CRP has no influence on the aggregation behavior of RBCs which leads to the fact that the clinical correlation between erythrocyte sedimentation rate (ESR) and CRP is indicated by other elevated protein concentrations such as fibrinogen, but not by the CRP concentration in

physiological ranges. This result is published in [78]. Regarding a deeper view, confocal microscopy allows to observe the deformation of cell membranes in dependency on the macromolecular concentration. By taking the amplitude of the interaction zones as a valid measure for their interaction energy the resulting bell-shape behavior is in good agreement with numerical analyses. Here the experimental interaction energy was extrapolated from numerical data. An analytic investigation performed by Thomas Pordgroski in combination with the numerical and experimental results allows to relate the shape transformation to a buckling process. The results will be published in [77].

A more direct approach is to measure the interaction energy between two RBCs with atomic force microscopy using single cell force spectroscopy (SCFS). Such investigations performed by Steffen and co-workers [180] indicate a bell-shape in good agreement with the depletion theory [143]. In the work presented here it is shown that this specific relation was mainly induced by viscosity effects of the solute dextran solutions. A bell-shape that is not in perfect agreement with all other observations is found for small cantilever velocities. These velocities are still influenced by the viscosity of the surrounding medium. Therefore, the velocity at which the viscosity influence does not influence the results anymore is quantified. This measurements are still in progress, but an answer is questionable.

Moreover, investigations of the local RBC elasticity were performed finding that the Young's modulus decreases with increasing dextran concentration while it does not change as a function of the fibrinogen concentrations. This result is in good agreement with surface acoustic waves (SAW) measurements that additionally indicate an adsorption of dextran onto RBCs while no adsorption for fibrinogen was suggested heretofore.

Since the 1970's a disagreement for the origin of RBC rouleaux formation is recurrent in the literature. On one hand, depletion theory accounts the osmotic pressure of the surrounding macromolecules as the reason for the aggregation. On the other hand, the bridging model assumes the physiosorption of macromolecules onto the cells as the key role of RBC clustering. The adsorption of macromolecules at the cell membranes is a necessary condition arguing that bridging is existing. This was already shown for dextran in the literature as well as encouraged in this work with several methods. In contrast, the results for fibrinogen show the tendency that it does not seem to adsorb onto RBCs. In addition, it was explained that bridging and depletion do not exclude each other, which is why an approach towards a new theory for RBC aggregation that combines the two existing theories, called "bridletion", was derived from colloidal physics [70]. Even if the bell-shape, especially the decreasing aggregation beyond the maximum clustering, is explainable with all three theories the cell shape change from discocytes to stomatocytes (induced by several macromolecules) was referred at least as an additional effect to understand the bell-shape. Progress is underway to investigate the influence of the cell shape on the bell-shape.

Resumé

Le cœur de ce travail est l'adhésion des globules rouges (RBCs). In vivo, ce processus d'agglomération pourrait avoir un rôle crucial dans la formation de thrombus et la coagulation du sang, alors que l'agrégation des RBCs est à l'origine de la propriété rhéo-fluidifiante du sang. La viscosité est principalement conférée par les RBCs. L'agrégation des RBCs a été induite artificiellement par ajout de succédanés du plasma (Dextran 70 kDa ou HEA 130 kDa) ou de protéines humaines (fibrinogène ou protéine C réactive) in vitro. Dans le cas de succédanés du plasma, l'agrégation des RBCs (c'est-à-dire la formation de rouleaux) augmentent avec la concentration en Dextran ou HEA jusqu'à atteindre un maximum. Une augmentation supplémentaire de la concentration entraîne une réduction de l'agrégation. Ce comportement est appelé « en cloche ». Globalement il est montré ici que le maximum de la cloche est atteint pour une concentration de 60 mg/mL de Dextran mais que la décroissance ne retourne pas à zéro, et donc qu'une désagrégation totale n'est jamais atteinte, contrairement à d'autres études [45, 47, 143, 180].

Par l'utilisation d'un rhéomètre commercial, il est possible de quantifier la dissociation des rouleaux en fonction du cisaillement ainsi que leur influence sur la viscosité, ce qui est bien établi depuis le siècle dernier. Afin de dissocier les effets sur la viscosité dus aux rouleaux de la viscosité des solutions de Dextran, il convient procéder à une normalisation des résultats. Une nouvelle manière de normaliser les suspensions de globules rouges, pertinente à la fois d'un point de vue physique et biologique, est proposée. Dans ce cadre, une courbe en cloche, en parfait accord avec la sédimentation des suspensions RBCs-Dextran, montre que la sédimentation n'a pas d'influence sur les résultats de rhéologie. Ces résultats sont publiés sous la référence [79]. La contrainte seuil, c'est-à-dire la contrainte de cisaillement minimale nécessaire pour observer un écoulement, reflètent ces résultats en tant que concept utile.

La microscopie permet l'observation, par exemple, d'échantillons biologiques vivant mais aussi de pouvoir étudier la formation de rouleaux de RBCs. Par microscopie confocale, il a été déterminé que le nombre de cellules agrégées rapporté au nombre total de cellule par unité de surface menait soit à un comportement « en cloche » (Dextran ou HEA) soit à une agrégation croissante pour le fibrinogène même à des concentrations au-delà de 160 mg/ml. Pour la CRP (protéine C réactive) utilisée dans des concentrations physiologiques, aucun changement n'a été observé à l'augmentation de la concentration. Cela signifie que la CRP n'a pas d'influence sur l'agrégation des RBCs, ce qui entraîne que la corrélation clinique entre le taux de sédimentation des érythrocytes (ESR) et la CRP est indiqué par des niveaux élevés d'autres protéines telles que le fibrinogène, mais pas uniquement par la CRP dans une gamme physiologique. Ce résultat est publié dans [78]. De manière plus poussée, la microscopie confocale permet aussi d'observer la déformation de la membrane cellulaire en fonction de la concentration en macromolécules. En prenant l'amplitude des zones d'interaction comme mesure valide de leur énergie d'interaction, le com-

portement en cloche des résultats est en bon accord avec les analyses numériques. Ici, l'énergie d'interaction a été extrapolée des données numériques. Une étude analytique menée par Thomas Podgorski, utilisant les données expérimentales et numériques permet de faire le lien entre le changement de forme des interfaces et un processus de flambage. Ces résultats sont publiés dans [77].

Une approche plus directe est de mesurer l'énergie d'interaction entre deux RBCs par microscopie à force atomique, en réalisant des mesures de spectroscopie de force sur cellule unique (SCFS). De telles expériences réalisées par Steffen et collaborateurs [180] ont montré une courbe en cloche en accord avec la théorie de la déplétion [143]. Dans le présent travail de thèse, il est montré que cette corrélation spécifique est principalement due à des effets de viscosités induits par les solutions de Dextran. Une courbe en cloche est aussi trouvée ici avec des vitesses de micro-levier plus faibles, mais cette dernière n'est pas en parfait accord avec les précédentes observations. Les vitesses utilisées ici sont elles aussi influencées par la viscosité ambiante. Ainsi, la vitesse maximale à laquelle la viscosité n'a pas d'influence sur la mesure est quantifiée. Les mesures sont à ce jour toujours en cours et la possibilité de trouver une réponse est toujours sujette à question.

D'autre part, des mesures de l'élasticité locale des RBCs ont montré que le module de Young décroît lorsque la concentration en fibrinogène augmente. Ces résultats sont en bon accord avec les mesures d'ondes de surface acoustiques (SAW) qui, de plus, montrent une adsorption du Dextran à la surface des RBCs alors que jusqu'à présent aucune adsorption ne semble avoir lieu pour le fibrinogène.

Depuis les années 1970, l'origine de la formation de rouleaux est régulièrement sujette à débat dans la littérature. D'une part, la théorie de la déplétion explique ces agrégats par la pression osmotique exercée par les macromolécules du milieu environnant. D'un autre côté, le modèle de pontage considère la physisorption de ces macromolécules comme l'élément clé de cette agrégation. L'adsorption de macromolécules à la membrane des cellules est une condition nécessaire pour l'existence du pontage. Cette étape a déjà été montrée dans la littérature dans le cas du Dextran et a aussi été fortement suggérée dans ce travail, et ce au travers de plusieurs méthodes expérimentales. A l'inverse, les résultats obtenus avec le fibrinogène vont plutôt dans la direction de la non-adsorption. De plus, il a été montré que déplétion et pontage ne sont pas mutuellement exclusifs. C'est la raison pour laquelle une nouvelle approche du problème, combinant les deux théories et appelée « pontlé-tion », a été dérivée de la physique des colloïdes [70]. Même si le comportement en cloche, notamment dans le cas de l'agrégation décroissante au-delà de l'association maximale, peut être expliqué par les trois théories, la déformation des cellules de discocytes à stomatocytes (induite par plusieurs types de macromolécules) a été démontrée comme un effet additionnel de compréhension du comportement en cloche. Les travaux de prise en compte de l'impact de la forme de la cellule sur le comportement en cloche sont en cours.

Zusammenfassung

In dieser Arbeit steht die Adhäsion roter Blutzellen (RBCs) im Zentrum des Interesses. In vivo kann dieser Clustering-Prozess eine signifikante Rolle für die Entstehung von Thromben und für die Blutkoagulation spielen, wobei die Aggregation roter Blutzellen verantwortlich für die Scherverdünnung von Blut ist. Rote Blutzellen sind der Bestandteil von Blut, der wesentlich für die Blutviskosität ist. Die Aggregation roter Blutzellen wurde in vitro künstlich durch die Zugabe von Plasmaexpandern (Dextran 70 kDa und HES 130 kDa) und menschlichen Proteinen (Fibrinogen und C-reaktives Protein) hervorgerufen. Für den Fall von Plasmaexpandern nimmt die Aggregation roter Blutzellen (Rouleaux-Formation) mit steigender Dextran- oder HES-Konzentration zu, bis ein Maximum erreicht ist. Eine weitere Erhöhung der Konzentration führt zu einer Abnahme der Zellaggregation. Dieses Verhalten wird hier "Glockenkurve" genannt. Mit verschiedenen Methoden wurde gezeigt, dass diese Glockenkurve ihr Maximum um 60 mg/ml Dextran erreicht und nicht ihr Ende, wie von anderen angenommen [45, 47, 143, 180].

Rheologie erlaubt die Quantifizierung des scherabhängigen Aufbrechens von Rouleaux und deren Einfluss auf die Viskosität, was seit dem letzten Jahrhundert bekannt ist. Um die Viskositätseffekte dieses Aufbrechens von den Viskositätseffekten der umgebenden Dextranlösungen zu separieren, ist eine Normierung notwendig. Die Art dieser Normierung für Suspensionen roter Blutzellen wurde erneuert in einer Weise, die relevant für ähnliche biologische und physikalische Systeme ist. In diesem Zusammenhang ergibt sich eine Glockenkurve, die in guter Übereinstimmung mit den Sedimentationsraten von RBC-Dextran-Suspensionen ist, womit gleichzeitig gezeigt wurde, dass die Sedimentation die rheologischen Daten nicht beeinflusst. Die rheologischen Resultate sind in [79] publiziert. Die Fließspannung als sinnvolles Konzept, d.h. die Schubspannung, bei der eine Flüssigkeit zu fließen beginnt, spiegelt diese Resultate wider.

Mikroskopie erlaubt die Beobachtung von z.B. lebenden biologischen Proben und die Untersuchung von Rouleauxformationen roter Blutzellen. Unter Verwendung von Konfokalmikroskopie wurde die Anzahl aggregierter Zellen im Vergleich zu der Gesamtanzahl von Zellen pro Einheitsfläche untersucht, was entweder zu einer Glockenkurve (für Dextran und HES) oder zu einer steigenden Aggregation für Fibrinogen bei Konzentrationen bis 160 mg/ml führt. Für CRP (C-reaktives Protein) bei physiologisch relevanten Konzentrationen wurde keine Änderung des Aggregationsverhaltens mit steigender CRP-Konzentration beobachtet. Dies bedeutet, dass CRP keinen Einfluss auf das Aggregationsverhalten roter Blutzellen hat, was dazu führt, dass die klinische Korrelation zwischen Blutsenkung (ESR) und CRP auf eine gleichzeitige Konzentrationserhöhung anderer Proteine, wie Fibrinogen, zurückzuführen ist, aber nicht auf die CRP-Konzentration in physiologischen Konzentrationen. Dieses Resultat ist in [78] publiziert. Bezugnehmend auf einen tieferen Einblick erlaubt Konfokalmikroskopie die Beobachtung der Zellmembrandeformation in Abhängigkeit der Makromolekülkonzentration. Die Amplitude der Interaktionszo-

nen wurde als passender Parameter angesehen, was zu einer Glockenkurve in guter Übereinstimmung mit numerischen Untersuchungen führte. Hierfür wurden die experimentellen Interaktionsenergien aus den numerischen Daten errechnet. Eine analytische Untersuchung von Thomas Podgorski in Kombination mit den numerischen und experimentellen Resultaten erlaubt es, die Formänderung in Verbindung zu einem Buckling-Prozess zu bringen. Diese Ergebnisse sind in [77] publiziert.

Eine direktere Methode zur Messung der Interaktionenergie zwischen zwei roten Blutzellen ist Atomkraftmikroskopie unter Verwendung von Einzelzellkraftspektroskopie (SCFS). Solche Untersuchungen wurden von Steffen und Mitarbeitern [180] durchgeführt und legen eine Glockenkurve in guter Übereinstimmung mit der Depletiontheorie [143] nahe. In der hier vorgestellten Arbeit wurde gezeigt, dass diese spezielle Relation hauptsächlich durch Viskositätseffekte der Dextranlösungen hervorgerufen wurde. Eine Glockenkurve, die nicht in perfekter Übereinstimmung mit allen anderen Beobachtungen steht, wurde für geringe Cantilever-Geschwindigkeiten gefunden. Diese Geschwindigkeiten werden immer noch durch die Viskosität des umgebenden Mediums beeinflusst. Daher wurde die Geschwindigkeit, bei der die Viskosität die Ergebnisse nicht mehr beeinflusst, quantifiziert. Diese Messungen sind noch im Gange, aber die Antwort ist fragwürdig.

Darüber hinaus wurden lokale Elastizitätsmessungen roter Blutzellen durchgeführt, was zu dem Ergebnis führte, dass die Elastizität mit steigender Dextranskonzentration abnimmt, während sie als Funktion der Fibrinogenkonzentration unverändert bleibt. Dieses Ergebnis ist in guter Übereinstimmung mit akustischen Oberflächenwellen (SAW), wie gleichzeitig eine Adsorption von Dextran an roten Blutzellen und keine Adsorption von Fibrinogen nahelegt.

Seit den 1970er Jahren herrscht eine Meinungsverschiedenheit in der Literatur über den Ursprung der RBC Roulauxformation. Einerseits verweist die Depletiontheorie auf den osmotischen Druck der umgebenden Makromoleküle als Grund für die Aggregation. Andererseits nimmt das Bridgingmodell eine Adsorption von Makromolekülen an die Zellen als Schlüsselrolle für die RBC-Aggregation an. Die Adsorption von Makromolekülen an den Zellmembranen ist eine notwendige Voraussetzung, wenn mit Bridging argumentiert wird. Dies wurde in der Literatur bereits für Dextran gezeigt und in dieser Arbeit mit verschiedenen Methoden untermauert. Im Gegensatz hierzu zeigen die Ergebnisse für Fibrinogen, dass es nicht an roten Blutzellen zu adsorbieren scheint. Ergänzend wurde erklärt, dass Bridging und Depletion sich nicht gegenseitig ausschließen, weshalb ein Denkansatz für eine neue Theorie für die Aggregation roter Blutzellen, welche die beiden existierenden Theorien vereinigt, genannt "Bridletion", aus der Kolloidphysik abgeleitet wurde [70]. Obwohl die Glockenkurve, speziell die Abnahme der Aggregation nach dem Maximum, mit allen drei Theorien erklärbar ist, wurde auf die Formänderung von Diskozyten zu Stomatozyten (hervorgerufen durch verschiedene Makromoleküle) als ein weiterer Effekt zum Verständnis der Glockenkurve verwiesen. Untersuchungen über den Einfluss der Zellform auf die Glockenkurve sind im Gange.

5 Appendices

In the appendix reference measurements and supplementary investigations are shown.

Starting with the explanation of the resolution limit of the rheometer MCR702, the rheological data for 36 % hematocrit instead of 45 % hematocrit are shown as well as the non-existing influence of BSA on the rheological measurements. The difference between the applied and measured shear stress using the AntonPaar MCR702 are depicted and the exact approximation values of the yield stress data are given.

Via the viscosity the concentrations of glycerin-water and dextran are related and the conversion from a molar to the used formulation via density measurements of the solutions are shown.

The dependency of the number of aggregated cells on the cellular volume fraction is presented. The MAI is given for fibrinogen as delivered by Sigma Aldrich, the pure salt that those concentrations are including, HES, CRP and gold colloids instead of using macromolecules to provoke the clustering process. With a PSCM it was shown that dextran 2,000 kDa can be found in between aggregated cells as well as dextran 70 kDa.

The amplitudes of the interfacial doublet shapes of washed (saltfree) fibrinogen are shown up to 160 mg/ml, which is close to the concentration where fibrinogen cannot be solved completely anymore. In addition, the complete data of the adsorption of macromolecules as well as the rheological adsorption for different hematocrit using dextran are depicted. In the end it is shown that dextran 70 kDa, fibrinogen as delivered by Sigma and CRP are not activating the calcium channels of RBCs.

All measurements were performed at room temperature of $23 \pm 0.5^\circ \text{C}$.

5.1 Rheology

The resolution limit of the rheometer MCR702 was measured and theoretically determined as depicted in fig. 5.1. The theoretical resolution limit was calculated with the following set of dependencies:

$$\eta_{min,1} = \tau_{min} / \dot{\gamma}_{max} \quad (5.1)$$

$$\eta_{min,2} = \tau_{min}/\dot{\gamma}_{min} \quad (5.2)$$

$$\eta_{max,1} = \tau_{max}/\dot{\gamma}_{min} \quad (5.3)$$

$$\eta_{max,2} = \tau_{max}/\dot{\gamma}_{max} \quad (5.4)$$

in which $\tau_{min} = Md_{min} \cdot A$, $\tau_{max} = Md_{max} \cdot A$ are minimum and maximum shear stresses and $\dot{\gamma}_{min} = \Omega_{min} \cdot M$, $\dot{\gamma}_{max} = \Omega_{max} \cdot M$ are minimum and maximum shear rates. $Md_{min,max}$ are minimum and maximum torques, $\Omega_{min,max}$ are minimum and maximum angular velocities, A and M are geometrical constants.

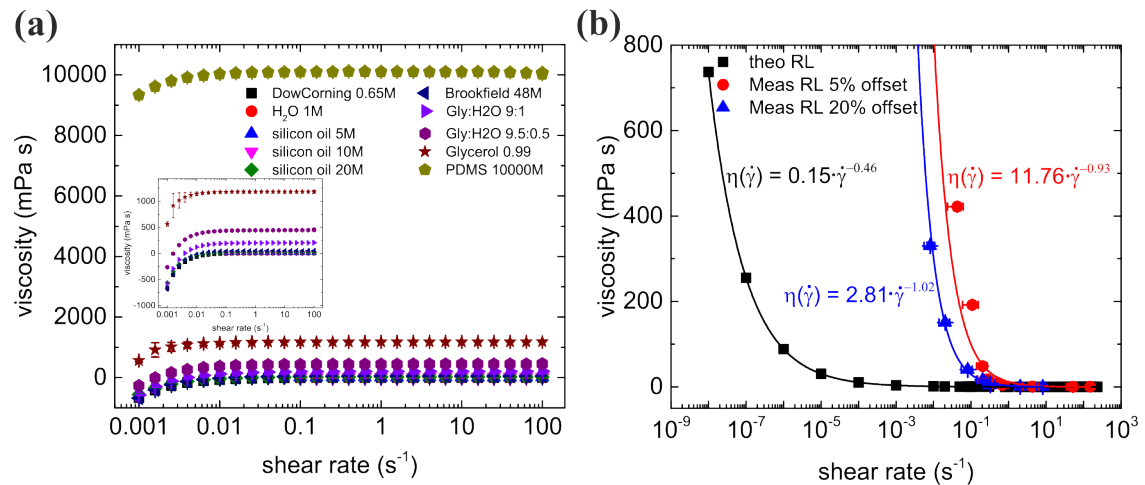


Figure 5.1: Rheological measurement of several Newtonian substances for the CC20 geometry. The appearing systematical error at low shear rates is a common effect of MCR702 due to calibration. (a) Allowing the offset of the curve to be 5% or 20% of the apparent viscosity (at 100 s⁻¹) leads to the measured resolution limit (Meas RL) for the MCR702 in comparison to the theoretical calculated resolution limit (theo RL). (b) Approximations were performed with a power law.

The dependency of the viscosities on the time average for rheological data over 25 s and 50 s was measured for the “up” protocol as it was performed and for the “up” protocol with stopping, removing the geometry and mixing the suspension up by hand with a small plastic stick after every measurement step as depicted in fig. 5.2 (a) for RBCs in a 60 mg/ml dextran solution. No significant difference between

the “up” protocol with and without mixing was found as well as no significant difference between the averaging times of 25 s and 50 s appeared. An example for the Newtonian behavior of dextran solutions is given for 60 mg/ml as well. The viscosity versus time is shown in fig. 5.2 (b) finding that a steady state is reached for all shear rates after approximately 20 s. Measurements were performed for 45 % hematocrit.

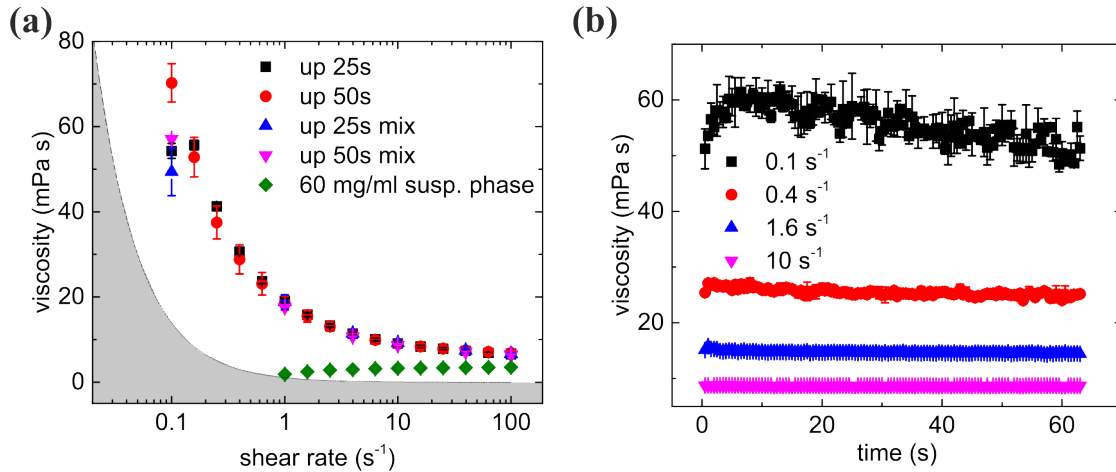


Figure 5.2: Control measurement for the “up” protocol where one shear rate was applied for 30 s or 60 s and averaged over 25 s or 50 s. “Mix” indicates a stop of the protocol, removing the inner cylinder of the CC20 and mixing the solution with a plastic stick in order to reduce potential sedimentation effects on the measurement result. “Susp. phase” is representing a pure dextran solution, here at 60 mg/ml (a). Time resolution shows that even for low shear rates of 0.1 s^{-1} a steady state is reached within approximately 30 s, which is valid for higher shear rates as well (b).

The shear thinning and bell-shape behavior for 36 % hematocrit suspended in several dextran concentrations as it was performed for 45 % hematocrit (see chapter 2.2.2.3) are illustrated in fig. 5.3. The viscosities are smaller than for a hematocrit of 45 %, which was expected.

The resulting normalized viscosities for the “up”- and “down” protocol as it was performed for 45 % hematocrit are depicted in fig. 5.4. The relative viscosities are smaller than for a hematocrit of 45 %, which was expected.

The position of the maximum for 36 % hematocrit as it was performed for 45 % hematocrit is shown in fig. 5.5.

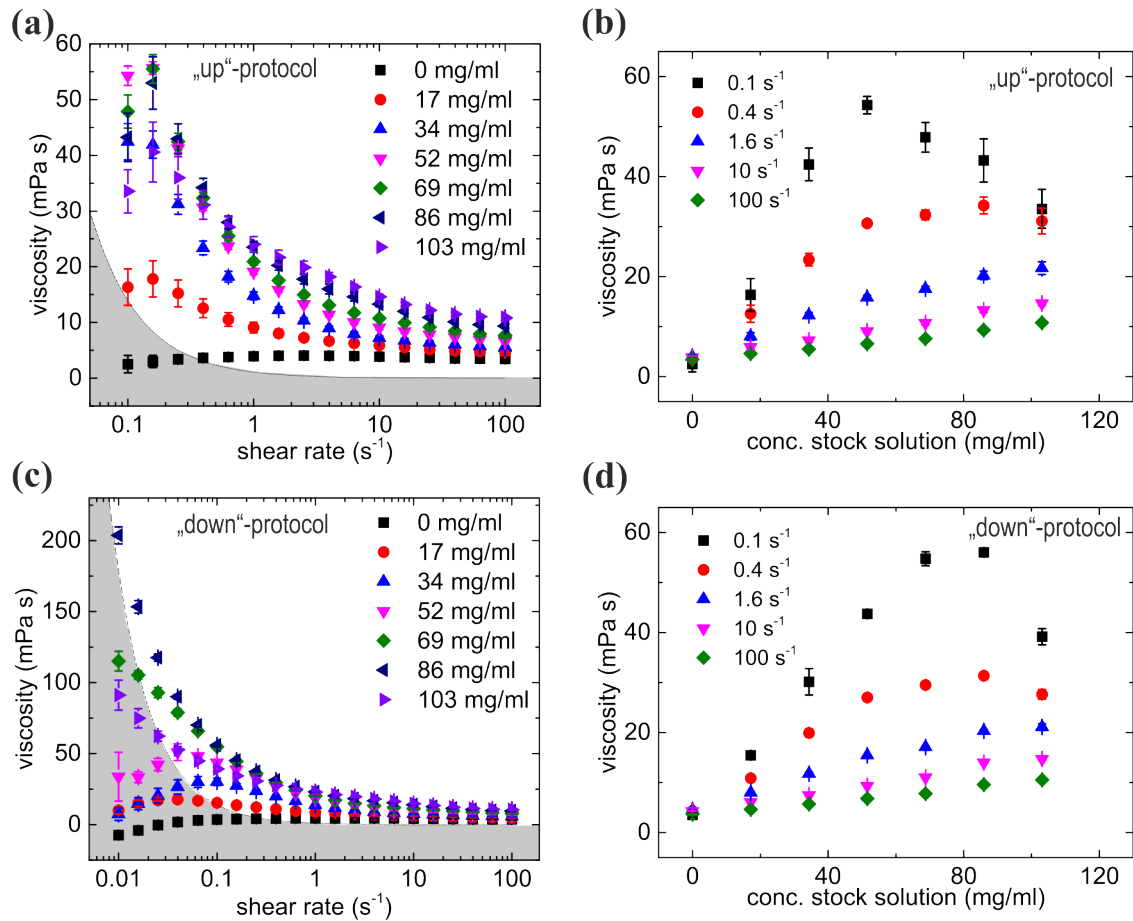


Figure 5.3: Shear rate dependent viscosities for different dextran concentration using the up protocol (a) and the down protocol (c). The viscosities in dependency on the concentration of the stock solution for appointed shear rates are depicted in (b) for the up protocol and in (d) for the down protocol.

In all rheological measurements neither BSA or HSA was added in order to influence the samples as low as possible. The influence of the addition of 1 mg/ml BSA on the supernatant and on the pellet for 45 % hematocrit are illustrated in fig. 5.6. No significant influence of BSA was found.

The difference of the applied and measured shear stresses by using the AntonPaar MCR702 in the SMT mode are depicted in fig. 5.7. The offsets are significant which leads to the fact that CS measurements have to be taken with care until AntonPaar solved this issue.

The exact approximation values for the three different applied yield stress models for 45 % hematocrit are shown in table 5.1. The most reasonable approximation is

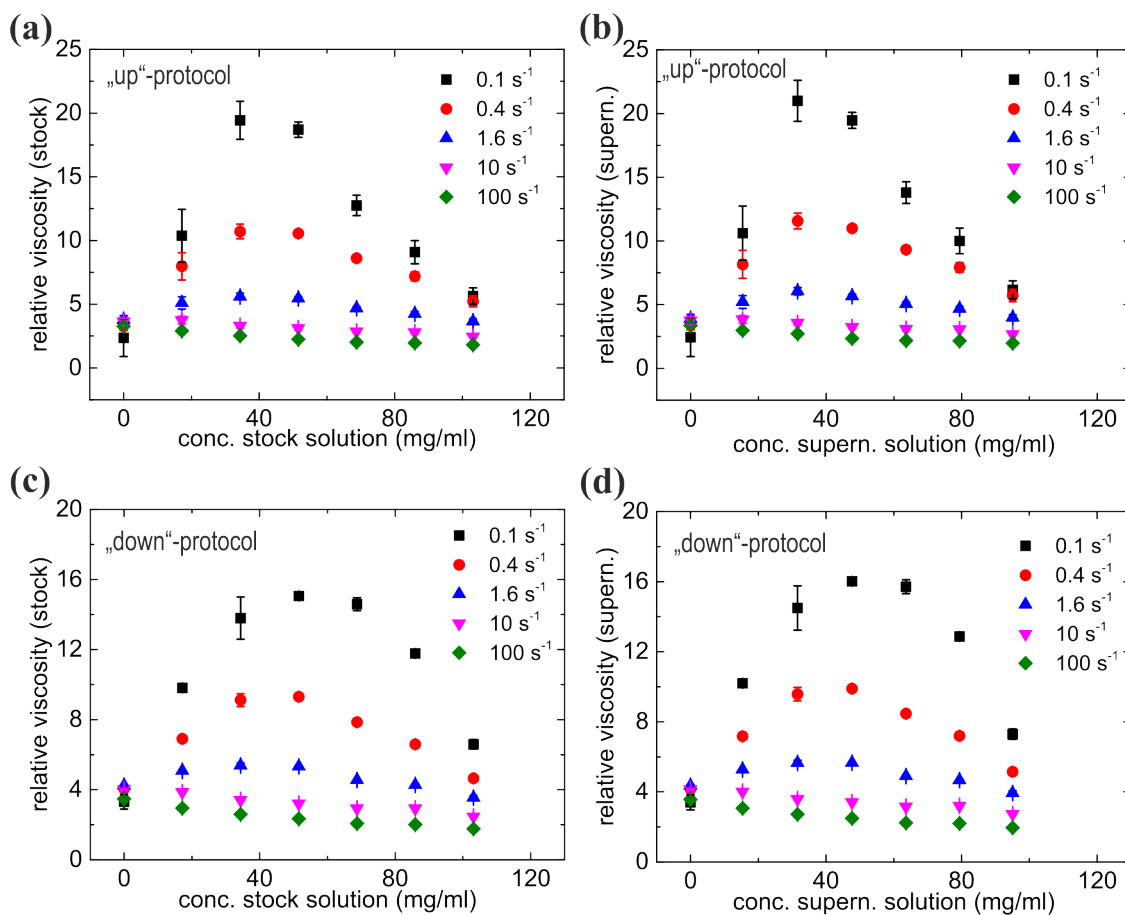


Figure 5.4: The normalization of shear thinning curves for 36% hematocrit at different shear rates for the up protocol (a, b) and for the down protocol (c, d). Normalizations with the viscosity of the stock solution (a, c) and with the viscosity of the supernatant solution (b, d).

given by the Casson model, because the Casson model is the only one that is based on potential disaggregation processes.

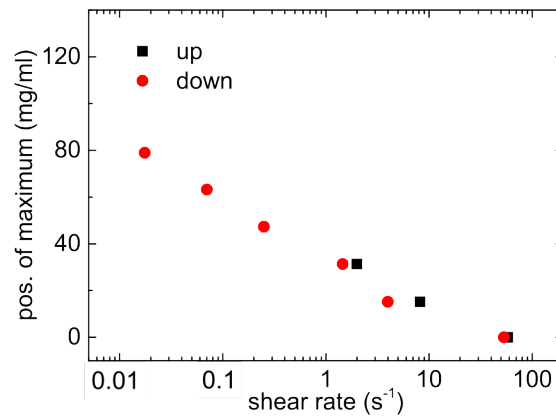


Figure 5.5: The position of maximum in dependency on the shear rate for 36 % hematocrit.

Model	Bingham	Herschel-Bulkley	Casson
Formula	$\sigma = \sigma_0 + \eta_B \dot{\gamma}$	$\sigma = \sigma_0 + K \dot{\gamma}^n$	$\sqrt{\sigma} = \sqrt{\sigma_0} + \sqrt{\eta_c \dot{\gamma}}$
Parameters	$\sigma_0; \eta_B$	$\sigma_0; K; n$	$\sqrt{\sigma_0}; \sqrt{\eta_c}$
0 mg/ml	1.72; 18.15	-0.34; 6.33; 0.92	0.87; 4.13
20 mg/ml	2.63; 16.6	0.58; 14.76; 0.8	1.25; 3.83
40 mg/ml	5.32; 13.22	1.36; 31.81; 0.68	1.81; 3.34
60 mg/ml	4.38; 11.34	2.9; 29.24; 0.75	1.63; 3.18
80 mg/ml	4.22; 9.01	1.15; 32.3; 0.76	1.53; 2.86
100 mg/ml	1.69; 7.08	-0.07; 33.81; 0.77	0.88; 2.6
120 mg/ml	-0.06; 5.11	1.25; 2.75; 1	-0.02; 2.28

Table 5.1: Approximation values of the yield stress models in relation to the dextran concentration regarding fig. 3.7.

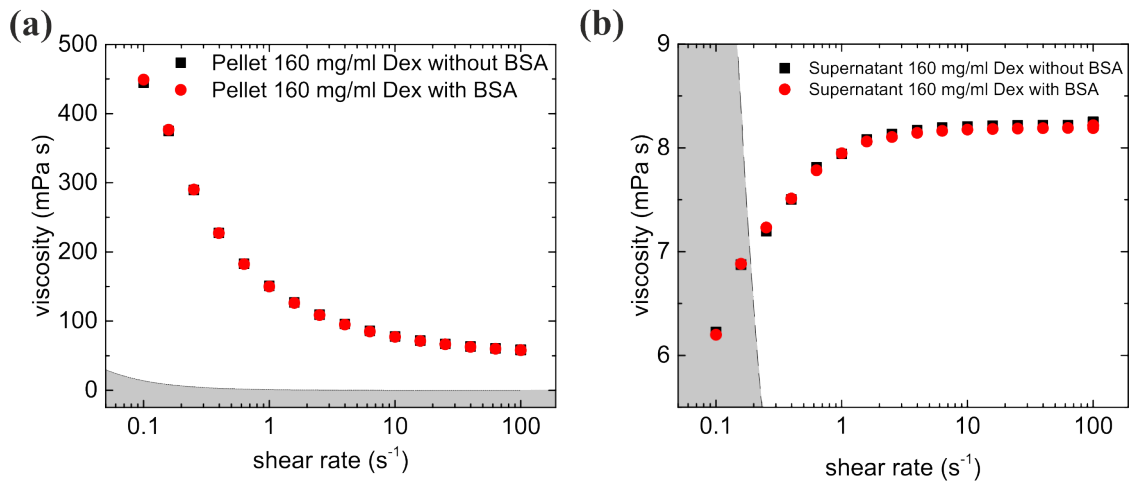


Figure 5.6: The influence of BSA on the pellet (a) and on the supernatant (b) for high dextran concentrations. At lower dextran concentrations the qualitative results is the same within the standard deviations. The resolution limit of the MCR702 is marked with gray areas.

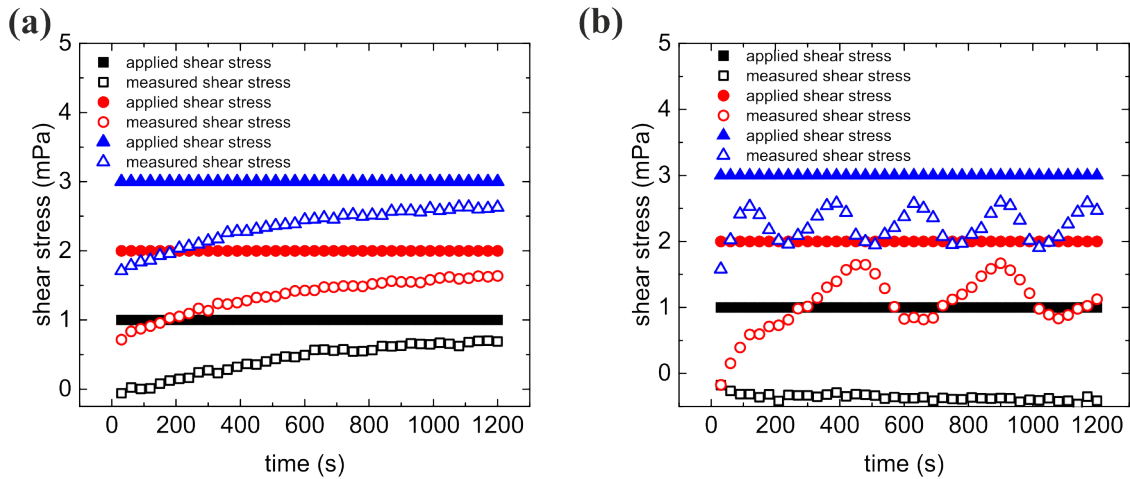


Figure 5.7: Shear stress dependency for the MCR702 with the CC20 geometry for (a) H₂O and (b) a 10M oil. The measured shear stress is in both cases significantly different from the applied stresses. Due to the oscillatory behavior of (b) an geometrical error in combination with a software are is assumed.

5.2 Concentration converting

The viscosities of different concentrations of glycerin in water and dextran in PBS were measured in order to compare their viscosities. The resulting relation is illustrated in fig. 5.8.

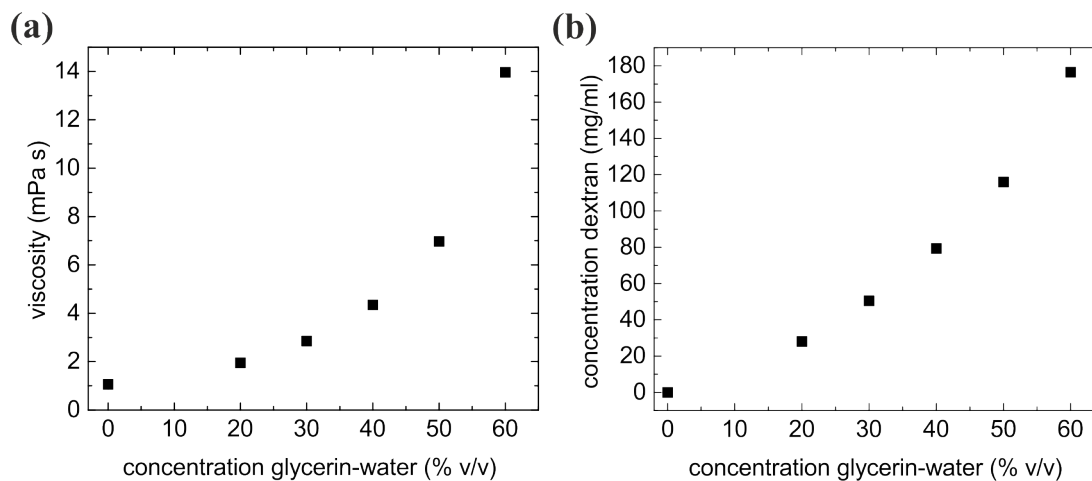


Figure 5.8: The viscosity of several glycerin-water concentrations (a) can be determined rheologically (the rheometer MCR702 with a CP50-2° was used at a shear rate of 100 1/s over three times 60s by an average of 10 s). Knowing the viscosity dependency of dextran 70 kDa concentrations from 3.1.1 they were related to the viscosities of several glycerin-water concentrations (b).

The formulation for all macromolecular solutions was to add “C” mg of the macromolecules to 1 ml of PBS, which was named “C” mg/ml. In order to be able to convert all presented data to a molar formulation the density of dextran 70 kDa and fibrinogen as delivered by Sigma Aldrich was measured and the concentrations of both formulations are compared in fig. 5.9 for both dextran 70 kDa and fibrinogen as delivered by Sigma Aldrich.

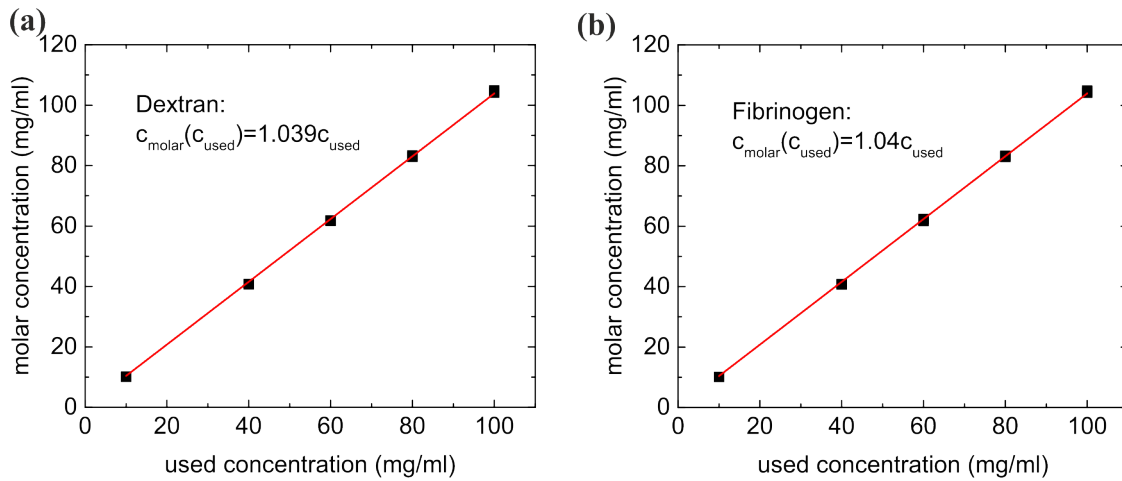


Figure 5.9: Conversion between the used formulation and the molar formulation for dextran 70 kDa and fibrinogen. Measurements were performed by density measurements of Karin Kretsch.

5.3 MAI

Most measurements of the MAI were performed at 10 % hematocrit. This was due to the fact that lower hematocrit concentrations show a very low aggregation affinity of RBCs as depicted in fig. 5.10.

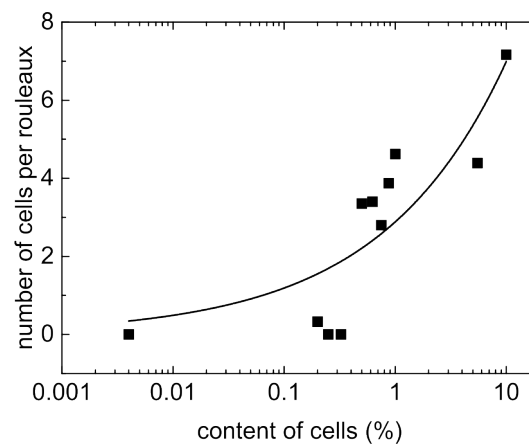


Figure 5.10: Hematocrit dependency for 60 mg/ml dextran. Hence, the hematocrit of the MAI was chosen to 10 %. The line is there to guide the eye.

The usage of 10 % hematocrit leads to several microscopic images that are investigated in 3.2 and shown in 5.11. It is remarkable that the RBCs are similar deformed by using fibrinogen as delivered by Sigma Aldrich (a) and the equivalent salt concentration (c) as well as that HES at high concentrations seems to change the cell shape to stomatocytes (b), which is an ongoing investigation process.

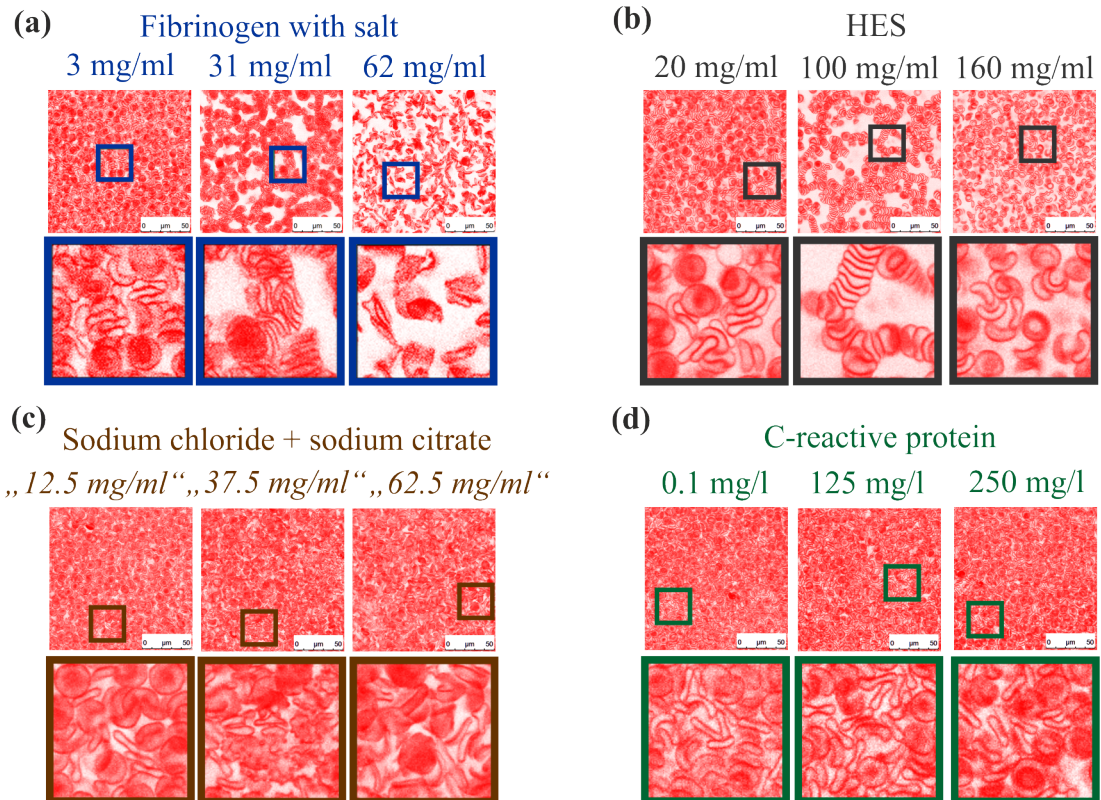


Figure 5.11: MAI for different concentrations of (a) fibrinogen that includes ca. 15% of sodium citrate and ca. 25% of sodium chloride as delivered by sigma, (b) HES, (c) 15% sodium citrate + 25% sodium chloride while the concentration is the equal fibrinogen concentration is given and (d) CRP.

Negatively charged gold particles instead of macromolecules suspended in distilled water as delivered lead to an aggregation and slight shape change of RBCs into spherocytes, which is most probably induced by water as illustrated in fig. 5.12.

For dextran 2,000 kDa the macromolecules were found in between the aggregated cells by a z-scan of 300 nm per step in a range from 0 to 12 μm in z-direction. Dextran in between the cells (upper images) can often be directly related to the cell membranes (lower images) as depicted in fig. 5.13.

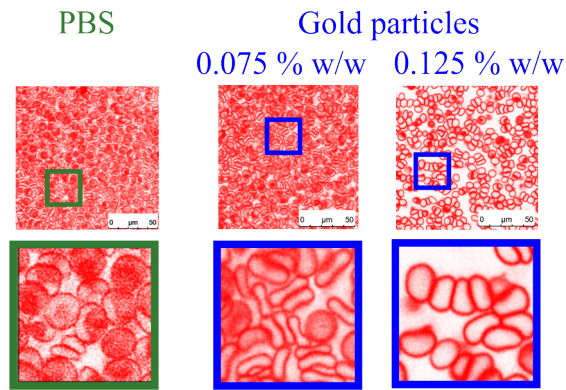


Figure 5.12: Microscopical images for 5 nm gold particles in distilled water instead of dextran. RBCs are marked red.

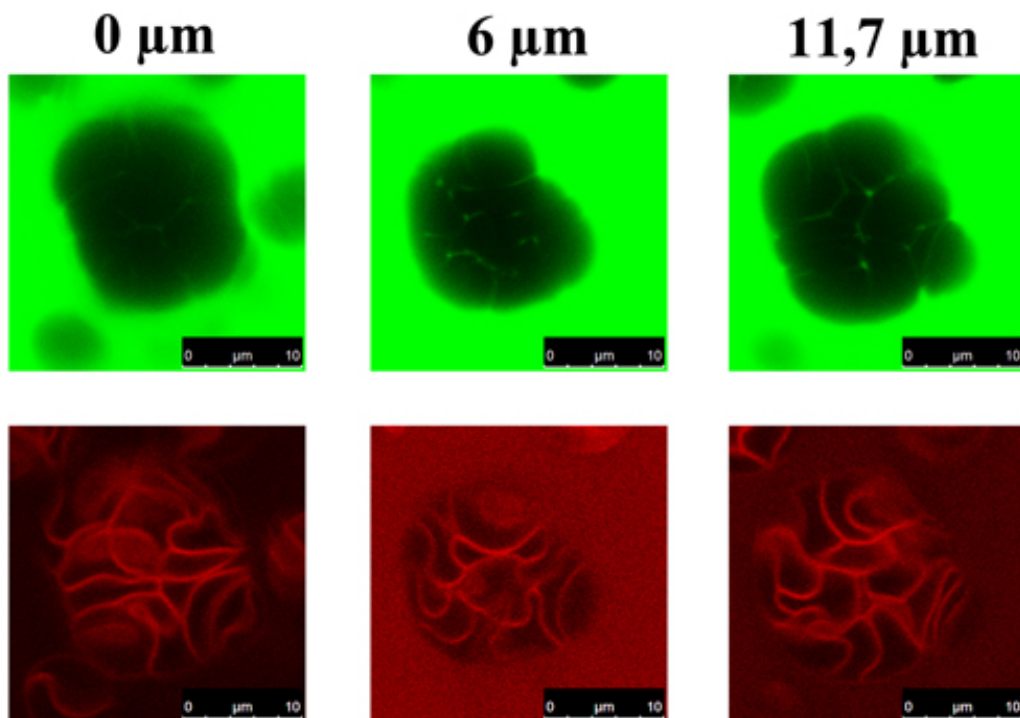


Figure 5.13: Exemplary images of confocal microscopic images for CellMask labeled RBCs surrounded by FITC-dextran 2000 kDa for different z-positions (it was scanned in 0.3 μm steps without a visible qualitative change). In the first row dextran is depicted in green, RBCs appear black. In the second row the corresponding images of the first row are depicted, while RBC membranes are marked in red and dextran is not visible. In most cases the dextran in between the RBCs is in good agreement with the membranes which is enhancing the probability of a dextran adsorption onto RBCs and therefore a bridging effect.

5.4 Supplements

The complete range of the interaction zones of RBC doublets for saltfree fibrinogen (compare fig. 3.44) up to 160 mg/ml is shown in fig. 5.14.

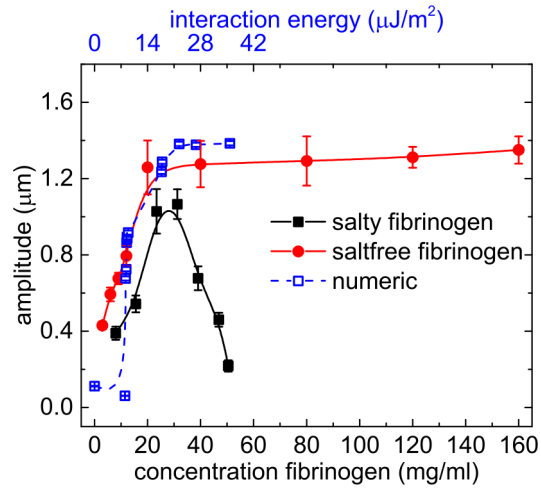


Figure 5.14: Amplitude of the interaction zones of a doublet up to the concentration of 160 mg/ml fibrinogen. Error bars are standard errors.

The complete range of the adsorption of macromolecules (compare fig. 3.24) is illustrated in fig. 5.15 (a), while their dependency on the rheological measured hematocrit is depicted in fig. 5.15 (b). With a decreasing hematocrit the total number of adhered macromolecules is decreasing most probably due to lower adsorptions of dextran 70 kDa onto the RBC membranes.

The presence of calcium by using dextran 70 kDa, fibrinogen as delivered by Sigma Aldrich and C-reactive protein shows no significant activation of the RBC calcium channels as shown in fig. 5.16.

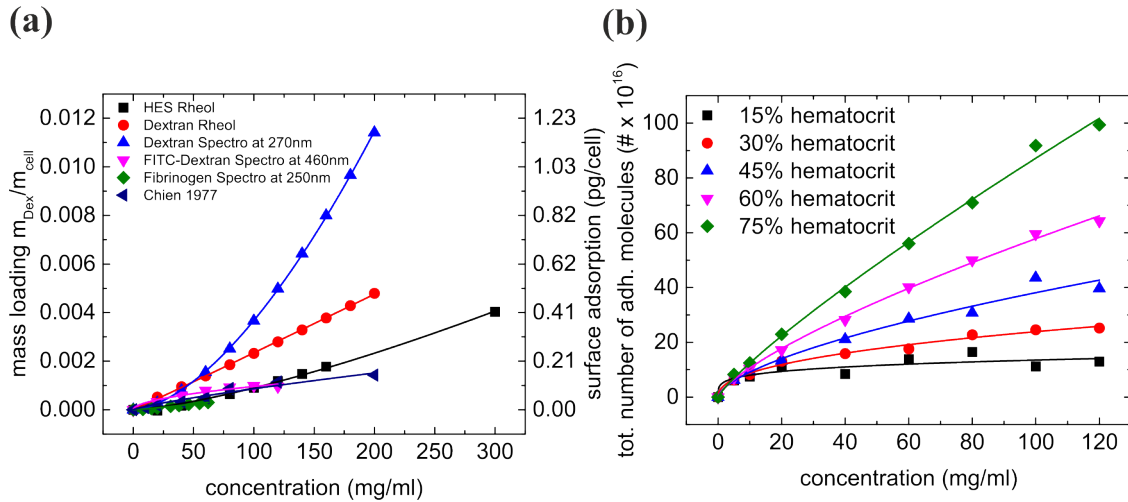


Figure 5.15: Complete adsorption curves measured with several methods where lines are indicating a Freundlich approximation (a) and rheological adsorption measurements for different hematocrits in dextran 70 kDa solutions (b). Lines are there to guide the eye.

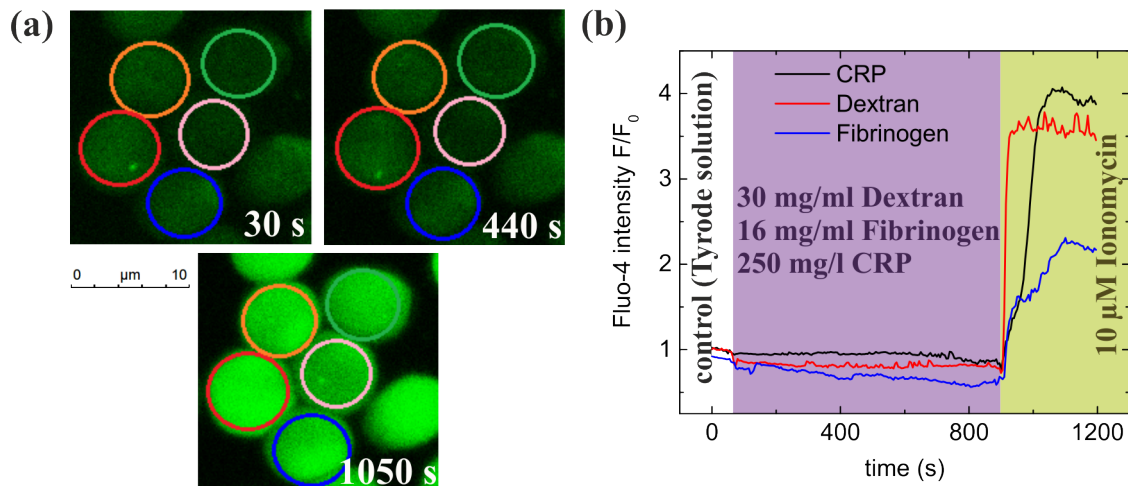


Figure 5.16: (a) Exemplary images for fluo-4 stained RBCs in tyrode solution for the control (30 s), after the addition of 250 mg/l CRP (440 s) and after adding 10 μM Ionomycin that is activating the Calcium channels (1050 s). Images for dextran and fibrinogen show a similar behavior. (b) Fluo-4 intensities of the measurements normalized by the control intensities (no addition of macromolecules) show no increase during the measurement, but a strong increase for all used macromolecules by adding Ionomycin as a positive control. The conclusion is that dextran, fibrinogen and CRP are not activating the calcium channels of the RBCs.

5.5 Tethers

Tethers, especially of RBCs, were investigated since the 1980th mainly by RM Hochmuth and some others [96, 97, 98, 99, 28, 40]. In these studies typically a RBC is attached via underinflation to a micropipet while e.g. a rather small bead in comparison to the RBC size is attached to another micropipet. Bringing the bead in contact with the RBCs leads to an adherence of integral proteins to the bead. By repulling the bead the protein is followed by a double lipid layer coming from the membrane and therefore the surface tension of the RBC is increasing. Typical pulling forces are in the range of $50 \text{ pN}/\mu\text{m}$ while the tether has a radius of ca. $10\text{-}20 \text{ nm}$ and longest tethers measured were in the range of $200 \mu\text{m}$.

As a side result while the AFM experiments in combination the confocal microscope (see chapter 3.5.2) tethers were observed at the same conditions (20 mg/ml dextran 70 kDa). By trying to catch a cell accidentally the top RBC of a (perpendicular orientated to the dish) triplet was adhered to the cantilever. Trying to remove the cell from the triplet leads to a tether formation as depicted in fig. 5.17 (a). Already within several micrometers the cells are deformed needle-like in direction of the tether/the other cell. The cantilever was moved in the upper left direction of the image that results in fig. 5.17 (b), in which the cantilever tip is in a similar position as in (d). The tether reached a length of ca. $50 \mu\text{m}$. Again accidentally a RBC doublet was touched with the tether at ca. its half length. The cantilever was moved out of the image in the upper right direction. A “three needle” RBC was resulting from this as illustrated in fig. 5.17 (c). This cell was attached to the tether of the first cell of the triplet (that was attached to the cantilever), its doublet corresponding cell (left) and the second cell of the triplet (lowest cell) that was still connected to the third cell of the triplet. The cantilever was moved ca. $150 \mu\text{m}$ in the upper right direction of the image until the doublet cell were disattached from the main tether. Moving back to the original position of the cantilever (close to the previously triplet) and moving it again to the position of image (b) led surprisingly to a round vesicle-like formation on the tether itself as depicted in fig. 5.17 (d) for brightfield and (e) for fluorescent imaging. Here the previously doublet cell reached nearly its original position in the doublet (compare (b)), while the top cell of the triplet is extremely deformed while the tether itself seems to be attached to the cantilever, because the original top RBC of the triplet is not visible anymore. In addition, by creating a tether between a single cell attached to the dish and the cantilever one tether were pulled out for $1200 \mu\text{m}$ which is enormously and the tether didn't brake up, but the the cantilever reaches the end of the dish, cause it was moved horizontally (data are not shown, cause just the distance was measured). Regarding the value mentioned above of ca. $50 \text{ pN}/\mu\text{m}$ the force this would lead to a total force of ca. 60 nN .

This observation may sounds arbitrary, but it includes one very important fact: Never tethers were observed which are that long, but they were always measured

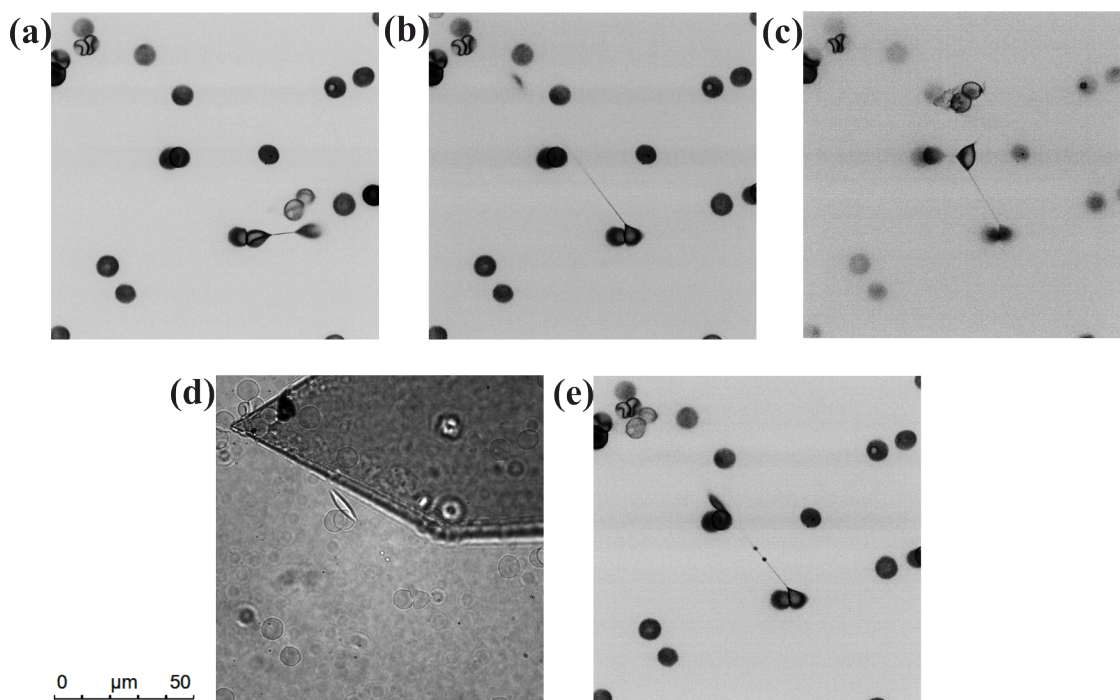


Figure 5.17: Tether pulled out from a RBC triplet for different positions of the cantilever. RBC membranes are marked in black.

in buffer solution and never in dextran. Therefore, it seems to be that dextran facilitates tether formations over a long range which could be related to the decreasing membrane stiffness by increasing dextran concentration as presented in chapter 3.5.1.

6 Acknowledgments

First, I want to give thanks to Prof. Dr. Christian Wagner and Prof. Dr. Thomas Podgorski for the intake of myself to your workgroups, for the freedom you forwarded to me to work out my own ideas, for all the discussions as well as the important and very helpful suggestions.

Vielen Dank an alle, die sich die Zeit genommen haben und diese Arbeit zum Teil oder komplett privat gelesen, erweitert sowie korrigiert haben (A. Christ, E. Terriac, P. Bohr, P. Steffen und L. Kästner).

I'm so grateful for all the discussions and facilities of Lars Kästner, Andreas Christ and Emmanuel Terriac. You were influencing my way of scientific thinking enormously. Emmanuel, thank you very much for all your help with the translations! Thanks to Othmane Aouane for supporting my thesis with your numerical results and realizing so many open questions. Karin und Elke: Vielen Dank für die Hilfe in so vielen Belangen! Thanks so much to the workgroups of AG Wagner, "AG" Podgorski, AG Lautenschlaeger and AG Lipp for the great moments beside the working and the help in many questions! Viviana, thank you so much for being there for scientific and personal issues.

Andi, du hast mich vor allem in der letzten Zeit sehr beeinflusst und ich denke, dass du mit sehr vielen Dingen absolut richtig liegst. Danke dafür und noch viel mehr für alles andere! Ina, vielen Dank für deine Unterstützung! Chris, du bist da, wenn ich real falle und für vieles andere, vielen Dank dafür!

Danke, dass du bei mir bist, Maggi!

Meine Eltern (Birgit und Gotthold): Dies ist nicht in Worte zu fassen. Aber sicher ist, dass es mir ohne euch niemals möglich gewesen wäre so weit zu kommen! Vielen, vielen Dank für alles, was ihr für mich getan habt!

Funding

The research leading to this results has received funding from the Saarland University, the center National de la Recherche Scientifique (CNRS), the German French University (DFH/UFA) and the German Research Foundation (DFG, SFB1026/7).

7 Publications

M Brust, O Aouane, M Thiébaud, **D Flormann**, C Verdier, L Kaestner, MW Laschke, H Selmi, A Benyoussef, T Podgorski, G Coupier, M Misbah and C Wagner. The plasma protein fibrinogen stabilizes clusters of red blood cells in microcapillary flows. *Scientific Reports*, 4:4348, 2014.

D Flormann, E Kuder, P Lipp, L Kaestner and C Wagner. Is there a role of C-reactive protein in red blood cell aggregation? *International Journal of Laboratory Hematology*, 37:474-482, 2015.

D Flormann, K Schirra, T Podgorski and C Wagner. On the rheology of red cell suspensions with different amounts of dextran: separating the effect of aggregation and increase in viscosity of the suspending phase. *Rheologica Acta*, 55:477-483, 2016.

D Flormann, O Aouane, L Kaestner, C Ruloff, S Svetina, C Misbah, T Podgorski and C Wagner. Red blood cells buckle during aggregation. submitted 2016.

List of Figures

- 1.1 (a) Single red blood cells in buffer solution can (b) aggregate into rouleaux induced by proteins or other macromolecules (here, the example of 8 mg/ml fibrinogen). Images were taken with a confocal microscope and cell membranes are marked in red by the cell membrane dye CellMask. (c) For the case of fibrinogen a further concentration increase does not lead to a disaggregation, i.e. even at c_2 and at higher concentrations the percentage of aggregated cells is assumed (and observed) to remain at 100 %. In contrast, for polysaccharides like dextran or HES a further concentration increase can lead to a complete disaggregation. The concentration c_1 at which 100 % of the RBC are aggregated is marked in red, while the concentration c_2 where no RBCs are aggregated is marked in blue. 2

- 2.1 Blood consists beside (aggregated) RBCs of the plasma (several proteins etc.) and the buffy coat (mainly white blood cells and platelets). The single components are just an illustration and the concentrations differ from the reality. 12

- 2.2 Sedimentation of blood in vitro leads to a separation between plasma, buffy coat and red blood cells. The single components are just an illustration and the concentrations differ from the reality. 13

- 2.3 A discocyte (a) can change its shape to a stomatocyte in a slight hypotonic environment (b) or to an echinocyte shape in an hypertonic environment in contact with glass or similar (c) or to a spherocyte shape in e.g. an hypotonic environment (d). 14

- 2.4 The red blood cell membrane formed out of a double lipid layer, several proteins, the glycocalyx and an underlying spectrin network. 15

- 2.5 Electrostatic potential surface diagram of (a) a fibrinogen monomer from [149] and (b) C-reactive protein from [186]. Negative charges are marked in red, positive charges are marked in blue. 18

- 2.6 If no macromolecules are present RBCs don't aggregate as depicted in the most left image. If 50 % of the surfaces of two cells is covered by macromolecules 50 % of the surfaces is uncovered and therefore the aggregation, i.e. the interaction energy is at the maximum (middle image). If 100 % of both cell surfaces is covered by steric-interacting macromolecules no free binding sites exist and the cells can't aggregate (most right image). Cells in between (upper left and right image) represent the intermediate state between maximum and minimum interaction energy. Macromolecules mainly adhered to the right cell of the cell pair are marked in green, while macromolecules mainly adhered to the left cell of the cell pair are marked in black. 21
- 2.7 A specific binding to proteins of macromolecules (black) between two red blood cells (red) (a) could be unspecific if no membrane proteins are involved (b). The glycocalyx is marked slightly red. Different sizes of macromolecules indicating the presence of imperfect macromolecules. 22
- 2.8 (a) The depletion of large spheres (marked in red) induced by small spheres (marked in green). The depletion layer is shown in blue and the forbidden areas are illustrated in black. (b) The depletion is changing by changing the sphere shape to a RBC shape. Small and greater green balls are indicating the presence of imperfect macromolecules, which do not have all the same size. 25
- 2.9 Red blood cells (a) could adsorb macromolecules which leads to bridging (b). By a further increase of the macromolecule concentration the cells could be fully covered by those molecules and can't bridge anymore, if the macromolecules can't adhere to themselves (c). Increasing the molecule concentration even more a depletion layer can appear, which leads again to an aggregation of the red blood cells (d). 28
- 2.10 A point scanning confocal microscope (a) scans the entire probe point by point and line by line (c). Out of focus light is marked in black. A spinning disc confocal microscope (b) scans the whole probe (d) using parallel curved lines (parallel scans are marked with the same color). 34
- 2.11 A confocal microscope is able to scan several areas in z-direction (e.g. from the bottom to the top of a sample, as shown here for a discocyte RBC) (a), which leads to a stack of images, where each image is representing one area in z-direction (b). In order to get a 3D view one can have a look to the reconstruction of the stacks from the side (c) or reconstruct the specimen by setting a surface threshold (d). . 35

2.12	Unidirectional shearing of a small volume element (here strongly magnified) with a linear velocity profile and constant shear rate for Newtonian fluids (a). The dependency of the shear stress on the shear rate differ for Newtonian, shear thickening and shear thinning fluids (red). The three basic approximation models for yield stress fluids (Bingham, Herschel-Bulkley and Casson model) are depicted in black (b) and discussed in chapter 2.2.2.4.	37
2.13	In rest or at low shear rates polymers are coiled (a). At high shear rates the polymers get stretched, which leads to an anisotropy of the fluid (b).	37
2.14	The AntonPaar MCR702 (a) is equipped (red rectangle, magnified in (b)) with two EC-motors (b) while a single motor (blue rectangle, magnified in (c)) is equipped with an optical encoder and an air bearing (c).	39
2.15	A cone-plate geometry (a) in comparison to a Taylor-Couette geometry (b), which has a significantly higher measurement position (c, left) and is realized with stainless steel (c, right). The inner diameter of the outer cylinder is 22 mm.	40
2.16	The shear thinning behavior of RBCs within the resolution limit of the rheometer MCR702 using the CC20 geometry (gray). If the RBCs are suspended in the buffer solution (black frame) the slight shear thinning behavior is caused by an elastic deformation and an orientation of the cells in flow direction (pink frame). If the RBCs are suspended in a 60 mg/ml dextran solution strong clustering appears resulting in a high viscosity (red frame). During shearing (indicated by blue arrows) most of the rouleaux break up and the cells become deformed elastically (green frame), which leads to a strong shear thinning behavior. The higher viscosity for the red curve at 100 s^{-1} is caused by the viscosity of dextran. Lines are there to guide the eye.	41
2.17	The linear Zener model represents a gel (a), which transfers to a viscoelastic fluid represented by the Maxwell model after the yield stress point (b).	42
2.18	Main components of the AFM (a) with no contact of the cantilever with the substrate, which is used for the measurement of the sensitivity (b). The cantilever in contact with the substrate (c) leads to a significant change in vertical deflection, which is used for the measurement of the spring constant (d).	46
2.19	The indentations into an elastic body (orange) of (a) the tip of a paraboloid, (b) a cone and (c) a quadratic pyramid.	48
2.20	The used cantilever tip in 3D (a) is shown from the side views (b). . .	48

- 2.21 The setup of a dual beam spectrometer includes a light source whose light is reduced to a single wave length by a monochromator. A dichroic mirror is splitting the beam into one that is passing the probe and reaching the sample detector and one that is directly reaching the reference detector. 50
- 2.22 If 45 % RBCs and macromolecules of a concentration c (a) are mixed with 55 % macromolecule solutions (b) it could lead to a sedimentation where the macromolecules are adsorbed to the RBC (c). The concentration of the supernatant is indicated by c_S while the concentration of the pellet is indicated by c_P 51
- 2.23 The SAW setup includes the in- and output IDT as well as the piezoelectric material on that the acoustic wave is transversally propagated. RBCs adhered to the cell-adhesive “CellTak” are taken as an example for a biofilm. 52
- 2.24 A surface acoustic wave (a) is changing its phase if e.g. a macromolecule adhere to the biological substrate and its amplitude if e.g. the substrate becomes more flexible (b). This behavior is (fully or nearly) reversible if the molecules don’t have an severe effect on the substrate (c), which can be shown in relation to the time (d). Colored areas are directly related to the letters of these figure. 53
- 2.25 On top of the filter inside a 15ml Vivaspin tube (a) the fibrinogen as provided by Sigma Aldrich dissolved in H_2O was added (b). After one centrifugation procedure some salt diluted in distilled water remains on the bottom of the 15 ml tube, while the fibrinogen can’t pass the 10 kDa filter (c). The lost volume was replaced by H_2O and after mixing the procedure was repeated at least 10 times (one hour between the addition of H_2O). 58
- 3.1 The viscosity of RBC-dextran suspensions for different dextran concentrations. (a) represents the “down” protocol and (b) represents the “up” protocol. Gray areas are the measured resolution limit of the MCR702 (with 20% tolerance, compare fig. 5.1). Respectively, in (b) and (d), the viscosities at a given shear rate for different dextran concentrations are depicted. Error bars indicate the standard deviation of at least three measurements. 65
- 3.2 If 45 % RBCs and macromolecules of a concentration c (a) are mixed with 55 % macromolecule solutions (b) it could lead either to a sedimentation where no macromolecules are actively involved which would be the case of no adsorption (c, upper graphic) or it could lead to a sedimentation where the macromolecules are adsorbed to the RBC (c, lower graphic). The concentration of the supernatant is indicated by c_S while the concentration of the pellet is indicated by c_P 66

3.3	Viscosity measurements of the supernatant of a 45 % and 36 % RBC-dextran suspension after sedimentation (a) and relative concentration in dependency on the concentration of the stock solution (b).	67
3.4	Relative viscosities of RBC-dextran suspensions for different shear rates with the (a) stock and (b) supernatant viscosities using the “up” protocol and (c) stock and (d) supernatant viscosities with the “down” protocol [79].	69
3.5	The viscosity of the pellet for different dextran concentrations using the “up” protocol (a). Gray areas are the measured resolution limit of the MCR702 (with 20% tolerance, compare fig. 5.1). Respectively, in (b) the viscosities at a given shear rate become related to the dextran concentrations. Error bars represent the standard deviation of at least three different measurements.	70
3.6	The position of maximum of normalized bell-shaped graphs, for the normalization with the stock solution and with the supernatant solution for both protocols (a) “up” and (b) “down”. In (a) the position of the maximum for the pellet is shown as well.	70
3.7	The three common model to approximate a yield stress are the Bingham model (a), the Herschel-Bulkley model (b) and especially for RBC suspensions the Casson model (c), which are shown for RBC-dextran suspensions by varying the dextran concentration. Additionally, a new idea for measuring the yield stress on the example of 60 mg/ml shows either a flow or at some point no flow anymore. Exact approximation values are depicted in table 5.1. The applied shear stresses are shown here. Gray areas are the measured resolution limit of the MCR702 (with 20 % tolerance, compare fig. 5.1).	75
3.8	The yield stress extrapolated by all three classical yield stress models (a) and compared to the new introduced resolution vs. flow method (b).	76
3.9	Image of cell sedimentation for different times at all investigated dextran concentrations (indicated in mg/ml at the first line) at a tube diameter of 25 mm. With increasing time a bell-shape behavior is clearly visible due to a strong sedimentation in the middle part (40-80 mg/ml), while a low sedimentation at the outer parts (0, 20, 100 and 120 mg/ml).	79
3.10	Position of the sedimentation front in % of filling levels in dependence on the time for the used dextran concentrations at different tube diameters. Error bars are representing the standard deviation of measurements for at least three healthy donors. Lines are there to guide the eye.	80

- 3.11 The sedimentation of RBC in dependency on the dextran concentration for tubes with the diameters 1.15 mm (a), 2.4 mm (b), 12 mm (c) and 25 mm (d) at different times. 25 mm reflects directly fig. 3.9. Error bars are representing the standard deviation of measurements for at least three healthy donors. Lines are there to guide the eye. 81
- 3.12 Sedimentation of the maximum sedimentation at 60 mg/ml dextran for different times. Error bars represent the standard deviation of measurements for at least three healthy donors. Lines are there to guide the eye. 82
- 3.13 Sedimentation of 45 % hematocrit in a 60 mg/ml dextran 70 kDa solution for three different times using a transparent CC20 geometry. Magnifications are marked in the same colors. 83
- 3.14 Measurements become not affected by sedimentation due to ca. 1 cm overfilling (100 % equals ca. 10 cm) 84
- 3.15 Microscopic imaging of dextran 70 kDa and saltfree fibrinogen for different concentrations in the first row and magnifications in the second row. Contacts at 90° angles of the cell membranes for saltfree fibrinogen are marked with a black circle (a). Microscopical aggregation indices for dextran 70 kDa (black curve), HES 130 kDa (red curve), saltfree (filtered) Fibrinogen (blue, filled triangles), Fibrinogen as delivered by Sigma Aldrich with approx. 40% salt (empty triangles) and C-reactive protein (green). Error bars represent the standard deviation of measurements for at least three healthy donors. Lines are guides to the eye (b). 88
- 3.16 Meta-analysis of several medical publications regarding the correlation between CRP concentration and ESR. Shortcuts are indicating the illness. The size of the measuring points is correlated with the number of patients (large: high number, small: low number). Error bars are either standard errors or standard deviations depending on the publication. The linear approximation (gray line) gives the overall tendency to guide the eye. 91
- 3.17 The sedimentation front (indicated with “sedimentation”) of washed RBC in PBS with the addition of several CRP concentrations in dependence on the time (a). No concentration dependency can be observed within the error bars (b). Line are there to guide the eye and images to are related to (from left to right) 0.0001 mg/ml, 0.125 mg/ml and 0.25 mg/ml of CRP. Error bars represent the standard deviations of at least three healthy donors. 92

3.18	MAI shows no significant increase of the RBC aggregation in the presence of CRP (a). Sedimentation measurements performed with an UV-Vis spectrometer show a rapid sedimentation of RBCs for the presence of fibrinogen and no effects for CRP compared to PBS (b). The analysis for the time of the inflection point confirms this result (c and d). Red lines are there to guide the eye and error bars represent the standard deviation of at least three measurements of three healthy donors.	93
3.19	Three dimensional adhered RBCs in relation to the adhesion strength and reduced volume theoretically observed by Svetina and Zihelr from [182] (a) and in relation the interaction energy varied by the dextran concentration for RBC in contact with the microscopy dish (b). From left to right the interaction zones are called: male-female, strong sigmoid or S and low sigmoid or S.	96
3.20	Overview of the observable doublets by varying the dextran concentration exemplary.	97
3.21	Observed RBC doublet shapes for saltfree fibrinogen (a), salty fibrinogen (c) and dextran while here the echinocyte shape was created by the glass effect (b) and numerics for the same reduced areas of 0.65 by varying the interaction energies (d).	99
3.22	RBC doublet contact zone distribution for saltfree fibrinogen (a), salty fibrinogen (b), dextran discocytes (c), dextran echinocytes (d).	100
3.23	Procedure of analyzing RBC doublet (a) and clusters larger then seven single cells (b) was performed by reducing the images to interaction zones (second column) and approximating the pixels with a sinus function.	101
3.24	Numerical simulations performed by Othmane Aouane [77] (a), dextran amplitudes compared to $\tau_1 = 0.65$ and $\tau_2 = 0.65$ (b), fibrinogen amplitudes compared to $\tau_1 = 0.65$ and $\tau_2 = 0.65$ (c) and the interaction energy in relation to the concentration for $\tau_1 = 0.60$ and $\tau_2 = 0.65$. Error bars represent the standard errors of 15 doublets for echinocytes and 30 doublets for all the other of at least three healthy donors. Thin error bars are in (d) represent the minimum and maximum interaction energies within the standard errors of the experimental data compared to the numerical amplitudes. Lines are there to guide the eye.	103
3.25	The parameters of analytical investigations performed by Thomas Podgorski [77] (a) lead to a bifurcation of the amplitude A of the changed interaction zone in depending on the rescaled interaction energy β for two reduced areas (b).	104

3.26	Exemplary images for clusters larger than seven cells (except for 10 mg/ml) for three dextran concentrations (a). At 10 mg/ml all observed aggregates contain four cells or less, cause no larger ones were observed. Only clusters of four cells were analyzed. The variation of the first three interaction zones for one dextran concentration can be severe (c), which was not observed by numerical simulation performed by Othmane Aouane [77] for different interaction energies at the same reduced areas of $\tau = 0.6$ (b).	105
3.27	Distribution of the first three interaction zones within a rouleau that consists of at least seven single RBCs. Only S- and male-female shapes were observed (a). Amplitudes of the first three interfacial shapes in dependence on the dextran concentration. For comparison data for echinocyte doublets are shown as well as numerical results for clusters of exact 7 cells and the same reduced volumes. Error bars are indicating standard errors.	106
3.28	Scanning electron microscopy (SEM) enables the high resolution imaging of the MLCT-O (a) and MLCT (b) cantilevers (Bruker). The magnification is marked with blue squares for MLCT-O (c) and with red rectangles for MLCT (d) cantilevers.	108
3.29	Illustration of the different Young's moduli of a RBC performing an AFM scan. The RBC, which has a much lower Young's modulus than the substrate, is marked in black for a color code up to 1 MPa (a). Assuming that the local Young's modulus of a RBC close to the edges is around 400 Pa as maximum the same cell as in (a) is shown with a color code up to 400 Pa (b).	109
3.30	Matching the valid area of measurement on RBC when dextran 70 kDa (at 60 mg/ml) is present (a) it leads to a "soft" curve while the inset is showing the magnification of the approximated area (b) as for all other representations in this figure. If the RBC is surrounded by PBS (c) and it's not matched properly the cantilever (respectively the AFM) feels the substrate which leads to a very high Young's modulus (d). If the RBC is matched properly with PBS in the surroundings (e) the resulting curve leads to moderate Young's modulus (f). . . .	111
3.31	The Young's moduli of RBCs by using a MLCT cantilever (Bruker) for an increasing fibrinogen and dextran concentration. Error bars representing the standard deviation of at least 20 different cells. Lines are there to guide the eye.	112
3.32	The force-distance curve while retracting the cantilever of two "adhered" cells for the case of dextran 150 kDa (a) leads to a bell-shape behavior regarding the interaction energy in dependency on the macromolecular concentration for both dextran 70 kDa and dextran 150 kDa. Measurements were performed by Patrick Steffen and published in [180].	113

- 3.33 The AFM cell-cell adhesion measurement is performed by an approach with three different velocities (a) that leads to the contact of the two cells, while three contact times were used (b). Retracting the cantilever could lead to a deformation of the cells (c) and after the detachment of the RBC the cantilever should come to its approaching or no-contact position (d) 115
- 3.34 Exemplary data for 40 mg/ml dextran 70 kDa are shown for a contact time of 0 s with a velocity of 5 $\mu\text{m/s}$ (a), 5 s with a velocity of 1 $\mu\text{m/s}$ (b) and 5s with a velocity of 0.1 $\mu\text{m/s}$ (c). The SCFS for PBS is shown as a reference for a contact time of 30 s with a velocity of 0.1 $\mu\text{m/s}$ (d). Insets in (c) and (d) show a magnification of the region of interest. 116
- 3.35 A mismatch of the RBCs in PBS at 5 $\mu\text{m/s}$ leads to strong interaction forces at 0 s contact time (a) and can lead to strong tether formations at 30 s contact time with an increase of interaction distance by 100% (b) in comparison to (a). 118
- 3.36 The interaction energy of SCFS versus on the dextran concentration by varying the extend/retract velocity from 0.1 over 1 to 5 $\mu\text{m/s}$ and the contact time (ct) from 0 over 5 to 30s. For high concentration of 80 mg/ml and more at 5 $\mu\text{m/s}$ the cells were not in contact anymore. Error bars represent the standard deviations of at least seven individual bottom cells using the same cell attached to the cantilever. Lines are there to guide the eye. 119
- 3.37 AFM measurements of the cantilever in BSA-dextran solutions without RBCs involved (a) compared with RBCs involved measurements for a velocity of 0.1 $\mu\text{m/s}$ and 0 s of contact time. This leads to a higher maximum force (b), a comparable interaction distance (c) and a higher interaction energy for measurements without RBCs involved as a function of the dextran concentrations (d). Due to the high error bars (standard deviation) for dextran measurements without RBCs one can assume that the dextran reference leads to at least higher interaction forces and therefore to slightly higher interaction energies. 120
- 3.38 Comparison between the SCFS and the glycerin-water reference regarding the maximum force (a), interaction distance (b), interaction energy with taken the RBC contact area into account (c) and interaction energy for glycerin-water without taken any area into account because it is not known (d). Error bars represent the standard deviation of at least seven measurements. The exact values of the measured glycerin-water concentrations are given at the second x-axis and related to the dextran concentrations via the viscosity as depicted in 5.8. 123

- 3.39 A 50 % v/v glycerin-water solution is used to measure the velocity dependency of the vertical deflection for 0.04 $\mu\text{m/s}$ (a) and 0.01 $\mu\text{m/s}$ (b). Both insets show the magnification of the retract curve in the potentially approximate-able range. Grey marked regions indicate possible integration areas. 124
- 3.40 If the cells overlap properly (a) they could show a deformed shape while retracting the cantilever (b). In the 3D side view one can see that they match properly (c) and deform during the retraction of the cantilever (d), which is depicted in a 3D reconstruction in (e) for the matching and (f) for the retraction. The cantilever position could be illustrated in the 3D reconstructions, because of side view images and the knowledge that the cantilever encloses an angle of 10° with the dish. 127
- 3.41 If the cells are not concentrically aligned (a) this could lead to an interaction between the upper cell and the coverslip or/and the lower cell and the cantilever (b). This happens as shown in the side view of the mismatch (c) and the retraction phase of the cantilever (d), while it is difficult to see the cell membrane in the original images due to bleaching effects. Therefore, the cell membranes are marked with black (c) and white (d) for a better visualization. The mismatch of the cells is depicted in (e) in a 3D reconstruction, while there is an mirroring by the centilever of the cell which is attached to the cantilever. Consequently, the scale bar is showing the area that is including the cells (the part above the scale bar is the mirrored part). Retracting the mismatched cells by ca. 20 μm that is taken by the cell itself only leads to a tether formation (f). The tethers are not touching the cells itselfs (even if it appears like this in the 3D reconstructions) but the coverslip and the cantilever, which is due to an over illumination of the cell-attached areas (d) and an over estimation of the threshold in case of the reconstruction (f). 128
- 3.42 SAW measurements for dextran indicates a mass increase with dextran concentration shown by an increasing phase (a) while the flexibility of RBCs increase with the dextran concentration shown by a decreasing amplitude (b). Grey areas are indicating the added dextran concentraion in mg/ml. 134
- 3.43 SAW results of the phase (a) and the amplitude (b) for RBC attached to the chip and fibrinogen flowed over. Reference signal (without cells) is higher then signal with cells. Grey areas are indicating the fibrinogen concentration in mg/ml. 135
- 3.44 Exemplary data for the absorption spectrum of fibrinogen for stock solutions and the corresponding supernatant solution after adding 45% of RBCs (a). The mass loadings and surface adsorptions resulting from rheological and spectroscopic measurements are compared with the data from Chien [55]. 136

- 3.45 Aggregated red blood cells (black) with FITC-dextran (white) in between nearly all cells (a) and the magnification of the red square (b). 138
- 3.46 If RBCs are surrounded by a macromolecular solution (a) one can try to wash the macromolecules out with PBS (b) which could lead to the ideal case that no macromolecules are in the solution anymore (c). Images in (b) show RBCs labeled with CellMask in black (i) left as well as dextran shown in white on the right image while RBCs appear black. RBCs labeled with CellMask in fibrinogen solution are shown in black (ii) on the left image while fibrinogen is shown in white on the right image (cells appear black here). 140
- 3.47 Measurements with ghosts in the presence of distilled water (a), dextran 70kDa at 40 mg/ml, HES at 40 mg/ml (c) and fibrinogen (salty) at 31 mg/ml (d) that were all solved in distilled water. RBC membranes are marked in black. 142
- 3.48 The osmolality for all used macromolecules in dependence on the concentration while the equivalent concentration of fibrinogen was used for the pure salt (green curve) that is typically attached to the protein. All macromolecules were solved in PBS. Error bars representing the standard deviation of at least three measurements. Lines are there to guide the eye. 143
- 3.49 Microscopical images of silica and PEG-labeled silica particles where RBCs are marked in red (a) lead to a microscopical aggregation index in dependence on the concentration of particles (b). 145
- 3.50 A 3D reconstruction of a cell (red, upper one) that is attached to the cantilever (dark yellow) while it is deforming itself slightly and a cell (red, lower one) attached to the coverslip (slightly marked in black). 146
- 5.1 Rheological measurement of several Newtonian substances for the CC20 geometry. The appearing systematical error at low shear rates is a common effect of MCR702 due to calibration. (a) Allowing the offset of the curve to be 5% or 20% of the apparent viscosity (at 100 s^{-1}) leads to the measured resolution limit (Meas RL) for the MCR702 in comparison to the theoretical calculated resolution limit (theo RL). (b) Approximations were performed with a power law. . . 158
- 5.2 Control measurement for the “up” protocol where one shear rate was applied for 30 s or 60 s and averaged over 25 s or 50 s. “Mix” indicates a stop of the protocol, removing the inner cylinder of the CC20 and mixing the solution with a plastic stick in order to reduce potential sedimentation effects on the measurement result. “Susp. phase” is representing a pure dextran solution, here at 60 mg/ml (a). Time resolution shows that even for low shear rates of 0.1 s^{-1} a steady state is reached within approximately 30 s, which is valid for higher shear rates as well (b). 159

5.3	Shear rate dependent viscosities for different dextran concentration using the up protocol (a) and the down protocol (c). The viscosities in dependency on the concentration of the stock solution for appointed shear rates are depicted in (b) for the up protocol and in (d) for the down protocol.	160
5.4	The normalization of shear thinning curves for 36% hematocrit at different shear rates for the up protocol (a, b) and for the down protocol (c, d). Normalizations with the viscosity of the stock solution (a, c) and with the viscosity of the supernatant solution (b, d).	161
5.5	The position of maximum in dependency on the shear rate for 36 % hematocrit.	162
5.6	The influence of BSA on the pellet (a) and on the supernatant (b) for high dextran concentrations. At lower dextran concentrations the qualitative results is the same within the standard deviations. The resolution limit of the MCR702 is marked with gray areas.	163
5.7	Shear stress dependency for the MCR702 with the CC20 geometry for (a) H ₂ O and (b) a 10M oil. The measured shear stress is in both cases significantly different from the applied stresses. Due to the oscillatory behavior of (b) an geometrical error in combination with a software are is assumed.	163
5.8	The viscosity of several glycerin-water concentrations (a) can be determined rheologically (the rheometer MCR702 with a CP50-2° was used at a shear rate of 100 1/s over three times 60s by an average of 10 s). Knowing the viscosity dependency of dextran 70 kDa concentrations from 3.1.1 they were related to the viscosities of several glycerin-water concentrations (b).	164
5.9	Conversion between the used formulation and the molar formulation for dextran 70 kDa and fibrinogen. Measurements were performed by density measurements of Karin Kretsch.	165
5.10	Hematocrit dependency for 60 mg/ml dextran. Hence, the hematocrit of the MAI was chosen to 10 %. The line is there to guide the eye.	165
5.11	MAI for different concentrations of (a) fibrinogen that includes ca. 15% of sodium citrate and ca. 25% of sodium chloride as delivered by sigma, (b) HES, (c) 15% sodium citrate + 25% sodium chloride while the concentration is the equal fibrinogen concentration is given and (d) CRP.	166
5.12	Microscopical images for 5 nm gold particles in distilled water instead of dextran. RBCs are marked red.	167

5.13	Exemplary images of confocal microscopic images for CellMask labeled RBCs surrounded by FITC-dextran 2000 kDa for different z-positions (it was scanned in 0.3 μm steps without a visible qualitative change). In the first row dextran is depicted in green, RBCs appear black. In the second row the corresponding images of the first row are depicted, while RBC membranes are marked in red and dextran is not visible. In most cases the dextran in between the RBCs is in good agreement with the membranes which is enhancing the probability of a dextran adsorption onto RBCs and therefore a bridging effect. . . .	167
5.14	Amplitude of the interaction zones of a doublet up to the concentration of 160 mg/ml fibrinogen. Error bars are standard errors. . . .	168
5.15	Complete adsorption curves measured with several methods where lines are indicating a Freundlich approximation (a) and rheological adsorption measurements for different hematocrits in dextran 70 kDa solutions (b). Lines are there to guide the eye.	169
5.16	(a) Exemplary images for fluo-4 stained RBCs in tyrode solution for the control (30 s), after the addition of 250 mg/l CRP (440 s) and after adding 10 μM Ionomycin that is activating the Calcium channels (1050 s). Images for dextran and fibrinogen show a similar behavior. (b) Fluo-4 intensities of the measurements normalized by the control intensities (no addition of macromolecules) show no increase during the measurement, but a strong increase for all used macromolecules by adding Ionomycin as a positive control. The conclusion is that dextran, fibrinogen and CRP are not activating the calcium channels of the RBCs.	169
5.17	Tether pulled out from a RBC triplet for different positions of the cantilever. RBC membranes are marked in black.	171

List of Tables

- 2.1 Overview of the main devices. 60
- 2.2 Overview of the main consumables. 61

- 3.1 Freundlich-coefficient and inverse Freundlich exponent for all data.
“r” stands for rheology, “s” for spectroscopy and “ra” for radioactivity
and “C” for Chien. 137
- 3.2 Summary of publications regarding depletion vs. bridging indica-
tions for dextran and fibrinogen with several methods over the years.
Shown are the intentions of the authors and no interpretation if the
conclusion is valid. Symbols are equivalent to the table 3.3. 147
- 3.3 Summary of depletion vs. bridging indications for dextran and fib-
rinogen with several here presented methods. “+” means “yes”; “-”
means “no”; “(+)” means “yes, but with restrictions”; “(-)” means
“no, but with restrictions”; “/” means “no statement”. 147

- 5.1 Approximation values of the yield stress models in relation to the
dextran concentration regarding fig. 3.7. 162

Bibliography

- [1] K Aalto, K Osterman, H Peltola, and J Raesaenen. Changes in erythrocyte sedimentation rate and c-reactive protein after total hip arthroplasty. *Clinical Orthopaedics and Related Research*, 184:118–120, 1984.
- [2] KN Adamik, ID Yozova, and N Regenscheit. Controversies in the use of hydroxyethyl starch solutions in small animal emergency and critical care. *Journal of Veterinary Emergency and Critical Care*, 25(1):20–47, 2015.
- [3] B Alberts, A Johnson, J Lewis, M Raff, K Roberts, and P Walter. *Molecular biology of the cell*. Garland Science, Taylor and Francis Group, 2002.
- [4] GI Amilo, MU Anokwute, MO Ifeanyichukwu, RC Chukwuanukwu, CC Onyenekwe, FC Ifediata, and SC Ezeah. Fibrinogen concentration and thrombin levels in pregnant women in nnewi, anambra state, south, eastern nigeria. *Journal of Biology, Agriculture and Healthcare*, 3(7):144–147, 2013.
- [5] S Amin, GV Barnett, JA Pathak, CJ Roberts, and PS Sarangapani. Protein aggregation, particle formation, characterization & rheology. *Current opinion in colloid & interface science (Elsevier Ltd.)*, 19(5):438–449, 2014.
- [6] RS Amos, TJ Constable, RA Crockson, AP Crockson, and B McConkey. Rheumatoid arthritis: relation of serum c-reactive protein and erythrocyte sedimentation rates to radiographic changes. *British Medical Journal*, 1:195–197, 1977.
- [7] M Anand and KR Rajagopal. A shear-thinning viscoelastic fluid model for describing the flow of blood. *International Journal of Cardiovascular Medicine and Science*, 4(2):59–68, 2004.
- [8] B Angelov and IM Mladenov. On the geometry of red blood cell. *Coral Press*, pages 27–46, 2000.
- [9] O Aouane, M Thiebaud, A Benyoussef, C Wagner, and C Misbah. Vesicle dynamics in a confined poiseuille flow: From steady state to chaos. *Physical Review E*, 90:033011, 2014.
- [10] AJ Apostolidis and AN Beris. Modeling of the blood rheology in steady-state shear flows. *Journal of Rheology*, 58:607–633, 2014.
- [11] RAS Ariens. Elevated fibrinogen causes thrombosis. *Blood*, 117:4687–4688, 2011.

- [12] JK Armstrong, HJ Meiselman, and TC Fisher. Covalent binding of poly(ethylene glycol) (peg) to the surface of red blood cells inhibits aggregation and reduces low shear blood viscosity. *American Journal of Hematology*, 56:26–28, 1999.
- [13] JK Armstrong, RB Wenby, HJ Meiselman, and TC Fisher. The hydrodynamic radii of macromolecules and their effect on red blood cell aggregation. *Biophysical Journal*, 87:4259–4270, 2004.
- [14] S Asakura and F Oosawa. Interaction between particles suspended in solutions of macromolecules. *Journal of polymer science*, 13:183–192, 1958.
- [15] S Badaire, CC Bizonne, JW Woddy, A Yang, and AD Strook. Shape selectivity in the assembly of lithographically designed colloidal particles. *Journal of american chemical society*, 129:40–41, 2007.
- [16] P Bagchi, PC Johnson, and AS Popel. Computational fluid dynamic simulation of aggregation of deformable cells in a shear flow. *Journal of biochemical engineering*, 127:1070–1080, 2005.
- [17] BJ Bain. *A beginner's guide to blood cells*. Backwell publishing, 2004.
- [18] BJ Bain. *Blood cells a particular guide*. Backwell publishing, 2006.
- [19] DW Ball. *The basics of spectroscopy*. Spie Press, Washington USA, 2001.
- [20] MP Barde and PJ Barde. What to use to express the variability of data: Standard deviation or standard error of mean. *Biostatistics*, 3(3):113–116, 2012.
- [21] PB Bareil, Y Sheng, YQ Chen, and A Chiou. Calculation of spherical red blood cell deformation in a dual-beam optical stretcher. *Optical Society of America*, 15 (24):16029–16034, 2007.
- [22] HA Barnes. The yield stress -a review or 'panta rhei'- everything flows? *Journal of Non-Newtonian Fluid Mechanics*, 81:133–178, 1999.
- [23] HA Barnes and K Walters. The yield stress myth. *Rheologica Acta*, 24:323–326, 1985.
- [24] G Barshtein, H Tamir, and S Yedgar. Red blood cell rouleaux formation in dextran solution: dependence on polymer concentration. *European biophysical journal*, 27:177–181, 1998.
- [25] D Barthes-Biesel. Motion and deformation of elastic capsules and vesicles in flow. *Annual Review of fluid mechanics*, 48:25–52, 2016.
- [26] O Baskurt, B Neu, and HJ Meiselman. *Red blood cell aggregation*. CRC Press New York, 2012.
- [27] M Berek. Grundlagen der tiefenwahrnehmung im mikroskop. *O Elsner Verlagsgesellschaft*, 62:189–223, 1927.

- [28] DA Berk and RM Hochmuth. Lateral mobility of integral proteins in red blood cell tethers. *Biophysical Journal*, 61:9–18, 1992.
- [29] K Bhadriraju and LK Hansen. Extracellular matrix- and cytoskeleton-dependent changes in cell shape and stiffness. *Experimental Cell Research*, 278(1):92–100, 2002.
- [30] E Biernacki. Samoistna sedymentacja krwi jako naukowa, praktyczno-kliniczna metoda badania. *Gazeta Lekarska*, 17:962–996, 1897.
- [31] GG Bilodeau. Regular pyramid punch problem. *Journal of Applied Mechanics*, 59:519–523, 1992.
- [32] EC Bingham. *Fluidity and plasticity*. McGraw-Hill, New York, 1922.
- [33] BD Biosciences. *BD Cell-Tak cell and tissue adhesive*, 2001.
- [34] RB Bird, RC Armstrong, and O Hassager. *Dynamics of Polymeric Liquids: Fluid Mechanics*. Wiley, New York, 1987.
- [35] S Black, I Kushner, and D Samols. C-reactive protein. *The Journal of Biological Chemistry*, 279(47):48487–48490, 2004.
- [36] H Bodemann and H Passow. Factors controlling the resealing of the membrane of human erythrocyte ghosts after hypotonic hemolysis. *Journal of Membrane Biology*, 8:1–26, 1972.
- [37] R Boehm and P Maybohm. *Notfallmedizin*. Georg Thieme Verlag KG Stuttgart, 2011.
- [38] CF Bohren and DR Huffman. *Absorption and scattering of light by small particles*. John Wiley and Sons, Weinheim, 1998.
- [39] D Bonn and MM Denn. Yield stress fluids slowly yield to analysis. *Materials Science*, 324:1401–1402, 2009.
- [40] N Borghi and F Brochard-Wyart. Tether extrusion from red blood cells: Integral proteins unbinding from cytoskeleton. *Biophysical Journal*, 93:1369–1379, 2007.
- [41] A Brooks, E Thomovsky, and P Johnson. Natural and synthetic colloids in veterinary medicine. *Topics in companion animal medicine*, accepted, 2016.
- [42] DE Brooks. The effect of neutral polymers on the electrokinetic potential of cells and other charged particles ii: Experimental studies on the dextran/erythrocyte system. *Journal of colloid interface science*, 43:701–713, 1973.
- [43] K Brummel, S Butenas, and KG Mann. An intergrated study of fibrinogen during blood coagulation. *Journal of biological chemistry* 274, 32:2286222870, 1999.
- [44] M Brust. *Rheological properties of Red Blood Cells*. PhD thesis, Saarland University, 2013.

- [45] M Brust, O Aouane, M Thiebaud, D Flormann, C Verdier, L Kaestner, MW Laschke, H Selmi, A Benyoussef, T Podgorski, G Coupier, C Misbah, and C Wagner. The plasma protein fibrinogen stabilizes clusters of red blood cells in microcapillary flows. *Scientific Reports*, 4:4348, 2014.
- [46] HJ Butt and M Jaschke. Calculation of thermal noise in atomic force microscopy. *Nanotechnology*, 6:1–7, 1995.
- [47] K Buxbaum, E Evans, and DE Brooks. Quantification of surface affinities of red blood cells in dextran solutions and plasma. *Biochemistry*, 21:3235–3239, 1982.
- [48] FA Carvalho, S Connell, G Miltenberger-Miltenyi, SV Pereira, A Tavares, RAS Ariens, and NC Santos. Atomic force microscopy-based molecular recognition of a fibrinogen receptor on human erythrocytes. *American chemical society*, 4:8:4609–4620, 2010.
- [49] N Casson. *Rheology of disperse systems*. Pergamon Press, Oxford, 1959.
- [50] MM Castellanos, JA Pathak, and RH Colby. Both protein adsorption and aggregation contribute to shear yield and viscosity increase in protein solutions. *Soft Matter*, 10(1):122–131, 2014.
- [51] S Chien. "Biophysical behavior of red cells in suspensions" in *The Red blood cell*, volume 1031-1033. Academic Press, New York, 1975.
- [52] S Chien and K Jan. Red cell aggregation by macromolecules: role of surface adsorption and electrostatic repulsion. *Journal of supramolecular structure*, pages 385–409, 1973.
- [53] S Chien and LA Jan. Ultrastructural basis of the mechanism of rouleaux formation. *Microvascular Research*, 5:155–166, 1973.
- [54] S Chien and LA Lang. Physiochemical basis and clinical implications of red cell aggregation. *Clinical Hemorheology*, 7:71–91, 1987.
- [55] S Chien, S Simchon, RE Abbott, and KM Jan. Surface adsorption of dextrans on human red cell membrane. *Journal of Colloid and Interface Science*, 62(3):461–470, 1977.
- [56] S Chien, S Usami, RJ Dellenback, and MI Gregersen. Shear-dependent deformation of erythrocytes in rheology of human blood. *American Journal of Physiology*, 219:136–142, 1970.
- [57] S Chien, S Usami, HM Taylor, JL Lundberg, and MI Gregersen. Effect of hematocrit and plasma proteins on human blood rheology at low shear rates. *Journal of Applied Physiology*, 21:81–87, 1966.
- [58] F Ciasca, M Papi, SD Claudio, M Chiarpotto, V Palmieri, G Maulucci, G Nocca, C Rossi, and MD Spirito. Mapping viscoelastic properties of healthy and pathological red blood cells at the nanoscale value. *Nanoscale*, 7:17030–17037, 2015.

- [59] C Cohen-Tannoudji, B Diu, and F Laloe. *Quantenmechanik*, volume Tome I and II. Walter de Gruyter, Berlin, 2010.
- [60] GR Cokelet, HJ Meiselman, and DE Brooks. *Erythrocyte mechanics and blood flow*. Alan R Liss, Inc. New York, 1980.
- [61] SS Datta, SH Kim, J Paulose, A Abbaspourrad, DR Nelson, and DA Weitz. Delayed buckling and guided folding of inhomogeneous capsules. *Physical Review Letters*, 109:134302, 2012.
- [62] PT Dawes, PD Fowler, S Clarke, J Fisher, A Lawton, and MF Shadforth. Rheumatoid arthritis: treatment which controls the c-reactive protein and erythrocyte sedimentation rate reduces radiological progression. *British Journal of Rheumatology*, 25:44–49, 1986.
- [63] AN de Belder. Dextran. Technical report, Amhersham Bioscience, 2003.
- [64] JT Dodge, C Mitchell, and DJ Hanahan. The preparation and chemical characteristics of hemoglobin-free ghosts of human erythrocytes. *Archives of Biochemistry and Biophysics*, 100(1):119–130, 1963.
- [65] C Duprat and HA Stone. *Fluid-structure interaction in low-reynolds-number flow*. RSC Soft Matter Series, 2015.
- [66] LEG Eriksson. On the shape of human red blood cells interacting with flat artificial surface - the 'glass effect'. *Biochimica et Biophysica Acta*, 1036:193–201, 1990.
- [67] EA Evans. Binding elastic modulus of red blood cell membrane derived from buckling instability in micropipet aspiration tests. *Biophysical Journal*, 43:27–30, 1983.
- [68] R Fahraeus. The suspension stability of the blood. *Physiological Reviews* 9, 2:241–274, 1929.
- [69] A Fall, F Bertrand, G Ovarlez, and D Bonn. Yield stress and shear bending in granular suspensions. *Physical Review Letters*, 103:178301, 2009.
- [70] R Fantoni, A Giacometti, and A Santos. Bridging and depletion mechanisms in colloid-colloid effective interaction: A reentrant phase diagram. *Journal of chemical physics*, 142:224905, 2015.
- [71] E Farag and DJ Doyle. The safety of hydroxyethyl starch (hes) - products now in doubt. Official Journal of Anesthesia Patient Safety Foundation, 2013.
- [72] DA Fedosov, W Pan, B Caswell, G Gompper, and GE Karniadakis. Predicting human blood viscosity in silico. *PNAS*, 108(29):11772–11777, 2011.
- [73] DA Fedosov, M Peltomaki, and G Gompper. Deformation and dynamics of red blood cells in flow through cylindrical microchannels. *Soft Matter*, 10:4258–4267, 2014.

- [74] J Feng, B Laderman, S Sacanna, and P Chaikin. Re-entrant solidification in polymer-colloid mixtures as a consequence of competing entropic and enthalpic attractions. *Nature materials*, 4109:61–65, 2014.
- [75] N Firooz, D Albert, D Wallace, M Ishimori, D Berel, and M Weisman. High-sensitivity c-reactive protein and erythrocyte sedimentation rate in system lupus erythematosus. *Lupus*, 20:588–597, 2011.
- [76] D Flormann. Untersuchung des aggregationsverhaltens roter blutzellen mit rheologie, sedimentation und mikroskopie. Master’s thesis, Saarland University, 2013.
- [77] D Flormann, O Aouane, L Kaestner, C Ruloff, S Svetina, C Misbah, T Podgorski, and C Wagner. The buckling instability of aggregating red blood cells. *submitted*, 2016.
- [78] D Flormann, E Kuder, P Lipp, C Wagner, and L Kaestner. Is there a role of c-reactive protein in red blood cell aggregation? *International Journal of Laboratory Hematology*, 37:474, 2015.
- [79] D Flormann, K Schirra, T Podgorski, and C Wagner. On the rheology of red cell suspensions with different amounts of dextran: separating the effect of aggregation and increase in viscosity of the suspending phase. *Rheologica Acta*, 55:477–483, 2016.
- [80] CF Quate, G Binnig, and C Gerber. Atomic force microscope. *Physical Review Letters*, 56 9:930–933, 1986.
- [81] PG De Gennes. *Scaling concepts in polymer physics*. Cornell university press New York, 1979.
- [82] M Godin, AK Bryan, and TP Burg. Measuring the mass, density, and size of particles and cells using a suspended microchannel resonator. *Applied physics letters*, 91:123121, 2007.
- [83] J Golstone, H Schoenbein, and R Wells. The rheology of red blood cell aggregates. *Microvascular Research*, 2:273–286, 1970.
- [84] W Gottwald and KH Heinrich. *UV/VIS-Spektroskopie*. Wiley-Vch, Weinheim, 1999.
- [85] N Gov, AG Zilman, and S Safran. Cytoskeleton confinement and tension of red blood cell membranes. *Physical Review Letters*, 90:228101, 2003.
- [86] KA Granath. Solution properties of branched dextran. *Journal of colloid science*, 13(4):308–328, 1958.
- [87] TMA Gronewold. Surface acoustic wave sensors in the bioanalytical field: Recent trends and challenges. *Analytica Chimica Acta*, 603:119–128, 2007.
- [88] E Guazzelli and J Hinch. Fluctuations and instability in sedimentation. *Journal of Fluid Mechanics*, 43:97–116, 2011.

- [89] B Gueslin, L Talini, B Herzhaft, Y Peysson, and C Allain. Flow induced by a sphere settling in an aging yield-stress fluid. *Physics of Fluids*, 18:103101, 2006.
- [90] CE Hall and HS Slayter. The fibrinogen molecule: Its size, shape and mode of polymerization. *Journal of Biophysical and Biochemical Cytology*, 5(1):11–17, 1958.
- [91] V Heinrich, K Ritchie, N Mohandas, and E Evans. Elastic thickness compressibility of the red cell membrane. *Biophysical Journal*, 81:1452–1463, 2001.
- [92] J Helenius, CP Heisenberg, HE Gaub, and DJ Muller. Single-cell force spectroscopy. *Journal of Cell Science*, 121:1785–1791, 2008.
- [93] WH Herschel and R Bulkley. Konsistenzmessungen von gummi-benzol-lösungen. *Kolloid Zeitschrift*, 39:291–300, 1926.
- [94] H Hertz. Miscellaneous papers. *London Macmillan*, page 146, 1896.
- [95] B Herzhaft and E Guazzelli. Experimental study of dilute and semi-dilute suspensions of fibers. *Journal of Fluid Mechanics*, 384:133–158, 1999.
- [96] RM Hochmuth and EA Evans. Extensional flow of erythrocyte membrane from cell body to elastic tethers i: Analysis. *Biophysical Journal*, 39:71–81, 1982.
- [97] RM Hochmuth and WD Marcus. Membrane tethers formed from blood cells with available area and determination of their adhesion energy. *Biophysical Journal*, 82:2964–2969, 2002.
- [98] RM Hochmuth, JY Shao, J Dai, and MP Sheetz. Deformation and flow of membrane into tethers extracted from neuronal growth cones. *Biophysical Journal*, 70:358–369, 1996.
- [99] RM Hochmuth, HC Wiles, EA Evans, and JT McCown. Extensional flow of erythrocyte membrane from cell body to elastic tethers ii: Experiment. *Biophysical Journal*, 39:83–89, 1982.
- [100] JF Hoffman. Physiological characteristics of human red blood cell ghosts. *The Journal of General Physiology*, pages 9–28, 1958.
- [101] H Hogevik, L Olaison, R Andersson, and K Alestig. C-reactive protein is more sensitive than erythrocyte sedimentation rate for diagnosis of infective endocarditis. *Infection*, 25:82–85, 1997.
- [102] JL Hutter. Comment on tilt of atomic force microscope cantilevers: Effect on spring constant and adhesion measurements. *Langmuir*, 21:2630–2632, 2005.
- [103] JL Hutter and J Bechhoefer. Calibration of atomic-force microscope tips. *Review of Scientific Instruments*, 64 (7):1868–1873, 1993.
- [104] CE Ioan, T Aberle, and W Burchard. Light scattering and viscosity behavior of dextran in semidilute solution. *Macromolecules*, 34:326–336, 2001.

- [105] KL Johnson, K Kendall, and AD Roberts. Surface energy and the contact of elastic solids. *Proceedings of the Royal Society of London*, 324:301–313, 1971.
- [106] A Jones and B Vincent. Depletion flocculation of nanaqueous sterically-stabilized particles 2: modifications to theory and further studies. *Colloids Surfaces*, 42:113–138, 1989.
- [107] A Jung. *Untersuchung einer Ca²⁺ induzierten Erythrozytenadhaesion mittels holographischer optischer Pinzetten*. PhD thesis, Universitaet des Saarlandes, 2009.
- [108] Fresenius Kabi. *Zusammenfassung der Merkmale des Arzneimittels: Voluven 6Infusionsloesung*, 2014.
- [109] L Kaestner, W Tabellion, P Lipp, and I Bernhardt. Prostaglandin e₂ activates chanelle-mediated calcium entry in human erythrocytes: an indication for a blood clot formation supporting process. *Thrombosis and Haemostasis*, 92:1269–1272, 2004.
- [110] B Kaoui, G Birois, and C Misbah. Why do red blood cells have asymmetric shapes even in a symmetric flow? *Physical Review Letters*, 103(18):188101, 2009.
- [111] LM Kern. *Untersuchung des adhaesionsverhaltens roter blutzellen mithilfe der holographischen optischen pinzette*. Master’s thesis, Saarland universitiy, 2016.
- [112] H Kiesewetter and F Jung. Blood fluidity and endothelial influences on microcirculation. *Journal of Molecular Medicine*, 64(20):1041–1096, 1986.
- [113] F Klumpers, U Goetz, T Kurtz, Christian Herrmann, and TMA Gronewold. Conformational changes at protein-protein interaction followed onlie with an saw biosenser. *Sensors and Actuators B*, 203:904–908, 2014.
- [114] S Knoche and J Kierfeld. Osmotic buckling of sperical capsules. *Soft Matter*, 10:8358–8369, 2014.
- [115] S Komura, K Tamura, and T Kato. Buckling of sperical shells adhering onto rigid substrate. *European Physical Journal E*, 18:343, 2005.
- [116] M Koralewski, F Reinholz, J Karon, and K Waraczewski. Optical and magne-tooptical properties of clinical dextran. *Acta Physica Polonica A*, 112(5):1119–1124, 2007.
- [117] I Kushner and JA Somerville. Estimation of the molecular size of c-reactive protein and cx-reactive protein in serum. *Biochimica et Biophysica Acta*, 207(1):105–114, 1970.
- [118] L Lanotte, J Mauer, S Mendez, DA Fedosov, JM Fromental, V Claveria, F Nicoud, G Gompper, and M Abkarian. Red cells dynamic morphologies govern blood shear thinning under microcirculatory flow conditions. *PNAS*, page 16080741113, 2016.

- [119] K Lee, M Kinnunen, MD Khokhlova, EV Lyubin, AV Priezzhev, I Meglinski, and AA Fedyanin. Optical tweezers study of red blood cell aggregation and disaggregation in plasma and protein solutions. *Journal of Biomedical Optics*, 21(3):035001, 2016.
- [120] T Lehmann. *UV/VIS-Spektroskopie*. Freie Universitaet Berlin, 2009.
- [121] AD Leung, KHK Wong, and J Tien. Plasma expanders stabilize human microvessels in microfluidic scaffolds. *Journal of biomedical materials research A*, 100A (7):1815–1822, 2012.
- [122] R Levy and M Maaloum. Measuring the spring constant of atomic force microscope cantilevers: thermal fluctuations and other methods. *Nanotechnology*, 13:33–37, 2001.
- [123] Malvern Instruments Limited. *Understanding the yield stress*, 2012.
- [124] CY Liu and S Chien, editors. *Fibrinogen, thrombosis, coagulation and fibrinolyses*. Springer Science and business media, New York, 1990.
- [125] D Lominadze and WL Dean. Involvement of fibrinogen specific binding in erythrocyte aggregation. *FEBS Letters*, 517(1-3):41, 2002.
- [126] N Mackman. Triggers, reargets and treatments for thrombosis. *Nature*, 7181:914–918, 2008.
- [127] N Maeda. Alteration of rheological properties of human erythrocytes by crosslinking of membrane proteins. *Biochimica et Biophysica Acta*, 735:104–112, 1983.
- [128] N Maeda, M Seike, S Kume, T Takaku, and T Shiga. Fibrinogen-induced erythrocyte aggregation: erythrocyte-binding site in the fibrinogen molecule. *Biochimica et Biophysica Acta*, 904:81–91, 1987.
- [129] MD Mager, V LaPointe, and MM Stevens. Exploring and exploiting chemistry at the cell surface. *Nature chemistry*, 3:582–589, 2011.
- [130] A Marucco, I Fenoglio, F Turci, and B Fubini. Interaction of fibrinogen and albumin with titanium dioxide nanoparticles of different drystalline phases. *Jounral of Physics: Conference Series*, 429:012014, 2013.
- [131] R McCahon and J Hardman. Pharmacology of plasma expanders. *Anaesthesia and Intensive Care Medicine*, 8:2:79–81, 2006.
- [132] EW Merrill, GC Cokelet, A Britten, and RE Wells Jr. Non-newtonian rheology of human-blood-effect of fibrinogen deduced by "subtraction". *Circulation Research*, 13:48–55, 1963.
- [133] EW Merrill, ER Gilliland, TS Lee, and EW Salzman. Blood rheology: Effect of fibrinogen deduced by addition. *Circulation Research*, 18:437–446, 1966.
- [134] LI Mi, L LianQing, X Ning, W YueChao, D ZaiLi, X XiuBin, and Z WeiJing. Atomic force microscopy imaging and mechanical properties measurement of red blood cells and aggressive cancer cells. *Science China*, 55:11:968–973, 2012.

- [135] Leica Microsystems. *Leica HyD for Confocal Imaging*, 2015.
- [136] M Minsky. Microscopy apparatus patent. *USA*, page 3013467, 1957.
- [137] M Minsky. Memoir on inventing the confocal scanning microscope. *Scanning*, 10:128–138, 1988.
- [138] E Mitsoulis. Flows of viscoplastic materials: models and computations. *Rheology Reviews*, pages 135–178, 2007.
- [139] ST Moerz. *Diffusion and adsorption of proteins in mesoporous environments*. PhD thesis, Saarland university, 2013.
- [140] N Mohandas and PG Gallagher. Red cell membrane: past, present and future. *Blood*, 112(10):3939–3948, 2008.
- [141] AN Morozov and W van Saarloos. An introduction essay on subcritical instabilities and the transition to turbulence in visco-elastic parallel shear flows. *Physics Reports*, 447:112–143, 2007.
- [142] V Narsimhan, AP Spann, and ESG Shaqfeh. Pearling, wrinkling and buckling of vesicles in elongational flows. *Journal of Fluid Mechanics*, 777:1–26, 2015.
- [143] B Neu and HJ Meiselman. Depletion-mediated red blood cell aggregation in polymer solutions. *Biophysical Journal*, 83:2482–2490, 2002.
- [144] DB Nguyen. *Phosphatidylserine exposure in red blood cells: A suggestion for the active role of red blood cells in blood formations*. PhD thesis, Saarland University, 2010.
- [145] DB Nguyen, L Wagner-Britz, S Maia, P Steffen, C Wagner, L Kaestner, and I Bernhardt. Regulation of phosphatidylserine exposure in red blood cells. *Cellular physiology and biochemistry*, 28:847–856, 2011.
- [146] P Nipkow. Patent. *Germany*, pages 30, 105, 1884.
- [147] Anton Paar. *Manual MCR702 TwinDrive*, 2014.
- [148] SW Paddock, editor. *Confocal Microscopy Methods and Protocols*, volume 122. *Methods in Molecular Biology*, Humana Press, Totawa, 1999.
- [149] SJ Park and D Khang. Conformational changes of fibrinogen in dispersed carbon nanotubes. *International Journal of Nanomedicine*, 7:4325–4333, 2012.
- [150] P Partal and JM Franco. Non-newtonian fluids. *Rheology*, 1, 2011.
- [151] EM Pasini, M Kirkegaard, P Mortensen, HU Lutz, AW Thomas, and M Mann. In-depth analysis of the membrane and cytosolic proteome of red blood cells. *Blood*, 108(3):791–801, 2006.
- [152] RB Pennell. *The red blood cell*. 2nd ed. Academic Press, New York, 1974.
- [153] M Perpeet, S Glass, T Gronewold, A Kiwitz, A Malave, I Stoyanov, M Tewes, and E Quandt. Saw sensor system for marker-free molecular interaction analysis. *Analytical Letters*, 39:1747–1757, 2006.

- [154] M Petran, M Hadravsky, MD Egger, and R Galambos. Tandem-scanning reflected-light microscope. *Journal of the Optical Society of America*, 58:661–664, 1968.
- [155] C Picart, JM Piau, H Galliard, and P Carpentier. Human blood shear yield stress and its hematocrit dependence. *Journal of Rheology*, 42(1), 1998.
- [156] P Poderick, G Ferris, K Wilson, H Halls, D Jackson, R Collins, and C Baigent. Towards evidence-based guideguide for the prevention of venous thromboembolism: systematic reviews of mechanical methods, oral anticoagulation, dextran and regional anaesthesia as thromboprophylaxis. *Health technology assess journal*, 9(49):1–78, 2005.
- [157] S Pongprasobchai, V Jianjaroonwong, P Charatcharoenwitthaya, C Komoltri, T Tanwandee, S Leelakusolvong, N Pausawasdi, W Srikureja, S Chainuvati, V Prachayakul, S Mantsathit, and U Kachintorn. Erythrocyte sedimentation rate and c-reactive protein for the prediction of severity of acute pancreatitis. *Pancreas*, 39:1226–1230, 2010.
- [158] PRAC. *PRAC recommends suspending marketing authorisations for infusion solutions containing hydroxyethyl-starch*, jun 2013.
- [159] A Pribush, D Zilberman-Kravits, and N Meyerstein. The mechanism of dextran-induced red blood cell aggregation. *European Biophysics Journal*, 36:85–94, 2006.
- [160] RL Price and WGJ Jerome, editors. *Basic Confocal Microscopy*. Springer Science and business media, New York, 2011.
- [161] S Ramankrishnan, R Grebe, M Singh, and H Smid-Schoenbein. Aggregation of shape-altered erythrocytes: An in vivo study. *Current Science*, 77(6):805–808, 1999.
- [162] MA Rao. *Rheology of fluid, semisolid, and solid foods*. Springer Science and business media, New York, 2014.
- [163] WH Reinhart, A Singh, and P Werner-Staub. Red blood cell aggregation and sedimentation: the role of the cell shape. *British Journal of Haematology*, 73:551–556, 1989.
- [164] M Rief, F Oesterhelt, B Heymann, and HE Gaub. Single molecule force spectroscopy on polysaccharides by atomic force microscopy. *Science*, 275:1295–1297, 1997.
- [165] CCW Ruppel and TA Fjeldly, editors. *Advances in surface acoustic wave technology, systems and applications*. World Scientific Publishing, Singapore, 2000.
- [166] WB Russel, DA Saville, and WR Schowalter. *Colloidal Dispersions*. Cambridge university press, 1999.

- [167] PS Sarangapani, SD Hudson, KB Migler, and JA Pathak. The limitations of an exclusively colloidal view of protein solution hydrodynamics and rheology. *Biophysical journal*, 105:2418–2426, 2013.
- [168] C Schaefer. *Elastic Flow Instabilities of Non-Newtonian Fluids in Shear Flows*. PhD thesis, Saarland University, 2013.
- [169] MD Schlesog, TMA Gronewold, M Tewes, B Schmid, M Famulok, and E Quandt. A love-wave sensor coupled with aptamers. In *European Conference on solid-state transducers*, number M2A3, pages 49–52, 2002.
- [170] H Schmid-Schoenbein, R Wells, and R Schildkraut. Microscopy and viscometry of blood flowing under uniform shear rate. *Journal of applied physiology*, 5:674–678, 1969.
- [171] G Schramm. *A partial approach to rheology and rheometry*. Thermo Haake GmbH, 2000.
- [172] US Schwarz and SA Safran. Physics of adherent cells. *Review of Modern Physics*, 85:1327–1381, 2013.
- [173] M Seigneuret and PF Devaux. Atp-dependent asymmetric distribution of sopinlabeled phospholipids in the erythrocyte membrane: Relation to changes. *Proceedings of national academy of science of the united states of america*, 12:3751–3755, 1984.
- [174] SJ Singer and GL Nicolson. Fluid mosaic model of structure of cell membranes. *Science*, 4023:720–731, 1972.
- [175] R Skalak and C Zhu. Rheological aspects of red blood cell aggregation. *Biorheology*, 27:309–325, 1990.
- [176] IN Sneddon. The relation between load and penetration in the axisymmetric boussinesq problem for a punch of arbitrary profile. *International Journal of Engineering Science*, 3:47–57, 1965.
- [177] RW Stark, T Drobek, and WM Heckl. Thermomechanical noise of a free v-shaped cantilever for atomic-force microscopy. *Ultramicroscopy*, 86:207–215, 2001.
- [178] P Steffen. Charakterisierung der zell-zell-adhaesion roter blutzellen mittels holographischer optischer pinzetten. Master’s thesis, Universitaet des Saarlandes, 2009.
- [179] P Steffen. *Quantification of red blood cell adhesion using holographic optical tweezers and single cell force spectroscopy*. PhD thesis, Universitaet des Saarlandes, 2012.
- [180] P Steffen, C Verdier, and C Wagner. Quantification of depletion-induced adhesion of red blood cells. *Physical Review Letters*, 110:018102, 2013.
- [181] Stoecker. *Taschenbuch der Physik*. Harri Deutsch Verlag, Frankfurt am Main, 2004.

- [182] S Svetina and P Ziherl. Morphology of small aggregates of red blood cells. *Bioelectrochemistry*, 73:84–91, 2008.
- [183] J Swenson, MV Smalley, and HLM Hatharasinghe. Mechanism and strength of polymer bridging flocculation. *Physical review letters*, 81:5840–5843, 1998.
- [184] Life Technologies. *CellMask plasma membrane stains*, 2014.
- [185] U Thelander and S Larsson. Quantification of c-reactive protein levels and erythrocyte sedimentation rate after spinal surgery. *Spine*, 17:400–404, 1992.
- [186] D Thompson, MB Pepys, and SP Wood. The physiological structure of human c-reactive protein and its complex with phosphocholine. *Structure*, 7(2):169–177, 1999.
- [187] D Tilley, WT Coakley, RK Gould, SE Payne, and LA Hewison. Real time observation of polylysine, dextran and polyethylene glycol induced mutual adhesion of erythrocytes held in suspension in an ultrasonic standing wave field. *European Biophysics Journal*, 14(8):499–507, 1987.
- [188] M Tomishige, Y Sako, and A Kusumi. Regulation mechanism of the lateral diffusion of band 3 in erythrocyte membranes by the membrane skeleton. *Journal of cell biology*, 142(4):989–1000, 1998.
- [189] M Tsujimoto, K Inoue, and S Nojima. Purification and characterization of human serum c-reactive protein. *Journal of Biochemistry*, 94(5):1367–1373, 1983.
- [190] D Turner, DR Mack, J Hyams, N LeLeiko, A Otley, J Markowitz, Y Kasirer, A Muise, CH Seow, MS Silverberg, W Crandall, and AM Griffiths. C-reactive protein (crp), erythrocyte sedimentation rate (esr) or both? a systematic evaluation in pediatric ulcerative colitis. *European Crohn's and Colitis Organisation*, 5:423–429, 2011.
- [191] L Unkila-Kallio, MJ Kallio, J Eskola, and H Peltola. Serum c-reactive protein, erythrocyte sedimentation rate, and white blood cell count in acute hematogenous osteomyelitis of children. *Pediatrics*, 93:59–62, 1994.
- [192] B Vincent. The calculation of depletion layer thickness as a function of bulk polymer concentration. *Colloids surfaces*, 50:241–249, 1990.
- [193] B Vincent, J Edwards, S Emmett, and A Jones. Depletion flocculation in dispersions of sterically-stabilized particles ("soft spheres"). *Colloids Surfaces*, 18:261–281, 1986.
- [194] JG White, WB Amos, and M Fordham. An evaluation of confocal versus conventional imaging of biological structures by fluorescence light microscopy. *Journal of Cell Biology*, 105:41–48, 1987.
- [195] CJ Wiedermann. Reporting bias in trials of volume resuscitation with hydroxyethyl starch. *The Central European Journal of Medicine*, 126:189–194, 2014.

- [196] HJ Woo and A Wallqvist. Spontaneous buckling of lipid bilayer and vesicle budding induced by antimicrobial peptide magainin 2: A coarse-grained simulation study. *Journal of Physical Chemistry B*, 115:8122–8129, 2011.
- [197] JF Wu, YH Yang, LC Wang, JH Lee, EY Shen, and BL Chiang. Comparative usefulness of c-reactive protein and erythrocyte sedimentation rate in juvenile rheumatoid arthritis. *Clinical and Experimental Rheumatology*, 25:782–785, 2007.
- [198] Y Yawata. *Cell Membrane The red blood cell as a model*. WILEY-VCH Verlag, Weinheim, 2003.
- [199] Y Zhao, X Sun, G Zhang, BG Trewyn, II Slowing, and VSY Lin. Interaction of mesoporous silica nanoparticles with human red blood cell membranes: Size and surface effects. *American Chemical Society Nano*, 5(2):1366–1375, 2011.
- [200] P Zihlerl and S Svetina. Flat and sigmoidally curved contact zones in vesicle-vesicle adhesion. *PNAS*, 104(3):761–765, 2007.